
Dissertation

Investigation on Fragmentation by Blasting

The influence of distorted blasthole patterns on fragmentation,
roughness of the remaining bench face and blast damage
behind it in model scale blasting

Mag. Radoslava Ivanova

19/11/2015

Investigation on Fragmentation by Blasting

The influence of distorted blasthole patterns on fragmentation, roughness of the remaining bench face and blast damage behind it in model scale blasting

Dissertation

by Radoslava Ivanova

Submitted to the Chair of Mining Engineering and Mineral
Economics

in fulfilment of the requirements of the degree of

Doktor der montanistischen Wissenschaften

at the

Montanuniversitaet Leoben

Supervisors:

Ouchterlony, Finn, Dr.mont. h.c. Dr.tekn.

Moser, Peter, Univ.-Prof. Dipl.-Ing. Dr.mont.

Declaration of Authorship

“I hereby declare that this report is my own work and that it contains, to the best knowledge and belief, no material previously published or written by another person nor material which to a substantial extent has been submitted for another module, except where due acknowledgement is made in the report.”

Radoslava Ivanova:

Acknowledgments

This thesis has been carried out at the Chair of Mining Engineering and Mineral Economics at the Montanuniversitaet, Leoben, with the support thereof.

As a doctoral student, I have had the pleasure of working with rock blasting experts, who have given me their continuous support and actively helped me throughout my research.

First, I would like to express my gratitude to my supervisor, Professor Finn Ouchterlony, for his invaluable, continuous assistance. Thank you very much, Finn! Thank you for being always there for us, your students, day and night. Without your assistance, finalizing this thesis would have not been possible. We have been working together for a few years now and I am happy that you have been my mentor throughout.

Next, I would like to thank Prof. Peter Moser for having given me the opportunity to work with applied blasting principles. Six years ago, he introduced me to the challenging world of blasting techniques and gave me the opportunity to experience it first-hand. Thank you, Prof. Moser, without your trust and continuous support; I would not be here now.

I would also like to thank Prof. José Angel Sanchidrián from Universidad Politécnica de Madrid, Spain, for his guidance and support.

Many thanks to Prof. Arnold Kräuter from the Chair of Mathematics and Statistics for his continuous assistance and support.

My grateful thanks also go to Peter Schimek and Gerold Wölfler, as well as all my colleagues at the Chair of Mining Engineering and Mineral Economics, Montanuniversitaet Leoben, for supporting me during these years.

Many thanks to the students of Mining Engineering at Leoben: Clara Villaro, Georg Glatz, Thomas Seidl, Juan Navarro, Stefanie Streit and Ganz Zhu for helping me with my blasting tests and the subsequent laboratory work.

Last but not least, I would like to thank all of my friends and especially DI Diego Herrera and Lorna Judge. Thank you for your kind support and for giving me so much joy outside of my work.

Abstract

Drilling and blasting are two of the most important parts of a quarry's production operation. An ineffective blasting, arising from drillhole deviations, significantly affects the overall performance of the process both technically and economically; it is believed to result in high quantities of fines, which have low commercial value, and in over-sized material, which requires further treatment. The larger the drillhole deviation, the smaller or larger the practical burden becomes. For high benches the difference between the theoretical and the practical burden values can become substantial. Blast damage and safety are other important aspects related to the drillhole deviation.

Very little is known about how drilling accuracy influences blast fragmentation though. The Kuz-Ram, a common blast model predicts a flatter sieving curve compared with that of a perfect drilling, but has an unchanged median fragment size. However, recent field study (Sellers et al., 2013), conducted in platinum mine in South Africa gave contradictory results.

This thesis summarizes the results from fifteen small-scale blasting tests in magnetic mortar, which were carried out in 2013 and 2014 with the aim of investigating how drillhole deviations influence fragmentation. In addition, characterization of the blast damage was accomplished by looking into the surface characteristics of the bench face and the development of internal cracks after the blast.

To minimize the geometrical and geological effects, the tests have been made with magnetite concrete blocks with dimensions of $660 \times 280 \times 210$ mm (L \times W \times H). The explosive source was a decoupled, 7 mm diameter, PETN-cord with a strength of 20 g/m, giving a theoretical specific charge (q) of 3.02 kg/m^3 over the volume of BLH = $0.07 \times 0.66 \times 0.21 \text{ m}^3$ corresponding to one burden unit. The specific charge was kept constant throughout the tests.

Six blasthole patterns, based on 3 rows with 7 holes each, have been tested: two reference patterns with a burden of 70 mm and spacing of 95 mm (S/B = 1.36) and four additional blasthole patterns with either a variation in burden or a variation in

both burden and spacing, used to represent stochastic or systematic drilling errors or blasthole pattern deformation.

Evaluation of the fragmented material from blasting has been completed by sieving it in the laboratory. The Swebrec function (Ouchterlony, 2005, 2010) was fitted to the experimental data.

The sieving results confirmed earlier findings though that the fragmentation gets finer with the number of rows shot, implying that blast damage from earlier rows has an influence on the blasting results. The fragmentation results were well reproduced by the basic three parameter Swebrec function.

Fragmentation analysis showed that there is no evidence if drill collaring errors, both stochastic and systematic to have a significant effect on the sieving curves, neither x_{50} nor n . This means that the fragmentation is not influenced by the blasthole patterns tested under these conditions: row by row blasting of 2D small scale models with unconfined bottom and drill patterns with collaring deviations and straight vertical holes.

The characteristics of the bench after each blast was evaluated along three horizontal lines out of a 3D-model of the bench face. The evaluation of the model was done with MATLAB, and the topography of the surface is then described by statistical parameters (D_{mean} and S_{norm}) corresponding to the backbreak/underbreak and micro roughness. The S_{norm} was judged later on as a parameter with no physical meaning of describing the bench surface characteristics.

The surface damage characteristics analysis showed that the blocks from session 2013 depicted a higher backbreak than blocks from session 2014. In four out of six drill patterns tested, the 2nd row produced more overbreak than 1st row, while the 3rd row shots resulted in a flatter surface independent of the chosen drill pattern. The smoothest surface damage was somehow achieved with S/4 shift pattern, however looking to the combined effect, the influence of the drillpatterns to the backbreak was insignificant.

The damage cracks behind the third row block remains were quantified by using a dye penetration method for crack visualization. The crack angles and their lengths, exposed by the dye, were then traced into the AutoCAD program. Eleven crack

families were identified, based on crack angles and lengths, and their connections and origin. As a result, mean crack density (MCD) and mean crack intersection density (MCID) were established. Due to a very high correlation between MCD and MCID values, the MCID values were removed from the further analysis.

Five out of eleven detected crack families showed an influence of the distorted drillhole patterns. The calculated mean crack density (MCD) showed that the six drillhole patterns have different degree of damage.

In addition the top surface damage was investigated using the same method for crack visualization. Crack detection was done before blasting, after each of the 1st, 2nd and 3rd rows. The analysis indicated that the cracks on the top underestimate the crack content in the interior specimens. The results obtained were combined with the fragmentation results, surface damage (D_{mean}) and MCD, to find how crack development from the previous blast would influence the fragmentation or damage in subsequent blasts.

To present in detail all of the afore mentioned work, this thesis is divided into four parts:

1. The first part contains a description of the drillhole deviation and its influence on the blast results, with regards to fragmentation, blast damage and safety.
2. In the second part, the set-up of both the experimental tests and the experimental methodology has been described. This includes the classification of the materials used for the blasting experiments, the blasthole patterns and the explosives used, the blast procedures followed, the surface roughness measurements, the surface crack detection procedures and the statistical tools used for data evaluation.
3. In the third part, the results and analysis of the material properties, fragmentation, surface roughness and crack detection have been presented. The analysis of the fragmentation obtained from the blasting experiments includes the analysis of the characteristic of the blast fragmentation curves and the analysis of the blast fragmentation results with respect to the specific particle sizes (e.g. x_{50}).
4. The final part examines the correlation between the fragmentation, surface damage characteristics and crack propagation properties of the material.

Zusammenfassung

Bohren und Sprengen sind zwei der wichtigsten Abläufe im Produktionsbetrieb von Steinbrüchen. Ineffektive Sprengtechnik, die aus Bohrlochabweichungen resultiert, hat signifikanten Einfluss auf die technische und wirtschaftliche Leistungsfähigkeit des gesamten Betriebes. Dies kann sowohl in wirtschaftlich minderwertigem Feinanteil als auch in aufwändig nachzubearbeitendem Grobkorn resultieren. Je größer die Bohrlochabweichung ist, desto größer oder kleiner ist die tatsächliche Vorgabe. Dies wiederum führt vor allem bei großen Etagenhöhen zu beträchtlichen Abweichungen zwischen der geplanten und der tatsächlichen Vorgabe. Die Schädigung durch Sprengungen sowie sicherheitsrelevante Aspekte sind weitere nicht zu unterschätzende Faktoren, die von Bohrlochabweichungen beeinflusst werden.

Über den Einfluss der Bohrgenauigkeit auf die Korngrößenverteilung nach dem Sprengen ist sehr wenig bekannt. Das bekannte Kuz-Ram-Modell prognostiziert für Bohrlochabweichungen eine flachere Siebkurve, wobei die mittlere Korngröße unverändert bleibt. Eine kürzlich durchgeführte Feldstudie in einem südafrikanischen Platinbergbau (Sellers et al., 2013) zeigte allerdings im Gegensatz dazu widersprüchliche Ergebnisse.

Die vorliegende Dissertation fasst die Ergebnisse von 15 Sprengversuchen im Kleinmaßstab zusammen, welche 2013 und 2014 mit dem Ziel der Untersuchung des Einflusses von Bohrlochabweichungen auf die Zerkleinerung durchgeführt wurden. Zusätzlich wurde die Schädigung durch Untersuchung der Bruchwandbeschaffenheit sowie der ins anstehende Gebirge eingetragenen Risse quantifiziert.

Um die geometrischen und geologischen Effekte zu minimieren, wurden die Versuche an Betonblöcken mit Magnetit-Partikeln mit den Dimensionen von 660 x 280 x 210 mm (L x W x H) durchgeführt. Der verwendete Sprengstoff war eine entkoppelte Sprengschnur (PETN) mit 7 mm Durchmesser und einem Lademetergewicht von 20 g/m. Dies resultierte beim gesprengten Volumen von $BLH = 0.07 \times 0.66 \times 0.21 \text{ m}^3$ in einer theoretischen spezifischen Lademenge (q) von

3.02 kg/m³. Diese spezifische Lademenge wurde während der gesamten durchgeführten Versuche konstant gehalten.

Fünf verschiedene Bohrraster, basierend auf 3 Reihen mit jeweils 7 Bohrlöchern wurden untersucht. Als Referenz diente ein Bohrraster mit einer Vorgabe von 70 mm und 95 mm Seitenabstand. Dies resultierte in einem Seitenabstand zu Vorgabe-Verhältnis (S/B) von 1.36. Dem gegenübergestellt wurden vier Bohrraster mit Variationen nur der Vorgabe oder einer Kombination von Vorgabe und Seitenabstand. Die untersuchten Bohrlochabweichungen waren stochastisch oder systematisch.

Die Zerkleinerung wurde mittels Siebanalyse verifiziert, wobei die Swebrec-Funktion (Ouchterlony, 2005, 2010) zur Beschreibung der Siebkurven herangezogen wurde.

Die Resultate der Siebanalyse bestätigten frühere Ergebnisse trotz der Tatsache, dass die Sprengungen feineres Material produzierten mit steigender Anzahl an Sprengungen. Dies impliziert den Einfluss der Vorschädigung durch vorangehende Sprengungen auf die Zerkleinerung. Die Ergebnisse der Zerkleinerung wurden mit der 3-parametrischen Swebrec-Funktion sehr gut beschrieben.

Die Analyse der Zerkleinerung zeigte, dass weder stochastische noch systematische Variationen der Bohrlochverläufe signifikanten Einfluss auf die Siebkurven haben. Da weder x_{50} noch n beeinflusst wurden, lassen diese Ergebnisse darauf schließen, dass die Zerkleinerung bei den untersuchten Bedingungen unverändert ist. Untersucht wurden dafür reihenweise Sprengungen in 2D kleinmaßstäblichen Modellen mit nicht eingespannter Bruchwandsohle und Bohrschema mit Variationen der vertikalen Bohrlöcher.

Die Beschaffenheit der gesprengten Bruchwand wurde nach jeder Sprengung anhand des Verlaufs von drei horizontalen Konturlinien aus dem 3D-Modell der Bruchwand bewertet. Die Auswertung des Modells wurde mit MATLAB durchgeführt, wobei die Topographie der Oberfläche mit statistischen Parametern (D_{mean} und S_{norm}) entsprechend dem Rückriss und Mikrorauigkeit beschrieben wurden. S_{norm} wurde später als Parameter ohne physikalische Bedeutung für die Beschreibung der Beschaffenheit der Bruchwand verworfen.

Die Auswertung der Bruchwandbeschaffenheit zeigte, dass die Blöcke der Testserie 2013 in mehr Rückriss als die Blöcke der Testserie 2014 resultierten. In vier der sechs untersuchten Bohrschemata resultierte die zweite Reihe in mehr Rückriss als die erste Reihe. Die Sprengversuche in der dritten Reihe resultierten in homogener ausgebildeten Oberflächen, unabhängig vom gewählten Bohrschema. Die homogenste Oberfläche wurde mit dem S/4-Bohrschema produziert, wobei der Einfluss des Bohrschemas auf den Rückriss nicht signifikant war.

Die erzeugten Risse hinter der dritten Reihe wurden mittels Farbeindringmittel visualisiert und quantifiziert. Die dadurch sichtbar gemachten Winkel und Längen der Risse wurden in AutoCAD digitalisiert. Die Risse wurden in elf Rissfamilien gemäß dem Winkel, der Länge, der Verbindungen und deren Ursprung kategorisiert. Resultierend daraus wurden die Parameter MCD (mean crack density) und MCID (mean crack intersection density) eingeführt. Aufgrund der hohen Korrelation der beiden Parameter wurde MCID nicht für die weitere Analyse herangezogen.

Fünf der elf detektierten Rissfamilien zeigten einen Einfluss der Bohrlochabweichungen. Der Parameter MCD zeigte, dass die sechs untersuchten Bohrschemata unterschiedliche Schädigungen hervorriefen.

Zusätzlich wurde die Schädigung an der Oberfläche der Testblöcke untersucht. Dafür wurde dieselbe Methodik wie für die interne Schädigung angewendet. Die Risse wurden vor sowie nach jeder Sprengung detektiert. Die Analyse zeigte, dass die Risse an der Oberfläche die erzeugten internen Risse unterbewerten. Die Resultate wurden in Relation gesetzt mit den Ergebnissen der Zerkleinerung, der Oberflächenbeschaffenheit (D_{mean}) und MCD. Somit konnte verifiziert werden, wie die erzeugten Risse durch vorangehende Sprengungen die Zerkleinerung und Schädigung von folgenden Sprengungen beeinflussen.

Um die gesamten Details der Untersuchungen zu präsentieren, wurde die Dissertation in vier Teile gegliedert:

1. Der erste Teil enthält eine Beschreibung von Bohrlochabweichungen und deren Einfluss auf das Sprengergebnis. Im Detail wird hierbei auf die Zerkleinerung, die Schädigung des anstehenden Gebirges und die Sicherheit eingegangen.

2. Im zweiten Teil werden der Versuchsaufbau und die Methodik der Sprengversuche erläutert. Dabei werden die eingesetzten Materialien, die Bohrschemata, der eingesetzte Sprengstoff sowie der Ablauf der Sprengversuche beschrieben. Weiters werden die Prozeduren für die Evaluierung der Oberflächenbeschaffenheit, die Quantifizierung der erzeugten Risse und die statistischen Methoden für die Auswertung der Daten erläutert.

3. Im dritten Teil werden die Resultate der Materialeigenschaften, der Zerkleinerung, der Oberflächenbeschaffenheit sowie der Rissausbreitung dargestellt. Die Evaluierung der Zerkleinerung enthält die detaillierte Analyse der Eigenschaften der Siebkurven sowie die Analyse von speziellen Kennzahlen (z.B. x_{50}).

4. Der vierte Teil untersucht die Zusammenhänge zwischen der Zerkleinerung, der Oberflächenbeschaffenheit und der Rissausbreitung.

List of symbols and abbreviations

A	rock mass factor, from literature $A = 4.76$ (at Vändle test site), corrected $A' \sim 3.9$ (Cunningham, 2005; Ouchterlony et al., 2006)
B	burden [m]
b	undulation parameter (exponent) in Swebrec function
C_1	coefficient of collaring error
C_2	coefficient that measures in-hole trajectory deviations
$C(n)$	correction factor, provided to calibrate the n-equation
COV	coefficient of variation [%]
2D	two dimensional
3D	three dimensional
D_{mean}	mean distance of the individual data points to the reference line
H	bench height or hole depth [m]
HF	hardness factor
JF	joint factor
KW-ANOVA	Kruskal-Wallis One-Way Analysis of Variance
L_b	bottom charge length [m]
L_c	column charge length [m]
L_{tot}	total charge length above grade [m]
l	drilled length [m]
MCD	mean crack density
MCID	mean crack intersection density
MWU-Test	Mann-Whitney-U-Test
n	Kuz-Ram uniformity index
n_s	uniformity factor governed by the scatter ratio;
P	cumulative mass passing at size x [m]
P_{max}	cumulative passing of grain class upper/lower [%]
P_0	sum of passing upper limit of grain class (oben-upper, in German) [%]
P_u	sum of passing lower limit of grain class(unten-lower, in German) [%]
Q	explosive charge weight [kg]
q	specific charge [kg/m^3]
r	Inter row-correlation factor
R^2	coefficient of determination
R_s	scatter ratio (for delay time $6\sigma_t/\tau_x$);
R	coefficient of correlation
RDI	rock density influence

RMD	rock mass description
RQ	research question
S	spacing [m]
S_{ANFO}	explosive strength, relative to ANFO [%]
SD	standard deviation for drilling error [m];
S_{Norm}	normalized slope inclination of the contour lines
T_r :	range of delay scatter for initiating system [ms]
T_x	desired delay between the holes[ms]
UCS	uniaxial compressive strength
VOD	velocity of detonation
x	fragment or mesh size variable [mm]
x_{30}	size at which the 30 % of the material is passing [mm]
x_{50}	median fragment size [mm]
x_{80}	size at which the 80 % of the material is passing [mm]
x_c	characteristic dimension [mm]
\varnothing_h	hole diameter [m]
σ_t	standard deviation of the initiation [ms]
α	significance level (= 5 % = 0.05)
μs	microseconds

Table of content

Declaration of Authorship	II
Acknowledgments	III
Abstract	IV
Zusammenfassung	VII
List of symbols and abbreviations	XI
Table of content	XIII
1. Introduction	1
Objectives	2
Scientific contribution	2
2. Literature review	4
2.1 Definition of drillhole deviation	4
2.2 Collaring and alignment deviation	5
2.3 Drilling deflection	6
2.4 Depth Deviation	7
2.5 Drillhole deviations: experiences, measurements and control	8
2.6 The effect of drillhole deviation on fragmentation	10
2.7 Drillhole deviation and blast damage	17
3. Test methodology and set-up	20
3.1 Blasting site Erzberg	20
3.2 Magnetite concrete	21
3.3 Testing blocks	22
3.4 Cylinders	23
3.5 Determination of physical and mechanical properties	24
3.5.1 Density	24
3.5.2 P-wave and S-wave velocity	25
3.5.3 Uniaxial compressive and tensile strength	25
3.5.4 E-modulus and Poisson's ratio	25
3.6 Blasthole pattern and drilling set-up	26
3.7 Explosives and delay time used	32
3.8 Blasting procedures	33
3.9 Pre-and post-blast visual control of the bench face	35
3.10 Sieving analysis	35
3.11 Particle size distribution and determination of x-values	37

3.12	Measurement of crack development	38
3.12.1	Crack detection on cut slices.....	39
3.12.2	Crack density analysis.....	43
3.12.3	Surface crack detection on the top of the testing blocks	45
3.12.4	Recognition of crack families.....	46
3.13	Surface characteristics analysis of the bench face.....	48
3.14	Statistical evaluation of the data.....	53
3.14.1	Mann-Whitney U- test.....	53
3.14.2	Kruskal-Wallis One-Way Analysis of Variance (KW-ANOVA)	55
3.14.3	Two samples t-test	57
3.14.4	One-way ANOVA F-Test:	58
4.	Results and analysis	59
4.1.	Material properties.....	59
4.1.1	Density	59
4.1.2	Uniaxial compressive and tensile strength	61
4.1.3	P-wave and S-wave velocity	61
4.1.4	Young's modulus and Poison's ratio	62
4.1.5	Sieving parameters of the cylinders	62
4.2.	Methodological question: Are the material properties from production sessions 2013 and 2014 comparable?.....	63
4.3.	Fragmentation results.....	65
4.3.1	Fragmentation results blast session 2013	66
4.3.2	Fragmentation: blast session 2014.....	73
4.3.3	Equivalent n-values and x_c for blast sessions 2013 and 2014.....	80
4.3.4	Summary of fragmentation findings.....	83
4.4.	Damage results	86
4.4.1	Results from visual bench face control.....	87
4.4.2	Surface damage	92
4.4.3	Interior damage results.....	98
4.4.4	Exterior blast damage results	109
4.4.5	Summary of the interior and exterior damage findings	111
4.5.	Correlation analysis.....	112
5.	Summary.....	117
6.	Further discussion about the results	122
7.	Recommendation for further tests	128

8.	Bibliography	132
9.	List of figures.....	144
10.	List of tables.....	151
Appendix 1	Magnetite concrete ingredients: data sheets.....	i
Appendix 2	Mechanical properties of mortar.....	iv
Appendix 3	Drill set-up.....	x
Appendix 4	Documentation of the blasting tests.....	xviii
Appendix 5	Sieving data and Swebrec fit summary.....	xxxiii
Appendix 6	Crack families detailed description.....	lv
Appendix 7	Crack families in horizontal sections on slices.....	lx
Appendix 8	Damage in individual blocks and patterns.....	lxxi
Appendix 9	Crack families on top of test blocks.....	lxxiii
Appendix 10	Surface damage analysis methodology.....	lxxxiv
Appendix 11	Surface damage characteristics diagrams.....	xcii
Appendix 12	Surface damage characteristics data.....	cvi

1. Introduction

Mining and quarry operations are continually working to reduce their operating costs, looking to optimize current performance with the aim of finding cost savings (Giltner and Koski, 2010). Optimization of blasting performance is a very important part of these and it may vary from quarry to quarry with respect to:

- desired fragment size distribution of blasted rock
- bench face stability
- vibration and noise, and the limits thereof.

The desired size distribution of fragmented rock varies for each quarry operation. Often quarries cannot use a large amount of fines (material with size less than 10-25 mm) and boulders can only be used for special building purposes. Blast optimization in terms of fragmenting material to the desired size may allow for significant cost savings in downstream processing stages.

The backbreak and damage to the remaining rock wall in open cast blasting is very important when considering the final pit wall design (Workman, 1991). A controlled backbreak will either allow a steeper pit angle to be used or that less rock wall support is necessary.

Blast vibration and noise levels are another aspect of the blast design; both are coming under increasing scrutiny and in many situations can be of prime importance.

On a daily basis, researchers in the bench blasting field attempt to optimize blasting performances to achieve the desired fragmentation, but the drillhole deviation is a problem that has been reported in quarry operations (Ouchterlony, 2002; Nielsen and Kristiansen, 1996; Olsen, 2009; Giltner and Koski, 2010; Sellers et al., 2013). Besides drillhole deviations, other factors seem to influence blasting: rock properties, blasthole pattern, ignition properties, explosive properties and the charging pattern (Da Gamma, 1983).

Furthermore, both the principal mechanisms of rock breaking with explosives, and the interaction between the rock mass and the induced stress waves, are still neither fully explained nor understood (Reichholf and Moser, 2000).

To date, scarcely any research has been done on the drillhole deviation effects on rock fragmentation and damage. Such research would be of great value to the mining and quarrying industries, since it would provide a better understanding of the mechanism of the effect of drillhole deviation, if any, on fragmentation. Due to the difficulties of studying blasting with distorted hole patterns on an industrial scale, small-scale tests were used herein.

Objectives

The primary objective of this thesis is to investigate how drillhole deviation affects the blast fragment size distribution.

The secondary objective is to investigate the blast damage behind the remaining bench faces when drillhole deviations exist.

The final objective is to investigate the relationship between the cracks generated by blasting and the blast fragmentation results.

To achieve these objectives, the following research questions (RQ) need to be answered:

- RQ1: Do the drillhole deviations have any influence on the fragmentation?
- RQ2: Do the drillhole deviations influence the blast damage and in what way?
- RQ3: Is there any connection between fragmentation and blast damage? If yes, then what is it?

Scientific contribution

Within the published literature, very few studies have been conducted that investigate and link measured drillhole deviations with measured fragmentation. Most of the existing studies report on drillhole deviation and discuss it along with other issues, related to the implementation of good blasting practices (Nielsen and Kristiansen, 1996; Olsen, 2008; Giltner and Koski, 2010).

To get a better understanding of the effect of drillhole deviations on both fragmentation and blast damage, this thesis introduces new ideas and results in the following directions:

1. Test of Kuz-Ram prediction of effect of drillhole deviations on value of uniformity index n in associated Rosin Rammler fragment size distribution.
2. Tests with well-defined stochastic drilling deviations (collaring error) in model scale row-wise bench blasts, starting with virgin and creating successively more blast damaged material under conditions where the blast waves radiate out and away from the breakage region
3. Use of stereo-photography to create calibrated 3D models of the remaining bench face after blasting and the calculation of measures of surface flatness (backbreak) and roughness
4. Use of dye penetrant technique on cut slices from the remaining material after blasting to visualize internal blast damage in the form of cracks, Categorization of these cracks into families and how the families react to drillhole deviations. Calculation of damage measures
5. An attempt to correlate bench front flatness and internal damage of blasted burden with fragmentation and back break

From the test experiments, all blast fragmentation and damage influencing parameters are investigated, presented and discussed in context.

2. Literature review

2.1 Definition of drillhole deviation

Drillhole deviation is defined as “the maximum deviation from the target position (m) in drilling/length of the hole (m) and given in %” (Rustan, 1998).

There are four causes of drilling deviation (see Figure 1):

- collaring deviation, d_c
- alignment deviation (horizontal direction and vertical inclination), d_a
- drilling deflection, d_d
- drillhole depth deviation, d_z .

Normally the size of the deviation is given either as a percentage of drillhole depth or in cm/m, with both giving the same numerical values.

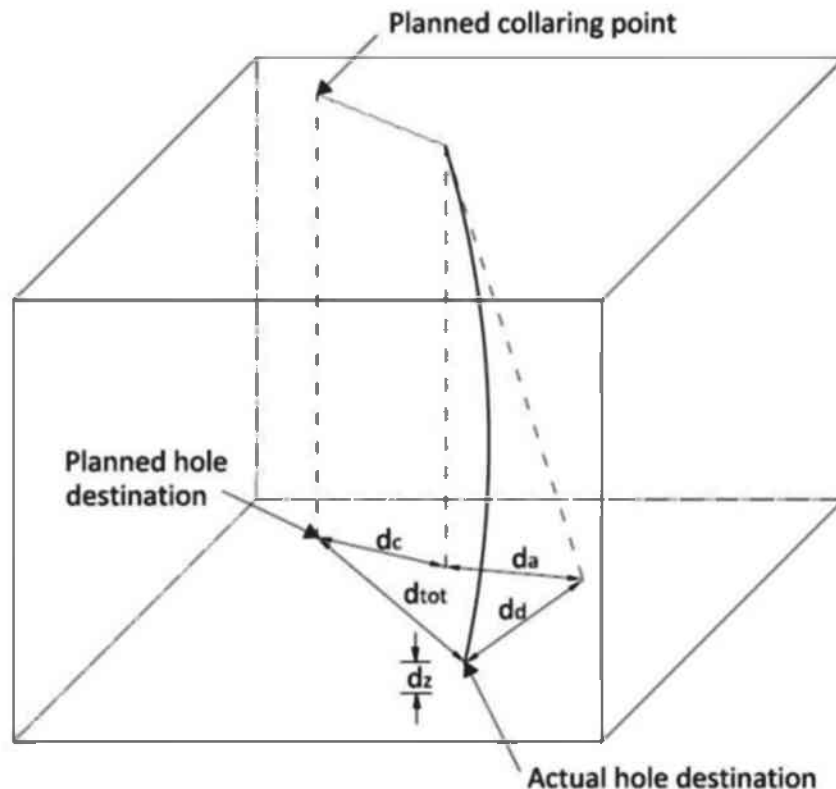


Figure 1: Diagrammatic representation of collaring d_c , alignment d_a , deflection d_d and vertical depth d_z deviations (Sinkala, 1989).

2.2 Collaring and alignment deviation

Collaring deviation is a lateral displacement from a planned location. It is therefore independent of any holes' depth. In general, it should not exceed the diameter of one drill bit.

$$d_c \leq D \quad \text{Equation 1}$$

where D is bit/hole diameter.

Alignment deviation is defined as angular, relative or percentage deviation from the intended angle of drilling in collaring (Cunningham et al, 2011).

Alignment deviation arises from inaccuracies while settings in the feed boom in its planned position. The alignment deviation is both horizontal/perpendicular in plane (azimuth angle) and vertical (inclination/dip angle). The azimuth angle deviation component becomes less important as the inclination approaches the vertical direction. The alignment deviation leads to a linear increase of the deviation of the hole. Alignment deviations with values less than 2 % (i.e. 20 mm/m) are considered good (Olsen, 2009). However alignment deviations larger than 50 mm/m are not unusual. Reasons for collaring and alignment deviations include: instability of the drilling rig; lack of precision during the surveying and setting-out process and in the tools/techniques used to align the feed beam; the topography at the collaring point; the drilling operator's experience and motivation (Ouchterlony, 2002).

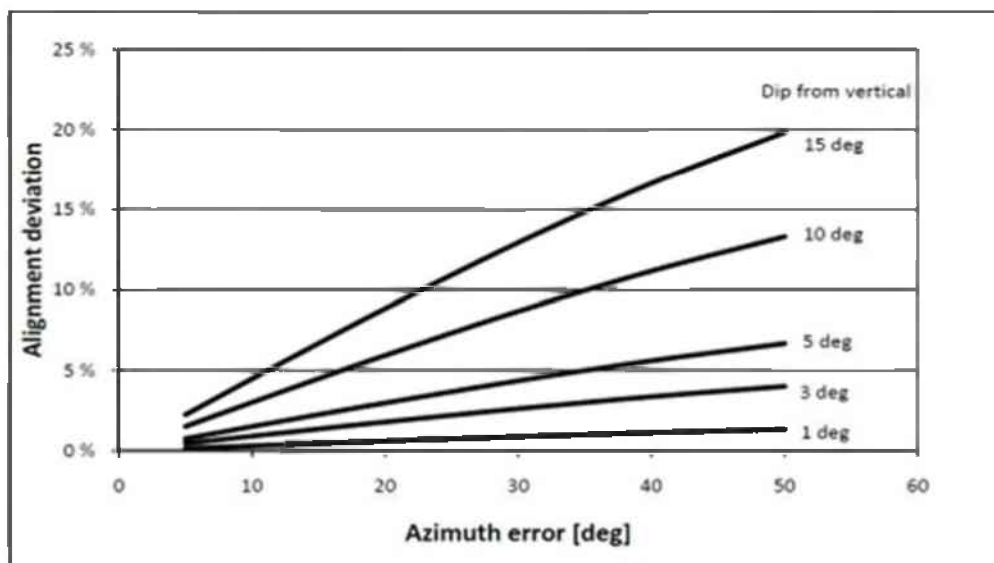


Figure 2: Alignment deviation (horizontally projected) as a function of dip angle and azimuth error (Olsen, 2009)

2.3 Drilling deflection

While collaring and alignment deviation arise from sources prior to drilling, deflection appears during the drilling process. It is mainly due to the pull-down pressure, which causes the drill-rod to bend and consequently to frequently follow the rock mass foliation (Olsen, 2009).

As a general rule, in quarries and open pit mines, where the bench heights are less than 20 m, deflections are only relevant to top-hammer drilling.

Studies show that the relative deflection increases with the drillhole length. Depending upon the loading conditions of the drill string, the deflection may increase by the power of two or three according to Euler's loading formulas (Olsen, 2009).

On average, the drillhole deflection varies from 20 cm to 100 cm in aggregate quarries with top-hammer drilling of 76 mm through 102 mm hole diameters. In some extreme cases a total deflection of 20 % of the drilled length can be measured. Figure 3 shows the deflection result as a function of the drillhole length. It can be seen that the deflection increases down the hole and varies from hole to hole.

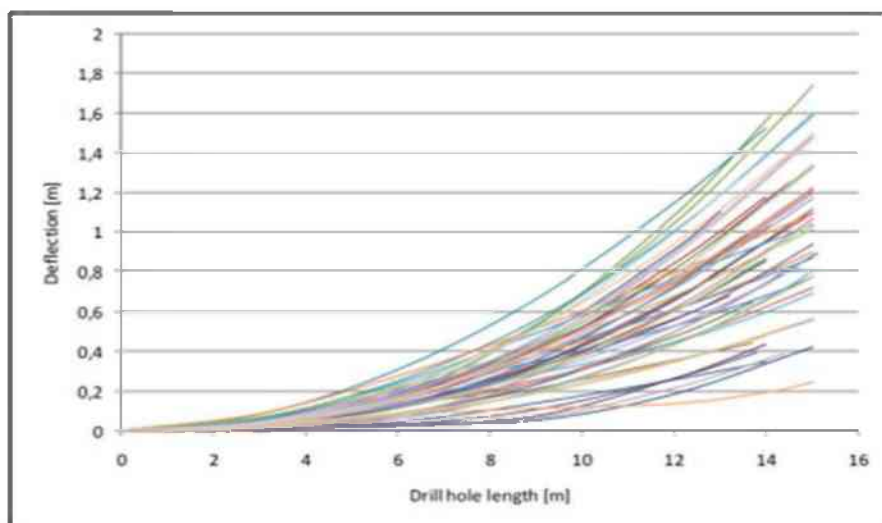


Figure 3: Deflection measures as a function of drillhole length (Olsen, 2009)

The deflection deviation may be randomly distributed, depending on the rock mass properties. In bedded and foliated rock, the drillholes are observed to either deflect parallel or normal to the bedding or foliation plane. The uniform deviation generally appears to be up-dip when the bedding inclination is less than 40°-50° to the horizontal, and to be down-dip otherwise (Olsen, 2009).

Severe deflections can be measured sometimes under “optimal” conditions. In homogenous rock, the deflection is random and usually small. Increased jointing frequency will lead to a more uniform deviation, converging towards the bedded rock conditions.

Sinkala (1988, 1989) gives a list of factors influencing the drilling deflection, some of which are:

- drillhole design, hole inclination/direction, hole diameter and hole length
- drilling parameters: thrust (feed), percussion pressure, torque, rotation speed, flushing, drill string weight, anti-jamming system
- equipment components: piston design, chuck/shank clearances, couplings and treads, stabilizer design, drill bit design, drill-rod design, rod/bit ratio, equipment wear
- rock mass and site properties: structure (bedding, jointing, fissuring or combinations), bedding dip relative to hole direction, joint frequency or bed thickness, rock hardness, cohesion between beddings/foliations, and bench floor conditions (rock debris or cleaned bench)

2.4 Depth Deviation

Drillhole depth deviations in bench blasting is the vertical displacement of the planned hole bottom position away from the planned level. Drilling without depth measuring instruments increases the chances of depth deviation and makes operator errors more probable. Joint fault material, rock debris and drill cuttings which fall into blastholes after drilling, reduce the hole’s depth and the planned extent of the charge column and the bottom charge. This error may be larger than the drillhole depth deviation itself. Smaller holes are more sensitive to this than larger holes. Often the operator drills the holes a couple of decimeters deeper than planned, due to the negative economic effects of the holes being too short (Olsen, 2009).

2.5 Drillhole deviations: experiences, measurements and control

During a normal bench drilling, the drilling deflection for 89 mm diameter holes appears to be under control when the bench is lower than 12-13 m (Bakken, 1994). When the drillhole diameter decreases or the bench height increases, the drilling deflection increases. In a road project in Sweden (Vägverket, 1984) it was shown that with a drill bit of 51 mm diameter and a drill string, the deviations were larger, when compared to equipment with a diameter of 64 mm.

Inside a round, the relative drillhole deviation between the neighboring holes is crucial to the functioning of the round. When the actual total drilling errors turn out to be much larger than the values planned, they may lead to a large variation of volumes thus to an uneven energy input into the rock from hole to hole. A typical example is shown in Figure 4, where a twisted blasthole pattern at the bottom is shown. The areas that are too small may increase the amount of fines, give more backbreak and cause less safety, while the big (vacant) areas may lead to increased vibrations, poor fragmentation and an uneven bench floor (Olsen, 2009).

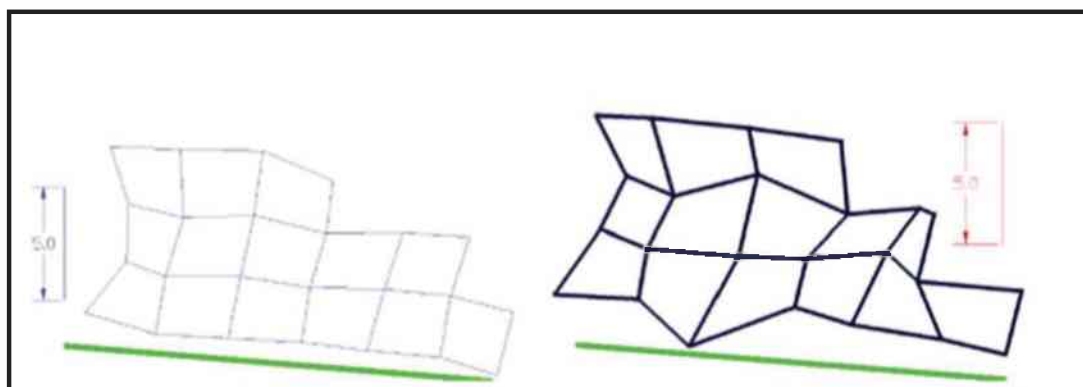


Figure 4: Poor drilling result in the bottom of blast. Left/right: Top/bottom coordinates. Green line indicates bench face (Spilling, 2004)

Extensive measurements and analysis of drillhole deviations have e.g. been conducted in the Akselberg marble quarry, as part of an optimization of the drill-blast–loading cost project (Ouchterlony, Ivanova et al., 2013). By bringing drillhole deviation under control (from the initial average deviation of 1.14 m to 0.45 m), the burden and spacing of the production blasthole patterns have been increased by 10 %, from the standard BxS = 2.7 x 3.4 m to 3.0 x 3.8 m for production (Ø89 mm holes)

and from BxS=3.0 x 4.0 m to 3.3 x 4.4 m for waste ($\varnothing 102$ mm holes). A bull's-eye scatter plot of hole bottoms from a blast at Round 1481 is shown in Figure 5.

The round 1481 (18 m bench height) was divided in two: one half was in production drilled with guide rods and increased pattern, and the other half in waste with the standard pattern and without guide rods. Accordingly, a close comparison with the standard pattern could be made, so that the influence of geological variations on the result was minimized. The plot below (Figure 5), is divided into four parts: $\varnothing 102$ mm production holes drilled with guides, $\varnothing 102$ mm production holes drilled without guides, $\varnothing 89$ mm helper holes (North and South part) and $\varnothing 76$ mm pre-split holes.

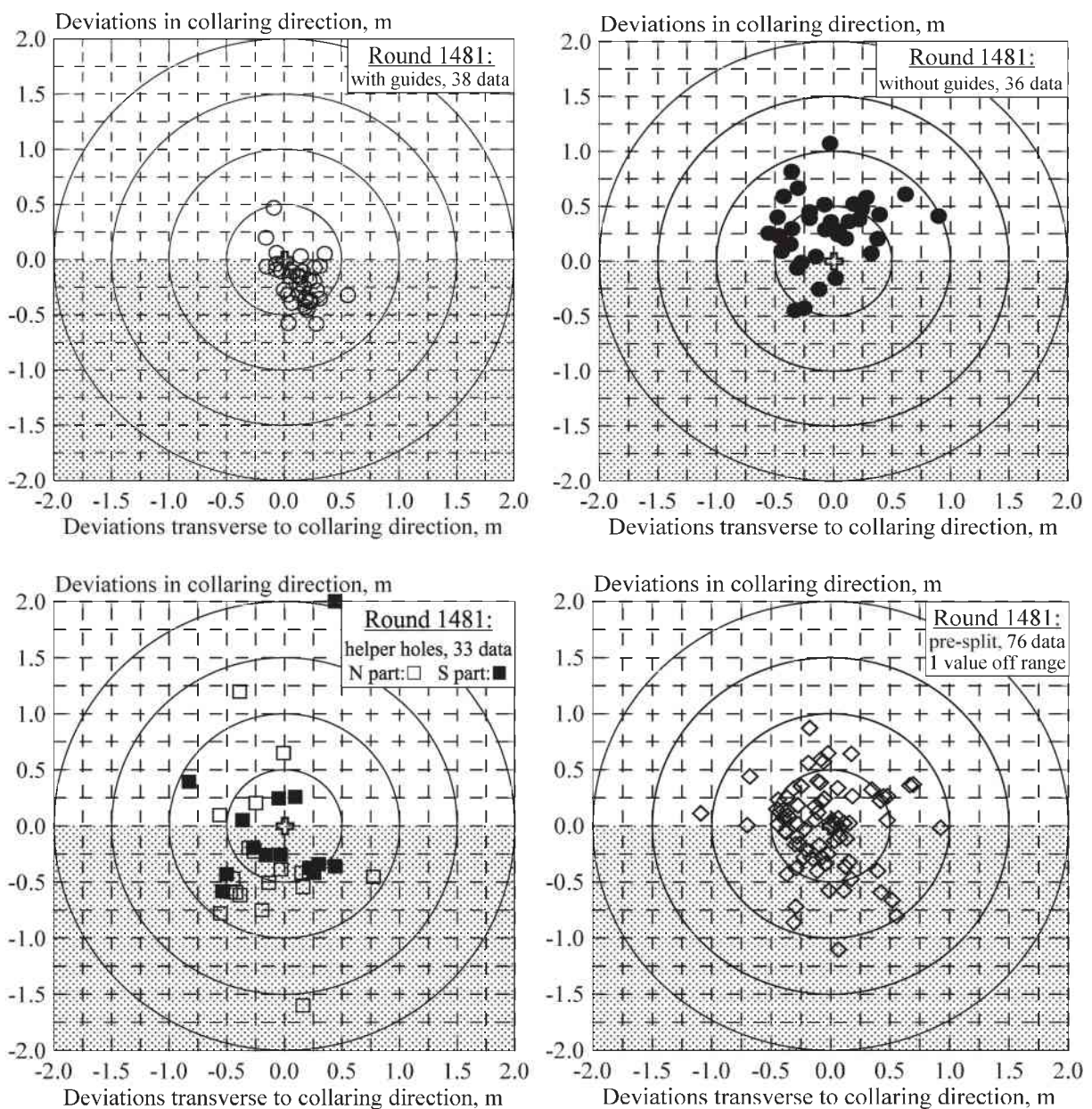


Figure 5: Bull's-eye drilling error for Round 1481's face (Ouchterlony, Ivanova et al. 2013)

The cross in the middle shows the planned end positions (bottoms) of the drillholes. The hatched area in the figure is the bench; the white area is the hole's bottom level in front of the bench. The radial bull's-eye error or drilling error is described as:

$$r(l) = c_1 \cdot l + c_2 \cdot l^2 \quad \text{Equation 2}$$

where, the l is the drilled length, c_1 a coefficient of collaring error and c_2 a coefficient that measures in-hole trajectory deviations (or drilling deflection, dd) (Ouchterlony et al., 2012).

Figure 5 shows that for round 1481, as seen in the collaring direction, most bottoms of the $\text{Ø}102$ mm production holes drilled without guides (upper right plot) scatter up to 1.1 m from the planned bottom positions in stochastic directions. This tends to increase the probability of burdens that are larger than planned, while the holes in the helper ($\text{Ø}89$ mm) and the pre-split rows ($\text{Ø}76$ mm) have an even larger scatter. For the $\text{Ø}102$ mm holes drilled with guides (upper left plot), the scatter is much smaller if not entirely within the 0.5 m limit set up by the quarry. In other words, for an 18-m high bench, the drilling error is only as half as large when drilling with guide rods, which is the result of suppressing the in-hole deviations (c_2), while the collar angle component c_1 is independent of using guide rods. The blast results showed that increasing the blasthole pattern and decreasing the specific charge by controlling the drillhole deviations is possible, without any substantial influence on the fragmentation result, loading and the hauling time.

The importance of reducing deviations has also been shown within the framework of a highway project in Södertälje, Sweden (Ouchterlony, 2002). Elliot (1999) and Sellers et al. (2013) also showed in projects, in small and large quarries, that without systematic surveying and control of blast geometry, an optimization of the drill and blast work is not possible.

2.6 The effect of drillhole deviation on fragmentation

In the published literature, there exist several models for fragmentation evaluation that refer to fragment size distribution of the muck material obtained after blasting. The Kuz–Ram model (Cunningham, 1983, 1987, 2005) is arguably the most widely

used fragmentation model. The model is based on the expression of the average fragment size constructed by Kunzetzov (1973) and a Rosin–Rammler distribution (Rosin and Rammler, 1933). The model consists of four equations; the first describes the fragmentation curve (Rosin–Rammler distribution), the second gives the value for the median fragment size (x_{50}) as a function of the blasting parameters, the third gives a value for the rock mass factor (A) and the last gives a value for the uniformity index (n). The Rosin–Rammler distribution can be written as:

$$P_{RR}(x) = 1 - e^{-\ln 2 \left(\frac{x}{x_{50}}\right)^n} = 1 - 2^{-\left(\frac{x}{x_{50}}\right)^n} \quad \text{Equation 3}$$

The distribution contains two parameters, the median size (x_{50}) and the uniformity index n , and it describes quite well the coarser part of the fragmentation but improperly models the finer part (Johansson, 2008).

The size distribution constant “ n ”, the so-called uniformity index, is a mathematical value expressing the variation in size of the grains or fragments that constitute the fragmented material:

$$n = \left[2.2 - \left(0.014 \cdot \frac{B}{\phi_h} \right) \right] \cdot \left(1 - \frac{SD}{B} \right) \cdot \sqrt{\left[\left(1 + \frac{S}{B} \right) / 2 \right]} \cdot \left[\frac{(L_b - L_c)}{L} + 0.1 \right]^{0.1} \cdot \left(\frac{L_{tot}}{H} \right) \quad \text{Equation 4}$$

where the symbols are described in the symbols list (see Page VIII). The median fragment size is given as (Cunningham, 1987):

$$x_{50} = A \cdot \left(\frac{1}{q^{0.8}} \right) Q^{1/6} \cdot \left(\frac{115}{S_{ANFO}} \right)^{19/30} \quad \text{Equation 5}$$

The rock mass factor is given by the following equation:

$$A = 0.06 \cdot (RMD + JF + RDI + HF) \quad \text{Equation 6}$$

where:

RMD: rock mass description [10-if powdered or friable, JF if joints are vertical; 50- if massive]

JF: Joint factor=JPS+JPA

JPS: Joint plane spacing [10, if average joint spacing $S_j < 0.1\text{m}$; 20, if $S_j < X_0$ oversize fragment; 50, if $S_j > X_0$ oversize fragment]

JPA: Joint plane angle [20, if the joints dip out of the face; 30, if strike is perpendicular to the face; 40, if the joints dip into the face]

RDI: rock density influence $(0.025 \cdot \rho) - 50$ [kg/m³]

HF: hardness factor, $=E/3$ if $E < 50$, or $\sigma_c/5$ if $E > 50$ and dependent on compressive strength σ_c [MPa] or Young's modulus E [GPa]

The characteristics size of the distribution (63.2 % passing) is expressed as (Cunningham, 1983):

$$x_c = \frac{x_{50}}{(0.693)^{\frac{1}{n}}} \quad \text{Equation 7}$$

Cunningham (2005) continued developing the n-formula and, in order to address the adverse effect of timing scatter on the uniformity, he invoked the scatter ratio. Thus he introduced the concept of the parameter 'scatter ratio', R_s , defined as:

$$R_s = \frac{T_r}{T_x} = 6 \frac{\sigma_t}{T_x} \quad \text{Equation 8}$$

where:

T_r is range of delay scatter for initiating system [ms]; T_x is the desired delay between the holes [ms]; σ_t is standard deviation in the initiation system [ms].

The higher the scatter ratio, the less uniform the fragmentation curve will be. The following algorithm has been introduced to the n-formula to illustrate the expected effect of precision on blasting results:

$$n_s = 0.206 + (1 - R_s/4)^{0.8} \quad \text{Equation 9}$$

where:

n_s is the uniformity factor governed by the scatter ratio.

Thus the n-formula has been developed to its current form (Cunningham 2005):

$$n = n_s \sqrt{\left(2 - \frac{30B}{d}\right)} \sqrt{\left(\frac{1+S/B}{2}\right)} \left(1 - \frac{SD}{B}\right) \left(\frac{L}{H}\right)^{0.3} \cdot c(n) \quad \text{Equation 10}$$

where $c(n)$ is a correction factor, provided to calibrate the n-equation, so that it agrees with measured values.

The median fragment size depends on the drill pattern (B and S) and the bench height, by means of the specific charge. Then changes to the specific charge caused

by variation in the drill pattern cause an effect on the median size. If the B/S ratio is changed and the burden B varied, so that the specific charge is kept constant, the distribution tilts about the mean and gets steeper as the S/B ratio increases.

The explosive mass per hole is directly proportional to the explosive density, blasthole cross sectional area and the length of the explosive charge. Therefore the median size could be changed by altering the explosive properties, but without affecting the uniformity exponent.

In Equation 4 (respectively at the improved Equation 10) this linear dependence between uniformity coefficient of fragmentation and drillhole deviation can be seen. The formula states that improving the drilling accuracy at a given specific charge should have no effect on x_{50} , but more accurate drilling should increase n . Cunningham (1983) added that, when a staggered pattern is employed, n increases by 10 %. Later, Cunningham (2005) explained that this phenomenon is caused by the more uniform distribution of the explosives (see Figure 6).

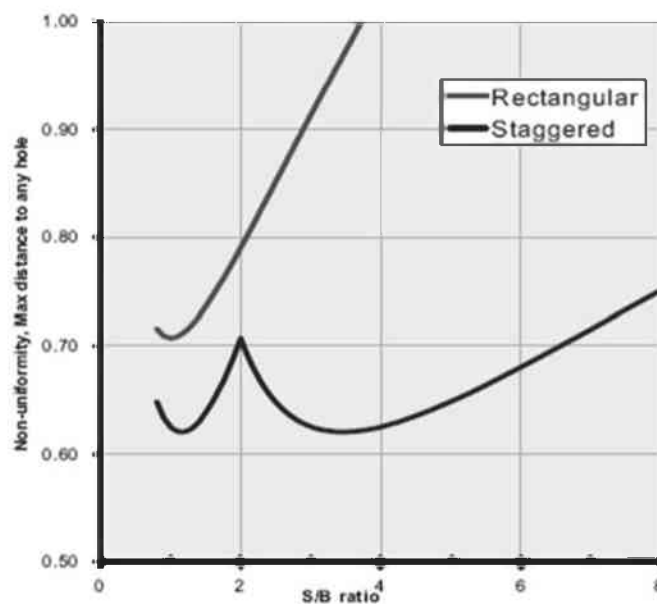


Figure 6: Effect of S/B ratio and layout on the maximum distance of any point and from any hole (Cunningham, 2005)

Hustrulid (1999) has also investigated the hypothesis that a staggered layout will lead to finer fragmentation, when compared to a rectangular layout. He explained that in both patterns the percentage of energy coverage is the same; however, the influenced region around a blasthole in the staggered pattern is giving a different

distribution of the “un-touched” areas and thus improved fragmentation (see Figure 7).

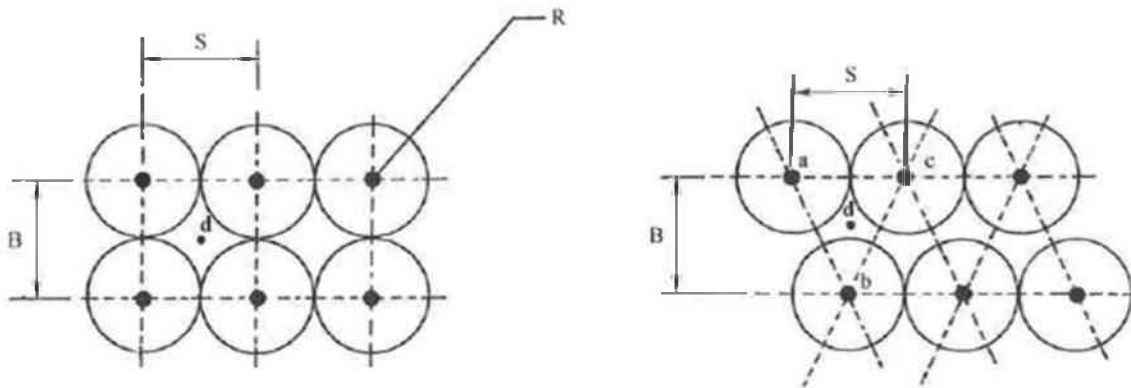


Figure 7: Square (left) and staggered layout (right) with influenced regions touching (Hustrulid, 1999)

Lownds (1983) investigated the effect of different variables (specific charge, blasthole pattern, drilling accuracy and delay time) on fragmentation, based on modeling bench blasting in Kimberlite with the SABREX model. He found that an increase of the drilling deviations had little effect on the characteristic fragment size x_c , but a significant effect on the size distribution; expressible, e.g., through changes in n , the uniformity coefficient of the Rosin-Rammler function (Rosin and Rammler 1933) (see Figure 8).

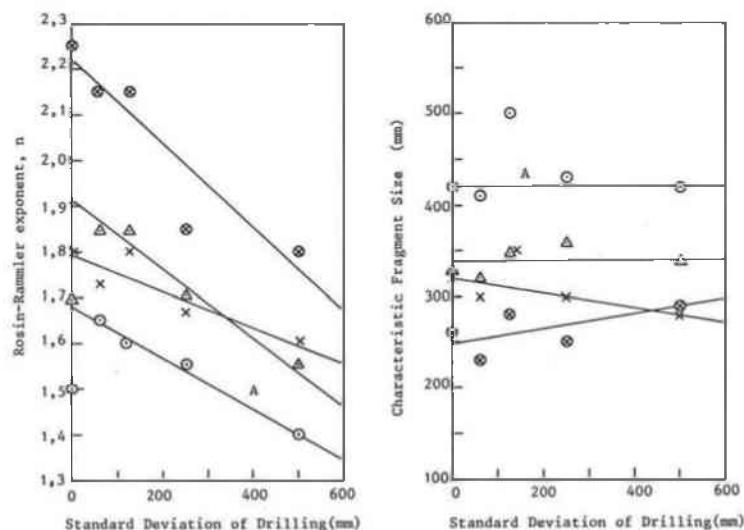


Figure 8: Dependence of n and x_c on drilling accuracy (Lownds, 1983)

The Kuz-Ram blast model described above (Cunningham, 1983, 1987, 2005) bases its predication equation for n on Lownds' (1983) findings. A recent study, conducted at quarries and platinum mines in South Africa (Sellers et al., 2013), measured the

effect on fragmentation of improvements in drilling accuracy. Drillhole deviations were measured and the fragmentation was evaluated using Split Desktop software, based on manually retouched images. The Split results are given in terms of x_0 , the same characteristic size as x_c and on n . The study indicated that there was a significant improvement in both the mean size and the uniformity index when drillhole deviation is reduced. Sellers et al. (2013) found that improving drilling lowers the characteristic fragment size from 242.3 mm to 188.5 and raises the uniformity index n from 0.89 to 1.24.

Looking to the formulas above, the results of Sellers et al. (2013) do not agree with the Cunningham formulas, which say that when the uniformity index changes, x_{50} should remain the same. Sellers et al. (2013) have found changes in both parameters. Reanalysis of Sellers' original data was conducted by Ouchterlony (2015).

Figure 9 shows the Sellers' data and an RR (Rosin Rammler) fit, plotted in a log-log scale. In this scale the n -value of the RR function equals the slope in the fines region but the RR representation systematically overestimates the steepness in this range.

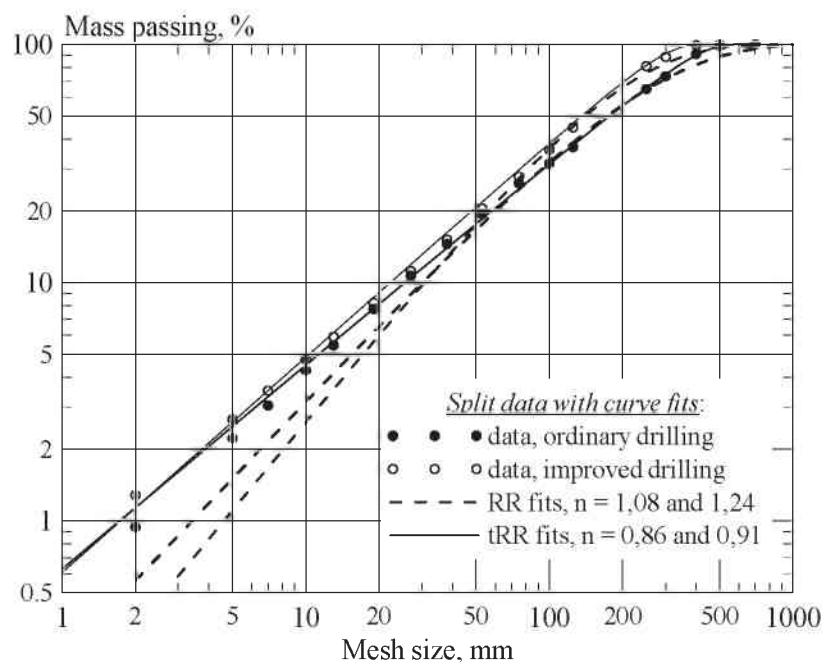


Figure 9: Comparison of RR and tRR fits to Split data from Sellers et al.(2013)

Ouchterlony (2015) has chosen to fit the RR function with transformed RR (tRR) function, e.g. in the form (Ouchterlony, 2009):

$$P(x) = 1 - 2^{[x/x_{50}(1-x_{50}/x_{max})/(1-x/x_{max})]^n} \quad \text{Equation 11}$$

The findings of the reanalysis found that while the improved drilling decreases x_0 from 238 to 187 mm, or x_{50} from 177 to 143 mm, the n -value hardly changed; it only increased slightly from 0.86 to 0.91.

Figure 9 shows how the accuracy of the curve fits are improved considerably in both the fines and coarse ranges by using the transformed RR function (tRR function). However, it doesn't answer the question as to why the results of Sellers'et al. (2013) contradict the Kuz-Ram formula.

The results of the Ouchterlony (2015) reanalysis are different from both Sellers' findings and the predictions in Kuz-Ram's equations. The contents of those findings indicated that using fragmentation models with functions that are either too simplistic, or over complex with too many parameters, may lead to questionable values of the predicted model parameters such as x_{50} and n . Table 1 gives a summary of the contradictory experiences found with regards to the Kuz-Ram fragmentation prediction formula.

Table 1: Literature findings summary of effects of drill hole deviations

Author	Statement based on	x_{50}	n	x_c
Kuz-Ram, Cunningham (1983)	Formulas, no field tests	same	increase	change
Lownds (1983)	SABREX simulation	(change)	increase	same
Cunningham (2005)	Improved Kuz-Ram model	Improved fragmentation		
Sellers et al. (2013)	Field test	(change)	increase	change
Ouchterlony (2015)	Re-calculations on Sellers data	change	same	change

From the table, it can be seen that there are the following contradicting experiences:

- The Kuz-Ram model who predict that n but not x_{50} , is influenced by drill hole deviation.
- Strictly speaking the consequence of constant x_{50} and changes in n would change the x_c value, see equation 7 (Cunningham, 1983). On the other side, Lownds (1983) did not find any changes in the x_c by drillhole deviation.
- Sellers, et al. (2013) reinterpreted findings that the deviations influence x_{50} and x_c but hardly n .

In addition the suggestion that n should increase by 10 % if the drilling pattern is staggered should be also kept in mind.

2.7 Drillhole deviation and blast damage

The drillhole deviation alters the planned blast layout by either narrowing or increasing the distance between the holes. The values of both spacing and burden would be modified, leading to the wrong amount of specific explosive energy being liberated inside the rock. In order to discuss the damage, the drillhole deviation is related to changes the burden.

When the explosive confinement or burden is excessive, the energy from the explosion has too much resistance for effective fracture and displacement of the rock, hence a bigger portion of the energy will be transformed into seismic energy, i.e. ground vibrations. This phenomenon is very common in pre splitting blasts, where blast vibration levels per unit weight of explosives five times higher to the conventional blast can be registered. If the burden is too small, then the explosion gasses escape and expand toward the free face at a very high speed, giving impulse to the rock fragments and projecting them uncontrollably, apart from provoking an increase of an air blast and noise (Jimeno et al., 1995).

Oriard et al. (1994) also underline the importance of explosives energy confinement and related high vibration level, saying that confinement is greatly affected by burden and spacing, drilling accuracy, amount of sub-drilling and stemming. Ramulu (1998), provide data from controlled field measurements, concluding that the burden distance influences vibration levels. The backbreak on the remaining wall is another issue associated with the drillhole deviations (Konya and Walter, 1991). Backbreak is defined as a fractured zone beyond the last row of blastholes (Jimeno et al., 1995). As a result of an excessive burden, backbreak may occur, thereby causing the explosive to break and crack the rock radially, further behind the last row of holes (see Figure 10).

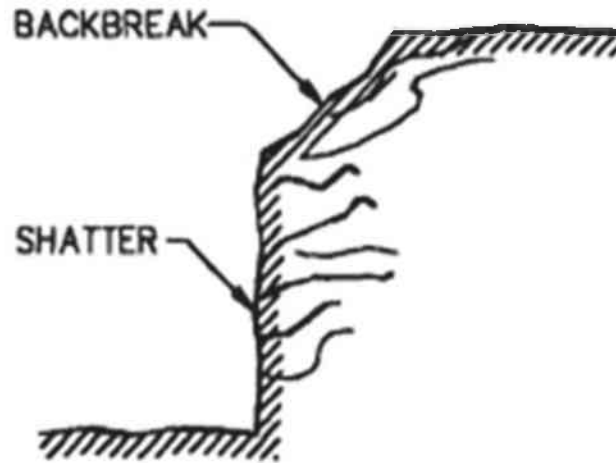


Figure 10: Backbreak due to excessive burden (Konya and Walter, 1991)

Improper delay timing from row-to-row can result in excessive confinement on the last rows in the shot, thereby causing backbreak. In general, the better the breakage obtained and the better the displacement in the row-by-row shot, the better the wall control. If sufficient energy is available to break rock properly in the burden, the added burden resistance placed against the hole, will cause an increased confinement and more fracturing (back shatter) behind the blast. If larger boulders are produced from the stemming area rather than the burden, an increased backbreak, especially on the top of the bench will result, subsequently causing problems with both drilling and wall stability.

The best approach to control backbreak on the wall is to control the effects of blasting by keeping the powerful energy released by the production blast sufficiently far away from the final wall to avoid damage. Different blasting techniques are used for different purposes depending on the specific excavation requirements (Konya and Walter (1991). A new contour blasting system – a bulk emulsions charging device, developed for use in both underground and open pit applications was also described by Ivanova et al. (2012). The system allows obtaining more stable drift and pit walls and at the same time prevents the leakage of the explosive into the cracks from the borehole.

Konya and Walter (1991) related the n -value with the potential for wall control, saying that the higher the n -value, the better the wall control. They also correlated the

backbreak with the mean fragment size, saying that the lower the mean value on a specific blast design is, the smaller the chance of causing a back shatter and backbreak beyond the excavation limit; giving values for n between 1 and 1.3 as a potential indicator of wall damage. They suggested that the Kuz–Ram fragmentation model, which uses the median symbol x_{50} but calls it the mean, can be also used not only for the fragment size estimation, but also to link the model with the potential backbreak issues.

3. Test methodology and set-up

3.1 Blasting site Erzberg

A series of small scale tests on magnetic mortar blocks were conducted at a blast site, located at the Erzberg iron mine, 30 km north of Leoben, Styria. The blast site belongs to the Chair of Mining Engineering at the Montanuniversitaet Leoben and its development was reported in a Master's thesis (Maierhofer, 2011).

The blast sessions were carried out in 2013 and 2014, hereafter called: blast session 2013 and blast session 2014.

The mortar was meant to be well-defined using the same composition which had given repeatable fragmentation results in other rock blasting tests (Johansson, 2008; Johansson and Ouchterlony, 2013).

Test blocks were mounted inside an inner yoke made from high strength concrete inside the outer yoke (see Figure 11). The gap between the inner yoke and the outer yoke was filled with compacted sand, which transmitted about 70 % of the energy of the blasting waves into the surrounding outer yoke (Maierhofer, 2011).

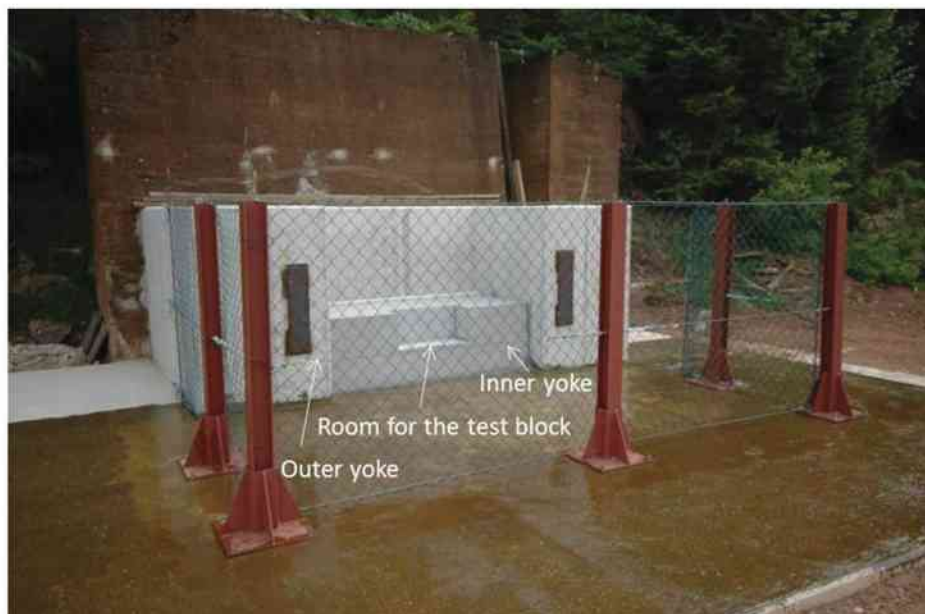


Figure 11: Yokes at the Erzberg blasting site. They allow waves to escape from a test specimen. The inner yoke has room for the test block (Schimek, 2013)

Both at the sides and the back, the test block is grouted into the inner yoke by using fast hardening cement, which has similar material properties as the blocks, thus minimizing the impedance difference. During the tests the area within the wire fence was covered with rubber mats and heavy non-woven felt in order to trap the blast fragments.

3.2 Magnetite concrete

The basic ingredients and proportions of the magnetite concrete can be seen in Table 2. These proportions are very similar to those used for small-scale tests at the Luleå Univ. Techn. (Johansson, 2008).

For the 2013 blast sessions, the magnetic concrete was produced by manufacturer (Luiki Betonwerke GmbH) in several batches; consequently, the produced samples within each batch should have identical properties. To verify repeatability in blasting properties, several test cylinders were produced from each batch.

For the 2014 blast sessions, the magnetic concrete, based on the same ingredients and proportions, was produced in the laboratory of the Montanuniversitaet using a 100 kg capacity cement mixer. In addition, several test cylinders were produced to verify the regularity and comparability of the tests.

Table 2 shows the ingredients of the magnetite concrete used in the 2013 and 2014 production sessions.

Table 2: Ingredients of the magnetite concrete blocks

Year/blast session	2013	2014
Ingredient	[%]	[%]
Portland cement CEM II / A-M 42.5 N	25.60	23.60
Water	12.65	19.44*
Glenium 361 (Plasticizer)	0.26	0.23
DCC-Defoamer	0.13	0.12
Magnetite powder (Ferroxon 618)	29.65	27.35
Quartz sand 0.1 - 0.5 mm (ME 31)	31.70	-
Quartz sand 0.1 - 0.4 mm (ME 01-04)	-	29.24

* Additional 8 l water was added for the 2014 production

In Table 2, a difference in the grain size of the quartz sand can be seen. In 2014, a grain size 0.1-0.4 mm was used instead of the 0.1-0.5 mm used in 2013, due to changes in the delivery from the factory. Appendix 1 shows a detailed description of the Quartz sands, ME31 and ME 01-04, used for the production. There was also a difference in the water content and grain size of the quartz sand used in 2013, compared to the one used in 2014. For production in 2014, 8 l of water was added to the recipe, to allow for a complete hydration of the concrete.

3.3 Testing blocks

The dimensions of the testing blocks used for blasting were 660×210×280mm (L×H×W) or approximately the same as those used by Johansson and Ouchterlony (2013). The reason for using the same dimensions was that there were a large number of blasting results is available for comparison.



Figure 12: Testing block with dimensions 660×280×210 mm

Three batches were produced for the 2013 blast session. For the 2014 blast session, due to the capacity of the mixer (100 kg), each block represented an individual batch. Table 3 gives a list of the blocks produced and tested for this thesis:

Table 3: List of the blocks produced and tested

Block #	Batch #	Block #	Produced in
1	1	CH01B02	2013
2	1	CH01B03	2013
3	1	CH01B04	2013
4	1	CH01B05	2013
5	3	CH03B01	2013
6	3	CH03B02	2013
7	-	B01	2014
8	-	B02	2014
9	-	B03	2014
10	-	B04	2014
11	-	B06	2014
12	-	B07	2014
13	-	B09	2014
14	-	B10	2014
15	-	B11	2014

Blocks were labeled with a code of the type CHxxByy, where

CH... batch ("Charge");

xx... batch serial number;

B... block;

yy... block serial number.

For the 2014 blast session there is no CH label, as each block corresponds to an individual batch.

3.4 Cylinders

At least three test cylinders of magnetite concrete were produced from each batch of concrete for the 2013 blast campaign, whereas only for two of the batches for 2014's campaign. The cylinders' dimensions were 142 mm (diameter) and 280 mm (height). Three cylinders from 2013 (one per batch) and four cylinders from 2014 (two from two selected batches), were blasted with 20 g/m detonating cords in 10 mm diameter blastholes. After blasting, sieving analyses were done to measure the repeatability of the fragmentation properties.

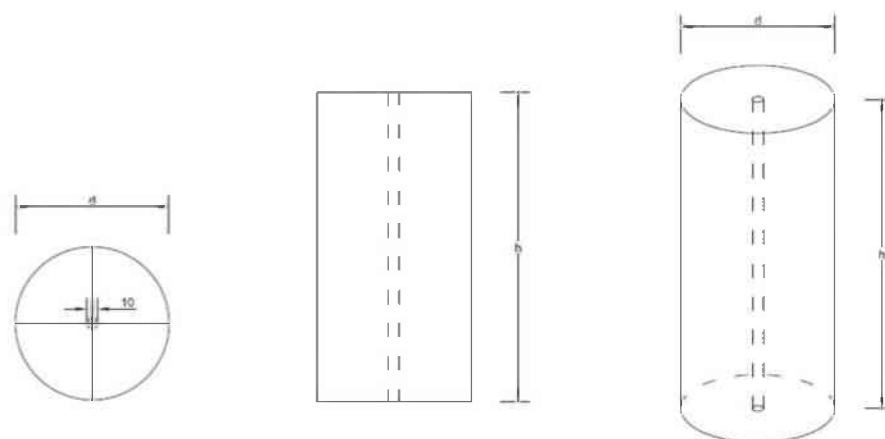


Figure 13: Cylinder sample geometry

As with the blocks, the cylinders were labeled with a code of the type CHxxByy, where:

CH... Batch ("Charge" in German);

xx... batch serial number;

Z... Cylinder;

yy... cylinder serial number.

The blasting results from the cylinders are presented and discussed further below in the report.

3.5 Determination of physical and mechanical properties

The physical and mechanical properties of the corresponding cylindrical core samples, which were produced from the same concrete batches as the blocks were determined at the laboratory. The aim was to define any factor or variable in the magnetic mortar properties that could have an effect on the fragmentation results. The methods for the determination of the physical and geotechnical properties of the samples are briefly described below.

3.5.1 Density

The density of the material was calculated in $[\text{kg}/\text{m}^3]$ by applying the mass-volume ratio method. Mass was obtained by weighing the specimens in a laboratory with a

scale AandDFG-150KAL (A&D company limited). Volumes, on the other hand, were calculated by applying volume equations to measured lengths, widths and heights. The lengths, widths, and heights of the blocks were measured several times at two opposite sides; whereas for the cylinders, their diameter was measured at several heights. Finally, for the volume calculation, the average values were used.

3.5.2 P-wave and S-wave velocity

The P-wave (longitudinal) c_p and the S-wave (shear) velocity c_s in [m/s] were measured by an ultrasound Light House UMPC device, before the blocks were grouted into the yokes. For determination of the P and S- wave velocities, the blocks were placed in between two transducers and then a high voltage pulse was applied to excite the device's piezoelectric crystal. The created waves were transmitted into the specimens and the times required for the wave to pass through them were used to determine wave velocities. The P and S-waves of every specimen were measured at three positions across the 28 cm width. The average of the three measurements was taken as the result.

3.5.3 Uniaxial compressive and tensile strength

The geotechnical properties of at least three core samples per batch, taken from the cylinders, were determined. The determination of the uniaxial compressive strength, in [MPa], and the Brazilian tensile strength, in [MPa], followed the ISRM Suggested Methods (Ulusay and Hudson, 2011).

3.5.4 E-modulus and Poisson's ratio

The modulus of elasticity, E-modulus, in [MPa], was calculated using the stress–strain diagrams obtained during uniaxial compressive strength tests. Poisson's ratio was determined as a ratio of the lateral strain to the axial strain within the linearly elastic region (Hohl, 2013). A detailed description of the methods and their testing procedures is given in a technical report (Restner, 1999).

3.6 Blasthole pattern and drilling set-up

The spacing and the burden for the reference blocks were 95 mm and 70 mm respectively, thus giving an S/B ratio of 1.36. For each block, three rows with seven blastholes were drilled. The 10-mm diameter blastholes were drilled at the laboratory using core-drilling equipment. After drilling, controlling the drill pattern was done using a measuring tape. No major differences with regards to the planned drilling were recorded. Figure 14 shows the blasthole pattern used for the reference blocks:

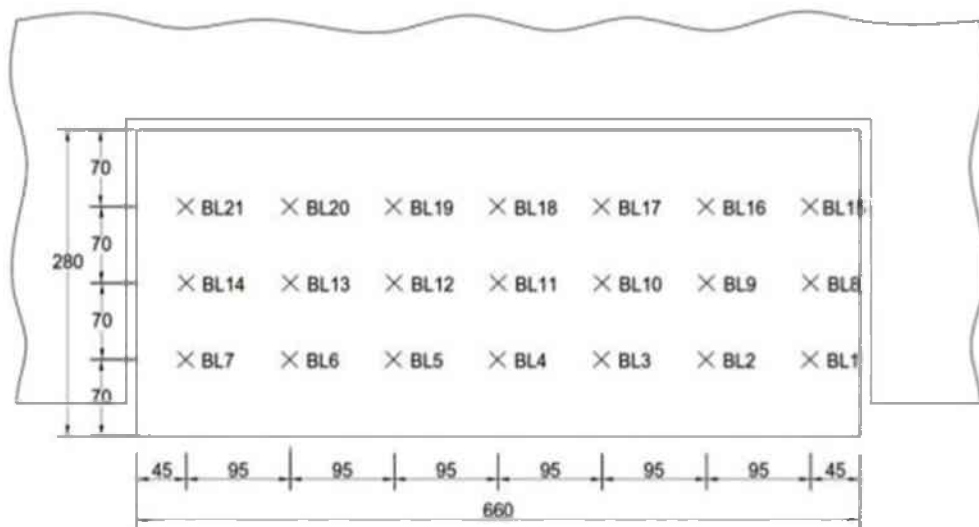


Figure 14: Reference block pattern

Drillhole deviations were designed by introducing a collaring error. The reason for choosing the collaring error was that the deviations should be exaggerated in order to see if there is any clear effect. As a first step for the design, variations in the spacing were eliminated, because the Kuz-Ram formula implies that the effect on fragmentation, due to variations in the spacing, should be smaller than the effect of changes in the burden, since on average a variation in spacing does not influence the specific charge and thus neither x_{50} . The influence on n would also even out on average. However, variations in the burden would show up as variation in the local specific charge, which has influence on x_{50} . That is why the initial design was made with displacement of holes with random uncorrelated variations in the burden.

The following design procedure was applied:

1. At the beginning, a sequence of the positions of the holes with rectangular (reference) pattern was taken. In Figure 15, the red-marked holes represent the normal holes, without the collaring position error, lying in a straight line.
2. A series of 200 pseudo random numbers for the burden variations in the range (-1.1) was taken and 13 sequences of 7 consecutive numbers with an average per set within ± 0.025 were selected.

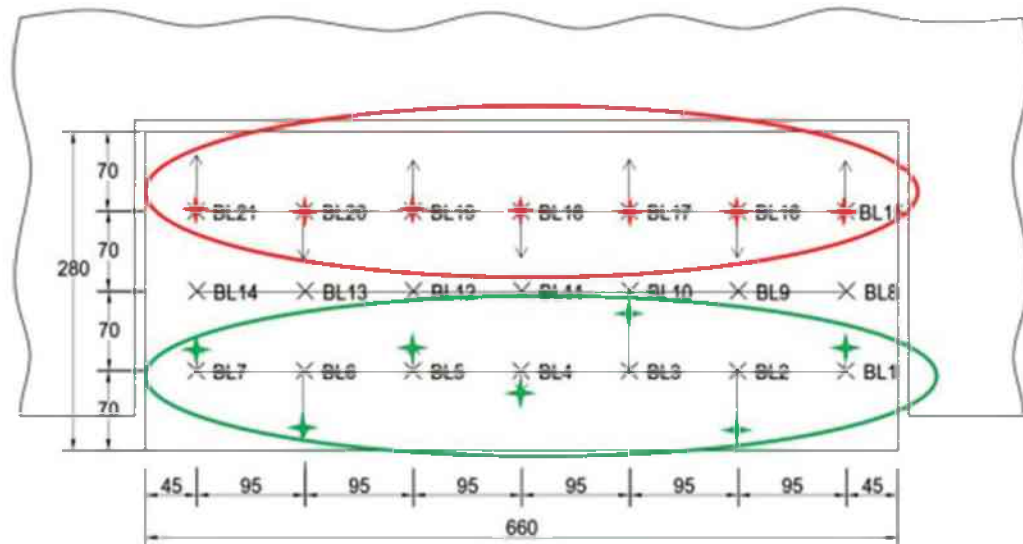


Figure 15: Deviation pattern designing

3. The 13 sequences were matched against each other and pairs with an inter-row correlation coefficient $|r| < 0.01$ were chosen.
4. A combination of hole deviations with a very low correlation and a stochastic pattern was selected (the green-marked holes in Figure 15).
5. The combination number 13-7-3 (see Figure 16) refers to one of these sequences 13 (row 1), 7 (row 2) and 3 (row 3) respectively. Adding the geometrical positions of the holes up (larger burden) with the holes down (smaller burden), the result is always near zero (± 0.025), thus a near constant breakage volume per row was achieved.
6. By choosing patterns with near constant breakage volume, the average q (specific charge) will, by definition, not be affected. Thus any fragmentation changes in the tests should be caused by the drillhole deviations, not by any changes in the specific charge.

7. The maximum deviation from the straight line was chosen to be 25 mm, comparable to the one in Akselberg (see Chapter 2.5) in terms of standard deviation, relative to burden $SD/B=0.638*25/70= 0.23$. Thus according to the Kuz–Ram model (Cunningham, 2005), $n \propto (1-SD/B)$ should decrease by about 25 %.

8. From a total of 13 combinations selected, two combinations of random drillhole deviation blasthole patterns were tested: combination 13-7-3 and combination 2-3-7.

The design of the displacement of the holes with random uncorrelated deviations and the numerical description of the set-up is given in Appendix 3.

The following figure shows the drillhole deviation blasthole patterns selected for the 2013 blast session tests.

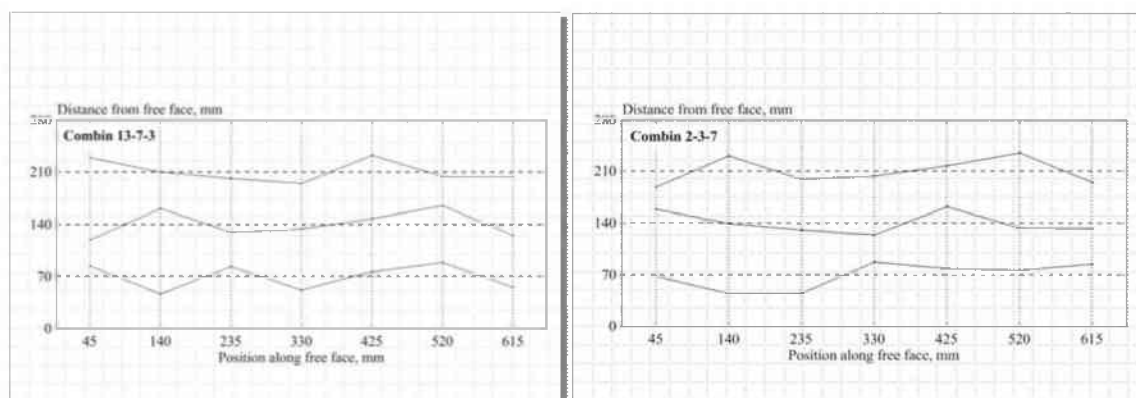


Figure 16: Drillhole deviation blasthole pattern 13-7-3 (1st burden deviation) on the left, and blasthole pattern 2-3-7 (2nd burden deviation) on the right

For the blast session 2014, two new designs were introduced: collaring errors in both the spacing and burden, and systematic collaring errors in spacing only ($\pm S/4$ shift) i.e., a staggered blasthole pattern. The following design steps were taken to create the burden and spacing variations:

1. The same rectangular blasthole pattern was used as a reference.
2. Two columns of 250 random, uniform variables, with a correlation coefficient $|r| < 0.01$ to use as Δx and Δy generators for variations in spacing (x) and burden (y) directions, were taken.
3. Applying the Box-Muller method (Box and Muller, 1958), two columns of normally distributed numbers with a mean of 0 and variance of 0.75 were calculated. The numbers followed the bivariate normal distribution well.

4. Working simultaneously with two independent parameters, made it harder to meet the same criteria as for the burden-only variation of 2013. Seven sequences of paired numbers were found for which: 1) $|\text{mean}(\Delta x)| < 0.2$ and $|\text{mean}(\Delta y)| < 0.1$, 2) $|\text{corr.}(\Delta x, \Delta y)| < 0.2$ and 3) $|\text{stdev}(\Delta x) - \text{stdev}(\Delta y)| < 0.2$.
5. For all pairs of sequences the Δx and Δy , the Δx with Δx and Δy with Δy correlations were calculated. Those for which both $|\text{corr.}| < 0.4$ were accepted as neighboring rows of holes with collaring errors.
6. An amplification factor $\lambda = 20$ mm (see below) was chosen so that $\Delta S = \lambda \Delta x$ defined the collaring error in the S-direction and $\Delta B = \lambda \Delta y$ the error in the B-direction. This corresponds to a drilling deviation SD/B of about 0.21.
7. The blasthole patterns were plotted and the burdens and edge hole positions were checked.

The starting and final bull's-eye diagrams for $(\Delta x, \Delta y)$ are shown in Figure 17.

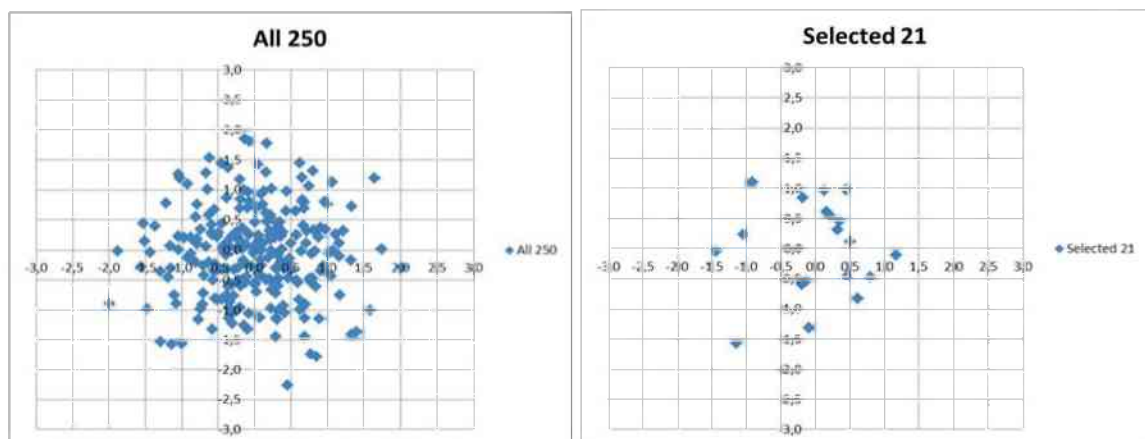


Figure 17: Bull's eye diagrams: 250 Box-Muller pairs $(\Delta x, \Delta y)$ (left) and the 21 values ultimately selected (right)

As a result of the above-described design set-up, the following criteria were met:

1. Blasthole pattern with almost uncorrelated collaring errors ΔS and ΔB .
2. Blasthole pattern with nearly uncorrelated collaring errors between rows.
3. Blasthole pattern with nearly the same average burden volume for each row and, as a consequence, nearly the same nominal specific charge.
4. Blasthole patterns where collaring errors in burden and spacing directions can be tested separately or together.

- The chosen $3 \cdot 7 = 21$ numbers Δx and Δy when put into order deviate somewhat from normal bivariate distribution CDF (see Appendix 3).

The selected distorted patterns for both sessions 2013 and 2014 are corresponding to the Sellers data (Sellers et al., 2013), where there were two cases:

- Case 1: with normal drilling 80 % of holes deflected more than 0.92 m
- Case 2: with improved drilling 40 % of holes deflected more than 0.52 m

By assuming normally distributed drilling errors, one obtains:

- Case 1: $\sigma = 0.78$ m and $R_{50} = 0.92$ m
- Case 2: $\sigma = 0.38$ m and $R_{50} = 0.45$ m

Where σ is the stdev and R_{50} is the median drilling deviation in m.

The R_{50} values are almost the same as Akselberg data (Ouchterlony et al., 2012) for drilling without and with guide rods (see Chapter 2.5).

In order to check the Cunningham (1983) suggestion that n -values should increase by 10 % in staggered pattern, the second design for the blast session 2014 was an staggered pattern; created by shifting the hole collaring positions in each row sideways by $+S/4$ in the first row, $-S/4$ in the second row and $+S/4$ in the third row to minimize edge effects in the block. In Figure 18, a schematic description of staggered pattern is given.

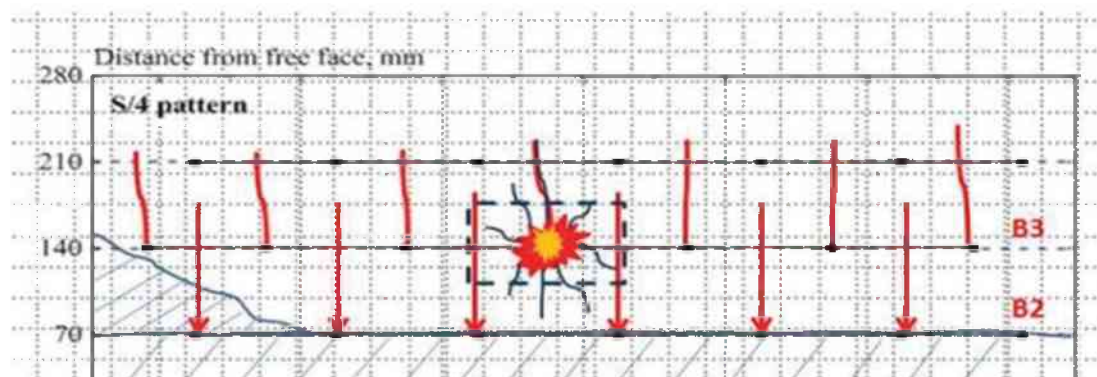


Figure 18: Schematic description of staggered pattern

Row 1 has been blasted and leaves long vertical damage cracks (Navarro, 2015). These cracks go straight back into the burden of row 2, and possibly into the burden of row 3. When the holes in row 2 are displaced by $S/4$, a staggered drillhole pattern is achieved. The holes in row 2 are more likely to be placed in undamaged rock with

better energy coupling. Consequently, the waves from these holes will bounce off the free face and damage cracks and will stay longer around the hole. The cracks from these holes are now spread into an uncracked volume with more wave energy in it. If the holes in row 2 are not displaced sideways, the coupling is worse, the energy is more diffused and the cracking spreads differently. This might be an explanation why an alternating pattern is considered to improve fragmentation (Cunningham, 1983). Combining the result with the 3D models of the crack damage, the effect of changes in spacing could be explained. Figure 19 shows the drillhole deviations selected for the blast session 2014. The numerical description of the design and sequence of the random numbers are given in Appendix 3.

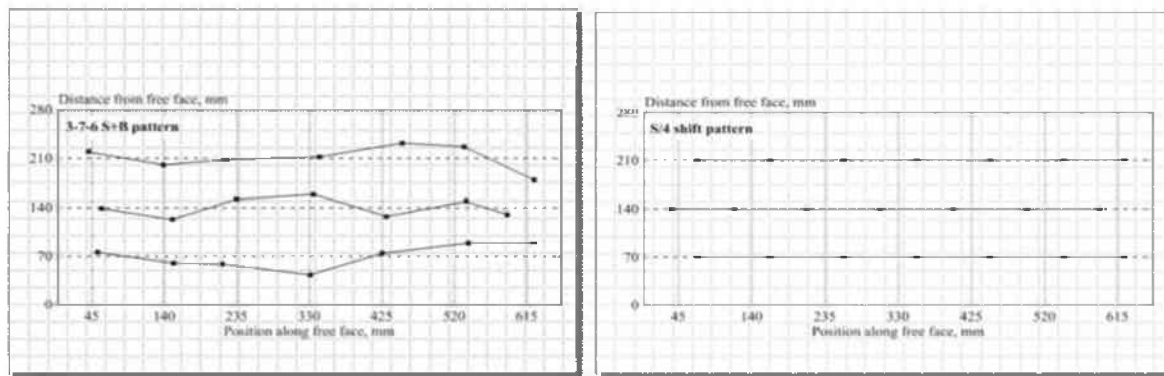


Figure 19: Drillhole deviation blasthole pattern 3-7-6 (S+B variations) on the left, and blasthole pattern S/4 shift on the right

Table 4 shows the blocks in both blast sessions and the deviation patterns tested:

Table 4: List of the blasthole patterns of blocks blasted

Block #	Batch #	Block #	Blasthole pattern	Blasted in blast session
1	1	CH01B02	1st burden deviation	2013
2	1	CH01B03	Reference	2013
3	1	CH01B04	1st burden deviation	2013
4	1	CH01B05	Reference	2013
5	3	CH03B01	2nd burden deviation	2013
6	3	CH03B02	2nd burden deviation	2013
7	-	B01	Reference	2014
8	-	B02	S/4 shift	2014
9	-	B03	S+B variations	2014
10	-	B04	S+B variations	2014
11	-	B06	Reference	2014
12	-	B07	S/4 shift	2014
13	-	B09	Reference	2014
14	-	B10	S+B variations	2014
15	-	B11	S/4 shift	2014

3.7 Explosives and delay time used

The explosive source was a decoupled \varnothing 7 mm, 20-g/m strength PETN-cord, giving a theoretical specific charge (q) of 3.02 kg/m^3 over the volume of $\text{BLH} = 0.07 \times 0.66 \times 0.21 \text{ m}$ corresponding to one burden unit. The decoupling ratio, i.e., hole diameter over the cord outer diameter, was $10/7 = 1.43$. The cord was not centered in the blasthole, but held to the front of the hole by means of plastic spacers that secured the cord segments. The cord was segmented into 28-cm pieces, where 21 cm of the cord were in-hole column charge plus a trunk line with connectors to each hole. By using a 5-g/m PETN-cord trunk line it was possible to adjust the delay times with high accuracy. With an average velocity of detonation of 7220 m/s (Schimek, 2012), the delay of $73 \mu\text{s}$ per blasthole; i.e., about 1.1 ms/m of burden, was arranged. The initiation was done by an electric detonator, connected to the trunk line that was arranged in loops on a piece of conveyor belt. The conveyor belt was used to protect the yoke from the detonation of the trunk line.

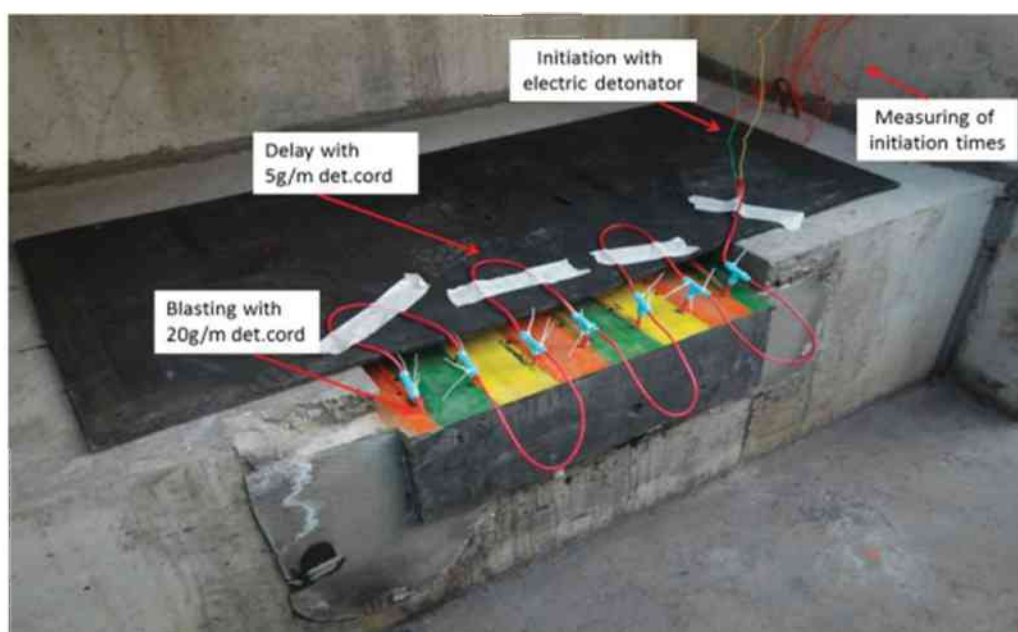


Figure 20: Arrangement of blasting and delay between holes

The firing sequence of all test blocks was from right to left in each row. The in-row delay time during tests was recorded with an oscilloscope Agilent MSO6014b; the delay results for each row are given in Appendix 4.

3.8 Blasting procedures

The model-scale tests made within this thesis had two different types of set-ups: blasting of cylinders and blasting of block specimens.

The cylinders set-up was carried to measure the repeatability of the fragmentation properties. At least one cylinder from each batch (three batches in 2013 and two in 2014, seven in total) was blasted in a blast chamber with covered opening (Maierhofer, 2011). The explosive source was a 20-g/m strength PETN-cord, giving a theoretical specific charge (q) of 1.26 kg/m^3 , with respect to the volume of the cylinders. After blasting, pictures were taken; the material was then collected and finally transported to the sieving laboratory for analysis.

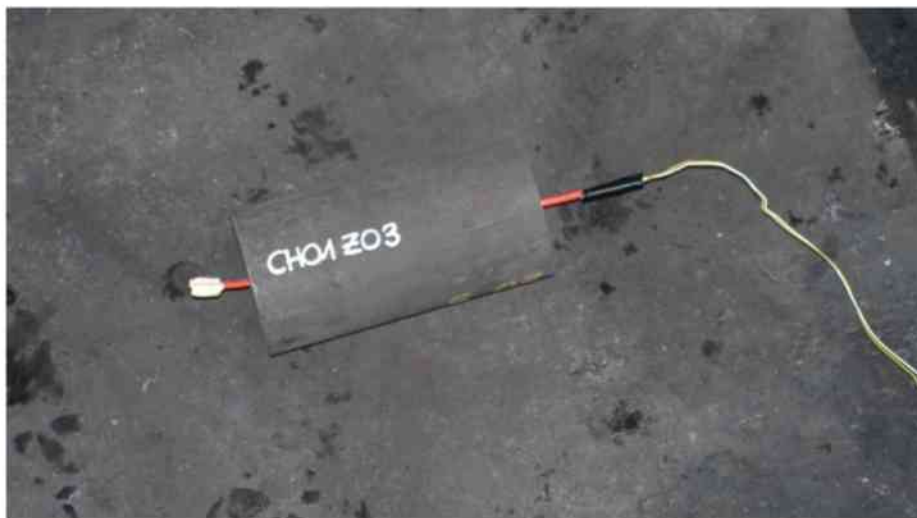


Figure 21: Cylinder prepared for blasting

For the tests of the concrete blocks with holes shots, the following procedure was followed:

- Controlling the geometry, wave velocity and physical and mechanical properties of the blocks in laboratory.
- Drilling the holes in the blocks in the laboratory by core drilling equipment.
- Controlling the geometry of the drilled holes by measuring tape.
- Transportation of the block to the blast site.
- Grouting the block into the inner yoke, leaving it overnight for grout to harden.

- Controlling the length of the drilled holes by using a metal stick. Cleaning or re-drilling in case some grouting material has stuck into the hole.
- Charge the row using segments of 20-g/m PETN-chord, inserted in each hole and connect with trunk line and detonator. The trunk line has a length appropriate to the desired delay time and guarantees that the detonation front travels from the detonator (delay no 0) and reaches the blastholes with a delay of 73 μ s; i.e., about 1 ms/m of the burden.
- Connecting of wire circuiting to each hole to measure delay times.
- Taking documentation pictures.
- Covering the blast site with geo-textile and rubber mats to avoid flying-rock and losses.
- Shooting.
- Post-blast control and assessment (see Chapter 3.9)
- Check of the delay time monitored.
- Taking BlastMetriX3D pictures: for each row blasted the bench surface was photographed with a 3D camera system, 3G Blast Metrix (Gaich et al., 2006).
- Muck collection: each row produced a certain amount of broken mortar material, which was contaminated by material from the yoke during the shots. A visual investigation of the material was done and the darker mortar fragments were separated from other material.
- Sweeping the blast site, collecting the loose material and storing it in labeled buckets.
- Transportation of the collected material to the laboratory for sieving.

3.9 Pre-and post-blast visual control of the bench face

Pre- and post-blast visual control of the bench face was done to investigate whether the bench face had been preconditioned either originally or in some way from the previous blasting. Such pre-conditioning may have had a significant effect on the blast result (Worsey, 1996). The assessment included the following: control of the crack existing within virgin block, check of the half casts, bench surface after blasting, breakage angle between blasted holes and deep trenches or visible blast damage.

3.10 Sieving analysis

After the blasted material was collected, the sieving analysis was completed according to the sieving standard of the Department of Mining Engineering (Grasedieck, 2006). From the sieving analysis, the particle size distribution: x_{30} , x_{50} and x_{80} were calculated. The blasted material was sieved as follows:

The grain sizes of the coarser material were analysed manually. Every single piece down to 14 mm was turned to fit through the mesh of the sieves. The following sieves were used in that procedure: 125; 100; 80; 63; 50; 40; 31.5; 25; 20; 14; 12.5; 10 mm. The two last sizes (12.5 and 10 mm) were used only for split material. The finer material was sieved using the following screen sizes: 6.3; 4; 2; 1; 0.5 mm. The screening stopped at a grain size of 0.5 mm because the lowest grains size in the ingredients of the magnetic mortar (Table 2) is 0.5 mm. A splitting of the material at 14 mm sieve was done when more than 3.0 kg of the material passed through. During each sieving step, a visual sorting process was carried out and if additional lighter pieces coming from the fast hardening cement or the yoke were found, then they were removed (see Figure 22). This material was weighed and then subtracted from the total mass of the material undergoing the sieving process.



Figure 22: Contaminating material removed and weighed

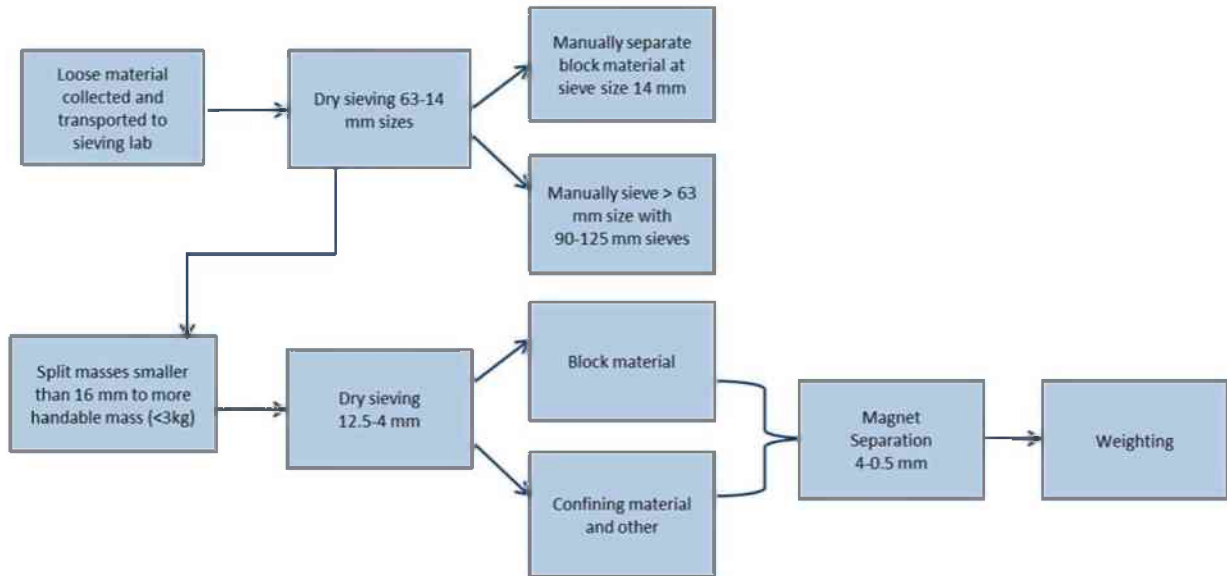
Using a magnet, material with a grain size of 4 mm was separated from the contamination material of the magnetic mortar. In sieves of 4 mm and below, a brush was used to clean and to reduce the amount of material being left on the sieve cloth.



Figure 23: Magnetic separation and brush cleaning of particles remaining on the mesh cloth

Table 5 summarizes the sieving procedure.

Table 5: Sieving procedure summary



3.11 Particle size distribution and determination of x-values

The results from the sieving analysis were plotted in a GGS-diagram (Schuhmann, 1940). This diagram is a log-log-plot, where the x-axis shows the screen size and the y-axis shows the cumulative mass passing. The passing “P” is calculated as follows:

$$P = 100 \cdot \left(\frac{x}{x_{max}} \right)^n \quad \text{Equation 12}$$

In addition, several x-values were calculated. The specific x-value was calculated with a linear interpolation between the two grain sizes next to the cumulative mass passing at 30 %, 50 % and 80 %. The calculation of x_{50} was e.g. done as follows:

$$x_{50} = x_u + \frac{x_0 - x_u}{P_0 - P_u} \cdot (P_{50} - P_u) \quad \text{Equation 13}$$

A way to describe slope of the particle size distribution around 50 % of the passing material is by a “coefficient of uniformity”. To determine this, the specific particle size x_{80} was divided by the specific particle size x_{30} . As the specific particle size x_{80} of a fragmentation process is larger than the specific particle size x_{30} , the minimum value must be always greater than 1 (Reichholf, 2003). The advantage of describing the particle size distribution with the uniformity exponent or with the “coefficient of uniformity” (x_{80}/x_{30}) respectively, is based on the evaluation of a section of the

distribution line, whereas a specific particle size (x_{80} , x_{50} or x_{30}) would only describe one point.

The tool used for fitting the fragmentation curve was the Swebrec function (Ouchterlony, 2005). The model includes three parameters: the median size (x_{50}), the maximum size (x_{max}) and an undulation parameter (b). This function describes the fragmentation distribution (coarse and fine parts) down to around 0.5 mm quite well. The Swebrec function is written as follows:

$$P(x) = \frac{1}{\left[1 + \frac{\left(\ln\left(\frac{x_{max}}{x}\right)\right)^b}{\ln\left(\frac{x_{max}}{x_{50}}\right)}\right]} \quad \text{Equation 14}$$

The undulation parameter b can be expressed as a function of the average size (x_{50}) and the maximum size (x_{max}) of the sieved material (Ouchterlony, 2005). The undulation parameter is then written as follows:

$$b = 0.5 \cdot x_{50}^{0.25} \cdot \ln\left(\frac{x_{max}}{x_{50}}\right) \quad \text{Equation 15}$$

The Swebrec function has been tested against several hundreds of sieved size distributions from blasting and crushing operations. This function is on average considered to give better fits, compared to all other functions (Sanchidrián et al.; 2009, 2012 and 2014).

Compared to the Kuz-Ram model for example, the Swebrec function takes into account the maximum size (x_{max}) of the blasted material. The function has been chosen for this thesis to fit to the sieved fragmented material in order to describe in more detail the two critical parameters: the maximum size (x_{max}) and the average size (x_{50}).

3.12 Measurement of crack development

The determination of blast-induced damage was done by investigating the crack development behind the shots with drillhole deviation and the reference shots (shots without drillhole deviation).

Both a dye penetration visualization technique and a 3D digital scale model method were applied for the visualization and assessment of the internal crack network (Navarro, 2015). With this technique, two main investigations were conducted: surface crack detection on cut slices and crack detection on the top of the testing blocks. Crack detection on the top of the blocks was made only for blast session 2014, due to the late development of crack detection method. The remaining parts of the blasted blocks in blast session 2013 were stored in the laboratory, so crack detection on cut slices was possible. A short description of the methodology is given below. A detailed description of the procedure can be found in Navarro (2015).

3.12.1 Crack detection on cut slices

After the blast tests of the blocks, fast-hardening cement was poured in front of the remains of the test-specimens behind row 3 to make it possible to remove them from the yokes in one piece and to enable them to be brought to the laboratory. The blast-induced cracks were detected and quantified by using dye penetration methodology on those specimens from the corresponding cut slices (Navarro, 2015).

The first step to visually detect the cracks was to trace them with a pen and to take documentation pictures from each side of the block remainder. A metric tape was used as a scale ruler, to help with further digital rescaling.



Figure 24: Surface cracks detection. Back side block CH01B04

Afterwards a dye penetrant on the back, up and down the surfaces of the testing block remain was applied, to detect a large number of cracks. Again documentation pictures were taken of all colored slices, using the same reference scale.

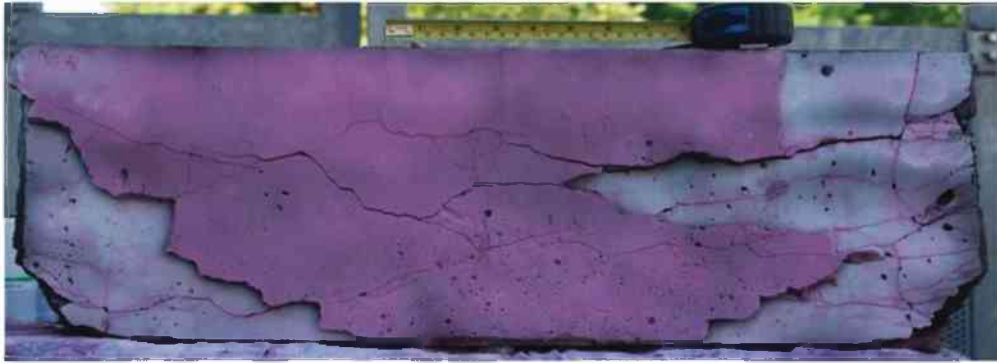


Figure 25: Dye penetrant application, block CH01B04

Once the block processing was finished, the detection of internal cracks in the testing block was carried out.

The block was cut into 5 horizontal slices by a diamond saw in the laboratory. The distance between the slices was roughly the same in each block, in order to allow comparison of cracks at the same level of the specimen. From those 5 slices 4 pairs of horizontal cutting faces, corresponding with the cut between slices, are used for the crack detection. The bottom of the remnant specimen (slice 5) was not used for the crack detection.



Figure 26: Distance between slices to cut the testing block CH01B04

Dye penetrant was applied to the surface of each slice. Each slice has top and bottom faces that should almost coincide with the bottom and top faces of the next or previous slices respectively. As the thickness of the machine saw used for cutting was only 5 mm, the separation between the adjacent faces was small compared to the lengths of most measured cracks; therefore, the face which displayed the highest number of visible cracks was used for the analysis.

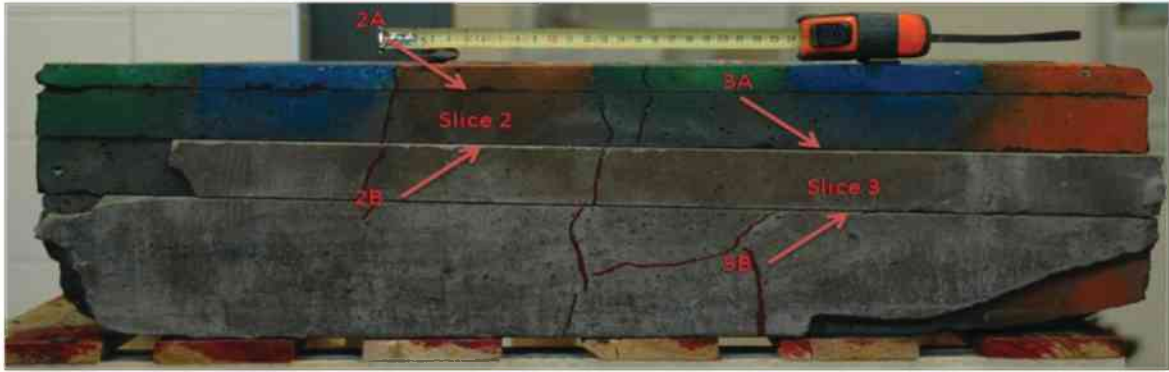


Figure 27: Clarification about the faces of the slices (e.g.3A-top, 3B-bottom) block CH01B04

The next step was to take photographs of the slices. In this case, photographs were taken after the cleaner was applied in order to observe cracks on the wet surface of the slice, and when the developer has been used.



Figure 28: Photo of the slice after using cleaner. Slice 2 block B04



Figure 29: Photo of the slice after using developer. Slice 2 block B04

To observe the cracks on the slice in greater detail, more pictures were taken after adjusting the camera zoom. Due to the limitations of the camera zoom, the whole block could not be covered by one picture. Thus, the surface of the slice was covered using three different pictures, dividing the surface into three sections (Figure 30).

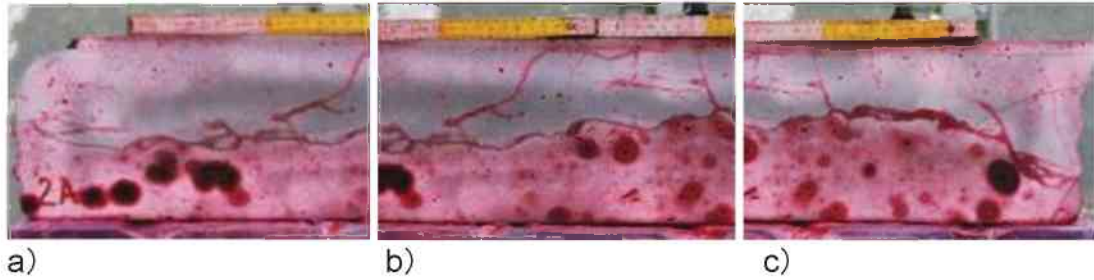


Figure 30: Photos by zoom adjusting a) left; b) middle and c) right part. Slice 2 block B04

From the pictures taken, the trace patterns of the testing block were used to construct 3D models in AutoCAD ® (Navarro, 2015). The cracks' traces on the pictures were drawn, and every visible line was considered as a crack. Attention was paid to the direction and continuity of the cracks in case there was a connection.

A boundary between the magnetite concrete and fast-hardening cement parts was also drawn (see Figure 31). The fast-hardening cement was checked for crack traces, which may have been created after blasting by the removal of the testing block from the yoke or during transportation.

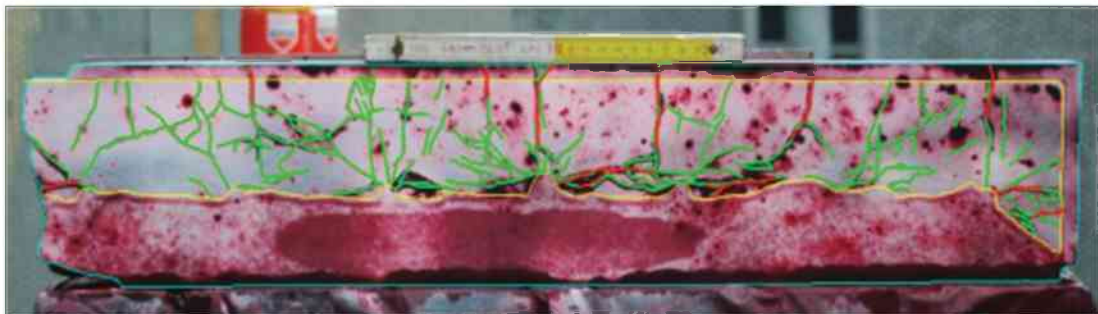


Figure 31: Drawing of crack traces horizontal slice. Slice 3 Block CH01B01

Figure 32 shows an example of digitized cracks on the horizontal sections of the testing block. These sections correspond to the bottom or top side of the slice surfaces, depending on which horizontal section displays better crack definition.

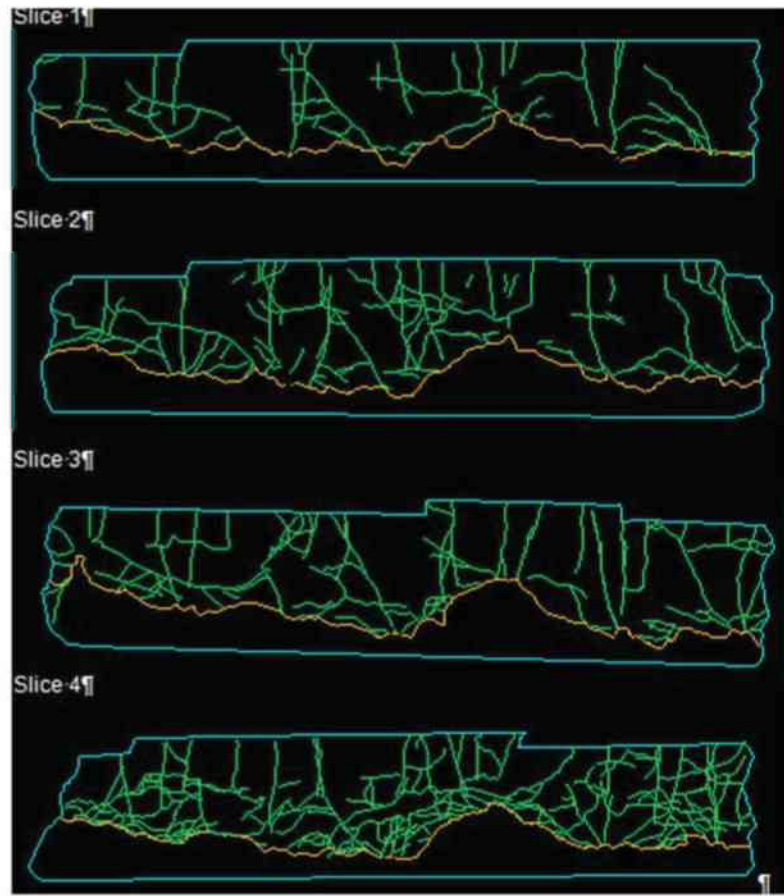


Figure 32: Digitized cracks on the horizontal sections. Slices 1-4 Block CH01B04

3.12.2 Crack density analysis

After the generation of the crack path, a calculation of the crack density was made, in order to detect where the damage (cracking) is concentrated within the slice (Navarro, 2015).

To carry out this analysis, the digital slice model was divided into a 2x2-cm grid (Figure 33), in which every square receives a value according to the number of cracks within its borders.

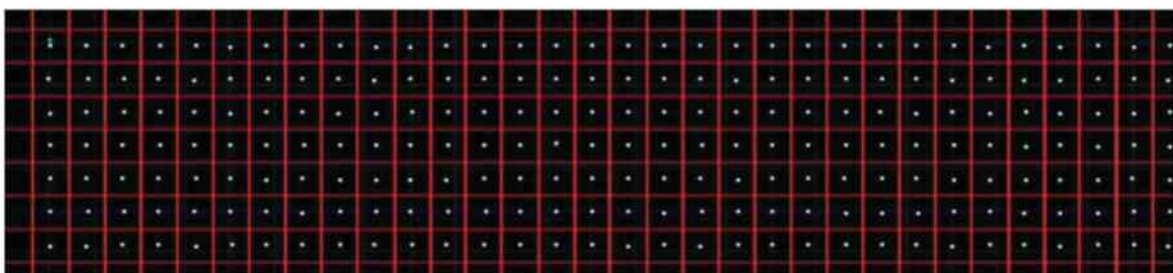


Figure 33: Grid 2x2 cm

The criteria for this choice were discussed by Navarro (2015). To create a damage map, which represents crack density in the slices, a computer program was written in MATLAB. Three values were taken as input of the code: X and Y coordinates of representative points; and a value containing the number of cracks. These named points are located inside each square in the grid as is shown in Figure 33.

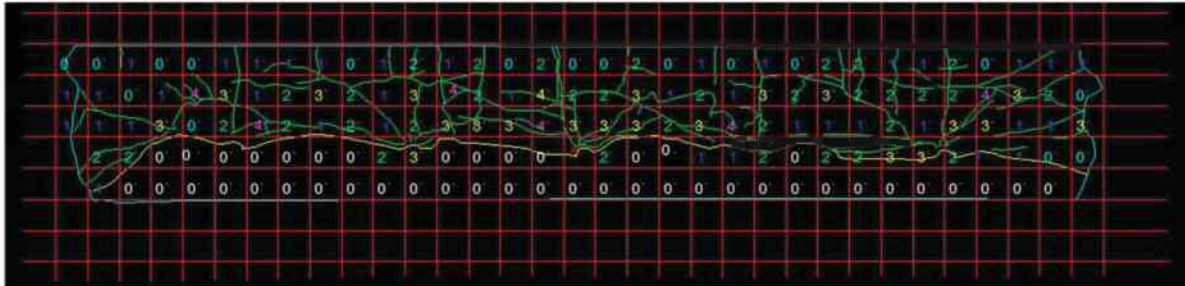


Figure 34: Grid 2x2 cm, representing the number of cracks (Navarro, 2015)

In Appendix 7 it can be seen, that the damage is not constant along the slices of the block. In addition, depending on which block is represented, the distribution of this damage changes between slices. For this reason, a measure was defined that would make the damage values comparable (Navarro, 2015). This measure was based on the number of density points established for each grid point. In this way, the mean value for all the numbers that belong to the same slice was calculated (Navarro, 2015). The parameter is the mean crack density (MCD) in the slice:

$$MCD_{value} = \frac{\sum_{i=1:N} i}{N} \quad \text{Equation 16}$$

where

N is the total number of grid points or 2x2 cm squares

i is number of cracks in the grid.

The totally created cracks in the testing block remnants are meaningful as one comparison figure, while the second figure, the MCD values take the length of these cracks into account.

Another way to quantify the block damage was to assume that the concentration of crack intersections along the slice is related to the blast fragmentation (Navarro, 2015), i.e., the more cracks that intersect in a specific region, the greater the damage

and the finer the fragmentation. The idea is similar to that for the Mean Crack Density. Thus the Mean Crack Intersection Density (MCID) value was defined as:

$$MCID_{value} = \frac{\sum_{i=1:N} i}{N} \text{ Equation 17}$$

where

N is the total number of grid points or 2x2 cm squares

i is number of cracks intersections in the grid

3.12.3 Surface crack detection on the top of the testing blocks

In addition to the cut slices, surface crack detection at the top of the testing blocks was made. Crack detection and documentation were done before blasting, after each of the 1st, 2nd and 3rd rows, using the same dye penetrant methodology (Navarro, 2015). Figure 35 below shows an example of the cracks introduced on the top of block after the blast in the 1st row. The crest behind the holes has been broken off.



Figure 35: Crack detection at the top of block after 1st row blast block B09

The block was divided into 4 sections according to the rows blasted (B1, B2, B3 and the remainder behind row 3). In this way, the same crack family definitions as those for the slices can be used. In each section, crack detection was done as if there is no other section or continuity of the crack. For example, a crack that goes further than one section was counted in both sections as different cracks, and was referred to the crack family to which it belongs in each section.

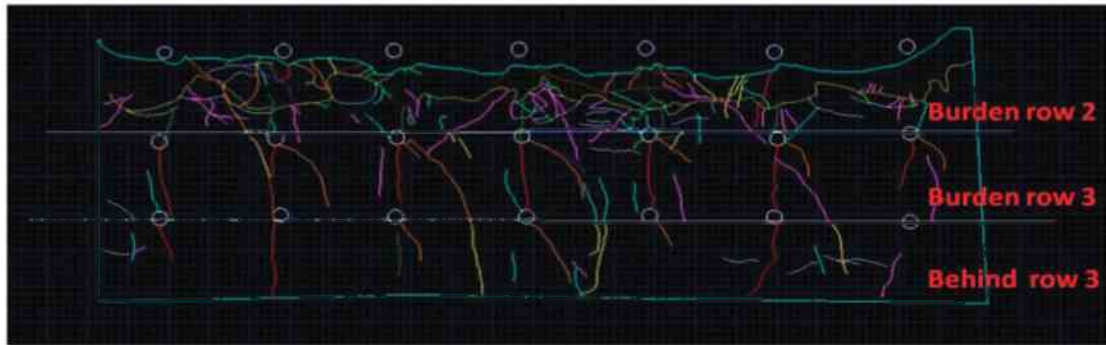


Figure 36: Detected cracks from blasting the 1st row of block B09

3.12.4 Recognition of crack families

Using the AutoCAD digitized cracks on the horizontal sections of the testing blocks, a division of crack patterns based on angles and lengths in slice surfaces was made. Different crack types were recognized on both the slices and the top surface area of the testing blocks hence they were grouped into eleven different crack families. These families were defined according to the angle and length of the crack, their origin and direction.

With regards to their lengths, the cracks were divided into two groups:

- long cracks (> 3 cm)
- short cracks (1-3 cm)

The following table shows the crack families recognized in this thesis. A detailed description of all cracks groups is given in Appendix 6.

Table 6: Crack families recognized

Colour	Description	Abbreviation
1	Cracks connecting with the borehole with an angle between 90° - 80°	CB 90° - 80°
2	Cracks connecting with the borehole with an angle between 80° - 30°	CB 80° - 30°
3	Cracks connecting with the borehole with an angle between 30° - 0°	CB 30° - 0°
4	Straight cracks between holes coming from the back side	SCB
5	Connections cracks between neighbouring boreholes	Connect
6	Parallel cracks to the bench surface	Parallel
7	Cracks with direction to the boreholes with an angle between 90° - 80°	CD 90° - 80°
8	Cracks with direction to the boreholes with an angle between 80° - 30°	CD 80° - 30°
9	Cracks with direction to the boreholes with an angle between 30° - 0°	CD 30° - 0°
10	Short radial cracks around the borehole	SC
11	Vertical cracks between boreholes, starting at face	VCB

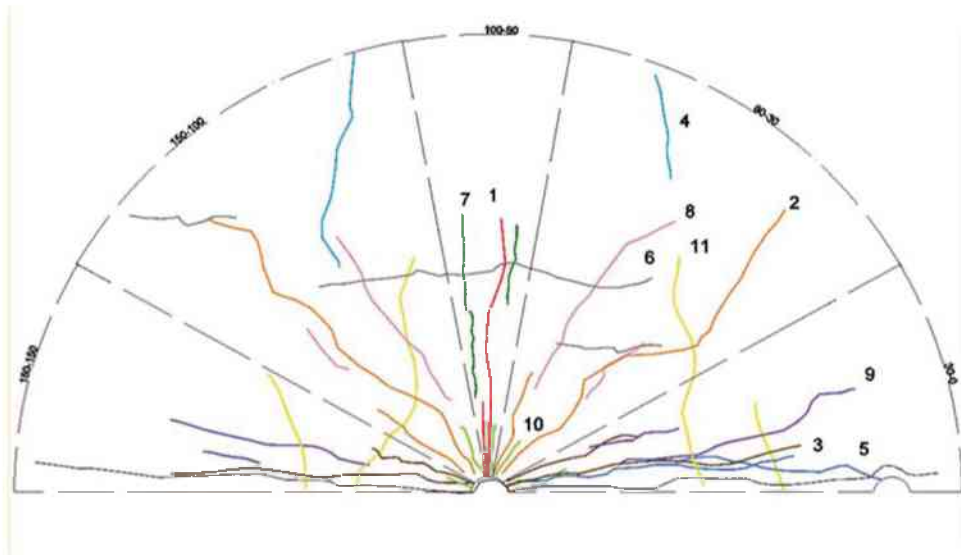


Figure 37: Graphical representation of the recognized crack families

Comparison of the cracks found in the published literature and the crack families recognized was done by Navarro (2015). He found several similar crack types as described by Ouchterlony et al. (1999 and 2000) and Saiang (2008) and the crack families analyzed in the horizontal sections, some of which are:

- a) Long and short radial cracks were found in both the Ouchterlony et al. (1999; 2000) and Saiang (2008) analyses. Six different radial crack families divided into 3 sectors were described in this work: 3 starting from the hole and 3 that develop a trajectory with a radial direction away from the hole.
- b) A notch root crack, defined in Ouchterlony et al. (1999), is the crack family defined as: Cracks from holes borehole with an angle between 90° - 80° .
- c) Arc shaped cracks defined by Ouchterlony et al. (1999) and Bow-shaped tangential cracks described by Saiang (2008), are similar to Cracks from holes with an angle between 30° - 0° . In addition, when a long crack (longer than 3 cm) of this family connects two holes, Connections cracks between neighboring holes can be included in this classification.
- d) Foliation cracks and Bench face cracks are quite similar to Parallel cracks but there are no foliation planes in our specimens.
- e) Structural cracks are also very similar to the crack family: Straight cracks between holes coming from the back side. However, since the blocks studied were made without foliations planes of joints, other generating mechanisms must have caused them.

- f) Short cracks from the hole are also found in both the Ouchterlony et al. (1999 and 2000) and Saiang (2008).

Only the cracks detected between the 1st and the 7th hole were taken for further analysis. The sections at both the left and right sides of the block were excluded from the analysis, to avoid possible influences from the break-out procedure.

The data generated was statistically evaluated in order to compare the cracks for different drillhole deviation blasthole patterns. The crack detection and analysis on the data has been done by Gang Zhu in 2013 and 2014 year and the data has been re-arranged and re-analyzed by Juan Navarro in 2014, due to development of the crack detection methodology.

3.13 Surface characteristics analysis of the bench face

The bench face was measured after each blast with a stereo-photography system Blast MetriX3D (Gaich et al., 2006), in order to get a model of the overall bench surface after blasting and see if there is any difference in the surface properties when drillhole deviation exists. The referencing and scaling was made by placing rulers and other well defined objects in the pictures (see Figure 38).

Two pairs of Range Poles with a space of 110 mm (center to center) between the top and bottom targets, and two Top Delimiters with 660 mm (end to end) distance between them were used.

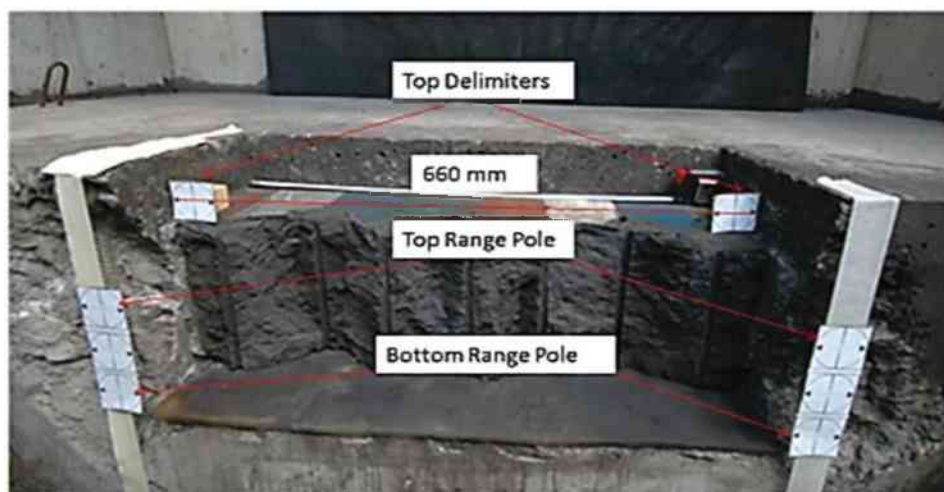


Figure 38: Taking stereo photographic pictures

A 3D model of the surface was constructed out of the paired pictures (left and right). The confining yoke was removed from the numerical models to facilitate the measurements and analysis.



Figure 39: 2D Projection of 3D model of blasted surface CH01B04 R02

Using the Blast Metrix software a triangular mesh of the bench face was generated. To enable further detailed analysis, the coordinates for each triangular point were extracted as csv-files (comma-separated values files).

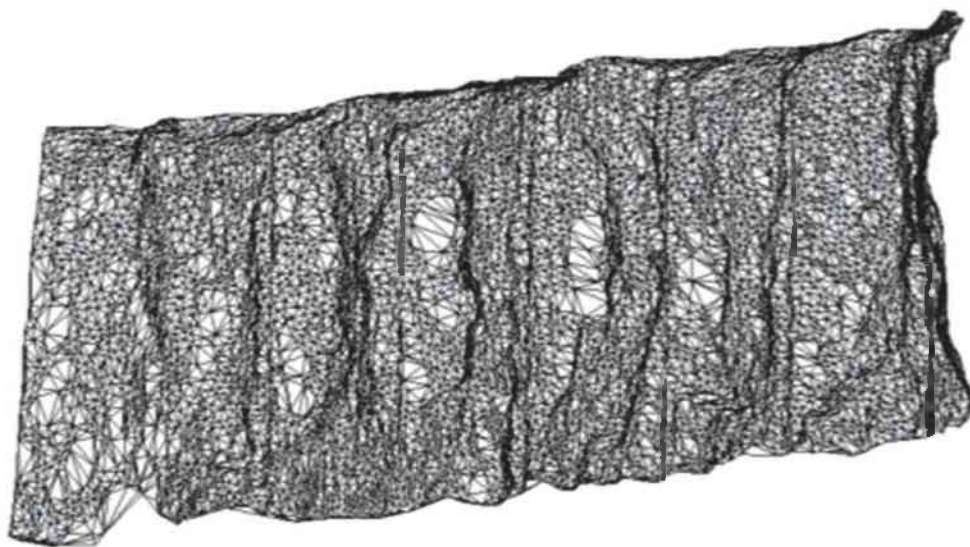


Figure 40: Capture of triangulation of the bench face imported into CAD

To analyze the backbreak, three horizontal contour lines were taken at 5, 10, and 15 cm height on the block (see yellow lines in Figure 39). The contour lines were further converted to CAD dxf. files (see Figure 41). Each contour line is represented by 700-1400 individual points.



Figure 41: 2D Projection of contour

The extracted data points are defined relative to the as-drilled center to center line of the holes, i.e. including the drilling errors when relevant.

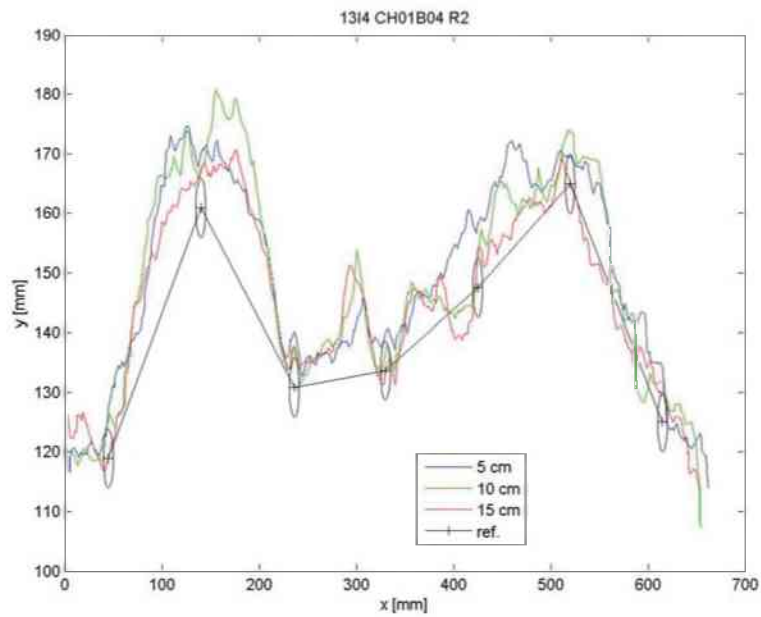


Figure 42: Projection of the contour and reference centre line of holes

The perpendicular distance to the contour line defines the surface deviation. The parts of the contour lines at the both sides of the block were excluded from the analysis and only the line parts between holes 1 and 7 were analyzed.

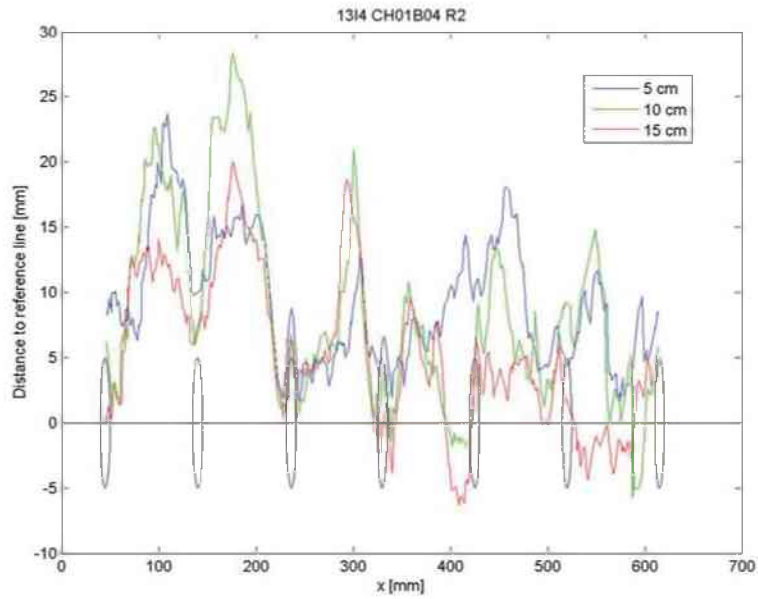


Figure 43: Perpendicular distance of contour to the reference line

To illustrate the backbreak and underbreak, a histogram plot of the deviation distances of the individual data points for all contour lines, as well as a combined value of three contour lines, was used. An analysis of the data based on the original CAD files was completed with MATLAB software. An example output is presented in the following diagram (Figure 44).

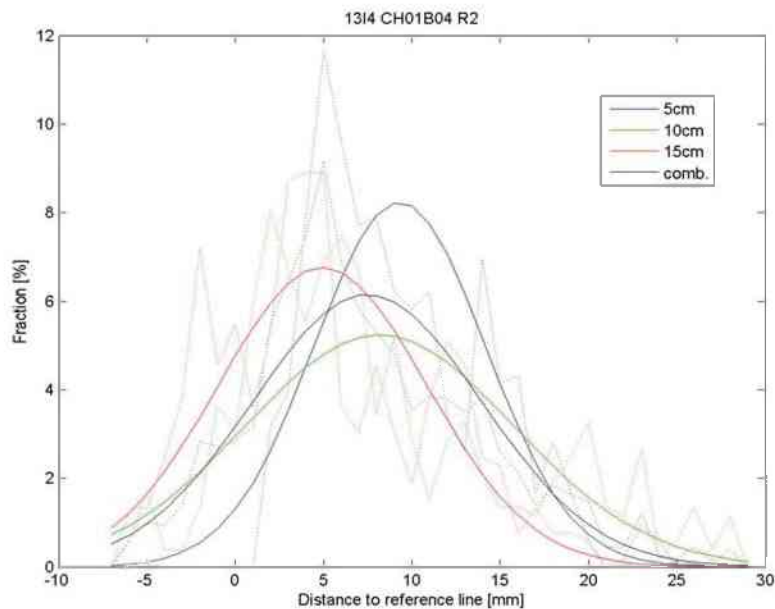


Figure 44: Distance of contour to the reference line histogram

The distances of the individual data points to the reference line was further presented as boxplots (see Figure 45).

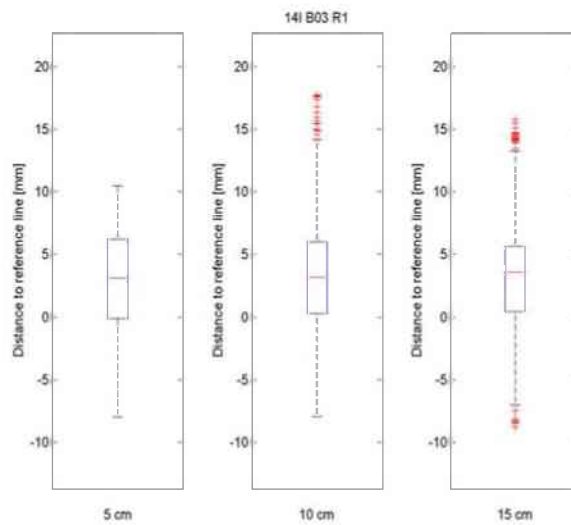


Figure 45: Boxplots distance of contour line to the reference line

The following parameters were calculated using a MATLAB code:

- **D_{mean} [mm]**

The mean distance of the individual data points to the reference line is a relative figure used to evaluate the broken out volume (Holloway et al., 1987). When D_{mean} is positive (+), then a backbreak occurred, when D_{mean} is negative (-) then underbreak is dominant. D_{mean} is calculated as follows:

$$D_{mean} = \bar{d} = \frac{\sum d}{n} = \frac{\sum_{i=1}^n d_i}{n} [mm] \quad \text{Equation 18}$$

where:

d... distance from an individual data point to the reference line

n... number of data points

- **S_{norm} [-]**

The normalized slope inclination of the individual sections of the contour lines is a comparative figure for the roughness of the contour line and it is calculated as below:

$$S_{norm} = \frac{\sum s_i \times \Delta x}{l} = \frac{\sum \frac{\Delta d_i}{\Delta x} \times \Delta x_i}{l} = \frac{\sum_{i=2}^n |d_i - d_{i-1}|}{x_{max} - x_{min}} \quad \text{Equation 19}$$

where:

d... distance from an individual data point to the reference line

n... number of data points

s_j ... inclination of connection line between two data points

x_i ... position of the data point measured from the left side of the block

l... projected surface length between holes 1 and 7.

A detailed description of both the procedure and the analysis of the surface characteristics are given in Appendix 10.

3.14 Statistical evaluation of the data

Four statistical methods were used to evaluate the data, with regards to fragmentation, surface roughness and quantification of the cracks: They are briefly described below. The choice of statistical tools for evaluation is based on the small amount of data. Many statistical methods are based on the assumption that the observed data are samples with a known distribution. However, due to the small amount of data in the samples, the distributions couldn't be determined. Thus, the following non-parametric methods were used for testing whether the samples originated from the same distribution. Too few data points in the compared groups may lead to inconsistent results of the MW U-test.

3.14.1 Mann-Whitney U- test

The Mann-Whitney U-test is used to compare differences between two independent groups when the dependent variable is either ordinal or continuous, but not normally distributed. This test is the non-parametric equivalent of the two sample t-test. The test implies the following assumptions (Conover, 1999):

- Both samples are random samples from their respective populations.
- In addition to independence within each sample, there is mutual independence between two samples.

- The measurement scale is at least ordinal.

The null hypothesis is that there are no differences between the means of the samples.

There are several marginally different ways given in the literature, for calculating Mann-Whitney U-test (Conover, 1999; Harmon, 2011; Scheskin, 1997). The calculation of Mann-Whitney U-test with regards to this thesis was carried out following the instructions for non-parametric testing in Microsoft Excel (Harmon,2011) using the following steps:

- 1) All data from the two groups have to be ranked together
- 2) The sums of the ranks for each group have to be calculated (R_1 and R_2)
- 3) The count of samples in each group is found (N_1 and N_2)
- 4) Calculation of U-statistics as:

$$U = N_1 \cdot N_2 + [(N_1(N_1 + 1)/2) - R_1] \quad \text{Equation 20}$$

- 5) Calculation of the mean μ_U and stdev. σ_U as:

$$\mu_U = \frac{N_1 \cdot N_2}{2} \quad \text{Equation 21}$$

$$\sigma_U = \sqrt{N_1 \cdot N_2 [(N_1 + N_2 + 1)/12]} \quad \text{Equation 22}$$

- 6) Calculation of the Z_{score} as:

$$Z_{score} = \frac{(U - \mu_U)}{\sigma_U} \quad \text{Equation 23}$$

- 7) Compare the Z_{score} to Z_{crit}

With degree of certainty 95 %, or significance level $\alpha=0.05$

For a one-trailed tests, $Z_{crit} = \text{NORMSINV}(\alpha) = \text{NORMSINV}(0.05) = -1.645$

For a two-trailed tests, $Z_{crit} = \text{NORMSINV}(\alpha/2) = \text{NORMSINV}(0.025) = -1.960$

- 8) The result is significant (so the null hypothesis can be rejected) if the absolute value:

$$|Z_{score}| > |Z_{crit}| \quad \text{Equation 24}$$

Too few numbers of observations in the groups compared may lead to a sum of the ranks of the individual groups which can't follow well the lower quantiles, this may lead to inconsistent results of the MWU-Test (Harmon, 2011). This issue has also been discussed by Nappier-Munn (2014) who suggested that the quality of the estimates will improve as the sample size increase, i.e. for more confidence in the results, larger samples should be evaluated.

3.14.2 Kruskal-Wallis One-Way Analysis of Variance (KW-ANOVA)

The Kruskal-Wallis One-Way Analysis of Variance (Kruskal and Wallis, 1952) is a rank-based non-parametric test that can be used to determine whether there are statistically significant differences between more than two groups of an independent variable on a continuous or ordinal dependent variable. The method was invented as an extension of the Mann-Whitney test, which can be used for only two independent samples (Graham, 2011).

The Kruskal-Wallis One-Way Analysis of Variance uses a Chi-Squared test statistic and cannot tell which specific groups of the independent variables are significantly differ from each other statistically; it only tells that at least two groups are different. The following are some of the characteristics of the Kruskal-Wallis One-Way Analysis of Variance:

- a. No assumptions are made about the type of underlying distribution.
- b. It is assumed that all groups have a distribution with the same shape.
- c. No population parameters are estimated, so there are no confidence intervals.

The Kruskal-Wallis One-Way Analysis of Variance is calculated following the steps below:

- 1) Rank all of the values, ignoring the group they belong to. The procedure for ranking is as follows: the lowest value gets the lowest rank. If two or more values are the same then they are "tied". "Tied" values get the average of the ranks that they would have obtained.

- 2) Calculate the total of the ranks for each group by adding together all of the ranks for each group in turn.
- 3) Find the value of “H”:

$$H = \left[\frac{12}{N(N+1)} \times \sum \frac{T_c^2}{n_c} \right] - 3(N + 1) \quad \text{Equation 25}$$

where:

N... is the total number of data points (all groups combined)

T_c... is the rank total for each group, and

n_c... is the number of data in each group.

The degrees of freedom (d.f.) are the number of groups minus one. Assessing the significance of H depends on the amount of data and the number of groups. H is statistically significant if it is equal to or larger than the critical value of Chi-Square (X²) for a particular d.f. value and the alpha (α) value.

Table 7: Critical Chi-Square (x²) values

d.f.	α=0.05	α=0.01	α=0.001
1	3.84	6.64	10.83
2	5.99	9.21	13.82
3	7.82	11.35	16.27

For the small samples (n<5), and in case there are no ties, the exact quintiles are re-calculated and the critical values are given in the following table (Conover, 1999).

Table 8: Critical Chi-Square (x²) values for small samples (Conover, 1999):

Sample size (n ₁ , n ₂ , n ₃)			d.f.	α=0.1	α =0.05	α=0.01
2	2	2	2	3.71	4.57	4.57
3	3	3	2	4.60	5.06	6.48
4	4	4	2	4.50	5.65	7.53

When the Kruskal-Wallis One-Way Analysis of Variance rejects the null hypothesis, it indicates that one or more pairs of samples do not have the same means, however it does not tell which pairs are different from each other (Conover, 1999). For this thesis the Kruskal-Wallis One-Way Analysis of Variance is abbreviated as KW-ANOVA.

3.14.3 Two samples t-test

The two-sample t-test is used to determine if two random population means are equal (Snedecor and Cochran, 1989). The following assumptions are taken into consideration:

- The two samples tested are independent
- Data should be normally distributed
- The two samples should have the same variance

The null hypothesis tested states that there is no difference between the means of the two populations, i.e. the difference is zero:

$$H_0: \mu_1 - \mu_2 = 0 \quad \text{Equation 26}$$

where

μ_1 is the mean of first population and μ_2 is the mean of the second population.

The null hypothesis tested can be rejected when:

$$H_a: \mu_1 - \mu_2 \neq 0 \quad \text{Equation 27}$$

The t-test statistics is calculated by following formula:

$$t = \frac{\bar{X}_1 - \bar{X}_2}{\sqrt{\left(\frac{(N_1-1)s_1^2 + (N_2-1)s_2^2}{N_1+N_2-2}\right)\left(\frac{1}{N_1} + \frac{1}{N_2}\right)}} \quad \text{Equation 28}$$

where:

X... is the sample mean

N... is the total number of data points

s.... is the sample variance

3.14.4 One-way ANOVA F-Test:

Analysis of variance (ANOVA) is a statistical model used to analyze the differences between group means and their associated procedures (such as "variation" among and between groups) (Strickland, 2014).

The following assumptions made by ANOVA are taken into consideration:

1. Homogeneity of variance: the populations have the same variance.
2. The populations are normally distributed.
3. Each value is sampled independently from the other values. In this way, each subject provides only one value. If a subject provides two scores, then the values are not independent.

These assumptions are the same as for a t-test of differences between groups except that they apply to two or more groups, not just to two groups. The null hypothesis tested by ANOVA states that the population means for all conditions are the same. This can be expressed as follows:

$$H_0: \mu_1 = \mu_2 \dots = \mu_k \text{ Equation 29}$$

One could reject the null hypothesis if only:

$$F > F_{crit} \text{ Equation 30}$$

Thus, the alternative hypothesis (H_a) is:

H_a : At least one mean value is not statistically equal.

The one-way ANOVA was implemented by the data-analysis tool in Microsoft Excel

4. Results and analysis

In this chapter, the results from the physical and mechanical parameters of the material, fragmentation results, blast damage in terms of crack density, and surface roughness results are presented and discussed. Statistical evaluation of the data is conducted to find out whether the material parameters derived from the mechanical tests, blast fragmentation and blast damage derived from the model scaled blasting tests are influenced by the drill hole deviations and if they are correlated or not.

4.1. Material properties

In this sub-chapter, the material properties' characteristics by quantitative estimation are described, with the aim of supporting the evaluation of fragmentation and blast damage results. Two batches of samples were tested in the laboratory for blast session 2013. The values of the individual core samples from blast session 2014 are presented as an average. The individual values of the samples can be seen in Appendix 2.

4.1.1 Density

The results for the 2 test sets of the Ø50mm magnetite concrete core samples cored from larger Ø 142 mm cylinders (blast sessions 2013 and 2014) are shown in Table 9.

Table 9: Average densities of core samples

Year	Batch	Density [kg/m ³]
2013	CH01 (4 samples)	2266
	CH03 (5 samples)	2280
	Average	2274
	Stdev	25
2014	14 samples average	1986
	Stdev	35

The average measured density of the core samples' subset for blast session 2013, differ from each other by much less than the standard deviation. The samples from the 2013

blast session have an average density, which is 14 % higher than those from the 2014 blast session.

Apart from the core samples, the density of the cylinders (used to measure the repeatability of the fragmentation properties) was also calculated in [kg/m³] by applying the mass-volume ratio method, described in Chapter 3.5. Table 10 gives the results obtained.

Table 10: Density of blasted cylinders

Year	Cylinder #	Density [kg/m ³]
2013	CH01Z03	2390
	CH02Z03	2369
	CH03Z03	2326
	Average	2362
	Stdev	33
2014	CH01Z01	2040
	CH01Z02	2018
	CH02Z01	2033
	CH02Z02	2005
	Average	2024
Stdev	16	

The measured density of the cylinders for each subset showed a high level of repeatability. The cylinders from blast session 2013 had an average value 17 % higher than that achieved in blast session 2014. Those values corresponded very well to the core samples' values. The density of a rock is a function of mineral composition, porosity and water saturation (Gardner et al., 1974). The additional 8 l water per batch added for a complete hydration of the concrete in the 2014 production session has to be taken into account. The density and compressive strength of concrete decrease when the water-cement ratio increases (Alawode and Idowu, 2011). Furthermore, the samples for blast session 2013 were produced with quartz sand with a larger grain size (0.1-0.5 mm), which differs from the sand in blast session 2014 (0.1-0.4 mm). Thus the results are influenced by the additional water content in the recipe, based on the fact that the finer sand size has a much larger specific area that required the use of more water.

4.1.2 Uniaxial compressive and tensile strength

Table 11 shows the results from the UCS (uniaxial compressive strength) and STS-splitting tensile strength (Brazilian test) for the blast sessions in 2013 and 2014.

Table 11: UCS and tensile strength of core samples

Blast session year	Batch	UCS [MPa]	STS [MPa]
2013	CH01 (4 samples)	61.9	5.4
	CH03 (5 samples)	54.2	5.5
	Average Stdev	58.1 5	5.5 -
2014	All 14 samples average	35.7	3.5
	Stdev	5	0.5

The average measured UCS values in blast session 2013 differ substantially from each other by nearly 12 %. Batch CH01 gave 61.9 MPa, while for batch CH03 the value is 54.2 MPa. A comparison of both blast sessions shows that the average UCS value for blast session 2013 is 63 % higher, compared to the value for blast session 2014. The average STS value for blast session 2013 is 57 % higher than the value for blast session 2014.

4.1.3 P-wave and S-wave velocity

The results for the P and S-wave velocities in both test sets of the blocks (blast sessions 2013 and 2014) are shown in Table 12. Due to the lack of suitable equipment in the laboratory, the S-wave velocity was not measured for blast session 2013.

Table 12: P and S- wave velocities of sessions 2013 and 2014

Blast session year	Batch	P-wave velocity [m/s]	S-wave velocity [m/s]
2013	CH01 (4 samples)	3809	
	Stdev	36	
	CH03 (5 samples)	3704	
	Stdev	81	
2014	All 14 samples average	3056	1989
	Stdev	36	36

4.1.4 Young's modulus and Poison's ratio

Table 13 shows the results from the E-modulus and Poison's ratio, measured during the UCS tests. It can be seen that, when compared to the 2013 blast session results, the Young modulus results from the 2014 blast session gave values approximately 40 % lower; on the other hand, when the same comparison is done with the Poison's ratio values, the values from the 2013 session are 40 % lower than the 2014 session.

Table 13: E-Modulus and Poisson's ratio values

Year	Batch	E-Modul [GPa]	Poisson's ratio [-]
2013	CH01 (4 samples)	24.3	0.13
	CH03 (5 samples)	23.5	0.12
	Average	23.9	0.12
	Stdev	0.5	0.03
2014	All 14 samples average	14.0	0.17
	Stdev	0.9	0.01

4.1.5 Sieving parameters of the cylinders

The sieving parameters x_{30} , x_{50} , x_{80} and coefficient of uniformity x_{80}/x_{30} of the blasted cylinders and a comparison of them for the blast sessions in 2013 and 2014 are summarized below. For blast session 2013, data for the batch CH02 used by Schimek (2013), is also given.

Table 14: Sieving parameters of the cylinders [mm] and coefficient of uniformity [-]

Blast session	Cylinder #	x_{30}	x_{50}	x_{80}	Coefficient of uniformity
2013	CH01Z03	8.4	15.5	24.6	2.92
	CH02Z03	8.8	15.9	26.4	3.01
	CH03Z03	8.0	14.3	22.8	2.86
	Average	8.4	15.2	24.6	2.93
	Stdev	0.33	0.70	1.49	0.08
2014	CH01Z01	8.1	13.2	22.2	2.74
	CH01Z02	8.4	13.3	22.1	2.63
	CH02Z01	8.1	13.6	24.4	3.03
	CH02Z02	7.6	13.5	23.3	3.08
	Average	8.1	13.4	23.0	2.87
	Stdev	0.29	0.15	0.95	0.22

The sieving parameters for the blast session 2013 show reasonably comparable results for the different batches. Similar characteristics for the median fragment size of the

mortar cylinders (x_{50}) could be also seen in the Johansson (2008) results, where 15 cylinders with the same properties and similar ingredients were blasted, and the average x_{50} was 15.3 mm with standard deviation of 1.1 mm. The sieving parameters of the cylinder's shots within blast session 2014 are also characterized by a high repeatability and a small variation between different batches.

4.2. Methodological question: Are the material properties from production sessions 2013 and 2014 comparable?

The testing block samples, produced in two different sessions 2013 and 2014 (see Chapter 3.3) were statistically evaluated, in order to see if their material properties are comparable. The statistical evaluation of the material properties for each session can be seen in the Table 15.

The material properties of the mortar from the different production cycles were significantly different. The complete set of data of the material property measurements can be found in Appendix 2.

Table 15: Statistical evaluation of the material properties with MWU-Test ($\alpha = 0.05$)

Material Property	Z _{score}	Z _{critical}	Sign.diff.
Density [kg/m ³]	2.00	1.64	Yes
Young's modulus [MPa]	3.46	1.64	Yes
UCS [MPa]	3.42	1.64	Yes
Brazilian tensile strength [MPa]	3.12	1.64	Yes
P-wave velocity [m/s]	2.77	1.64	Yes

Statistical evaluation of the data was also conducted to find out whether the fragmentation parameters between 2013 and 2014 show any significant difference between them. Table 16 summarizes the Mann-Whitney U-Tests results of the sieving parameters (x_{30} , x_{50} and x_{80}).

Table 16: Statistical evaluation of cylinders sieving parameters with MWU-Test ($\alpha = 0.05$)

Parameter	Z _{score}	Z _{critical}	Sign. diff.
x_{30}	1.06	1.64	No
x_{50}	2.12	1.64	Yes
x_{80}	1.41	1.64	No

The results showed that the specimens in blast session 2014 gave finer x_{50} fragmentation values, compared to the specimens in blast session 2013 and this difference in x_{50} values is significant. The x_{30} and x_{80} fragmentation values did not show significant differences.

In his thesis, Reichholf (2003) stated that *“the rock mass density influences the blast energy transfer into the rock, and thus, affects the blastability and the fragmentation.”* Moreover, Rustan et al. (1995) established from model scale blast tests that x_{50} increased with the rock mass density. Rustan (2010) considered as important parameters the density of the explosive (ρ_e), the density of the rock mass (ρ_r) and the sound wave velocity in the rock mass (c_p) for determination of energy transformation from explosive to the rock mass. With regards to the acoustic impedance ratio Z_R of two adjacent contacting materials, he gives a formula for the contact acoustic impedance of rock and explosive, stating that *“for maximum energy transfer from the explosive to the rock mass according to classical wave transmission theory, Z_R should be equal to 1”* (Rustan, 2010). Ramulu and Sinha (2011) have conducted full scale blast tests in four different benches at Kamptee mine, trying to match the impedance, by adapting the explosive properties to rock impedance, so as to achieve Z_R equal or near to 1. The rock mass characterization was done by MASW seismic profiling technique, the fragmentation size distribution analysis was done by image analysis software FRAGALYST. The results indicated that selection of proper explosives with impedance matching to the rock impedance clearly improved the fragmentation (mean fragment size was reduced about 15-20 %) and reduced the back break about 50 %.

With regards to the Kuz-Ram formula for the median fragment size (see equation 6), the x_{50} is a function of A (rock mass factor, see equation 7) and explosive charge and strength. The rock factor A is a function of JF, RMD, HF and RDI. In blast sessions 2013 and 2014 the explosive charge and properties are constant, while the RDI value ($(0.025 \cdot \rho) \cdot 50$) would change because of the different density values. Calculations of the changes in A, with regards to the rock density, showed that the $\Delta A/A$ was estimated to be roughly 18 %. Moreover if the effect on c_p is added (Kou and Rustan, 1993), the changes in the x_{50} values would be even larger, up to 30 % (see also Appendix 2). The following table shows the density, specific charge and x_{50} of the individual blast sessions.

Table 17: Specific charge, density and cylinder's sieving parameters

Year	Cylinder #	Density [kg/m ³]	Specific charge [kg/m ³]	x ₅₀ [mm]
2013	CH01Z03	2390	1.29	15.45
	CH02Z03	2369	1.27	15.92
	CH03Z03	2326	1.23	14.26
	Average Stdev	2362 33	1.26 0.03	15.21 0.86
2014	CH01Z01	2040	1.29	13.24
	CH01Z02	2018	1.27	13.34
	CH02Z01	2033	1.29	13.61
	CH02Z02	2005	1.27	13.54
	Average Stdev	2024 16	1.28 0.01	13.43 0.17

Summarizing the findings it can be stated that the two sessions 2013 and 2014 showed significantly different results in the material properties of the cylinders. This is a result of the variations in the production ingredients in both sessions (see Table 2). The statistical evaluation of the fragmentation data using MWU-Tests, also showed that the identically blasted cylinders from blast sessions 2013 and 2014 showed significant differences in x₅₀ values, however not in the x₃₀ and x₈₀. These cases cannot be explained directly. Based on the findings discussed above, the conclusion from both material properties and fragmentation is that the blastability of the cylinders in sessions 2013 and 2014 is different; therefore, blast sessions 2013 and 2014 are treated separately.

4.3. Fragmentation results

The fragmentation results for the sessions in both 2013 and 2014 and the subsequent statistical evaluation of the data have been described in this chapter. The statistical evaluation was done to obtain a comparison of fragmentation when different deviation patterns were tested. The complete results of the sieving analyses are contained in Appendix 5, where the retained mass and mass passing % data, as well as the Swebrec function fits are given.

4.3.1 Fragmentation results blast session 2013

The percentile size passing values x_p for $P = 30, 50$ and 80% for the blast session 2013, obtained by linear interpolation of the sieving data are summed up in the table below.

Table 18: Sieving parameters blast session 2013

Block	Row	x_{30} [mm]	x_{50} [mm]	x_{80} [mm]	Coefficient of uniformity x_{80}/x_{30}
CH01B03 (Reference)	1	26.08	57.61	91.35	3.50
	2	9.94	21.36	73.09	7.35
	3	8.50	17.51	43.12	5.07
CH01B05 (Reference)	1	15.64	32.43	64.29	4.11
	2	10.41	22.42	54.45	5.23
	3	7.71	14.54	37.00	4.80
CH01B02 (1st burden deviation)	1	13.74	30.14	110.05	8.01
	2	11.63	23.61	61.67	5.30
	3	10.12	19.95	52.05	5.14
CH01B04 (1st burden deviation)	1	13.56	25.87	84.61	6.24
	2	9.77	18.96	47.81	4.89
	3	7.53	13.86	33.84	4.49
CH03B01 (2nd burden deviation)	1	16.55	54.42	117.74	7.11
	2	10.87	25.61	79.76	7.34
	3	8.96	18.09	46.15	5.15
CH03B02 (2nd burden deviation)	1	20.28	44.74	88.13	4.35
	2	9.53	24.53	79.05	8.30
	3	9.78	19.38	55.32	5.66

Referring to Table 18, the general observation is that the largest scatter in the data is observed in row 1, when compared to rows 2 and 3. It is not possible to make a direct comparison of the data, since blast influencing parameters in terms of deviation blasthole patterns has been changed. With reference to that, the data has been divided in individual groups.

The coefficient of variation (COV [%]) i.e. relative standard deviation within each group has been calculated as a ratio of the standard deviation to the mean, multiplied by 100. The following criteria were established:

- When COV between 0 and 10 % - good repeatability (low scatter)
- When COV between 11 and 20 % - acceptable repeatability (moderate scatter)
- When COV between 21 and more % - bad repeatability (high scatter)

The following comparison between the Reference blocks can be made:

- The repeatability of x_p data from blocks CH01B03 and CH01B05 in the first row is bad and the coefficient of variation is in the range 25-40 %. The coefficient of variation in x_{80}/x_{30} values is 11 %.
- For the second row, the two reference blocks show good repeatability of the results except in the x_{80} values, where the coefficient of variation is 21 %. The coefficient of variation in x_{80}/x_{30} values is 24 %.
- For the third row the two reference blocks do show an acceptable repeatability of the results: the coefficient of variation lies in the range 7-13 %. The coefficient of variation in x_{80}/x_{30} values is 4 %.

The following comparison between the 1st deviation pattern blocks can be made:

- Blocks CH01B02 and CH01B04 show an acceptable repeatability of the results in row 1 except for the x_{80} value: the coefficient of variation of the data goes up to 19 %. The coefficient of variation in x_{80}/x_{30} values is 18 %.
- For the second row the 1st burden deviation pattern blocks show acceptable repeatability of the results: the coefficient of variation of the data lies in the range 12-18 %. The coefficient of variation in x_{80}/x_{30} values is 6 %.
- For the third row, the repeatability is bad and the coefficient of variation of the data lies in the range 21-30 %. The coefficient of variation in x_{80}/x_{30} is 10 %.

The following comparison between the 2nd deviation pattern blocks can be made:

- For the first row of the 2nd burden the deviation pattern blocks do show acceptable repeatability of the results; the coefficient of variation of the data is in the range 14-20 %. The coefficient of variation in x_{80}/x_{30} values is 34 %.
- The second and third row results shows acceptable repeatability of the result, except the x_{80} values, where the coefficient of variation for the third row is 13 %. The coefficient of variation in x_{80}/x_{30} values is 6 %.

No clear and consistent trend in the data can be seen with respect to the drillhole deviation (distorted patterns). It would be difficult to find any significant effect on the fragmentation caused by the changes in blasthole pattern.

Figure 46 gives a plot of the median fragment size x_{50} from Table 18 versus deviation patterns plotted row wise.

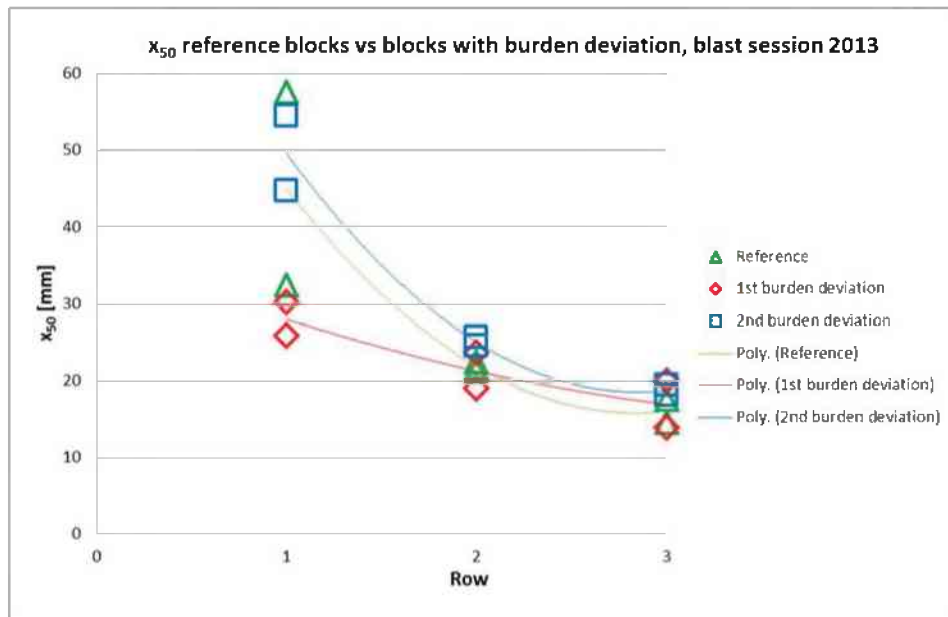


Figure 46: Percentile size x_{50} values plotted row wise, blast session 2013

It can be seen that x_{50} decreases with increasing row number. This is probably an effect of the first preconditioning of the mortar by the blasting of the 1st row, which causes backbreak and radial cracks in the previously intact material, see e.g. Johansson and Ouchterlony (2013) and Schimek et al. (2013). The third row, in turn, undergoes preconditioning from both rows 1 and 2 blasted in respective order. In the photographic documentation from Dal Farra (2012) and Navarro (2015), it was deduced that some cracks reaching the third row were in fact generated from blasting row 1. The COV in the fragmentation in the second and third rows appears to be somewhat smaller, compared to the fragmentation in the first row.

The average fragment size x_{50} for Row 1 is, with an exception in 1st burden deviation and one in Reference pattern, larger than half the nominal burden $B/2 = 35$ mm. This corresponds to a fragmentation behavior, which can be described as “dust and boulders”, i.e., relatively few large blocks and a fines tail (Johansson and Ouchterlony, 2013).

Figure 47 (see next page) shows the result of the sieving analysis of block CH01B05 (2nd burden deviation), fitted with the Swebrec function, which represents a typical “dust and boulders” behavior. The fines tail is well described by the Swebrec function, with an amplitude of less than 100 ($d = 85$ %). The large blocks are so few that it becomes difficult to describe the fragmentation by a continuous sieving curve; the latter is rather a continuous fines tail, with a discrete coarse part added.

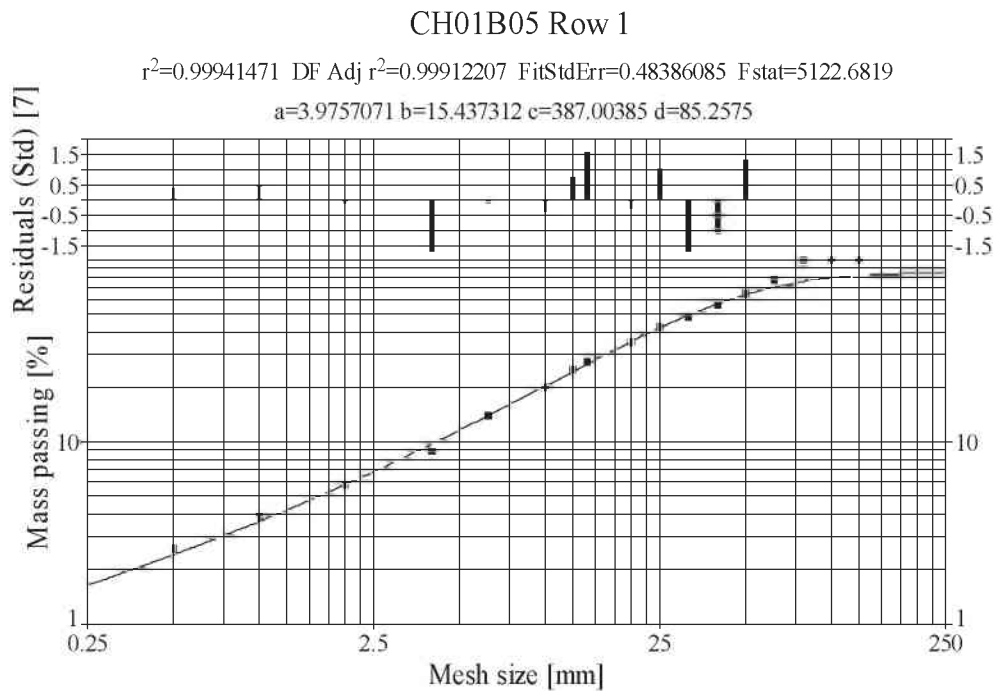


Figure 47: Sieving curve block CH01B04 and Swebrec curve fit (1st burden deviation)

Dust and boulders behavior in the first row is well known and Rustan et al. (1983) found that “dust and boulders” behavior occurs when the burden exceeds half the critical one ($B_{crit.}$); the closer one gets to the critical burden, the more sensitive the x_{50} and fragmentation become. Similar results were also found by Johansson and Ouchterlony (2013), who linked this mechanism with contribution to the large scatter in the 1st row.

For the second and third rows, Figure 48 shows that not only is the fragmentation finer, but the scatter is also smaller. It means in a sense that blast damage from previous rows improves the fragmentation and may help to decrease the scatter in the following rows’ results.

The second and third rows’ sieving curves were in general very well described by both three and five parameter Swebrec functions with 100 % amplitude (see also Appendix 5), i.e., there is much less dust and boulders type fragmentation in these rows. The data for the percentile size values x_{30} in Table 18 show pretty much the same behavior as the x_{50} data, see Figure 48.

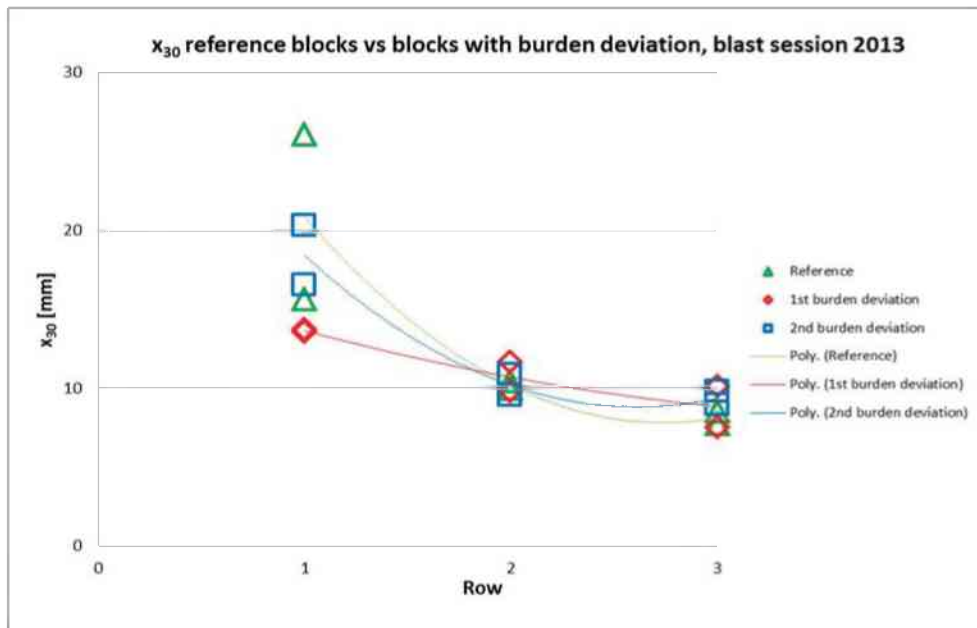


Figure 48: Percentile size x_{30} values plotted row wise, blast session 2013

Looking to the x_{80} values a large scatter in the data can be seen, especially for rows 1 and 2. For the third row the scatter is smaller.

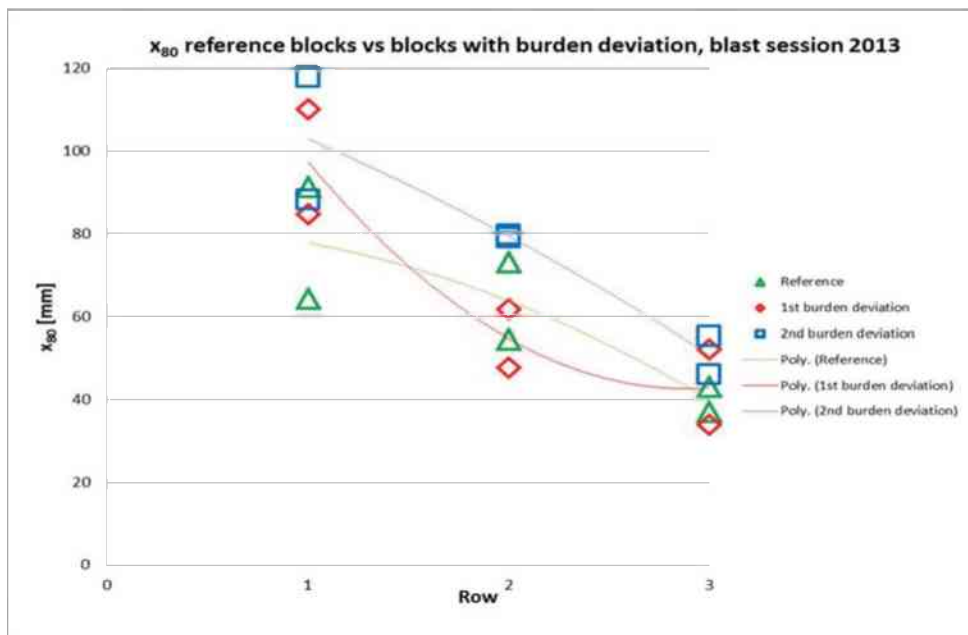


Figure 49: Percentile size x_{80} values plotted row wise blast session 2013

Summarizing the data, it can be seen that the largest scatter in the data has been observed in row 1 and that the values for x_{80} exhibit the largest scatter, compared to the values for x_{50} and x_{30} . In rows 2 and 3 the scatter is lower, in the third row there are almost no instances for dust and boulders behavior.

KW-ANOVA statistical evaluation of the sieving parameters was conducted for the sieving parameters, i.e., to find out if specific groups are significantly (statistically) different. The following groups have been compared for x_{80} , x_{50} and x_{30} values, for rows 1, 2 and 3 respectively (see Table 19):

- All three patterns together 1 row.
- All three patterns together 2 row.
- All three patterns together 3 row.

The results of the statistical evaluation showed with 95 % level of confidence that there is no significant difference between the means of the groups for x_{80} , x_{50} , x_{30} parameters within rows 1, 2 and 3 respectively. This was one reason why the testing in 2014 used three blocks for each drilling pattern instead of two.

Table 19: Statistical evaluation of the sieving parameters with the KW-ANOVA ($\alpha=0.05$), 3x5 data, blast session 2013

Row	Comparison x_{80}	H	$X^2(0.05)$	Sign.diff.
1	All three patterns together	1.14	4.57	No
2	All three patterns together	3.71	4.57	No
3	All three patterns together	2.00	4.57	No

Row	Comparison x_{50}	H	$X^2(0.05)$	Sign.diff
1	All three patterns together	3.43	4.57	No
2	All three patterns together	3.43	4.57	No
3	All three patterns together	1.14	4.57	No

Row	Comparison x_{30}	H	$X^2(0.05)$	Sign.diff
1	All three patterns together	3.43	4.57	No
2	All three patterns together	0.29	4.57	No
3	All three patterns together	1.14	4.57	No

Figure 50 shows the coefficient of uniformity for blast session 2013. The coefficients of uniformity (x_{80}/x_{30}) of the 1st row of the two Reference blocks are 3.5 and 4.1, of the 1st burden deviation is 8.0 and 6.2 and that of the 2nd burden deviation are 7.1 and 4.3. The low coefficient of uniformity values are due to the coarser blast fragmentation result in the first row obtained. It can be seen in 2nd row that there is a scatter in the data between the blocks from individual groups, representing the same blasthole pattern (see Reference and 2nd burden deviation patterns). In the 3rd row this scatter is not apparent.

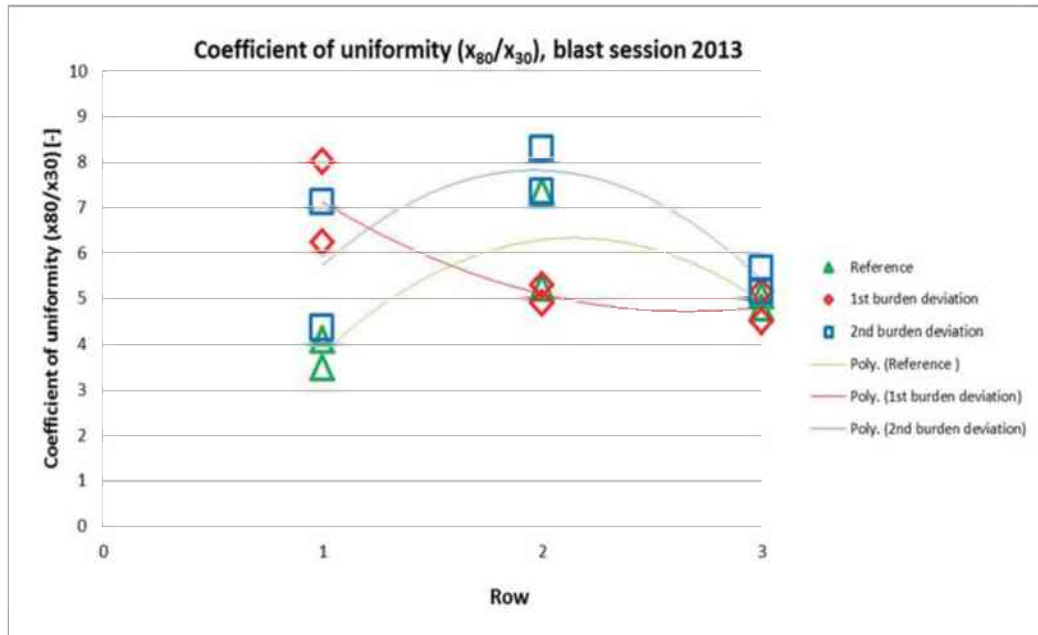


Figure 50: Coefficient of uniformity, blast session 2013

KW-ANOVA statistical evaluation of the Coefficient of uniformity was conducted, i.e. to find out if specific groups are significantly (statistically) different. The individual groups which have been compared for rows 1, 2 and 3 respectively are shown in the table below.

Table 20: Coefficient of uniformity x_{80}/x_{30} evaluation with KW-ANOVA ($\alpha=0.05$), 3x5 data, blast session 2013

Row	Comparison x_{80}/x_{30}	H	$X^2(0.05)$	Sign.diff.
1	All three patterns together	3.71	4.57	No
2	All three patterns together	2.57	4.57	No
3	All three patterns together	3.43	4.57	No

Although the scatter in the data apparent, which was larger in the first and second row, an influence on the coefficient of uniformity cannot be noticed. The results of the statistical evaluation showed with 95 % level of confidence that there is no significant difference between the means of the coefficient of uniformity parameters within rows 1, 2 and 3 respectively.

4.3.2 Fragmentation: blast session 2014

The complete results of the sieving analyses for each test are contained in Appendix 5, where the retained mass and mass-passing percentages, as well as the Swebrec function fits are given. The x_p -values for blast session 2014 are summed up in Table 21. The general observation from the table is again that the largest variance in the data is observed in row 1, compared to rows 2 and 3. The data has also some outliers, which will be discussed later in the chapter. It is not possible to make a direct comparison of all the data since different deviation patterns have been used. Hence, the data has been divided in individual groups.

Table 21: Sieving parameters blast session 2014

Block	Row	x_{30} [mm]	x_{50} [mm]	x_{80} [mm]	Coefficient of uniformity (x_{80}/x_{30})
B01 (Reference)	1	56.96	90.63	>125	
	2	12.28	29.07	67.07	5.46
	3	9.06	19.63	50.85	5.61
B06 (Reference)	1	11.34	22.03	48.47	4.27
	2	8.65	18.6	44.07	5.09
	3	5.83	12.61	33.94	5.82
B09 (Reference)	1	16.95	38.05	83.93	4.95
	2	8.07	16.37	39.24	4.86
	3	5.86	12.76	36.44	6.22
B03 (S+B variations)	1	9.41	23.69	71.03	7.55
	2	7.23	16.58	45.86	6.35
	3	9.17	19.25	49.62	5.41
B04 (S+B variations)	1	9.02	20.58	61.3	6.8
	2	6.3	15.67	53.5	8.49
	3	6.52	13.97	37.48	5.75
B10 (S+B variations)	1	19.07	43.76	103.83	5.44
	2	11.7	25.58	101.59	8.68
	3	9.44	18.62	42.23	4.47
B02 (S/4 shift)	1	19.67	46.92	90.01	4.58
	2	21.64	49.19	89.24	4.12
	3	11.42	22.02	48.24	4.23
B07 (S/4 shift)	1	30.14	79.13	102.74	3.41
	2	15.43	39.55	81.46	5.28
	3	8.80	17.8	42.68	4.85
B11 (S/4 shift)	1	17.83	39.12	90.75	5.09
	2	11.73	28.27	71.78	6.12
	3	10.89	21.49	48.83	4.49

The following comparison between the Reference blocks can be made:

- Block B01 gives very different values, compared to blocks B06 and B09, e.g., the variation in the 1st row is huge see the x_p values compared to B06 and B09, due to the very coarse fragmentation obtained. Thus block B01 was considered as an outlier and excluded from the further analysis, but kept in the further presentation of D_{mean} and the crack data analysis further in the report.
- Blocks B06 and B09 do not show good repeatability of the results in the 1st row; the coefficient of variation in x_{80} , x_{50} and x_{30} values, lies in range 28-38 %. The COV in x_{80}/x_{30} values is about 10 %.
- For the 2nd and 3rd rows, blocks B06 and B09 show a good repeatability of the results and the COV values are low (COV 5-9 % in 2nd and 0.1-4 % in 3rd row). The COV in x_{80}/x_{30} values lies in range 3-5 %.

The following comparison between the S+B variations pattern blocks can be made:

- Blocks B03 and B04: show good repeatability of the results in 1st row except for the x_{80} value. Block B10 has nearly double the x_{80} , x_{50} and x_{30} -values for the 1st row compared to B03 and B04. For the row 1 shots, the average COV lies in range 28-45 %. The COV in x_{80}/x_{30} values is about 16 %.
- For the second row COV lies in the range 28-45 %. The blocks B03 and B04 give a good repeatability of the results except the x_{80} for B04 (Table 21). Block B10 has nearly the double values for the x_{80} , 47 % higher values for x_{30} and 38 % higher value for x_{50} compared to B03 and B04. This explains the large values of COV. The COV in x_{80}/x_{30} values is about 17 %.
- For the third row, the COV lies in the range 14-19 % with acceptable repeatability. The COV in x_{80}/x_{30} values is about 13 %.

The following comparison between the S/4 shift pattern blocks can be made:

- For the first row of the S/4 shift pattern, the blocks do not show good repeatability of the results; the COV lies in range of 8-39 %. The COV in x_{80}/x_{30} values is about 20 %.

- The second row results do not show good repeatability of the results in x_{30} and x_{50} values where the COV is between 27-31 %, whereas for the x_{80} the COV is 11 %. The COV in x_{80}/x_{30} values is about 19 %.
- In the third row B02 and B11 gave similar results and B07 shows up to 28 % variation in the result. This is why the COV lies in the range of 7-14 %. The COV in x_{80}/x_{30} values is about 7 %.

Figure 51 gives an overview of the x_{50} reference blocks versus deviation patterns and rows respectively.

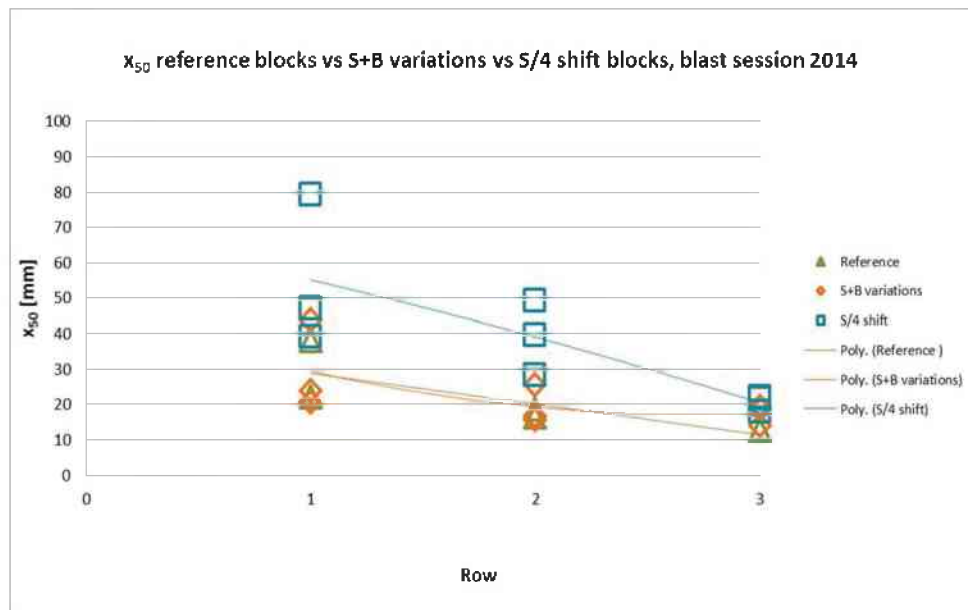


Figure 51: Percentile size x_{50} values plotted row wise for blast session 2014

From the Figure 51, it can be seen that there is the same tendency as in blast session 2013 for the x_{50} values to decrease with increasing row number. This phenomenon was described in the previous chapter. The scatter in the fragmentation in the third row appears to be smaller, compared to that in the first and second rows; it can be seen by comparing the COV values of the 1st row, with the values of rows 2 and 3. The general trend seen in Figure 51 is that the percentile size x_{50} for the S/4 shift pattern tends to be the highest. This behavior, contradicts the literature findings (Cunningham, 1983) who suggested that the fragmentation should be improved by shooting with a staggered pattern. The fragmentation in Row 1 can be described as “dust and boulders”, i.e. relatively few large blocks and a fines tail (see Appendix 5). Figure 52 shows the result of the sieving analysis of block B07 (S/4 shift), fitted with the Swebrec function, which is

a typical example of “dust and boulders” behavior. The fines tail is described by the Swebrec function with an amplitude of less than 100 ($d = 74\%$).

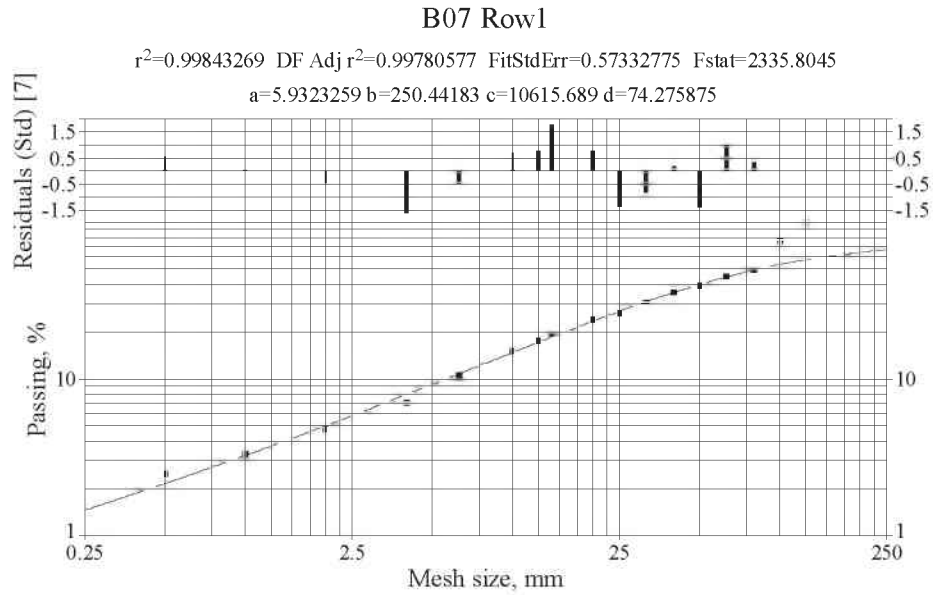


Figure 52: Sieving curve 1st row block B07 and Swebrec curve fit (S/4 shift)

For the second and third rows, the fragmentation is finer, and the scatter is smaller too. Figure 53 gives an example of a sieving curve for the third row, block B07 (S/4 shift), where it can be seen that the curve is well described by the Swebrec function.

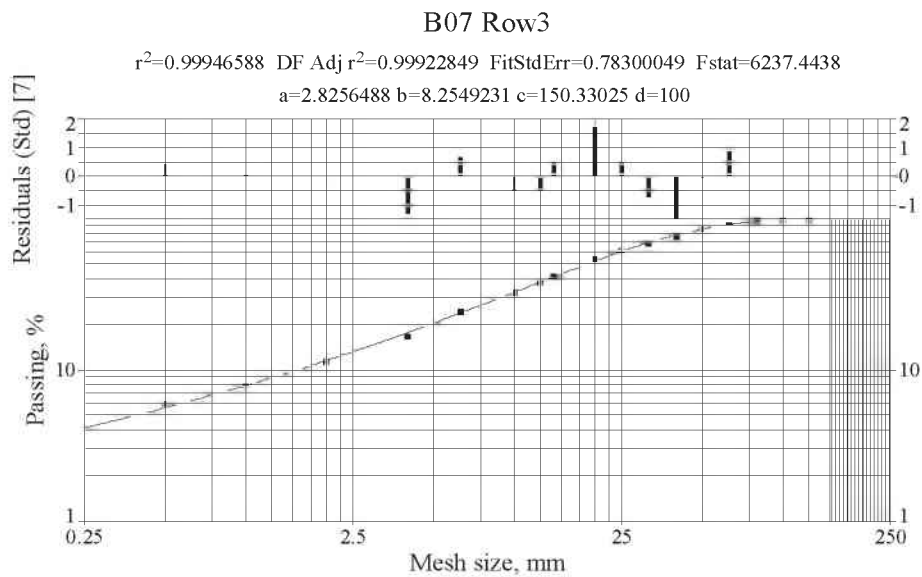


Figure 53: Sieving curve 3rd row block B07 and Swebrec curve fit (S/4 shift)

Looking to the x_{80} (see Figure 54) the tendency for the values to decrease with the increase of the row number is not apparent. A large scatter in the data can be seen, especially in the first and second rows. For the third row the x_{80} values show a scatter that is smaller. The S/4 shift pattern shows the largest x_{80} values compared to the Reference and S+B variations patterns.

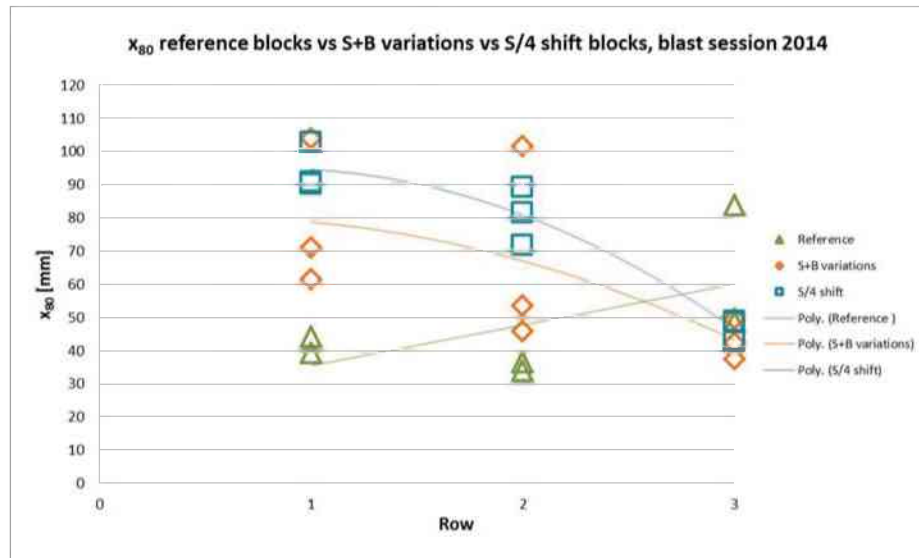


Figure 54: Percentile size x_{80} values plotted row wise for blast session 2014

The x_{30} values (see Figure 55) show that there is a large scatter in the data for row 1. For the second and third rows the scatter is substantially smaller. The S/4 shift pattern shows the largest x_{30} values compared to the one in the other two patterns.

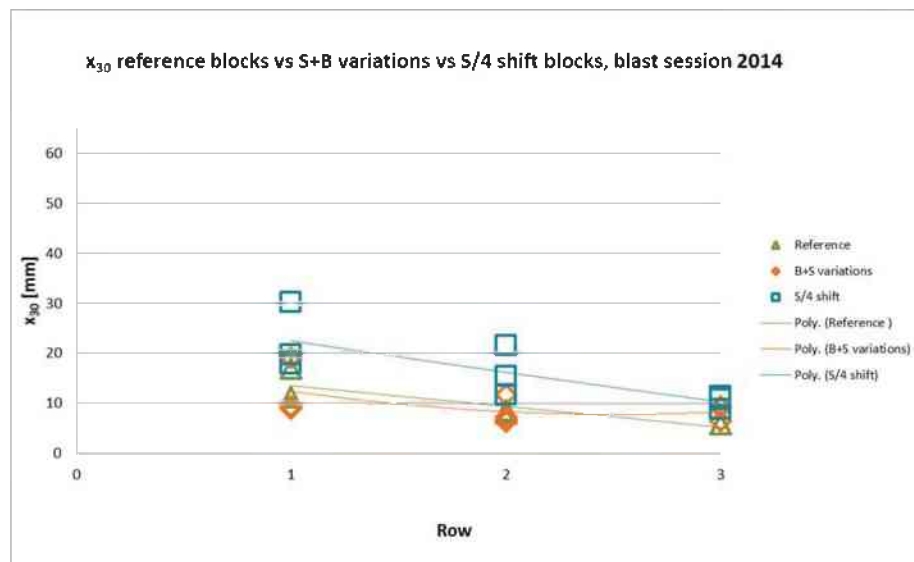


Figure 55: Percentile size x_{30} values plotted row wise for blast session 2014

Summarizing the data, it can be seen that the largest scatter in the data has been observed in row 1 (and that the values for x_{80} exhibit the largest scatter, compared to the values for x_{50} and x_{30}). For row 2 the scatter is substantial for the S/4 shift pattern; while in row 3 the scatter is lower. This is also supported by the sieving parameters and curves, described by the Swebrec function (Appendix 5).

Statistical evaluation of the sieving parameters was conducted in order to determine their significance, i.e., to find out if specific groups are significantly (statistically) different, by means of KW-ANOVA. The following specific groups have been compared for x_{80} , x_{50} and x_{30} values, rows 1, 2 and 3 respectively:

- All three patterns together 1st row.
- All three patterns together 2nd row.
- All three patterns together 3rd row.

The KW-ANOVA of the sieving parameters showed that there is no significant difference between the means of the groups for x_{80} , x_{50} and x_{30} , within rows 1, 2 and 3.

Table 22: Statistical evaluation of the sieving parameters with the KW-ANOVA ($\alpha=0.05$), 3x3 data, blast session 2014

Row	Comparison x_{80}	H	$X^2(0.05)$	Sign.diff.
1	All three patterns together	0.62	5.06	No
2	All three patterns together	0.82	5.06	No
3	All three patterns together	2.29	5.06	No

Row	Comparison x_{50}	H	$X^2(0.05)$	Sign.diff.
1	All three patterns together	2.22	5.06	No
2	All three patterns together	4.62	5.06	No
3	All three patterns together	2.76	5.06	No

Row	Comparison x_{30}	H	$X^2(0.05)$	Sign.diff.
1	All three patterns together	2.76	5.06	No
2	All three patterns together	5.06	5.06	No
3	All three patterns together	3.82	5.06	No

Looking to the coefficient of uniformity values, it can be seen that the coefficient of uniformity varies for the blocks from individual groups, representing the same drill pattern (see Figure 56). The scatter for rows 1 and 2 is the highest, as pattern S+B

variations depicts the highest value (see also Appendix 5, Table 59), whereas this scatter is lower for row 3.

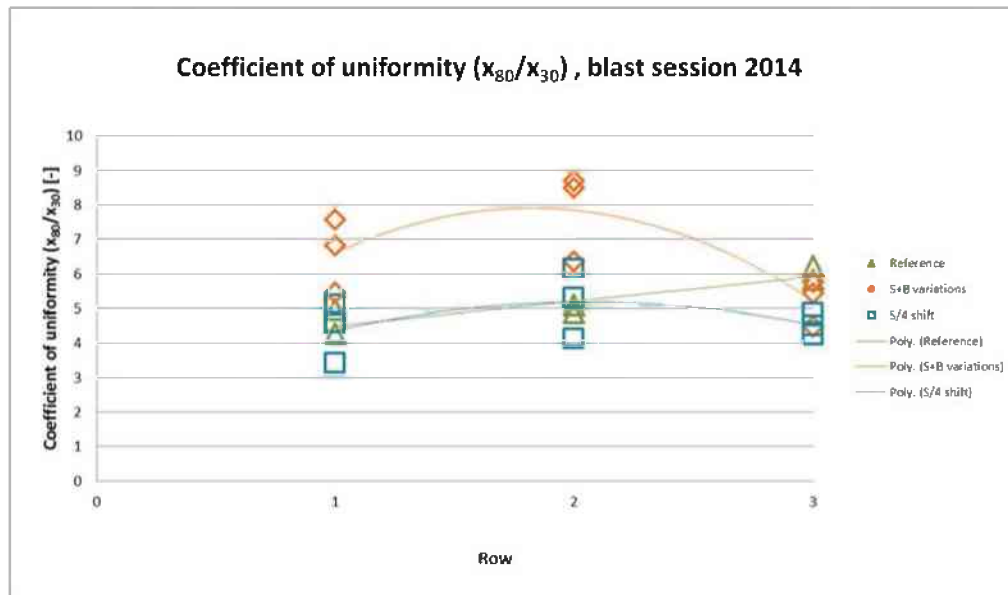


Figure 56: Coefficient of uniformity, blast session 2014

KW-ANOVA of the coefficient of uniformity was conducted i.e., to find out if specific groups are significantly (statistically) different. The individual groups which have been compared for rows 2 and 3 respectively are shown in the table below.

Table 23: Coefficient of uniformity x_{80}/x_{30} statistical evaluation with KW-ANOVA ($\alpha=0.05$), 3x3 data blast session 2014

Row	Comparison x_{80}/x_{30}	H	$\chi^2(0.05)$	Sign.diff.
1	All three patterns together row1	5.00	5.06	No
2	All three patterns together row 2	5.42	5.06	Yes
3	All three patterns together row 3	5.07	5.06	Yes

The KW-ANOVA evaluation of the coefficient of uniformity showed that the groups in the second and third rows are significantly different. From Figure 56 it can be seen that only the S+B variation pattern differs. It can be seen that the H-statistic in both row 1 and row 3 is pretty close to the critical Chi-squared values. Since the small samples exact quintiles are re-calculated and the new critical values are used (see also Chapter 3.14), the decision with regards to the null hypotheses can be different (Gregory and Foreman, 2009). As the results in rows 2 and 3 present borderline data, they may be questioned and interpreted as barely significant.

4.3.3 Equivalent n-values and x_c for blast sessions 2013 and 2014

From the sieving curves, equivalent n or uniformity index-values were calculated from fitting a Rosin-Rammler function to the x_{30} and x_{80} values in order to see if there were any changes when the distorted blasthole patterns were tested. The steps for equivalent n-calculation can be written as follows, starting from the RR cumulative fragment size distribution function:

$$P = 1 - 2^{-(x/x_{50})^n} \quad \text{Equation 31}$$

and rearranged as:

$$1 - P = 2^{-(x/x_{50})^n} \Rightarrow \frac{1}{(1-P)} = 2^{(x/x_{50})^n} \quad \text{Equation 32}$$

$$\ln\left[\frac{1}{(1-P)}\right] = \ln 2 \cdot (x/x_{50})^n \quad \text{Equation 33}$$

$$\left[\frac{\ln(1/(1-0.8))}{\ln(1/(1-0.3))}\right]^{1/n} = (x_{80}/x_{30}) \quad \text{Equation 34}$$

The calculated value $\ln(B)$, where B is the ln-ratio inside the brackets [...] is =1.506 thus the equivalent n-value can be written as:

$$n_{equiv.} = \frac{\ln B}{\ln(x_{80}/x_{30})} \Rightarrow \frac{1.506}{\ln(x_{80}/x_{30})} \quad \text{Equation 35}$$

For this equivalence to be meaningful, the equivalent x_{50} -value calculated from the x_{30} - x_{80} fit has to be nearly the same as the interpolated x_{50} -values in Table 18 and Table 21. This is typically not the case when there is an extreme dust and boulders effect. Then there is kink in the mass passing curve (see Figure 52) which destroys the agreement between the two x_{50} values. Thus the row 1 data have been checked and some n_{equiv} values judged as invalid, among them the data for the outlier block B01. The following figures give a plot-summary of the corresponding n-values for the blast sessions 2013 and 2014 respectively. The numerical data is given in Appendix 5.

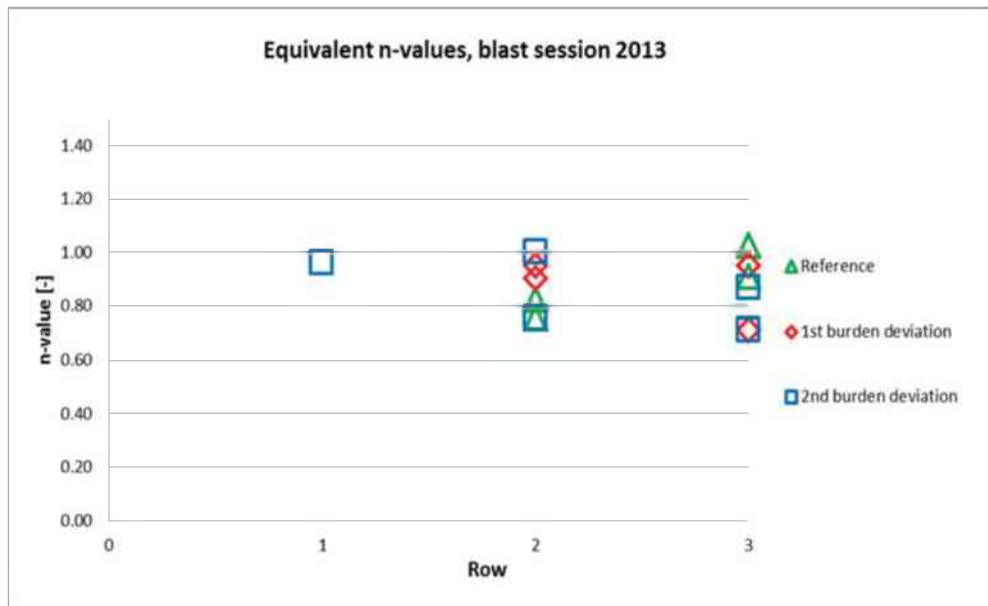


Figure 57: Equivalent n-values, blast session 2013 without invalid values

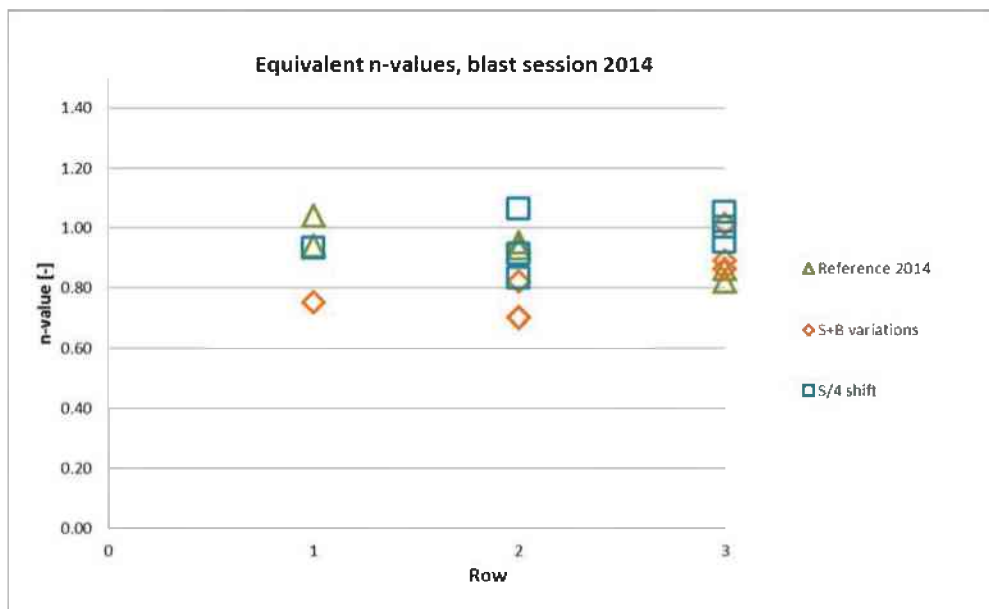


Figure 58: Equivalent n-values, blast session 2014 without invalid values

Similar average equivalent n-values can be seen in both session 2013 and 2014 reference patterns. The equivalent n-value for the blocks from the groups 2nd burden deviation shows a very small decrease, but the 1st burden deviation data remain the same. A general tendency in Figure 57 and Figure 58 (see also Appendix 5) is that the equivalent n-values for the staggered pattern are the highest and for the S+B variations the lowest.

The S/4 shift pattern showed a 9 % higher n-value compared to the reference pattern, while the S+B variations pattern with uncorrelated collaring errors ΔS and ΔB in S and B directions respectively has shown a 7 % decrease in the n-value (see also Appendix 5 Table 58). A summary of the statistical evaluation with KW-ANOVA, of the valid equivalent n-values is given in the following table.

Table 24: Statistical evaluation of n-values values with the KW-ANOVA $\alpha=0.05$), 3x2 and 3x3 data, blast sessions 2013 and 2014

Row*	Comparison blast session 2013	H	X ² (0.05)	Sign.diff.
2	All three patterns together row 2	1.50	4.57	No
3	All three patterns together row 3	2.21	4.57	No
Row*	Comparison blast session 2014	H	X ² (0.05)	Sign.diff.
2	All three patterns together row 2	5.14	5.06	Yes
3	All three patterns together row 3	4.20	5.06	No

*The invalid values in row 1 have been excluded from the analysis

The KW-ANOVA of the equivalent n-values showed, that there was no significant difference between the means of the groups for Reference blocks, 1st and 2nd deviation pattern blocks in blast session 2013.

In blast session 2014 the row 2 results showed that there was a significant difference between the means of the groups, when all three patterns were combined. From Figure 58, it can be seen that the S+B values are the one which cause the variation in the results. From Table 24 it can be also seen that the H-value in row 2 is marginally on the wrong side of Chi-squared. Moreover the both values are close to the border, thus the conclusion may be not very exact. The analysis also shows that there was no significant difference between the group means in row 3 when the data for Reference blocks, S+B deviation and S/4 shift pattern blocks were combined.

Additionally to the equivalent n-values, the equivalent x_c sizes from the sieving curves, equal to the fragment size at 63.2 % passing, were calculated, to see if there were any changes when the distorted blasthole pattern were tested. The calculation of x_c was done by a linear interpolation between the two fragment sizes next to the cumulative mass passing at 63.2 %, as follows:

$$x_c = x_u + \frac{x_0 - x_u}{P_0 - P_u} \cdot (P_{63.2} - P_u) \quad \text{Equation 36}$$

A summary of the equivalent x_c -values is given in Table 59, where the data in the first row has been excluded when calculating averages, due to the large scatter in the values, as well as block B01, which was considered as an outlier.

Table 25 gives the KW-ANOVA evaluation of the equivalent x_c -values in sessions 2013 and 2014.

Table 25: Statistical evaluation of x_c -values values, with the KW-ANOVA ($\alpha=0.05$), 3x2 and 3x3 data, blast sessions 2013 and 2014

Row	Comparison blast session 2013	H	$X^2(0.05)$	Sign.diff.
2	All three patterns together row 2	3.43	4.57	No
3	All three patterns together row 3	2.57	4.57	No

Row	Comparison blast session 2014	H	$X^2(0.05)$	Sign.diff.
2	All three patterns together row 2	5.42	5.06	Yes
3	All three patterns together row 3	5.07	5.06	Yes

In blast session 2013 there is no significant difference between the means of the groups for Reference blocks, and 1st and 2nd burden deviation pattern blocks. In blast session 2014, the analysis shows that there was a significant difference between the group means when the data from reference, S+B variations and S/4 shift patterns in 2014 are combined.

From the Table 25, it can be seen that in both cases, blast session 2014 row 2 and row 3, the H statistic is very close to the critical Chi-squared values. Therefore as the result represents borderline data, it may be interpreted as barely/or not significant (see Chapter 4.3.2)

4.3.4 Summary of fragmentation findings

Summarizing the data, in both sessions 2013 and 2014 it can be seen that the variation of the sieving parameters of row 1 is quite large. The majority of the tests showed an average size x_{50} larger than half the burden. The corresponding size distributions are characterized as showing “dust and boulders” behavior. Because of this the first intact or “free” row with virgin material is not a good representation of a real blast situation. Moreover the bench front is unrealistically even and smooth, thus a detailed analysis of the results from row 1 would be less meaningful and has been excluded.

Continuing to the rows 2 and 3 results, there is a finer fragmentation and almost no tendency for dust and boulders behavior. The data reveal a smaller scatter, which is more apparent in the x_{50} and x_{30} values, than in x_{80} . Looking to the x_{50} percentile values, it was seen that a somewhat coarser fragmentation was achieved with S+B variations and the S/4 shift patterns in both rows 2 and 3, while for the rest of the blasthole patterns, no effect on x_{50} was detected.

Despite those findings the overall statistical evaluation of all the x_{30} , x_{50} and x_{80} values showed that the fragmentation was not significantly influenced by any of the tested types of drillhole deviations. Moreover, the bad repeatability of the fragmentation data between block pairs with the same blasthole pattern was observed. The large average relative differences (18 % in session 2013 and 24 % in session 2014) underline the difficulty of finding any significant effect of the pattern changes that have been made. Continuing to the x_c results, the statistical evaluation, see Table 25 showed no statistical difference between the means of the pattern groups in session 2013, while the values in session 2014 showed statistical differences between the means of the pattern groups. Again when looking to the data, it can be seen that the data is borderline and that mainly the values in S+B variation stick out.

Table 26 shows a summary of the average effect on the equivalent n-values of the different blasthole patterns, where the obtained and expected changes in n-values are given as $\Delta n = n_{\text{equiv}} - n_{\text{ref}}$. The average n_{equiv} value for the respective reference blocks derived from Equation 34 are used.

Table 26: Expected and obtained equivalent n-values, blast sessions 2013 and 2014

Pattern	n	Obtained Δn	Expected Δn
Reference 2013	0.88	-	-
1st burden deviation	0.88	0 %	-23.0 %
2nd burden deviation	0.84	-4.6 %	-23.0 %
Reference 2014	0.89	-	-
S+B variations	0.83	-6.8 %	-15.0 %
Total effect (excl. S/4 shift)		-3.0 %	-
S/4 shift	0.97	(+9.0 %)	+10.0 %

It can be seen that the average equivalent n-values in both blast session 2013 and 2014 reference patterns are very similar. The equivalent n-value for the blocks with 1st

burden variation does not change, while the values in 2nd burden deviation shows only about a 5 % decrease. In the S+B variations pattern the decrease in the average equivalent n-value is the lowest, about 7 %. Those changes are far away from the expected ones with regards to the Kuz-Ram formula (see Chapter 2.6 and Table 26).

If the observed changes are significant is also questionable. The statistical evaluation of the equivalent n values, in Table 24 showed that the only significant difference between the means of the groups was in row 2, session 2014, when all three patterns were compared and, mainly caused by the variations in the S+B variations pattern (see Figure 58). The data was borderline, i.e. barely significant.

If one calculates the effect in all three samples from S+B variations for row 2, with regards to the equivalent n-values, the expected changes for row 2 would be a reduction of the value of 21 %. On the other hand, in row 3, the reduction is only 6 %. If one assumes that the changes in the equivalent n-values should be equal, i.e. the same effect is acting on the equivalent n-values for all deviation patterns, the average effect on all the reference pattern is only 3 %, thus it is highly doubtful if a systematic effect of drillhole deviations on fragmentation exists, at least for the patterns with collaring deviations and straight vertical holes studied here in row-by-row blasting of 2D models with an unconfined bottom.

Comparing the effect on staggered (S/4 shift) pattern on the fragmentation it can be seen that the equivalent n-values increase by 9 %.

Evaluation of the fragmentation data of Shimek (2015) was done to check the effect of the staggered pattern. He has blasted 2 blocks with S/B ratio 1.57, 4 rows with 5 blastholes per row, one reference block and one with a staggered pattern. The evaluation of his sieving data showed that the average equivalent n-values decreased for the staggered pattern: from 1.05 to 0.89. Schimek's results are contrary to the results found in this thesis; moreover the combined result points to no effect of the staggered pattern, which is contrary to the literature findings (Cunningham, 1983, 2005).

With regards to the uniformity coefficient x_{80}/x_{30} values, the statistical evaluation showed no difference between the values in session 2013, while in session 2014, there was a difference for the data in rows 2 and 3, where H statistic was very close to the critical

Chi-squared values. As the results are borderline data, they may be interpreted as almost insignificant (see Chapter 4.3.2, Table 23).

Summarizing the findings, the analysis showed that the percentile size values x_p (P= 30, 50 and 80 %) were not affected by the drillhole deviation patterns tested. The uniformity coefficient x_{80}/x_{30} results did not show very convincing results about any influence either. The uniformity coefficients x_{80}/x_{30} may be seen as a transformation of the equivalent n -values, which gave similar borderline values in session 2014.

All the statistically significant results were borderline data, i.e. the H value lay very close to the Chi-square limit. Thus what is a significant difference for one variable x_{30}/x_{80} , n_{equiv} , x_c or x_{50} , may be insignificant for others. A slightly smaller α would have removed this inconsistency. The tables for both KW-one way ANOVA test and MWU-test don't make it possible to calculate the p-values for the tests. Taking into account that the samples per pattern blasted were 2 in blast session 2013 and 3 in blast session 2014 the results with regards to fragmentation may be questioned and treated as insignificant ones. More data would help give a more conclusive answer for the fragmentation results.

4.4. Damage results

In this thesis "Damage" is related to both the surface and interior of the remaining rock. Three different formats were used for the damage related investigation. Firstly, the surface damage on the crest and the bench face was investigated by both visual observation and investigation of back break (surface unevenness) and surface roughness. Then the interior damage was observed by investigating the crack development in cut slices of block remnants and then the exterior damage was observed on the top surface on the testing blocks. A detailed description of the results is given later in the report.

4.4.1 Results from visual bench face control

The row-wise blasting of the 3 rows with 7 holes for the blocks in 2013 and 2014 was always initiated from the right side of the block.

Figure 59 gives an example of a bench surface front view of a blasted block with reference pattern. The breakout angle between the holes was approximately 180° , at the edges of the block this angle was somewhat smaller. After each blast, all seven half-casts were visible. At the top of every blasthole a thin section flaked off. An excessive backbreak with deep trenches behind the second and third rows was observed in block B01 (Appendix 4). All the bench surfaces of the reference block B06 had deep trenches in both left and right sides. Similar surfaces can be seen in the other Reference blocks.



Figure 59: Front view after blasting of Reference block B06 row 1

For the testing blocks with the 1st burden deviation pattern, the breakout angle between the holes followed the pattern and was in this sense different from 180° break out in the reference blocks. Figure 60 gives an example of the bench surface for the 1st burden deviation pattern. After each blast, all seven half-casts were visible. At the top of every blasthole a thin section flaked off. In some of the rows, several deep trenches could be seen. An excessive backbreak was observed in block CH01B02, row 3. The fresh blasted bench surface became rougher for this pattern. After blasting of the rows 1 and 2, several clearly visible cracks, going to the next row burden were detected.



Figure 60: Front view after blasting of 1st burden deviation pattern CH01B02, row 1

For the testing blocks with the 2nd burden deviation pattern, the breakout angle between the holes again followed the drill pattern. Figure 61 gives an example of the bench surface after the 2nd deviation pattern. The side angles of the testing blocks were influenced by the pattern. After each blast, all seven half-casts were visible, except hole 5 for CH03B02, Row 1 (see Figure 61). An excessive backbreak was observed in block CH03B02, Rows 2 and 3. The fresh blasted bench surface was rougher for this pattern and deep trenches were visible in some rows. After the blasting of the first row, one clearly visible crack going to the next row burden was detected, for CH03B01.



Figure 61: Front view after blasting of 2nd burden deviation pattern CH03B02, row 1

For the testing blocks with the S+B variations pattern, the breakout angle between the holes again followed the drilled pattern. Figure 62 gives an example of the bench

surface after Row 1 blasted in B+S variations pattern. After each blast, all seven half-casts were visible. The fresh blasted bench surface was rougher for this pattern and deep trenches were visible. An excessive backbreak was observed in most of the rows. No visible cracks were observed behind the holes or going to the next row burden.



Figure 62: Front view after blasting of S+B variations pattern B04 row 1

For the S/4 pattern, the bench surface in between the blastholes was very smooth and regular and had comparable bench surface properties as the Reference pattern, see Figure 63. No surface cracks behind the holes or going to the next row burden were detected. The only backbreak was observed at B07, Row 3 (see Appendix 3)



Figure 63: Front view after blasting of S/4 shift pattern B07 row 1

The results of the visual bench face control in session 2013 and session 2014 are given in following tables. The corresponding documented pictures of the blocks, taken before and after blasting of each row, are given in Appendix 4.

Table 27: Overview of the visual bench face control: blocks blast session 2013

Block #	Row #	Visible half casts, holes #	Breakage angle between holes	Visible cracks behind holes #	Deep trenches	Other observations
CH01B03 (Reference)	1	1-7	follows pattern	no	left	crest flaking
	2	1-7	follows pattern	no	left, right	crest flaking
	3	1-7	follows pattern	no	no	crest flaking, air pockets observed in yoke
CH01B05 (Reference)	1	1-7	follows pattern	no	right	crest flaking
	2	1-7	follows pattern	no	left, right	crest flaking
	3	1-7	follows pattern	no	no	crest flaking
CH01B02 (1st burden dev.)	1	1-7	follows pattern	2,4,7	left, right	crest flaking, crack 7 goes to 3 row burden
	2	1-7	follows pattern	2,7	left, right	crest flaking
	3	1-7	follows pattern	no	left, right	large backbreak
CH01B04 (1st burden dev.)	1	1-7	follows pattern	no	left, right	crest flaking
	2	1-7	follows pattern	5	left, right	crest flaking
	3	1-7	follows pattern	no	left	crest flaking
CH03B01 (2nd burden dev.)	1	1-7	follows pattern	7	right	crest flaking
	2	1-7	follows pattern	no	no	crest flaking
	3	1-7	follows pattern	no	no	crest flaking
CH03B02 (2nd burden dev.)	1	not #5	follows pattern	no	left	crest flaking
	2	1-7	follows pattern	no	left, right	backbreak
	3	1-7	follows pattern	no	no	backbreak

Table 28: Overview of the visual bench face control: blocks blast session 2014

Block #	Row #	Visible half casts, holes #	Breakage angle between holes	Visible cracks behind holes #	Deep trenches	Other observations
B01 (Reference)	1	1-7	follows pattern	no	left	crest flaking
	2	1-7	follows pattern	2,4	left, right	backbreak
	3	1-7	follows pattern	no	left, right	crest flaking
B06 (Reference)	1	1-7	follows pattern	no	no	crest flaking
	2	1-7	follows pattern	no	left, right	backbreak
	3	1-7	follows pattern	no	no	crest flaking
B09 (Reference)	1	1-7	follows pattern	no	right	crest flaking
	2	1-7	follows pattern	no	left, right	crest flaking
	3	1-7	follows pattern	no	no	crest flaking
B03 (S+B variations)	1	1-7	follows pattern	no	left	backbreak
	2	1-7	follows pattern	no	left	backbreak
	3	1-7	follows pattern	no	right	crest flaking
B04 (S+B variations)	1	1-7	follows pattern	no	left	backbreak
	2	1-7	follows pattern	no	left, right	backbreak
	3	1-7	follows pattern	no	left, right	crest flaking
B10 (S+B variations)	1	1-7	follows pattern	no	left, right	crest flaking
	2	1-7	follows pattern	no	right	backbreak
	3	1-7	follows pattern	no	right	crest flaking
B02 (S/4 shift)	1	1-7	follows pattern	no	left	crest flaking
	2	1-7	follows pattern	no	left, right	crest flaking
	3	1-7	follows pattern	no	left	crest flaking
B07 (S/4 shift)	1	1-7	follows pattern	no	no	crest flaking
	2	1-7	follows pattern	no	no	crest flaking
	3	1-7	follows pattern	no	no	backbreak
B11 (S/4 shift)	1	1-7	follows pattern	no	no	crest flaking
	2	1-7	follows pattern	no	left, right	crest flaking
	3	1-7	follows pattern	no	left, right	crest flaking

4.4.2 Surface damage

This Chapter describes the main results, for the surface damage characteristics of the bench face, achieved by blasting using different blasthole patterns. The method of measuring the blasted surface characteristics was described in Chapter 3.13. The numerical data are given in Appendix 12 (see Table 82 and Table 83).

Two parameters, D_{mean} and S_{norm} were used to quantify the surface damage characteristics: D_{mean} , defined as the mean distance of the individual data points to the reference line (see equation 18); and S_{norm} , defined as the normalized slope inclination of the individual sections of the contour lines (see equation 19). For each horizontal contour line, at heights of 5, 10 and 15 cm, the D_{mean} data are plotted both individually and then combined into a single average value for the whole surface, where a positive D_{mean} (+) represents a backbreak and a negative D_{mean} (-) represents an underbreak. With regards to S_{norm} , it was found that the values were not reproducible (see Appendix 11) thus the results are only presented there.

The D_{mean} data are given in Figure 64. Each D_{mean} value represents a specific line height (3 values) and row no. (1-3) in specific block of a given pattern group (2 or 3 samples); altogether 54 data for blast session 2013 and 72 data for blast session 2014. The main results are given below, covering several evaluations of D_{mean} dependency on: mortar batch; height of contour line; blasthole pattern and row.

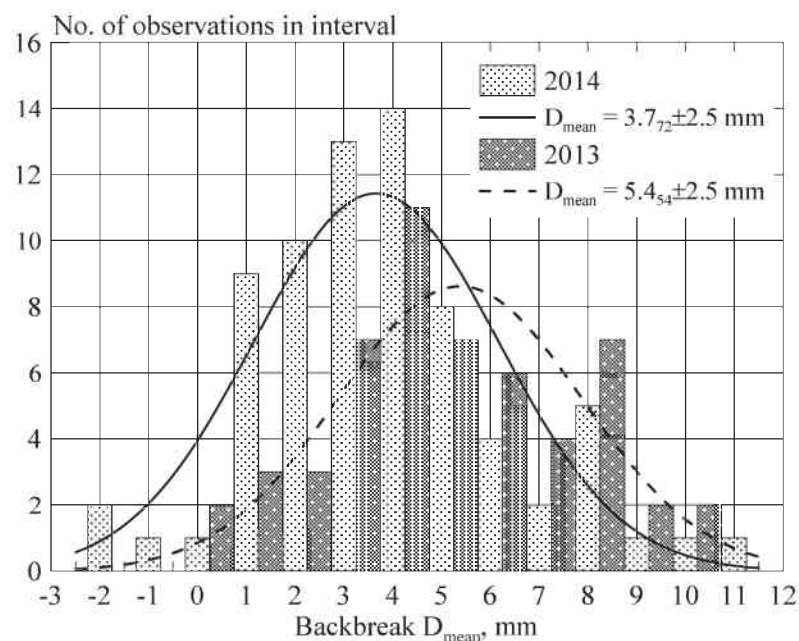


Figure 64: D_{mean} for individual blocks, blast sessions 2013 and 2014

Figure 64 shows a histogram-plot of the D_{mean} data for individual lines. The mean backbreak for both sessions is around half of the borehole diameter and both histograms in Figure 64 follow the normal distribution reasonably well. Thus a two-sample t-test was used to determine if the two population means of the D_{mean} values are equal. The results are given in the table below.

Table 29: Statistical evaluation of D_{mean} -values, with the two-sample t-test of variance ($\alpha=0.05$)

Combination	t	p-value	t_{crit}	Sign.diff.
Session 2013 / Session 2014	3.77	0.0026	1.98	Yes

The test showed that the specimens in blast session 2013 gave significantly higher D_{mean} values, compared to the specimens in blast session 2014. This result can be correlated with the different mechanical properties of the material in blast sessions 2013 and 2014, thus leading to changes in the surface characteristics. Figure 65 shows the average D_{mean} values vs. P-wave velocity per block, plotted for blast sessions 2013 and 2014.

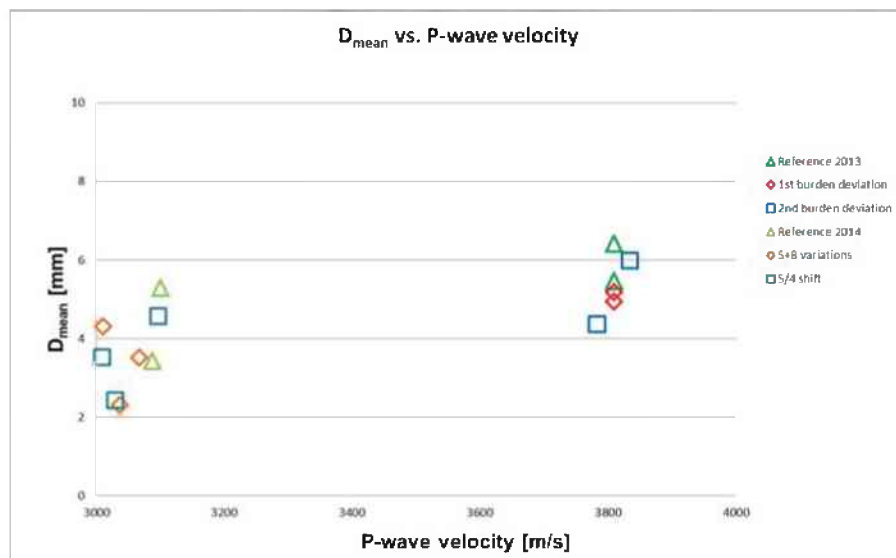


Figure 65: D_{mean} vs. P-wave velocity

Figure 65 shows that D_{mean} is positively correlated with the P-wave velocity. The same is true for the D_{mean} vs. E_{dyn} , density and UCS. No literature reference was found for the correlation between backbreak and any material properties (P-wave velocity, density, E_{dyn} or UCS).

To evaluate the effect of line height on D_{mean} , the average D_{mean} values over rows and pattern group (class) have been calculated for each height, leaving three averages per

height and class. For each class ANOVA has then been used to evaluate if the variation with line height is significant (3 classes with 6 data each in blast session 2013 and 3 classes with 6 or 9 data in blast session 2014). The results are presented in Table 30.

Table 30: Statistical evaluation of D_{mean} of the individual line heights and patterns with the One-way ANOVA ($\alpha = 0.05$), per block, blast sessions 2013 and 2014

Drill Pattern group	F	F _{crit}	p-value	Sign.diff.
Reference (2 blocks)	0.01	3.68	0.99	No
1st burden deviation (2 blocks)	0.01	3.68	0.99	No
2nd burden deviation (2 blocks)	0.58	3.68	0.57	No
Reference (2 blocks)	0.09	3.68	0.91	No
S+B variation (3 blocks)	1.37	3.40	0.27	No
S/4 shift (3 blocks)	0.06	3.40	0.93	No

The evaluation showed that there was no significant difference between the mean D_{mean} values from the individual classes. It means that there is no visible influence of the line height compared to variations with row and chance.

Figure 66 shows a box and whisker plot of the D_{mean} data with median (the middle line) and indicated outliers for each blasthole pattern blasted in blast sessions 2013 and 2014. Each data set is based on the three horizontal contour lines for the 1st, 2nd and 3rd row and blocks with the same blasthole pattern.

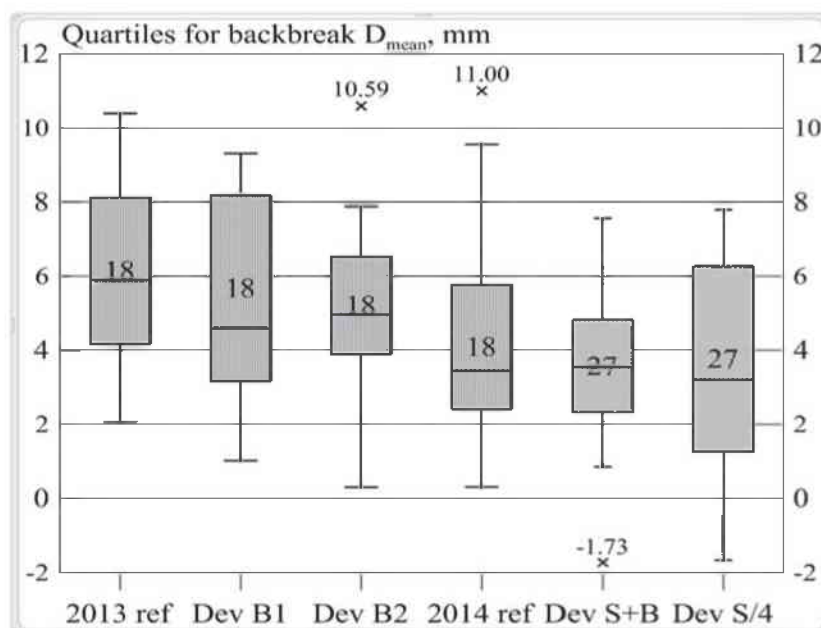


Figure 66: D_{mean} data for individual blasthole pattern groups, blast sessions 2013 and 2014

From Figure 66, it can be seen that the groups with both reference and distorted patterns showed no clear trend of either larger or smaller backbreak. Therefore to evaluate the “combined” effect of the individual D_{mean} values, since the influence of the line height is insignificant, the D_{mean} data from the height classes have been merged and average D_{mean} values for each pattern group calculated. For each year ANOVA has then been used to evaluate if the variation with drill pattern is significant (3 groups with 18 data each in blast session 2013 and 3 groups with 18 or 27 data each 2014). The result is shown in the following Table 31.

Table 31: Statistical evaluation of average D_{mean} of the average rows and line heights with One-way ANOVA ($\alpha = 0.05$), 6 blocks x 3 rows data (session 2013) and 8 blocks x 3 rows data (session 2014)

Comparison D_{mean}	Block	F	F_{crit}	p-value	Sign. diff.
Blast session 2013	all blocks	0.64	3.17	0.53	No
Blast session 2014	all blocks	0.92	3.13	0.40	No

The results in both blast sessions 2013 and 2014 showed that there was no significant difference between the mean D_{mean} values from the individual blocks and blasthole patterns. This means, that looking to the combined effect (see Figure 66) the influence of the blasthole patterns on the backbreak is insignificant. Figure 67 (blast session 2013) and Figure 68 (blast session 2014) show the D_{mean} values for the individual contour lines plotted row-wise.

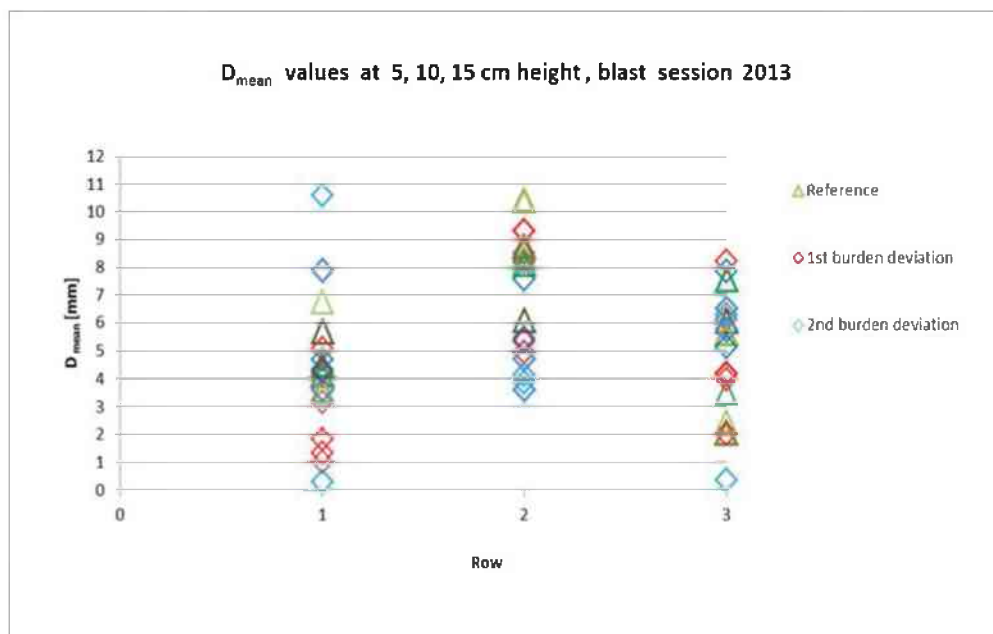


Figure 67: D_{mean} values at 5, 10 and 15 cm height, session 2013

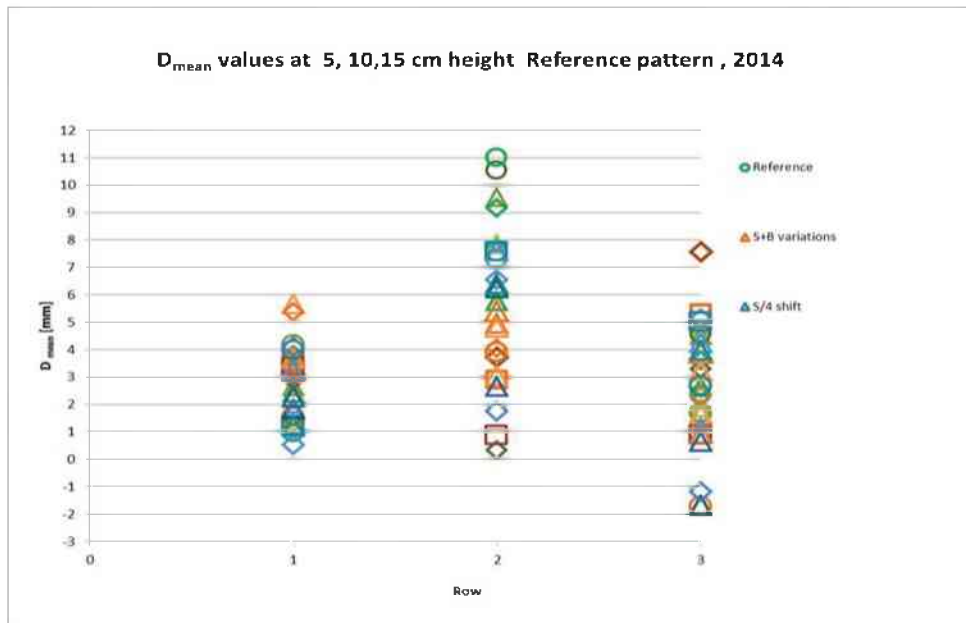


Figure 68: D_{mean} values at 5, 10 and 15 cm height, blast session 2014

A statistical evaluation of the individual D_{mean} data was carried out using the MWU-Test to see if there is a difference between the values from the rows 1, 2 and 3 (see Figure 67 and Figure 68), for the different blasthole patterns. The MWU-Test was chosen as method for analysis, due to the small number of the groups tested as well as the small number of data points. The results for blast session 2013 are given in Table 32.

Table 32: Statistical evaluation of D_{mean} data of the individual rows and line heights with MWU-Test ($\alpha = 0.05$), 6x2 data, blast session 2013

Drill Pattern	Rows	Z_{score}	Z_{critical}	Sign.diff.
Reference	1 to 2	2.72	1.64	Yes
	1 to 3	0.16	1.64	No
	2 to 3	2.56	1.64	Yes
1 st burden deviation	1 to 2	2.56	1.64	Yes
	1 to 3	1.28	1.64	No
	2 to 3	2.24	1.64	Yes
2nd burden deviation	1 to 2	0.01	1.64	No
	1 to 3	0.48	1.64	No
	2 to 3	1.12	1.64	No

The analysis in blast session 2013 showed that the D_{mean} values from row 2 were significantly different from the values of rows 1 and 3 for the reference and 1st burden variation patterns, i.e. for these patterns significantly more backbreak was observed in the second row. In the 2nd burden deviation pattern blocks, the D_{mean} values of rows 1,

2 and row 3 showed no significant differences, i.e., there was no trend for more backbreak in the second row. The results from the statistical evaluation of the individual D_{mean} data using the MWU-Test for blast session 2014 are given in Table 33.

Table 33: Statistical evaluation of D_{mean} of the individual rows and line heights with MWU-Test ($\alpha = 0.05$), 2x6 (B01 excluded) and 2x9 data, blast session 2014

Drill Pattern	Rows	Z _{score}	Z _{critical}	Sign.diff.
Reference	1 to 2	1.92	1.64	Yes
	1 to 3	0.16	1.64	No
	2 to 3	1.92	1.64	Yes
S+B variations	1 to 2	0.39	1.64	No
	1 to 3	1.19	1.64	No
	2 to 3	1.10	1.64	No
S/4 shift	1 to 2	2.78	1.64	Yes
	1 to 3	0.39	1.64	No
	2 to 3	2.69	1.64	Yes

The analysis for individual levels in both reference pattern and S/4 shift pattern, showed that mean D_{mean} values from row 2 were significantly different from those of rows 1 and 3, i.e. more backbreak was observed in the second row. In the S+B variations pattern, none of the D_{mean} values showed a significant difference, i.e., there was no trend for more backbreak in the second row.

4.4.2.1. Summary of the surface damage findings

Summarizing the results, the specimens in session 2013 gave higher D_{mean} values, compared to the specimens in blast session 2014 and this difference in D_{mean} values is significant, i.e. there is a difference between the results for the different mortar batches. This result can be correlated with the different mechanical properties of the material in blast sessions 2013 and 2014, leading to changes in the backbreak.

The evaluation in Table 30 showed that there was no significant difference between the mean D_{mean} values for the individual heights and patterns in any of the rows. It indicates that there is no influence of the line height compared to variations with row and chance for the same pattern, and the repeatability of the samples blasted with the same drill pattern is reasonable. It can be seen that the influence of the height level is no stronger than the variation within the pattern groups for all rows and patterns.

The results in both sessions 2013 and 2014, showed that there was no significant differences between the mean D_{mean} values from the individual blocks, i.e. the “combined” effect (see Figure 66) of the drilling patterns on the backbreak is insignificant. This means that the backbreak is not influenced by the blasthole patterns under these conditions: row-by-row blasting of 2D small scale models with an unconfined bottom, patterns with collaring deviations and straight vertical holes.

From Table 32 and Table 33 it was observed that in four out of six drill patterns, the D_{mean} value is significantly larger after row 2, than after rows 1 and 3. These results are correlated to both the visible deep trenches and backbreak, reported in Table 27 and Table 28. The correlation between the numerical values and the visual observations are discussed later in Chapter 4.5. For rows 1 and 3 there is no significant difference in D_{mean} . The 2nd burden deviation and S/4 shift patterns did not show a trend for larger 2nd row D_{mean} values, see also Appendix 12 (Figure 159 and Figure 160).

4.4.3 Interior damage results

In this subchapter, a description is presented of the main results with regards to both the interior crack development and the analysis of the number of cracks developed by blasting in the different drill pattern groups.

The procedure for the quantification of the crack development (described in Chapter 3.12) was developed and improved during the blasting tests (Navarro, 2015). The crack detection was mainly done on cut slices from remnants of the blocks behind the third row. Slice 1 corresponds to the upper part of the block remnants (see Figure 26) and Slice 4 corresponds to the bottom part. These remnants contain the total of the pre-conditionings from the previous row blasts. Crack families were identified based on angles, lengths and origin (see Figure 37). The analysis was carried out by studying the number of cracks from each family. The data is given in Appendix 7, see Table 65.

The cracks in the slices were analyzed in order to see if there was any difference, when different drillhole deviation patterns were tested. The cracks were then compared with regards to the different drillhole patterns blasted as well as with regards to the height position of the slice. The obtained results are given in terms of:

- number of detected cracks per block
- statistical evaluation of the individual crack families
- number of cracks in the different cut slices
- mean crack density (MCD)
- statistical evaluation of the damage introduced in drill pattern groups
- statistical analysis of damage on the different slices

Since the cracks created after each blast were traced by using dye-penetrant spray and categorized in 11 crack families followed by the calculation of the mean crack density (MCD) and the mean crack intersection density (MCID), these measures (see also Chapter3.12.4) need to be evaluated according to the value they add to the description of the damage. Table 34 shows a correlation matrix between total number of cracks created in each slice and the corresponding MCD and MCID values.

Table 34: Correlation coefficient R matrix for total number of cracks created, MCD and MCID values, blast sessions 2013 and 2014

	Total Cracks	MCD [-]	MCID [-]
Total Cracks	1.00		
MCD [-]	0.64	1.00	
MCID [-]	0.57	0.98	1.00

Figure 69 shows a linear regression between the MCD and MCID values. The complete set of data can be found in Appendix 7, Table 62.

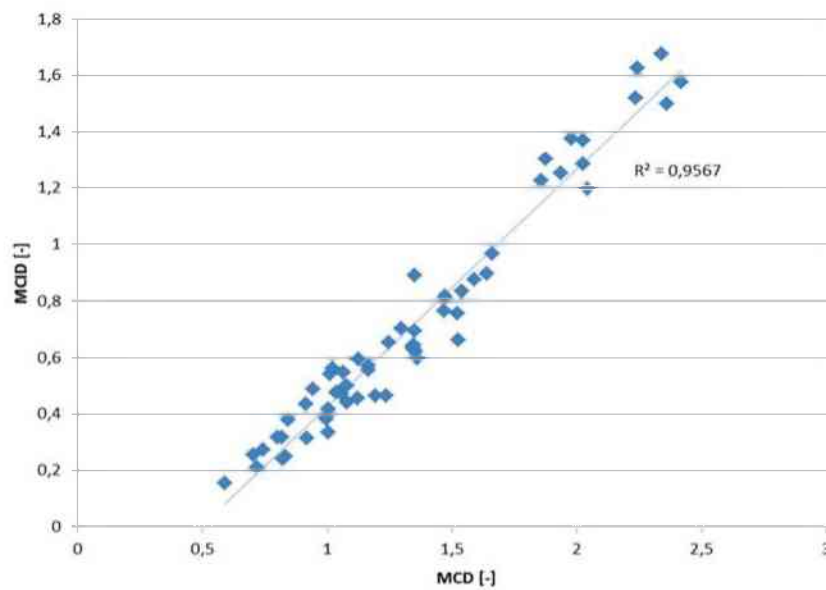


Figure 69: MCD vs MCID, blocks session 2013 and 2014

The presentation of the data is divided into sessions 2013 and 2014. The information about session and pattern is determined by the individual block number, where:

Session 2013: 3 pattern groups of 2 blocks each, overall 6 blocks

Session 2014: 3 pattern groups of 3 blocks each, overall 9 blocks

The analysis begins with comparison of the blast sessions 2013 and 2014, considering the pattern groups and blocks for each group. As the number of cracks in fragmentation outlier block B01 is similar to the number of cracks in the other blocks with the same pattern (see Table 65), this block is also included in the analysis. Then the data is divided in blast sessions 2013 and 2014, to investigate if the individual numbers of cracks in the different families depend on pattern and slice number. Since the number of cracks in some families is very small and may vary relatively much, pattern average numbers have been used.

4.4.3.1 Blast session 2013 vs blast session 2014 interior damage

One comparison of the interior damage, achieved by blasting using different blasthole patterns is shown in Figure 70, where a summary of the number of cracks per block from each pattern, blast sessions 2013 and 2014 is given.

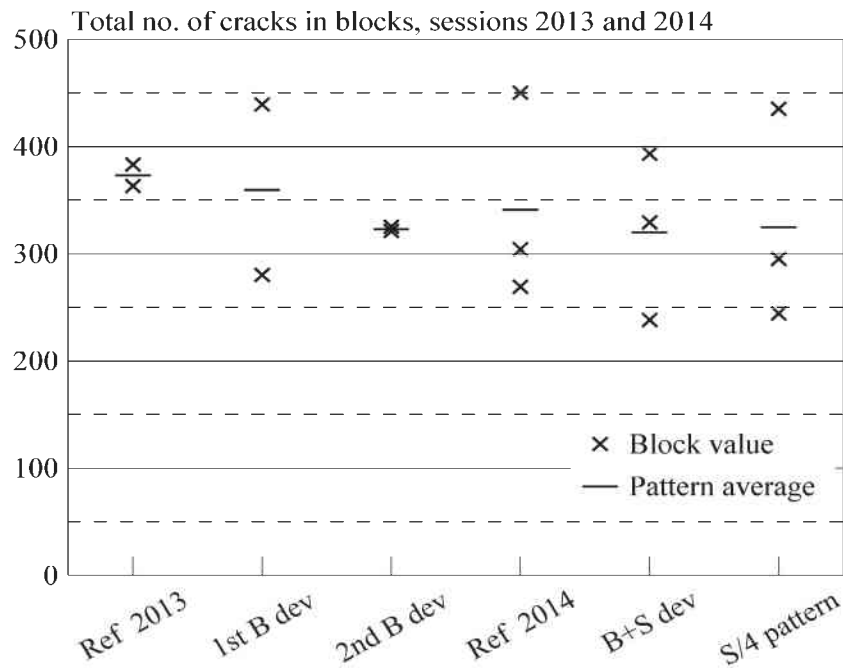


Figure 70: Number of cracks in blocks for blast sessions 2013 and 2014

From Figure 70 it can be seen that both number of cracks per block and the pattern average per block show no clear tendency for either larger or smaller degree of damage, i.e. similar values are observed. The average MCD values for blocks from different patterns, blast sessions 2013 and 2014 are given in Figure 71.

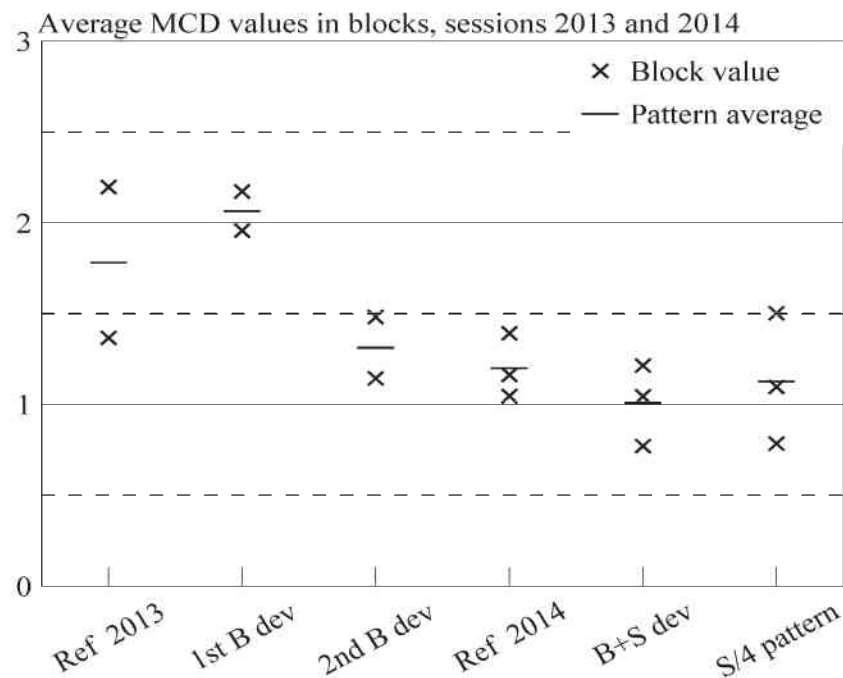


Figure 71: MCD values for blast sessions 2013 and 2014

It can be seen that the average MCD values for the reference and first burden deviation (1st B dev.) patterns from 2013 are slightly higher than for the rest of the patterns. For the latter, similar values are observed. The scatter in reference blocks 2013 and S/4 shift blocks appear to be larger compared to the ones in the other blocks.

A MWU-Test was used to determine if the two population means of the total number of cracks as well as the MCD values showed significant differences. The result is given in the table below.

Table 35: Statistical analysis of damage session 2013 vs. session 2014 with the MWU-Test ($\alpha = 0.05$), 2 session groups x 6 blocks in 2013 and 9 blocks 2014

Comparison	Z _{score}	Z _{critical}	Sign.diff
Total number of cracks	0.70	1.64	No
MCD	2.35	1.64	Yes

The statistical evaluation of the number of cracks showed that blast session 2013 gave a similar degree of damage as blast session 2014. The MCD data however, showed significantly different degrees of damage. The average number of cracks per slice data is given in Table 36. Each value represents the average number of cracks in a specific slice of a given pattern group (2 or 3 blocks); altogether 12 (3x4) data for blast session 2013 and 12 (3x4) data for blast session 2014.

Table 36: Average number of cracks and average MCD values per slice, blast sessions 2013 and 2014

Blast session 2013						
Drill pattern	Reference		Dev B1		Dev B2	
	Ave	MCD	Ave	MCD	Ave	MCD
Slice 1	91.5	1.55	68.0	0.76	58.0	0.91
Slice 2	84.0	1.52	96.5	2.19	81.5	1.31
Slice 3	97.5	1.94	101.5	2.24	90.5	1.55
Slice 4	100.0	2.10	93.5	2.00	93.0	1.50
Average	93.3	1.8	89.9	1.8	80.8	1.3
Stdev	7.1	0.3	15.0	0.7	16.0	0.3

Blast session 2014						
Drill pattern	Reference		S+B var.		S/4 shift	
	Ave	MCD	Ave	MCD	Ave	MCD
Slice 1	74.7	1.12	80.7	1.00	78.0	0.99
Slice 2	85.3	1.20	80.7	1.03	83.0	1.18
Slice 3	84.3	1.20	80.7	1.02	77.0	1.06
Slice 4	96.7	1.30	78.0	1.00	86.7	1.30
Average	85.3	1.2	80.0	1.0	81.2	1.1
Stdev	9.0	0.1	1.4	0.0	4.5	0.1

From Table 36 it can be seen that the average number of cracks per slices as well as MCD values in both sessions 2013 and 2014 showed no clear tendency for either larger or smaller degree of damage. The variations in the results may be explained with either different material properties of the mortar in sessions 2013 and 2014 (see also Chapter4.2) or inconsistency in the crack detection procedure. The crack detection was done by two different students with no previous experience (Gang Zhu in blast session 2013 and Stefanie Streit in blast session 2014), so for that reason the judgement quality and repeatability of the cracks detection procedure could probably be questioned.

The data from two sessions don't follow the normal distribution well. Therefore the average numbers of cracks in the slices as well as the average MCD values were statistically evaluated with KW-ANOVA method, to compare the degree of damage on average between blast session 2013 and blast session 2014. The statistical evaluation results are given in Table 37.

Table 37: Statistical analysis of average number of cracks in slices and average MCD values with the KW-ANOVA ($\alpha = 0.05$), 6 pattern groups x 4 slices data blast sessions 2013 and 2014

Session 2013 / Session 2014	H	X ²	Sign.diff.
Average cracks in slices	7.29	11.07	No
MCD	10.94	11.07	No

The statistical analysis of the average number of cracks created and the MCD values on the different slices showed no significant differences, i.e. the damage was not slice number dependent in the six drill pattern groups in sessions 2013 and 2014. The general conclusion that can be drawn from the statistical analyses is that the slices from six drillhole patterns contained similar degree of crack damage, for both average and total number of cracks per block.

4.4.3.2 Blast session 2013

The average crack numbers for each family are given in Table 38. The detected number of cracks for the blast session 2013 was statistically evaluated with regards to the crack families (see Table 38), where the individual number of cracks from each slice of the reference pattern blocks was compared to the individual number of cracks from each slice of 1st burden deviation and the 2nd burden deviation pattern blocks. The statistical

evaluation of all the crack families showed no significant difference between the numbers of cracks for different deviation patterns, except for the family CD 80⁰-30⁰.

Table 38: Statistical evaluation of individual crack families with the KW-ANOVA ($\alpha = 0.05$), 6 block groups x 4 slices data, blast session 2013

Crack family	Ave no of cracks per block			KW-ANOVA test		
	Ref.	1st B dev.	2nd B dev.	H	X ²	Sign. diff.
CB 90-80	11	10.5	14	3.75	11.07	No
CB 80-30	45.5	41	29	7.95	11.07	No
CB 30-0	22	22.5	24	4.11	11.07	No
SCB	44	35	26.5	9.53	11.07	No
Connect	40.5	39	46	4.25	11.07	No
Parallel	32.5	33	29	3.14	11.07	No
CD 90-80	12	13	14.5	6.3	11.07	No
CD 80-30	53.5	69.5	63	11.35	11.07	Yes
CD 30-0	60	56.5	46.5	7.65	11.07	No
SC	20	11.5	11	10.91	11.07	No
VCB	32	28	19.5	5.24	11.07	No
Total	373	359.5	323			

The total number of cracks in the four slices of the reference, 1st burden deviation and 2nd burden deviation pattern blocks is shown in Figure 72.

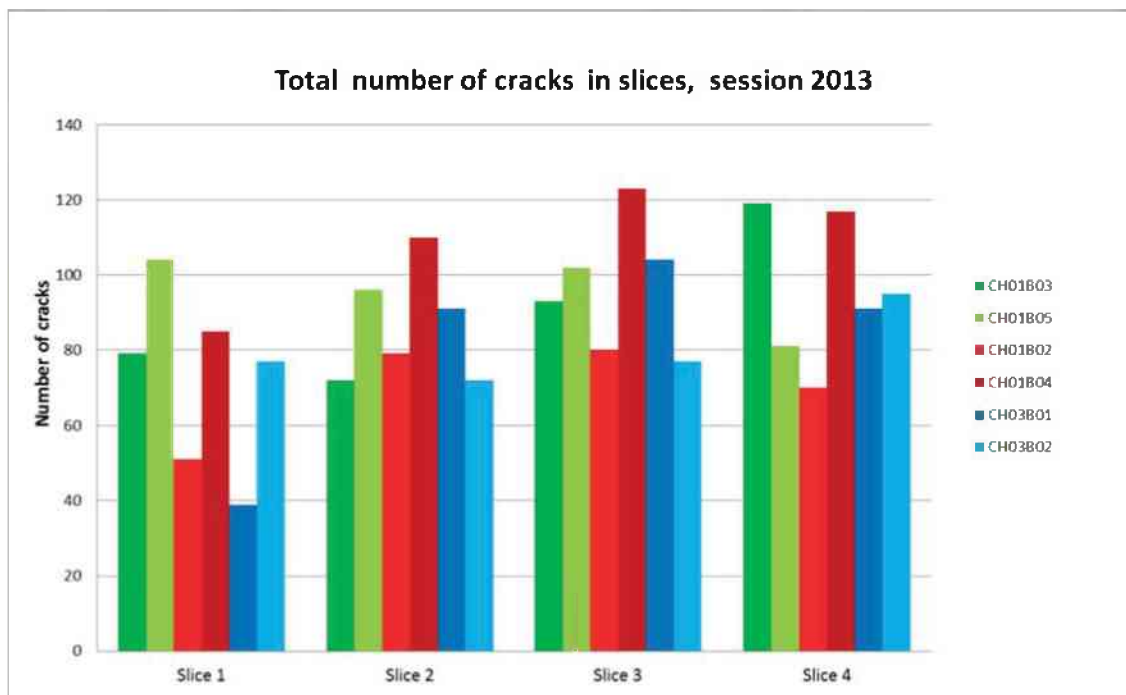


Figure 72: Total number of cracks in different slices, blast session 2013

From the Figure 72, it can be seen that there are variations both in number of cracks in slices for blocks from different patterns and in number of cracks in slices for blocks from the same patterns. Table 39 shows the total number of cracks, as well as the damage

results of the mean crack density (MCD), calculated for the individual slices and blocks, session 2013.

Table 39: Total number of cracks in slices and MCD values, blast session 2013

Slice	Total cracks					
	Reference		1st burden deviation		2nd burden deviation	
	CH01B03	CH01B05	CH01B02	CH01B04	CH03B01	CH03B02
Slice 1	79	104	51	85	39	77
Slice 2	72	96	79	110	91	72
Slice 3	93	102	80	123	104	77
Slice 4	119	81	70	117	91	95
Average	90.8	95.8	70.0	108.8	81.3	80.3
Stdev	20.8	10.4	13.4	16.7	28.8	10.1

Slice	MCD values					
	Reference		1st burden deviation		2nd burden deviation	
	CH01B03	CH01B05	CH01B02	CH01B04	CH03B01	CH03B02
Slice 1	1.06	2.03		1.53	0.82	1.01
Slice 2	1.06	1.98	2.34	2.04	1.59	1.02
Slice 3	1.47	2.42	2.24	2.24	1.86	1.25
Slice 4	1.88	2.36	1.94	2.02	1.66	1.30
Average	1.4	2.2	2.2	2.0	1.5	1.1
Stdev	0.4	0.2	0.2	0.3	0.5	0.1

The statistical evaluation of the data in Table 39 about the influence of the pattern based on total crack number and MCD values per block is given in Table 40.

Table 40: Statistical analysis of cracks in slices and MCD values with the KW-ANOVA ($\alpha = 0.05$), 6 blocks groups x 4 slices data, blast session 2013

Blast session 2013	KW-ANOVA test		
	H	X ²	Sign. diff.
Total number of cracks in slices	10.31	11.07	No
MCD	15.96	11.07	Yes

The KW-ANOVA evaluation showed that the number of cracks in slices in the 6 blocks groups is not significantly different, while the MCD values are significantly different. From Table 40 it can be seen that for the number of cracks in slices, the H-statistic is relatively close to the critical Chi-squared values. As the results present borderline data, they may be interpreted as almost significant. Thus the general conclusion that can be drawn from the statistical analyses is that the blocks from three drill patterns showed different degrees of damage in session 2013. The total number of cracks, as well as the MCD values for the session 2013 were also evaluated with regards to the possible effect of slice number, where the number of cracks from slice 1 of reference, 1st burden

deviation and 2nd burden deviation patterns was compared to the number of cracks from slices 2, 3 and 4 (i.e. to check if the damage was slice number dependent). The result is presented in Table 41.

Table 41: Statistical analysis of damage on the different slices with the KW-ANOVA ($\alpha = 0.05$)
4 slices groups x 6 blocks data, blast session 2013

Blast session 2013	KW-ANOVA test		
	H	X ²	Sign. diff.
Total number of cracks in slices	3.97	7.81	No
MCD	4.30	7.81	No

The statistical analysis of the total number of cracks created and the MCD values on the different slices showed no significant differences, i.e. the damage was not slice number dependent in the three drill pattern groups in session 2013. The data, treated with linear regression analysis showed basically the same results

4.4.3.3 Blast session 2014

The average crack numbers for each family are given in Table 42. The detected number of cracks for the blast session 2014 was statistically evaluated with regards to the crack families (see Table 42), where the individual number of cracks from each individual slice of reference pattern blocks was compared to the individual number of cracks from each slice of S+B variations and the S/4 shift pattern blocks.

The statistical evaluation of the crack families when the three drilling patterns were compared showed significant differences between the means of the following crack families: CB 80⁰-30⁰, Connection between holes, Parallel, CD 80⁰-30⁰ and CD 30⁰-0⁰. The number of cracks for the crack families which were identified to be significantly different can be seen in Appendix 7.

Table 42: Statistical evaluation of crack families with the KW-ANOVA ($\alpha = 0.05$), 9 blocks groups x 4 slices data, blast session 2014

Crack family	Ave no of cracks per block			KW-ANOVA test		
	Ref.	S+B var.	S/4 shift	H	X ²	Sign. diff.
CB 90-80	10.7	9.7	13.3	12.30	15.51	No
CB 80-30	22.3	25	39.3	19.91	15.51	Yes
CB 30-0	22.7	38.3	39.3	13.92	15.51	No
SCB	23.7	23	21.3	15.26	15.51	No
Connect	47.3	52.7	40	25.80	15.51	Yes
Parallel	39.3	36.7	38.7	25.03	15.51	Yes
CD 90-80	14	11.7	10.7	14.12	15.51	No
CD 80-30	63.3	45.3	41	25.08	15.51	Yes
CD 30-0	54	46.7	35.3	24.48	15.51	Yes
SC	5	8.3	13.3	11.15	15.51	No
VCB	38.7	22.7	32.3	15.01	15.51	No
Total	341	320	325			

The number of cracks in the four individual slices for the reference, S+B variations and S/4 shift pattern blocks is shown in Figure 73. It can be seen that there are variations in both number of cracks in slices for blocks from different patterns, as well as in number of cracks in slices for blocks from the same patterns.

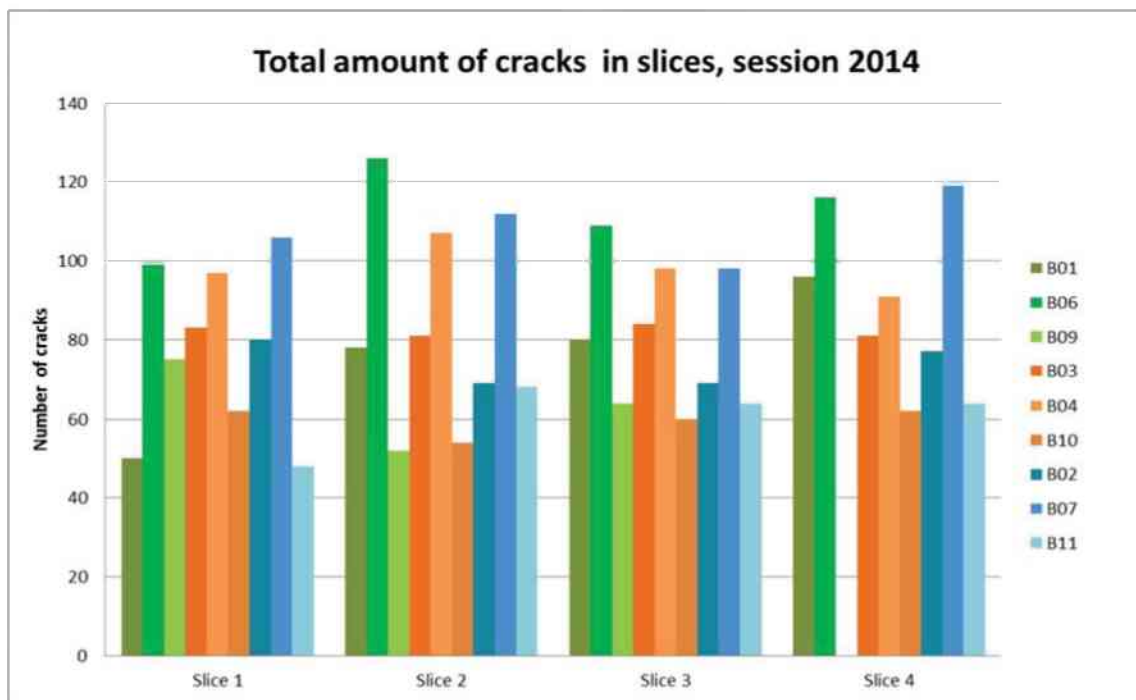


Figure 73: Total number of cracks in different slices and blocks, blast session 2014

Table 43 shows the total number of cracks, as well as the damage parameter mean crack density (MCD), calculated for the individual slices and blocks for session 2014.

Table 43: Total number of cracks in slices and MCD values, blast session 2014

Slice	Total cracks								
	Reference			S+B variations			S/4 shift		
	B01	B06	B09	B03	B04	B10	B02	B07	B11
Slice 1	50	99	75	83	97	62	80	106	48
Slice 2	78	126	52	81	107	54	69	112	68
Slice 3	80	109	64	84	98	60	69	98	64
Slice 4	96	116	-	81	91	62	77	119	64
Average	76.0	112.5	47.8	82.3	98.3	59.5	73.8	108.8	61.0
Stdev	19.1	11.4	33.2	1.5	6.6	3.8	5.6	8.9	8.9

Slice	MCD values								
	Reference			S+B variations			S/4 shift		
	B01	B06	B09	B03	B04	B10	B02	B07	B11
Slice 1	0.83	1.36	1.16	1.07	1.19	0.74	0.92	1.47	0.59
Slice 2	1.12	1.52	0.94	1.04	1.35	0.72	1.00	1.54	1.01
Slice 3	1.34	1.34	0.92	1.00	1.24	0.82	1.12	1.36	0.70
Slice 4	1.35	1.35	1.16	1.08	1.08	0.80	1.34	1.64	0.84
Average	1.2	1.4	1.0	1.0	1.2	0.8	1.1	1.5	0.8
Stdev	0.2	0.1	0.1	0.0	0.1	0.0	0.2	0.1	0.2

The statistical evaluation of the data in Table 43 about the influence of the pattern based on number of cracks and MCD values per block is given in Table 44.

Table 44: Statistical analysis of cracks in slices and MCD values with the KW-ANOVA ($\alpha = 0.05$), 9 blocks groups x 4 slices data, blast session 2014

Blast session 2014	KW-ANOVA test		
	H	X ²	Sign. diff.
Total cracks in slices	30.04	15.51	Yes
MCD	27.68	15.51	Yes

The KW-ANOVA evaluation showed that the number of cracks in slices and the MCD values in the 9 blocks groups are significantly different, i.e. blasting of the blocks with three drill patterns generated different degrees of damage.

To analyse the data more precisely, i.e. to compare only what is the effect of stochastic collaring errors on the interior blast damage, the systematic S/4 shift pattern should be excluded from the analysis. This statistical evaluation with respect to effect of drill pattern is given in Table 45.

Table 45: Statistical analysis reference samples vs. samples with stochastic collaring errors, of number of cracks in slices and MCD values with the KW-ANOVA ($\alpha = 0.05$), 6 blocks groups x 4 slices data, blast session 2014

Blast session 2014	KW-ANOVA test		
	H	X ²	Sign. diff.
Total cracks in slices	19.2	11.07	Yes
MCD	17.1	11.07	Yes

The conclusion from the Table 45 is that the blocks with reference drill pattern and the blocks with stochastic collaring drilling errors (S+B variations), showed different degrees of damage. The number of detected cracks from the individual crack families is given in detail in Appendix 7. The total number of cracks, as well as the MCD values for the session 2014 were evaluated with regards to the possible effect of slice number, where the number of cracks from slice 1 of reference, S+B variations and S/4 shift patterns was compared to the number of cracks from slices 2, 3 and 4 (i.e. to check if the damage was slice number dependent). The result is presented in Table 46.

Table 46: Statistical analysis of damage on the n different slices with the KW-ANOVA ($\alpha = 0.05$), 4 slices groups x 9 blocks data, blast session 2014

Blast session 2014	KW-ANOVA test		
	H	X ²	Sign. diff.
Total cracks in slices	0.25	7.81	No
MCD	1.12	7.81	No

The statistical analysis of the total number of cracks created and, the MCD on the different slices showed no significant differences, i.e. the damage is not slice number dependent in the three drill pattern arrangements in session 2014.

4.4.4 Exterior blast damage results

As described in Chapter 3.12.2, using the procedure of crack detection at the top of the testing blocks made it possible to investigate the cracks created after each blasted row (see also Chapter 3.12.3). The procedure was made only for blast session 2014. Figure 74 shows the average number of detected cracks in the different burden areas (sections) on blocks from the same pattern group before and after blasting the individual rows.

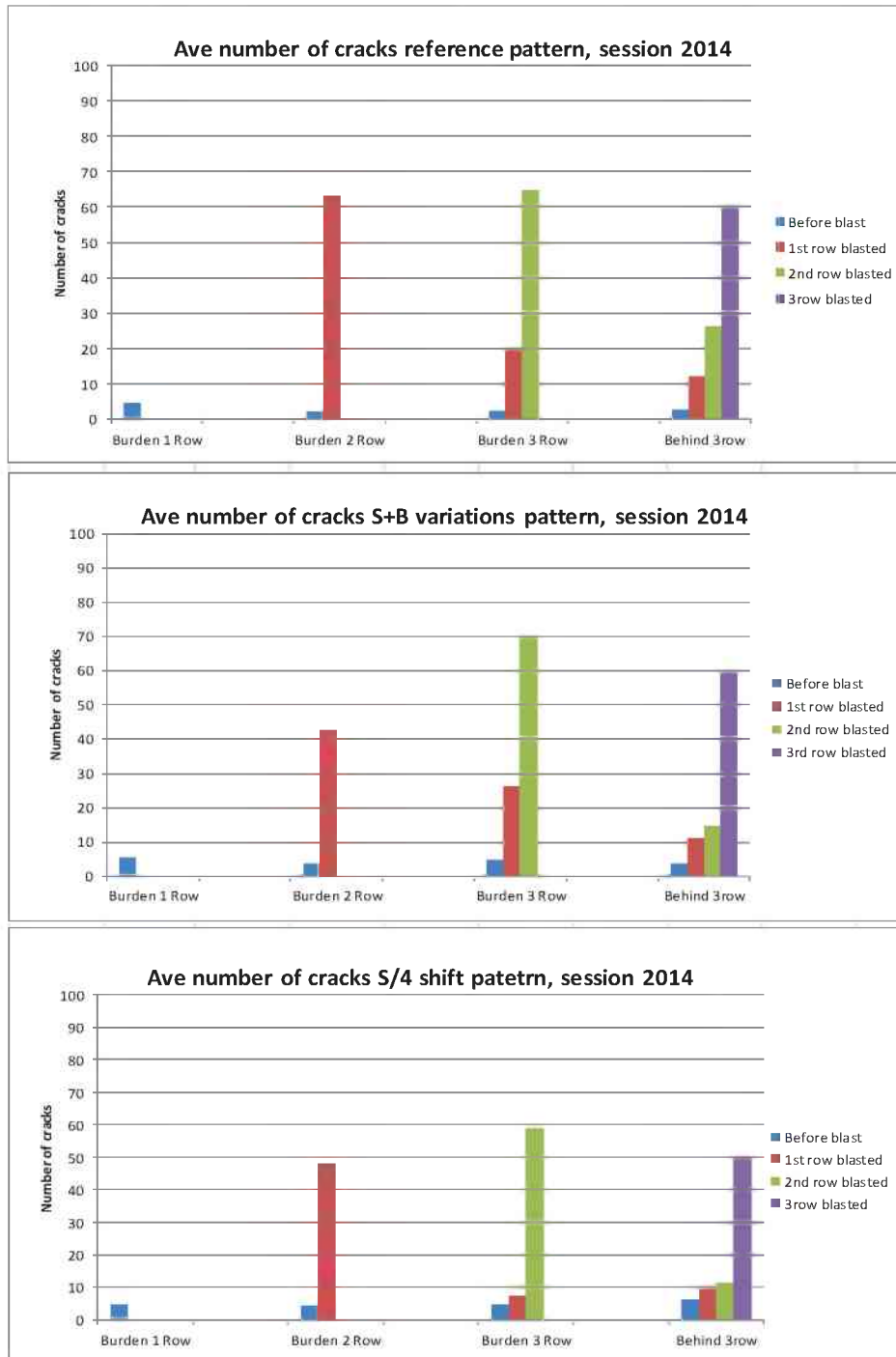


Figure 74: Average number of cracks in different regions of blocks from reference drill pattern groups: reference (upper); S+B variations (middle), S/4 (lower).

The first burden section exists only until the first row is shot, i.e. one observation of surface cracking is possible. The second burden section exists till the second row is blasted, so two surface crack counting were made, etc. The blue bars represent cracks present before any blasting was done, the violet bars represent the cracks observed on the top of the block remnants after the third row was shot. This value represents a “slice

0” when compared to the interior damage in slices 1-4. From the Figure 74 it can be seen that the largest number of cracks is created directly behind the rows blasted. The average number of cracks on the top surface behind the row 3 (56 ± 11) is significantly lower than the average one in the slices (82 ± 21), see also Table 81 in Appendix 9. One reason is the breakage or flaking off of the crest flaked off (see also Chapter 4.4.1), as a result of row blasting. Therefore it can be concluded that the cracks on the top underestimate the cracks content in the interior specimens.

4.4.5 Summary of the interior and exterior damage findings

Several conclusions can be drawn from the investigations of the interior and exterior damage, see also Navarro (2015).

In blast session 2013 only one crack family-CD 80^0-30^0 was influenced by the distorted blasthole patterns, while in blast session 2014 five crack families were: CB 80^0-30^0 , CB 30^0-0^0 , Connection between holes, CD 80^0-30^0 and CD 30^0-0^0 . Despite that the crack numbers of those families showed significant differences, the total number of cracks created on the different slices showed no significant differences. In his thesis, Schimek (2015) has also obtained similar results by the statistical evaluation of his data.

In blast sessions 2013 the three drillhole patterns with different preconditioning generated different degrees of damage in terms of number of cracks. The same results were observed in the blast session 2014. Excluding the pattern with systematic drilling errors (S/4 shift) and comparing only the blocks with the reference drill pattern with the blocks with stochastic collaring drilling errors (S+B variations), they contained different degrees of damage (see also Table 45). Comparison of the two blast sessions 2013 and 2014, showed that the slices from six drillhole patterns with different preconditioning gave similar degrees of damage in terms of the number of cracks in the block remnants but different degrees of damage in terms of the corresponding MCD values. The reason for this difference may lie in that the differences in the crack length distributions may be picked up by the MCD values.

The statistical analysis of the number of cracks created in the six drill pattern groups in both blast sessions 2013 and 2014, as well as the MCD values on the different slices

showed no significant differences, i.e. the damage was not slice number dependent, i.e. independent of cutting height. The highest degree of exterior damage was observed directly behind the row, however the top crack surface data underestimates somewhat the interior damage on the cut slices.

Summarizing the findings of Chapter 4.3.3 it can be stated that the interior damage, i.e. the number of cracks created in the testing block remnants is dependent on the drillhole deviations in both blast sessions 2013 and 2014.

4.5. Correlation analysis

Several correlation analyses have been done, to investigate the relationship between different fragmentation results and thus to help to answer the scientific questions in Chapter 5 in the thesis.

To start with, for the results from the qualitative visual bench face control, a relative comparison with the damage was done, i.e. to see how the presence of excessive backbreak and deep trenches agree with both the surface damage results and the number of the top cracks behind the blasted rows. Table 47 gives a summary of the parameters used for the relative comparison.

In session 2013, it can be seen that in most of the cases (except CH03B01) higher D_{mean} values are usually correlated with deep trenches behind the blasted rows and a backbreak observation. This result can be also seen in the documentation pictures given in Appendix 4. In session 2014, where the cracks on the top of testing blocks were traced, it can be seen that in most of the cases the deep trenches on the fresh blasted surface are giving a higher backbreak (D_{mean} values). It can be seen that the higher number of cracks on the top of the block after blasting are usually correlated with crest breakage and deep trenches.

Table 47: Correlation table for damage, blast sessions 2013 and 2014

Block #	Row	D _{mean}	Visible cracks behind holes #	Top cracks behind blasted row	Deep trenches	Other observations
CH01B03	1	5.14	no	-	left	crest flaking
	2	8.56	no	-	left, right	crest flaking
	3	2.67	no	-	no	crest flaking
CH01B05	1	4.59	no	-	right	crest flaking
	2	8.20	no	-	left, right	crest flaking
	3	6.41	no	-	no	crest flaking
CH01B02	1	2.37	2,4,7	-	left, right	crest flaking
	2	7.71	2,7	-	left, right	crest flaking
	3	5.46	no	-	left, right	excessive backbreak
CH01B04	1	3.20	no	-	left, right	crest flaking
	2	7.47	5	-	left, right	crest flaking
	3	4.11	no	-	left	crest flaking
CH03B01	1	2.74	7	-	right	crest flaking
	2	4.32	no	-	no	crest flaking
	3	6.00	no	-	no	crest flaking
CH03B02	1	7.72	no	-	left	crest flaking
	2	5.48	no	-	left, right	backbreak
	3	4.67	no	-	no	backbreak
B01	1	2.06	no	25	left	crest flaking
	2	8.17	2,4	82	left, right	backbreak
	3	3.66	no	51	left, right	crest flaking
B06	1	3.3	no	145	no	crest flaking
	2	4.46	no	94	left, right	backbreak
	3	2.54	no	70	no	crest flaking
B09	1	2.47	no	113	right	crest flaking
	2	9.90	no	97	left, right	crest flaking
	3	3.49	no	63	no	crest flaking
B03	1	3.30	no	73	left	backbreak
	2	4.00	no	73	left	backbreak
	3	5.59	no	65	right	crest flaking
B04	1	3.52	no	118	left	backbreak
	2	2.60	no	95	left, right	backbreak
	3	0.79	no	59	left, right	crest flaking
B10	1	4.27	no	49	left, right	crest flaking
	2	4.60	no	86	right	backbreak
	3	1.63	no	47	right	crest flaking
B02	1	1.65	no	50	left	crest flaking
	2	7.24	no	50	left, right	crest flaking
	3	4.79	no	42	left	crest flaking
B07	1	2.56	no	81	no	crest flaking
	2	7.20	no	90	no	crest flaking
	3	0.75	no	63	no	backbreak
B11	1	2.51	no	62	no	crest flaking
	2	3.60	no	71	left, right	crest flaking
	3	1.14	no	44	left, right	crest flaking

A correlation matrix, constructed for a single block to investigate the possible relation between the data, is given in Table 48.

Table 48: Correlation matrix, constructed to find relation between data

	Row1	Row 2	Row 3
D_{mean} before blast	$D_{\text{mean}, 0}$	$D_{\text{mean}, 1}$	$D_{\text{mean}, 2}$
N_{tot} before blast	N_0	N_1	N_2
x_{30}	$x_{30,1}$	$x_{30,2}$	$x_{30,3}$
x_{50}	$x_{50,1}$	$x_{50,2}$	$x_{50,3}$
x_{80}	$x_{80,1}$	$x_{80,2}$	$x_{80,3}$
n_{equiv}	$n_{\text{equiv}, 1}$	$n_{\text{equiv}, 2}$	$n_{\text{equiv}, 3}$
D_{mean} after blast	$D_{\text{mean}, 1}$	$D_{\text{mean}, 2}$	$D_{\text{mean}, 3}$
N_{tot} after blast	$N_{\text{tot}, 1}$	$N_{\text{tot}, 2}$	$N_{\text{tot}, 3}$

Two sets of damage variables are used for the correlation analysis: The D_{mean} and N_{tot} values before blasting are referring to “initial state” parameters, i.e. parameters which may have an influence on the blasting process; the x_p , D_{mean} and N_{tot} values after blast, are referring to “result” parameters, i.e. parameters created as a result of blasting and most probably influenced by the initial state parameter values. The $D_{\text{mean},0}$ value represents the surface damage (backbreak) of the bench face before blast, equal to 0 as the surface is not damaged before blasting of the first row. The $D_{\text{mean},1}$, $D_{\text{mean}, 2}$ and $D_{\text{mean},3}$ are the surface damages, created after blasting of the rows 1, 2 and 3 respectively. In this sense the $D_{\text{mean},1}$, which is the damage/backbreak result behind blasted row 1 is the initial one before blasting row 2, etc. The $N_{\text{tot},0}$ represents the cracks on the block top surface present before any blasting was done, the $N_{\text{tot},1}$, $N_{\text{tot},2}$, $N_{\text{tot},3}$, are the cracks created after blasting the rows 1, 2 and 3 respectively. In this sense the $N_{\text{tot},1}$, is the resulting damage/ crack number behind blasted row 1, and the initial one before blasting row 2, etc. The x_{p1} , x_{p2} and x_{p3} are the fragment sizes, created after blasting of the rows 1, 2 and 3 respectively, n_{equiv} represents the n-equiv. values, calculated from fitting a Rosin-Rammler function to the x_{30} and x_{80} values (see also Chapter4.3.3).

For blast session 2013, a joint correlation matrix for 6 blocks of 6 matrix rows in Table 48 (without N_{tot} values) with 18 columns (6 blocks x 3 blasting rows) was created. For blast session 2014, a correlation matrix for 9 blocks of 8 matrix rows with 27 columns (9

blocks x 3 blasting rows) was created. The complete set of data used for the correlation analysis can be found in Appendix 7, Table 63 and Table 64.

Table 49 shows a correlation matrix between the damage parameters D_{mean} and the percentile fragment sizes x_{30} , x_{50} and x_{80} and n_{equiv} in blast session 2013.

Table 49: Correlation matrix for D_{mean} values, n_{equiv} , x_{30} , x_{50} and x_{80} percentiles, blast sessions 2013

	D_{mean} before	x_{30}	x_{50}	x_{80}	n_{equiv}	D_{mean} after
D_{mean} before	1					
x_{30}	-0.76	1				
x_{50}	-0.73	0.93	1			
x_{80}	-0.73	0.67	0.79	1		
n_{equiv}	0.74	-0.60	-0.61	-0.65	1	
D_{mean} after	0.13	-0.08	-0.17	-0.33	0.57	1

Table 50 shows a correlation matrix between parameters D_{mean} , the number of top surface cracks N_{tot} , n_{equiv} and the x_{30} , x_{50} and x_{80} percentile sizes for blast session 2014.

Table 50: Correlation matrix for D_{mean} values, n_{equiv} , number of cracks N , x_{30} , x_{50} and x_{80} percentiles, blast session 2014

	D_{mean} before	N_{tot} before	x_{30}	x_{50}	x_{80}	n_{equiv}	D_{mean} after	N_{tot} after
D_{mean} before	1							
N_{tot} before	0.62	1						
x_{30}	-0.46	-0.54	1					
x_{50}	-0.54	-0.59	0.95	1				
x_{80}	-0.60	-0.71	0.80	0.87	1			
n_{equiv}	0.47	0.46	-0.56	-0.61	-0.60	1		
D_{mean} after	-0.02	0.10	-0.10	-0.05	0.02	0.22	1	
N_{tot} after	-0.31	0.03	-0.34	-0.27	-0.18	-0.11	0.22	1

The following conclusions can be drawn from the correlation matrixes:

1. A reasonably high correlation was found between the x_{30} , x_{50} , x_{80} percentile fragment sizes for both sessions 2013 and 2014, especially between x_{30} and x_{50} (0.93 to 0.95).
2. The correlation of the percentile fragment sizes with D_{mean} or N_{tot} was found to be slightly negative, i.e. when D_{mean} or N_{tot} increases the fragmentation gets finer. The correlation coefficient is not very high though but a general trend between both parameters is visible (-0.46 to -0.76).

3. In both sessions 2013 and 2014 the correlation found between the backbreak before blasting and the backbreak after blasting was virtually zero (-0,02 to 0.13).
4. In session 2013 the backbreak D_{mean} after blasting showed a slightly positive correlation with n_{equiv} values, while in session 2014 the backbreak after blasting was virtually uncorrelated with all other parameters.
5. A relatively high positive correlation was found between the backbreak before blasting and the cracks existing in the burden section on the top of the blocks before blasting for session 2014 (corr. coeff. 0.62).
6. In session 2014 virtually no correlation was found between the initial top surface cracks and the subsequent top surface cracks.
7. The 2014 correlation of the n_{equiv} value with D_{mean} or N_{tot} was found to be slightly positive, i.e. when D_{mean} or N_{tot} increases the n_{equiv} value increase. The correlation coefficient is not very high though (0.46 to 0.74).

5. Summary

In this thesis five blast drill patterns has been tested, based upon 15 test blocks, to investigate the effect of drillhole deviations on fragmentation. The design of the drillhole deviation was made with a distortion of a rectangular drillhole pattern, with random uncorrelated variations in the burden alone, in spacing and burden together and with systematic variations in spacing. This made it possible to perform exaggerated deviations with good accuracy keeping the specific charge almost constant and thus not influencing the expected x_{50} values very much with changes in q . The performance of the small-scale tests allowed a relatively large number of tests under relatively reproducible conditions to be done and therefore to deliver a sufficient number of data for a detailed analysis of the research questions. However some aspects could only be only superficially investigated and these need and additional work for improvement the methodology.

The findings with regards to the literature study can be summarised as follows:

- The drillhole deviation was defined as a maximum deviation from the target position (m) in drilling length of the hole (in m), expressed in %. It was found to be a function of drilling machines settings, rock and its geological conditions and human mistakes.
- A literature review of about 40 articles was performed to summarize the existing knowledge about drillhole deviations and their influence on the blasting results. Very few of these studies link the drillhole deviations directly to the fragmentation, blast damage, vibrations, noise and flyrock. Some authors concluded anyway from their investigations that blasting results are strongly influenced by drillhole deviations (see Chapter2).
- With regards to how fragmentation is influenced by the drillhole deviations, two contradictive experiences were found in the literature: the Kuz-Ram model, which predicts that n but not x_{50} , is influenced by drill hole deviations (based upon modeling); and the reinterpreted field tests findings of Sellers et al. (2013), which indicate that the deviations influenced x_{50} and x_c but hardly n . In addition, a suggestion that n should increase by ten per cent if the drilling pattern is staggered (Cunningham, 1987) was added.

The findings with regards to the methodology can be summarized as follows:

- The different production sessions 2013 and 2014 showed significantly different results in the material properties. The statistical evaluation of the fragmentation results showed that the identically blasted comparison cylinders from blast sessions 2013 and 2014 showed significant differences in x_{50} values, however not in the x_{30} and x_{80} values. This difference could not be explained directly. It was concluded that the blastability of the cylinders in sessions 2013 and 2014 was different; therefore it was decided that blast sessions 2013 and 2014 would be treated separately.
- The comparison of the blasted cylinders from the same production sessions showed comparable results for the different batches, i.e. a high repeatability and a small variation between different batches.
- The fragmentation and surface damage results taken from identically blasted testing blocks from different production sessions, leads to a conclusion that only a relative comparison of results from different production sessions is meaningful.
- While the evaluation of the D_{mean} values showed meaningful results, the S_{norm} values showed a high inconsistency in the first results. Thus S_{norm} was not further used.
- The total number of created cracks in the testing block remnants is a meaningful damage parameter as are the MCD values which include the length distribution of these cracks.
- The created cracks on the top of the block after blasting are most probably influenced by a breakage of the flaked off crest and therefore underestimate the crack contents in the interior of the specimens, i.e. they are not an appropriate representation of the interior damage created.
- The chosen Swebrec function described the fragmentation obtained quite well in the size range 0.25 mm and up, i.e. it was an appropriate tool for the curves fitting in this thesis.

The main conclusions of this thesis are given as answers to the research questions posed in the introduction:

RQ 1: Do the drillhole deviations have any influence on the fragmentation?

Despite that a small effect was observed in the x_{50} percentile values, i.e. coarser fragmentation was achieved with stochastic (S+B variations) and systematic (S/4 shift) error patterns in both rows 2 and 3. The statistical evaluation of all the x_{30} , x_{50} and x_{80} values showed that the fragmentation was not significantly influenced by any of the tested drillhole deviation patterns. The evaluation of the corresponding n_{equiv} values showed a small indication for changes for the S+B variations and S/4 patterns. However the average effect on all the patterns was found to be only 3 %. Thus it is highly questionable if a systematic effect of drillhole deviations on fragmentation exists in our tests. The statistical evaluation of the effect of the drill hole deviations on the n_{equiv} values was borderline, i.e. barely significant. Thus if those changes are significant is also questionable. It should be added that the variation of the fragmentation data between block pairs with the same blasthole pattern was almost as large as the expected effect of the drillhole deviation, i.e. around 20 %. This illustrates the difficulty of finding any significant effect of the pattern changes that have been made.

Answer: Drillhole deviations may have an influence on the fragmentation, but not under our conditions: patterns with collaring deviations and straight vertical holes, row-by-row blasting of 2D models with an unconfined bottom. If there is any effect, most probably this effect is hidden by the low repeatability of the data. In addition the number of tests is quite small and this may affect the statistical evaluation of the data. More data would help to achieve a more conclusive answer for the fragmentation results.

RQ 2: Do the drillhole deviations influence the blast damage and in what way?

The backbreak differences between blocks from the same production session didn't seem to be significant, i.e. they were not influenced by the different drillhole patterns under our testing conditions. The backbreak behind the 2nd row blasts was for four pattern groups out of six significantly larger than behind rows 1 and

3. The 3rd row blasts produced flatter surfaces with a similar backbreak as the 1st row.

Despite the different material properties, when compared the sessions 2013 and 2014 gave on average similar degrees of interior crack damage, i.e. the crack contents for the different drillhole patterns were on average the same. However the mean MCD values were different, i.e. the crack length distributions were probably different.

Looking to the blast sessions 2013 and 2014 separately, it was found that the blocks from the three stochastically distorted drillhole patterns generated different degrees of damage, both in terms of crack contents and of MCD values. Five crack families were influenced by the distorted drillhole patterns, i.e. were larger: CB 80^0-30^0 , CB 30^0-0^0 , Connection between holes, CD 80^0-30^0 and CD 30^0-0^0 , while the other crack families were not. The statistical analysis of the number of cracks created on the different slices showed that the damage was not slice number (height of cut) dependent. With respect to the exterior damage it was found that the highest degree of damage occurred directly behind the row blasted, however it could be questioned how representative these data are since the number of visible cracks on the top surface behind row 3 is significantly smaller than the number of cracks on any of the slices cut through the interior of this region.

Answer: Yes, the drillhole deviations influence the blast damage to a certain extent. The surface damage (backbreak) in the testing block remains the same with an unexplained higher value behind row 2. The number of created interior cracks and their length distribution are influenced by the drillhole deviations.

RQ 3: Is there any connection between the fragmentation and blast damage?

The fragmentation gets finer with increasing row number for all the six drill patterns tested. This was explained as a probable effect of the first preconditioning of the mortar by the blasting of the previous row, which causes backbreak and radial cracks in the previously intact material. There is a slight negative correlation coefficient between the percentile fragment sizes and D_{mean} or N_{tot} , but high enough to show a general trend. This general trend was also observed for S/4 shift pattern. This pattern produced the lowest backbreak D_{mean}

and the lowest number of cracks which tends to give coarser fragmentation than the reference pattern.

A slight positive correlation was found between n_{equiv} and D_{mean} or N_{tot} , i.e. when D_{mean} or N_{tot} increase the n_{equiv} value increases. A positive correlation was found between the deep trenches, backbreak and the cracks created on the top of the blocks before and after blasting of the rows, i.e. more backbreak would create also more cracks, i.e. a larger degree of exterior damage. In neither of sessions 2013 and 2014, clear evidence was found that damage from the previous row would influence the damage in the subsequent row blasted.

Answer: Yes, most likely there is a connection between fragmentation and blast damage. Our correlation coefficients are however not very strong. They may e.g. be influenced by either our varying test conditions (drillhole deviations) or the low repeatability but there is a relationship between the fragmentation and the blast damage.

6. Further discussion about the results

As a result of the different blastability in sessions 2013 and 2014, based on the different material properties, the fragmentation and damage results from the different sessions were treated separately. In the Chapter 4.2, a number of references are given, to link the rock and rock mass parameters influence on the blast results.

Reichholf and Moser (2000) did a literature review of more than 100 articles, to link the influence of rock and rock mass parameters to the blast fragmentation results. They have found that “*all rock mechanical and structural parameters have an influence on the blasting result, as well as joints and joint filling materials.*” They pointed that in the Kuz-Ram model some of the general parameters are considered (RMR-system), however for a more accurate and generally applicable fragmentation prediction model, more parameters have to be included.

Later on, in his thesis, Reichholf (2003) has presented the following summary, about the influence of rock properties on the blastability and blast fragmentation results (see Table 51). The authors of the sources are also added to the table.

Summarizing Table 51, it can be seen that all the mechanical and structural rock mass parameters have an effect on the blasting results. In our tests, the two sessions 2013 and 2014 showed significantly different results in the material properties of the density (14 %), uniaxial compressive strength (63 %), Young modulus (40 %), P-wave velocity (29 %). In addition the grain size of the quartz sand used for the magnetic mortar production was also different in session 2013 (0.1-0.5 mm) and in session 2014 (0.1-0.4 mm). All of these parameters, according to Table 51, are considered to have an influence on the blasting results. Thus, the decision to treat the blast session separately is supported by the literature findings

Table 51: Summary of the literature review about influence of rock and rock mass parameters on blastability and fragmentation (Reichholf, 2013)

Rock and rock mass parameters influence on	Blastability	Fragmentation	Author, year
ROCK PROPERTIES			
Compressive strength	Yes/No	Yes/No	Sunu et al. (1989), Latham (1999), Worsey et al. (1986), Rustan (1992) Rustan et al. (1995)
Tensile strength	Yes	No	Worsey et al. (1986), Sen (1992), Rustan (1992), Cunningham (1987)
Shear strength	Yes	No	Rustan and Lin (1987), Leins and Thum (1970)
Acoustic Impedance	Yes	Yes	Rustan (1992), Rustan et al. (1995)
Young's Modulus	Yes	Yes	Yang (1983), Scott (1996), Rustan (1992)
Poisson's ratio	Yes	No	Yang (1983), Scott (1996), Rustan (1992)
Mineral content and grain size	Yes	Yes	Müller (1990), Bohloli (1997)
Angle of internal friction	Yes	Yes	Jimeno et al. (1995)
Density	Yes	Yes	Rustan et al. (1995)
P-wave velocity	Yes	Yes	Reichholf (2003), Rustan et al. (1995)
Porosity	Yes	Yes	Jimeno et al. (1995), Rustan et al. (1995)
Specific energy	Yes	Yes	Jimeno et al. (1995), Rustan et al. (1995)
Strain rate	Yes	Yes	Chitombo et al. (1999)
Fracture toughness	Yes	Yes	Chitombo et al. (1999)
JOINT PARAMETERS			
Joint status (open / closed)	Yes	Yes	Fourney et al. (1993, 1997), Rustan et al. (1983)
Joint width	Yes	Yes	Fourney et al. (1997)
Joint frequency	Yes	Yes	Bohloli (1997), Rustan and Lin (1987)
Type of joint filling material	Yes	Yes	Bhandary (1996), Sen (1992), Fordyce et al. (1993)
Shear strength of filling material	Yes	Yes	Sen (1992), Fordyce et al. (1993)
Friction properties of filling material	Yes	Yes	Lu et al. (1998)
Joint distance to a borehole	Yes	Yes	Reichholf (2003)
Angle of incidence - stress wave to joint face	Yes	Yes	Reichholf (2003)
JOINT ORIENTATION			
Joint orientation with respect to the bench face	Yes	Yes	Singh et al. (1983), Bhandari (1983), Rustan et al. (1983)

In all blocks with reference and S/4 shift patterns, the breakout angle between the holes was approximately 180° , at the edges of the block this angle was somewhat smaller. For the rest of the patterns this angle was different, following the drill pattern, i.e. the blast contours were removed as planned and the blasting was done properly.

The thin section flaking off phenomenon at the top of each blasthole was also observed in other small scale blasts (Wimmer, 2007), where it was assumed that the reflections of tensile waves at the free surface may be the reason for broken off thin sections at the bottom of blasted cubes. A reason may be also the 20 g/m detonating cord used for blasting, projected a few centimetres from the blastholes.

The backbreak D_{mean} data agree well with the visual observations of the back surface, i.e. the deep trenches on the fresh blasted surface gave somehow a higher backbreak. The backbreak differences between blocks from the different production sessions 2013 and 2014 seem to be significant, i.e. session 2013 gave higher D_{mean} values (see chapters 4.3.2). However the blocks from the same blast session, which were shot in different way didn't seem to be significantly different. Johansson and Ouchterlony (2013) have also investigated the bench surface characteristics (backbreak) and the crack development speed of a blasted magnetite blocks applying different delay times. They found values that were similar with our average values of backbreak (see also Appendix 12), for shots with the same delay: for 73 μs (4-5 mm) mm and stated that the minimum backbreak was created with delay $\Delta t = 0$, i.e. when blasting simultaneously.

The internal damage has been measured in the remaining part of blocks. The crack families which were found to be affected have similar shapes as the cracks found by Ouchterlony et al. (1999, 2000) and Saiang (2008) in their work: CB $80^\circ\text{-}30^\circ$, CB $30^\circ\text{-}0^\circ$ (long and short radial cracks from hole), Connection between holes (longer than 3 cm cracks connecting two holes), CD $80^\circ\text{-}30^\circ$ (cracks developing a trajectory with a radial direction away from the hole) and CD $30^\circ\text{-}0^\circ$ (Bow shaped tangential cracks). Saiang, (2008) has found that those cracks, along with rock parameters and explosive properties were influenced also by the blasting geometry.

With regards to fragmentation, it was found that when blasting in intact material (row 1) the scatter is large and the fragmentation is coarse, showing "dust and boulders" behavior. For the second and third row, the scatter is smaller, the fragmentation is finer and the sieving curves follow the Swebrec function well. The tests of Johansson and

Ouchterlony (2013), Schimek (2013; 2015) showed similar behavior: “dust and boulders behavior” in row 1 and the fragmentation in subsequent rows being much more even than that of the first row. They linked this with the fact that the first row contained virgin material and the second row contained already cracked material, i.e. the blast damage from previous rows helps to improve the fragmentation and may help to decrease the scatter in the fragmentation results in subsequent rows, like is discussed under RQ3.

Most other model scale blasting tests known from the literature are done in virgin material. Katsabanis et al. (2014) e.g. an did investigation about the optimization of fragmentation by using different delay times, in similar blocks but only virgin material (one–row blasting). They also found a similar “dust and boulders” behavior.

Winzer and Ritter (1980) investigated pre-conditioned specimens and found that the pre-existing structural discontinuities in the rock play a dominant role in the overall fragmentation of the rock by interacting with the stress waves to produce new fractures or to further develop themselves. They also suggest that these new fractures are most likely a result from shear stresses that develop because of the passage of the P wave over the discontinuity and a lesser number develop in tension at the free face with the reflection of the P wave. Our correlation results between the pre-existing cracks in the blasted rows and the fragmentation result was negative, i.e. they confirm the literature findings that more pre-existing cracks will generate finer fragmentation.

The influence of the drillhole deviation on the fragmentation results, based on evaluation of the six drillhole patterns tested in this thesis, showed that our results support neither the Kuz-Ram model nor the reinterpreted results from the South African study (Sellers et. al., 2013). Preliminary results to this effect were reported by Ivanova et al. (2015) and the further detailed investigation in this thesis strengthened those findings.

Moreover, there are several interpretations of the effect of the drillhole deviation on the fragmentation, which are different to the one stated in Kuz-Ram prediction model. The weaknesses of the Kuz-Ram prediction model has been described in the literature (Reichholf and Moser, 2000; Ouchterlony, 2005; Spathis, 2004; Cunningham, 2005). Later on, Ouchterlony (2015) analysed in details the Kuz-Ram formula (Cunningham 1983, 1987, 2005), underlining the need of suitable function for representing of fragmentation.

In the Chapter 2, the ability of the Kuz-Ram model was discussed, and our findings are just pointing another weakness of the model. The Kuz-Ram model (Cunningham, 1983) n-value prediction is to a large part based on earlier simplistic modelling of bench blasting in Kimberlite with the SABREX model (Lownds, 1983). It may be also questioned how accurate this modelling is for the other aspects. Compared to this modelling our small scale tests are more realistic. Verification of the other aspects of the SABREX model that enter into the Kuz-Ram n-equation may be done in field tests.

With regards to the S/4 shift pattern, our tests demonstrated that the n_{equiv} value has increased 9 % by shooting a staggered pattern. This finding corresponds well with the literature, i.e. Cunningham (1987) who suggested an increase by 10 % for a staggered pattern. On the other hand a somewhat a coarser fragmentation was obtained with this pattern, compared to the reference one and thus contradicting other literature findings (Hustrulid, 1999).

Schimek (2015) has blasted 2 blocks with the same layout as ours, one reference block and one with a staggered pattern to find the influence on n. He found out that the staggered pattern gave somewhat improved fragmentation. His result showed that the average equivalent n-values decreased for the staggered pattern: from 1.05 to 0.89, which is also contradicting result. Again we have two results, pointing in different directions, which combined point at no effect.

Konya and Walter (1991) related the n-value with the potential for wall control, saying that the higher the n-value, the better the wall control. In their description, they are describing the backbreak as the damage observed on the wall and crest, i.e. as our D_{mean} (see also Figure 10), and shatter as cracking i.e. roughly as our N_{tot} . They correlated the backbreak with the Kuz-Ram median x_{50} fragment size (calling x_{50} the mean), saying that “the lower the mean value on a specific blast design is, the smaller the chance of causing a back shatter and overbreak beyond the excavation limit”. Thus our relatively high negative correlation (from - 0.54 to - 0.73) between x_{50} and both D_{mean} and N_{tot} do not support those findings. Moreover, the positive correlation found between n_{equiv} values with both D_{mean} (backbreak) and N_{tot} (generated crack damage) also does not agree with Konya and Walter (1991).

Due to the high variations in the data no firm conclusions can be drawn to answer if drillhole deviations significantly affect the fragmentation. Such variations may arise from

the blast features, rock mass properties, but also from the difficulties existing in the experimental set-up and measurements. The bad repeatability of the fragmentation data between block pairs with the same blasthole pattern, the average relative difference observed in our tests, the statistical evaluation of the data with small number of samples (Higgins and Green, 2011) only underline the difficulty of finding any significant effect of the pattern changes that have been made. A more precise performance of the tests as well as more data would help give a more conclusive interpretation of the results.

7. Recommendation for further tests

This thesis was limited to small-scale blasting and did not cover any full-scale tests, though a discussion concerning earlier published full-scale experiments is provided (see Chapter 2). The magnetite mortar material selected for the testing blocks, contributed to a good optical surface characterization procedure directly after blasting of each row, as well as for fast magnetic separation in the sieving process. The chosen arrangement using blasting mats on a wire mesh around the blasting site, avoided extensive secondary breakage. Handling of the blasted material as well as documenting the blasting tests was easy and fast.

Despite the advantages of the small scale vs. full scale blasting, conducting small scale blasting comparable to normal bench blasts, is not easy to do. The inhomogeneous nature of the rocks would always create scatter in the data (Winzer et al., 1983). As shown in Chapter 4.1, even small variations in the ingredients might have a large influence on the physical and mechanical properties of the mortar material, leading to possible differences in the fragmentation results. Consequently, it was harder to manufacture mortar blocks with repeatable material properties than we thought to begin with.

Several factors should be taken into account when choosing the production method. The production of the test specimens in the precast concrete plant was expensive; even though experienced personnel were involved in the production, control of the exact ingredients proportion and the curing conditions (humidity and temperature) was not possible. The size of the batches produced was 680 kg, so up to 5 testing blocks were produced out of the same batch. This increases the repeatability of the mechanical properties and probably also of similar fragmentation characteristics for this batch of testing blocks.

On the other hand, the specimen production in the laboratory allowed for a better control of the ingredients proportions. Curing the specimens to laboratory standards was possible by using the climate chamber in the university's laboratory. However, using a 120 kg capacity cement mixer only allowed one block per individual batch. The actual mixing was done by PhD students with no previous experience, but under

supervision, so for that reason the quality and repeatability of the batches could be improved.

The borehole drilling using drill laboratory equipment was done with precision and the post-drilling control of the collaring and bottom positions did not show any deviations from the original plan. The limiting factors in this case were the length of the blasthole and the inability of the equipment to drill angled holes with drill hole alignment deviations.

Testing at the Eisenerz blast site is restricted by the weather conditions; consequently it is only possible to blast 15-16 samples per season. This number is insufficient for the subsequent proper statistical evaluation of the data if the blocks are divided into too many groups. The size of a specimen (approximately 100 kg) makes it hard to handle. The fast hardening cement used for grouting the testing blocks into the yoke was the correct choice due to similar physical characteristics of the materials.

The blasting arrangement with the 20 g/m detonating cord worked properly and the delay time of 73 μ s per blasthole with the 5 g/m PETN-cord trunk line showed repeatable values with small scatter (see Appendix 4). At the beginning of this research it was decided to try to use 140 μ s delay per blasthole, which required a longer length of the delay-timing cord. This choice was critical and several cut-offs were observed. Therefore the initiation procedure has to be improved either by choosing a detonating cord with a lower strength (1, 2 or 3 g/m) or by finding another alternative initiation of the blastholes if delay times longer than 73 μ s are to be used.

For the documentation pictures of the blasts, the use of comparable camera positions for every blast-documentation was essential. Comparable light conditions would be of advantage for the generation of the 3D-models and shade should be provided during documentation of the bench face to avoid direct sunlight with shadows lines.

The D_{mean} parameters for the surface roughness seem to give a good description of the blasted surface. The method of taking 3 horizontal contour lines along the blasted bench face, developed for the calculation of reference figures for the roughness of the blasted bench face, was simple and fast. The parameter D_{mean} gave reasonable results and a proper description of the roughness of the fresh blasted surface. Due to the observed irregularities along the bench face the horizontal contour lines should be split up into smaller sections. Single parameters for the sections between the individual

blastholes would result in more data for the statistical analysis of the blasted bench face.

S_{norm} it is not a meaningful parameter for the physical description of the fresh blasted bench face however and other ways to describe the small scale roughness of the blasted bench face should be found.

The BlastMetrix3D software package generated a 3D-model with a dense mesh of data points along the bench face. Due to the known coordinates of these data points, this mesh could be used for further analysis. The surfaces of the individual blasted benches could be merged to calculate the exact blasted volume per row.

The crack detection procedure, using dye penetrant spray, worked well although the repeatability of the results is dependent on the personal performing the work.

The same method of crack detection used at the top of the testing blocks was a good was to study the cracks generated after each blasted row. The procedure would give better results if the surface were cut flat with a diamond saw during the block preparation and if the crest flaking were suppressed.

The crack detection on cut slices worked well, although the testing block remains had to be broken out of the yoke and this procedure was rather rough. Therefore, a better procedure of breaking out the testing block remnants after the blasting tests should be used, i.e. removal of remains either from left or from the right side and with better tools.

The classification of the cracks in crack families was a good choice although a smaller number of different crack families may be better for more efficient analysis, e.g. relating them to different ranges of fragment sizes (Zhu, 2015).

As an alternative to a direct detection of introduced cracks and the damage in the remaining testing block, a method which is able to detect cracks in-situ should be investigated. Destruction of the testing block could be avoided with methods like P-, S-wave or other ultrasound measurements. A related method is the Schmidt hammer rebound test. Preliminary tests using Schmidt hammer rebound test were made during 2014. The results were promising but not conclusive. Its use should be considered in future tests.

To better link the surface roughness to the number of interior cracks in the remaining testing block, the used contour lines for the determination of the distance of the

individual data points to the reference line (D_{mean}) should be evaluated at the same height level as that at which the slices are cut that are used for the detection of the introduced cracks. Even if height doesn't seem to influence the number of cracks created, slices cut at 5, 10 and 15 cm from bottom to top should be used.

The sieving analysis of the blasted material should be done according to sieving standards. Ensuring similarity for all optical sorting and magnetic separation process for all investigated samples is essential.

Finally the number of repetitions for the different blast arrangements should be increased, i.e. each pattern group should consist of more blocks. It would help the statistical analysis and would probably remove some of the uncertainties in the results that have occurred in this thesis.

8. Bibliography

- Alawode, O. and Idowu, O. 2011. Effect of water-cement ratios on the compressive strength and workability of concrete and lateritic concrete mixes. *The Pacific Journal of Science and Technology*, Vol.12: 99-105.
- Bakken, R. 1994. Production blasting in open pits In *Proc. blasting seminar*, Lanzarote, January (10), Nitro Nobel Sweden: 10-17.
- Bhandari, S.1983. Influence of joint directions in blasting. *Proc. 9th Conference on Explosives and Blasting Technique*, ISEE, Annual meeting, Dallas, Texas: 359–369.
- Bhandari, S. 1996. Changes in fragmentation processes with blasting conditions. *Fragblast 5. Proc. 5th Int. Symp. for rock fragmentation by blasting*, B. Mohanty (ed.), Montreal: 301-312.
- Bohloli, B. 1997. Effects of the geological parameters on the rock blasting using the Hopkinson Split Bar. *Int. J. Rock. Mech. and Min. Sci.* Vol. 32: 3-4.
- Box, G. E. P. and Muller, M. E. 1958. A Note on the Generation of Random Normal Deviates. *Annals of Mathematical Statistics*, Vol. 29 (2): 610–619.
- Chan, Y. and Walmsley, P. 1997. Learning and understanding the Kruskal-Wallis one-way analysis of-variance by-ranks test for differences among three or more independent groups. *Journal of Phys. Therapy*, Vol. 77(12):1755-62.
- Chitombo, G., Guest, A., Djordjevic, N. and La Rosa, D. 1999. In search of an improved understanding of the fundamentals of rock breakage under controlled dynamic loading. *Fragblast 6. Proc. 6th Int. Symp. for Rock Fragmentation by Blasting*, Marshalltown, South Africa: 73-79.
- Conover, W. J. 1999. *Practical Nonparametric Statistics*, 3rd Edition. Wiley and Sons, ISBN 978-0-471-16068-7.

- Cunningham, C. V. B. 1983. The Kuz-Ram model for prediction of fragmentation from blasting. *Fragblast 1. Proc. 1st Int. Symp. on Rock Fragmentation by Blasting*, R. Holmberg and A. Rustan (eds.), Luleå University of Technology, Sweden: 439-454.
- Cunningham, C. V. B. 1987. Fragmentation estimations and the Kuz-Ram model – four years on. *Fragblast 2. Proc. 2nd Int. Symp. on Rock Fragmentation by Blasting*, W. Fournery and R. Dick (eds.), SEM, Bethel CT: 475-487.
- Cunningham, C. V. B. 2005. The Kuz-Ram fragmentation model–20 years on. *Third EFEE World Conf. Explosives and Blasting*, R. Holmberg et al. (eds.), EFEE: 201–210.
- Cunningham, C., Fournery, W., Simha K. and Spathis, A. 2011. *Mining and Rock Construction Technology Desk Reference. Rock mechanics, drilling and blasting*. CRC press, A. Rustan (ed.) Taylor and Francis group, Balkema. London, UK.
- Dal Farra, E. 2012. Initiation delay effects on fragmentation and face geometry in small-scale blasting tests. Master Thesis. Politecnico di Torino, Italy.
- Da Gama, D. C. 1983. Use of comminution theory to predict fragmentation of jointed rock masses subjected to blasting. *1st Int. Symp. on Rock Fragmentation by Blasting*, R. Holmberg and A. Rustan (eds.), Luleå University of Technology, Sweden: 565-580.
- Elliott, R., Ethier, R. and Levaque, J. 1999. Lafarge Exshaw finer fragmentation study. *Proc. 25th Ann. Conf. on Explosives and Blasting Technique Vol. 2*, SEM, Bethel CT: 333-354.
- Fordyce, D. L., Fournery, W.L., Dick, R.D. and Wang, X.J. 1993. Effect of joints on stress wave transmission. *Fragblast 4. Proc. 4th Int. Symp. on Rock Fragmentation by Blasting*, H-P. Rossmannith (ed.), Balkema, Rotterdam: 211-220.
- Fournery, W., Barker, W. and Holloway, D.C. 1993. Fragmentation in jointed rock material. *Fragblast 1. Proc. 1st Int. Symp. on rock fragmentation by blasting. Vol. 2*, Lulea, Sweden: 505-532.
- Fournery, W., Dick, R. D., Wang, X. J. and Weaver, T. A. 1997. Effects of weak layers on particle velocity measurements. *Rock Mechanics and Rock Engineering*, Vol. 30: 1-18.

Gaich, A., Moser, P., Zechmann, E. and Grasedieck, A. 2006. The SMX Blast Metrix – A new tool to determine the geometrical parameters of a blast based on 3D imaging. *Fragblast 8. Proc. 8th Int. Symp. on Rock Fragmentation by Blasting*, Editec, Santiago, Chile: 80-84.

Gardner, G. F., Gardner, L. W. and Gregory A. R. 1974. Formation velocity and density—the diagnostic basics for stratigraphic traps, *Geophysics*, Vol 39 (6): 770-780.

Giltner S. G. and Koski A.E. 2010. The application of a blast audit for production improvement. *Fragblast 9. Proc. 9th Int. Symp. on Rock Fragmentation by Blasting*, Sanchidrián (ed), Taylor and Francis Group, London: 723-730.

Graham Hole Research Skills Kruskal-Wallis Hand-out, 2011. The Kruskal-Wallis Test. 2011. Version 1.0. Retrieved from: [http://www.sussex.ac.uk/Users/grahamh/RM1web/KruskalWallis %20Handoout2011.pdf](http://www.sussex.ac.uk/Users/grahamh/RM1web/KruskalWallis%20Handoout2011.pdf).

Grasedieck, A., 2006. Die natürliche Bruchcharakteristik (NBC) von Gesteinen in der Sprengtechnik; Dissertation. (The natural breakage characteristics of rocks in blasting), Montanuniversitaet Leoben, Austria. Chair of Mining Engineering and Mineral Economics.

Gregory, W. and Foreman, D. 2009. *Nonparametric Statistics for Non-Statisticians: A Step-by-Step Approach*. John Wiley and Sons.

Harmon, M. 2011. *Non-parametric testing in excel. The excel statistical master*. ISBN: 978-0-9833070-4-4. Retrieved from : http://excelmasterseries.com/New_Manuals.php.

Higgins, J. and Green S. 2011. *Cochrane Handbook for Systematic Reviews of Interventions*. The Cochrane collaboration, Willey and Blackwell, London , UK.

Hohl, W. 2013. Prüfbericht TR_2013_007. Internal document, Montanuniversitaet Leoben, Chair of Mining Engineering and Mineral Economics.

Holloway, D.C., Bjarnholt, G. and Wilson, W. H. 1987. A field study of fracture control techniques for smooth wall blasting. *Fragblast 2. Proc. 2nd Int. Symp. on Rock Fragmentation by Blasting*, W. Fournery and R. Dick (eds.), SEM Betchel, CT: 646-656.

Hustrulid, W. 1999. Blasting principles for open pit mining 1. General design concepts. Balkema, Rotterdam.

Ivanova, R., Ganster, M., Moser, P. and Bauer, F. 2012. Development of a new contour blasting system using bulk emulsions. ISEE, Proceedings of the 39th Annual Conference on Explosives and Blasting Technique. February 12-15, 2012, Nashville: 253-264.

Ivanova, R., Ouchterlony, F. and Moser, P. 2015. Influence of distorted blasthole patterns on fragmentation as well as roughness of, and blast damage behind, remaining bench face in model-scale blasting. *Fragblast 11*. Proc. 11th Int Symp. on Rock Fragmentation by Blasting, A. Spathis, P. Gribble, A. Torrance and N. Little (eds.) AusIMM, Carlton VIC: 693-706.

Jimeno, C. L., Jimeno, E. L. and Carcedo, F. J. A. 1995. Drilling and blasting of rocks. Geomining Technical Institute of Spain. Balkema, Rotterdam.

Johansson, D., Ouchterlony F. and Nyberg U. 2007. Blasting against aggregate confinement, fragmentation and swelling in model scale blasting. Proc 4th EFEE World Conference on Explosives and Blasting, P. Moser (ed.), European Federation of Explosives Engineers: 13-26.

Johansson, D. 2008. Fragmentation and waste rock compaction in small-scale confined blasting; Licentiate thesis. Lulea University of Technology, Sweden. Division of Mining and Geotechnical Engineering.

Johansson, D. and Ouchterlony, F. 2013. Shock wave interactions in rock blasting: the use of short delays to improve fragmentation in model-scale. *Rock Mech. and Rock Eng.* Vol. 46 (1): 1-28.

Katsabanis, P., Omid, O., Rielo, O. and Ross, P. 2014. Examination of timing requirements for optimization of fragmentation using small scale grout samples. *Blasting and Fragmentation*. Vol. 8 (1): 35-53.

Konya, C. J. and Walter, E. J. 1991. Rock blasting and overbreak control. Washington, DC. US Department of Transportation, National Highway Institute, Federal Highway Administration: 139-195.

Kou, S. and Rustan, A. 1993. Computerized design and result prediction of bench blasting. *Fragblast 4. Proc. 4th Int. Symposium on Rock Fragmentation by Blasting*, H. P. Rossmannith (ed.), Technical University Vienna, Balkema Rotterdam: 263-271.

Kruskal, W., and Wallis, A. 1952. Use of Ranks in One-Criterion Variance Analysis. *Journal of the American Statistical Association*, Vol. 47 (260): 583-621.

Kuznetsov, V. M. 1973. The mean diameter of the fragments formed by blasting rock. *Soviet Mining Science, Institute of Mining, Siberian Branch, Academy of Sciences of the USSR, Novosibirsk*, Vol. 9: 144-148.

Latham, J. P., Munjiza, A., and Lu, P. 1999. Components in an understanding of rock blasting. *Fragblast 6. Proc. 6th Int. Symp. on Rock Fragmentation by Blasting*, The South African Institute of Mining and Metallurgy: 173-182.

Leins, W. and Thum, W. 1970. Ermittlung und Beurteilung der Sprengbarkeit von Gestein auf der Grundlage des spezifischen Sprengenergieaufwandes. *Forschungsbericht des Landes Nordrhein–Westfalen*, Nr. 2118, Westdeutscher Verlag GmbH, Köln und Opladen.

Lownds, C. 1983. Computer modelling of fragmentation from an array of shotholes. *Fragblast 1. Proc 1st Int Symp on Rock Fragmentation by Blasting*, R. Holmberg and A. Rustan (eds.), Lulea University of Technology: 455-468.

Lu, P. and Latham, J. P. 1998. A model for the transition of block size during fragmentation blasting of rock masses. *Fragblast Int. Journal of Blasting and Fragmentation*, P. Rossmannith (ed.): 341-368.

Maierhofer, E. 2011. Development of a blasting area and blasting tests with concrete blocks in half scale to research different fragmentation phenomena; Master thesis. *Montanuniversitaet Leoben, Austria. Chair of Mining Engineering and Mineral Economics.*

Müller, B., 1990. Erarbeitung der Sprengtechnologie für verschiedene Festgebirge und die Beurteilung des Sprengergebnisses. Nobel Hefte, Heft 3 / 4 Juli: 92-102.

Napier-Munn, T.J. 2014. Statistical methods for mineral engineers. How to design experiments and analyse the data. Julius Kruttschnitt Mineral Research Centre. SMIJKMRC: 168-177.

Navarro, J. 2015. Quantification of blast-induced cracks. Master thesis, Montanuniversitaet, Leoben, Austria: Chair of Mining Engineering and Mineral Economics.

Nielsen, K. and Kristiansen, J. 1996. Blasting-crushing-grinding: Optimisation of an integrated comminution system. Fragblast 5. Proc 5th Int Symp on Rock Fragmentation by Blasting, B. Mohanty (ed.) Balkema. Rotterdam: 269-277.

Olsen, V. 2008. Rock quarrying: Prediction Models and Blasting Safety. Doctoral Thesis. Norwegian University of Science and Technology Trondheim, Norway.

Oriard, L. L. 1994. Vibroseis operations in an urban environment, Bulletin of Association of Engineering Geologists, Vol. 31 (3): 343-346.

Ouchterlony, F., Olsson, M. and Båvik, S. 1999. Bench blasting in granite with holes with axial notches and radial bottom slots. Fragblast 6. Proc. 6th Int. Symp. on Rock Fragmentation by Blasting, South African Institute of Mining and Metallurgy, Johannesburg: 229-239.

Ouchterlony, F., Olsson, M. and Båvik, S. 2000. Perimeter blasting in a 130 m road cut in gneiss with holes with radial bottom slots. Explosives and Blasting Technique, R. Holmberg (ed.), Balkema, Rotterdam: 225-234.

Ouchterlony, F. 2002. Drill Hole Deviations in a Road Cut Perimeter. Experiences from Measurements at Sodertalje. Fragblast 7. Proc. 7th Int. Symp. on Rock Fragmentation by Blasting, W. Xuguang (ed.), Metallurgical Industry Press, Beijing: 341-354.

Ouchterlony, F. 2003. Influence of blasting on the size distribution and properties of muckpile fragments, a state-of-the-art review. MinFo project P 2000-10, Energy optimisation in comminution, Swebrec, Lulea Sweden.

Ouchterlony, F. 2005. The Swebrec[®] function, linking fragmentation by blasting and crushing. *Mining Technology*, Trans. Inst. Min. Metal A 114: A29-A44.

Ouchterlony, F. and Moser, P. 2006. Likenesses and differences in the fragmentation of full-scale and model-scale blast. *Fragblast 8. Proc. 8th Int. Symp. on Rock Fragmentation by Blasting*, Editec SA, Chile: 207-220.

Ouchterlony, F., Olsson, M., Nyberg, U., Andersson, P. and Gustavsson, L. 2006. Constructing the fragment size distribution of a bench blasting round using the new Swebrec function. *Fragblast 8. Proc. 8th Int. Symp. on Rock Fragmentation by Blasting*, Editec SA, Chile: 332-344.

Ouchterlony, F. 2009. A common form for fragment size distributions from blasting and a derivation of a generalized Kuznetsov's x_{50} -equation. *Fragblast 9. Proc. 9th Int. Symp. on Rock Fragmentation by Blasting*, J.A. Sanchidrián (ed.), Taylor and Francis Group, London: 199-208.

Ouchterlony, F. 2010. Fragmentation characterization; the Swebrec function and its use in blast engineering. *Fragblast 9. Proc. 9th Int. Symp. on Rock Fragmentation by Blasting*, J.A. Sanchidrián (ed.), Taylor and Francis Group, London: 3-22.

Ouchterlony, F., Ivanova, R., Moser, P. and Seidl, T. 2013. Results of monitoring of rounds with enlarged pattern at Akselberg. Internal report, Montanuniversitaet Leoben, Austria. Chair of Mining Engineering and Mineral Economics.

Ouchterlony, F. 2015. The median versus the mean fragment size and other issues with the Kuz-Ram model. *Fragblast 11. Proc 11th Int Symposium on Rock Fragmentation by Blasting*, A. Spathis, P. Gribble, A. Torrance and N. Little (eds.) AusIMM, Carlton VIC: 109-120.

Ramulu, M., Chacraborty, A., Raina, A., Choudhury, P. and Thote, N. 2005. Influence of burden size on blast induced ground vibration in open cast mines. *Proc. 3rd EFEE World Conference on Explosives Engineering*, R. Holmberg et al. (eds.), EFEE, UK: 103-109.

Ramulu, A., Sinha, A and Jha, A. K. K.2011. Blast optimisation with impedance matching using surface-wave tomography at open cast coal mine. EFEE Lisbon Conference Proceedings R. Holmberg (ed.): 229-243.

Reichholf, G. and Moser, P. 2000. The influence of rock and rock mass parameters on the blasting results in terms of fragmentation. Explosives and Blasting Technique, R. Holmberg (ed.). Balkema, Rotterdam: 171-178.

Reichholf, G. 2003. Experimental investigation into the characteristic of particle size distributions of blasted material; Doctoral thesis, Montanuniversitaet Leoben, Austria. Chair of Mining Engineering and Mineral Economics.

Restner, U. 1999. Test report (Meßbericht) from the Department of Geophysics – internal paper. Montanuniversitaet Leoben, Austria, Department of Geophysics.

Rosin, P. and Rammler, E. 1933. The laws governing fineness of powdered coal. Journal of the Institute of Fuel, Vol 7: 29-36.

Rustan, A., Vutukuri, V. and Naartijärvi, T. 1983. The influence from specific charge, geometric scale and physical properties of homogeneous rock on fragmentation. Fragblast 1. Proc. 1st Int Symp. on Rock Fragmentation by Blasting, R. Holmberg and A. Rustan (eds.), Lulea: Lulea University of Technology: 115-142.

Rustan, A. and Lin, N. (Nie, S.). 1987. New method to test the rock breaking properties of explosives in full scale. Fragblast 2. Proc. 2nd Int. Symp. on Rock Fragmentation by Blasting, W. Fournery and R. Dick (eds.), SEM, Bethel CT: 36-47.

Rustan, A. 1992. A composite formula for mean fragment calculation in rock blasting. 4th Int. Symp. on Explosives Technology and Ballistics (NIXT 92), Pretoria, RSA: 1-11.

Rustan, A., Vutukuri, V. and Naartijärvi, T. 1995. The influence from specific charge, geometric scale and physical properties of homogeneous rock on fragmentation. Controlled fragmentation and contours in rock blasting, theoretical and technical approaches. Lulea University of Technology. Sweden. Division of Mining Engineering.

Rustan, A. 1998. Rock blasting terms and symbols. A dictionary of symbols and terminology in rock blasting and related areas like drilling, mining, and rock mechanics. Rotterdam: Balkema: 60-61.

Rustan, A. 2010. A new principal formula for the determination of explosive strength in combination with the rock mass strength. *Fragblast 9. Proc. 9th Int. Symp. on Rock Fragmentation by Blasting*, J.A. Sanchidrián (ed.), Taylor and Francis Group, London: 155-162.

Saiang, D. 2008. Blast Induced damage. A summary of SVEBEFO investigations. Technical Report. Rock Mechanics, Lulea University of Technology, Sweden. Department of Civil and Environmental Engineering.

Sanchidrián, J. A., Segarra, P., López, L. and Ouchterlony, F. 2009. Evaluation of some distribution functions for describing rock fragmentation data. *Fragblast 9. Proc. 9th Int. Symp. on Rock Fragmentation by Blasting*. J. A. Sanchidrián (ed.), Taylor and Francis Group, London: 239-248.

Sanchidrián, J. A., Ouchterlony, F., Moser, P., Segarra, P. and López, L. 2012. Performance of some distributions to describe rock fragmentation data. In *J. Rock Mech. Min. Sci.* Vol. 53: 18–31.

Sanchidrián, J. A., Ouchterlony, F. and Moser, P. 2014. Size distribution functions for rock fragments. In *J. Rock Mech. Min. Sci.* Vol. 71: 381-394.

Scheskin, D. 1997. Handbook of parametric and non-parametric statistical procedures. Chapman & Hall/CRC Press. Taylor and Francis Group, Boca Raton.

Schimek, P. 2012. Experimental blast fragmentation research in model-scale bench blasts. Research report. 2012. Montanuniversitaet Leoben, Austria. Chair of Mining Engineering and Mineral Economics.

Schimek, P. 2013. Experimental blast fragmentation research in model-scale bench blasts. Research report, 2013. Montanuniversitaet Leoben, Austria. Chair of Mining Engineering and Mineral Economics.

Schimek, P., Ouchterlony, F. and Moser, P. 2013. Experimental blast fragmentation research in model-scale bench blasts. *Measurement and Analysis of Blast Fragmentation*, J. Sanchidrián and A. K. Singh (eds.), Taylor and Francis Group, London: 51-60.

Schimek, P., Ouchterlony, F. and Moser, P. 2015. Influence of blasthole delay-timing on fragmentation as well as roughness of and blast damage behind a remaining bench face through model scale blasting. *Fragblast 11. 11th Int Symp. on Rock Fragmentation by Blasting*, A. Spathis, P. Gribble, A. Torrance and N. Little (eds.) AusIMM, Carlton VIC: 257-267.

Scott, A., 1996. Blastability and blast design. *Rock fragmentation by blasting. Proc. 5th Int. Symp. on Rock Fragmentation by Blasting*, B. Mohanty (ed.), Balkema, Rotterdam: 27-36.

Schuhmann, R. 1940. Principles of comminution. 1-size distribution and surface calculation. *Tech. Publs. AIME, Vol. 1189 (11)*.

Sellers, E., Kotze, M. and Mthlane, M. 2013. Quantification of the effect of inaccurate drilling on the risk of poor fragmentation and increased blast hazard. *Fragblast 10. Proc. 10th Int Symp. on Rock Fragmentation by Blasting*, K. Singh and A. Sinha (eds.), CRC Press, New Delhi: 153-163.

Sen, G. 1992. *Rock property influence on fragmentation at rock blasting—a literature review: ISSN 0349-3571, Lulea University of Technology, Sweden. Division of Mining and Rock Excavation.*

Singh, P. and Sarma, K. 1983. Influence of joints on rock blasting—a model scale study. *Fragblast 1. Proc. 1st Int. Symp. on Rock Fragmentation by Blasting, Vol. 2*, R. Holmberg and A. Rustan (eds.), Lulea, University of Technology, Sweden: 533-554.

Sinkala, T. 1988. *Drill hole deviations governed by the rock structure - How, why, what to do. Swedish Rock Engineering Research Foundation, Report BeFo 141:1/88, Sweden.*

- Sinkala, T. 1989. Hole deviations in percussion drilling and control measures: theoretical and field studies. Doctoral Thesis. Lulea University of Technology, Sweden. Division of Mining Equipment Engineering.
- Snedecor, G. and Cochran, W. 1989. Statistical methods. 8th ed., Iowa State University Press, Ames, IA.
- Spathis, A. T. 2004. A correction relating to the analysis of the original Kuz-Ram model. *Fragblast, International Journal for Blasting and Fragmentation*, 8(4): 201-205.
- Spilling, E. 2004. Blasthole deviation control. Master thesis, Department of Civil and transport engineering. NTNU, published in Norwegian.
- Strickland, J. 2014. Predictive modelling and analytics. Published by Lulu Press, Inc Colorado.
- Sunu, M. Z. and Singh, R. N. 1989. Application of modified rock-mass classification system to blasting assessment in surface mining operations. *Mining Science and Technology*, Vol. 8: 285–296.
- Ulusay, R. and Hudson, J. A. 2011. *The Complete ISRM Suggested Methods for Rock Characterization, Testing and Monitoring*.
- Vägverket. 1984. Drilling of straight holes. Dept. Data Report. Swedish National Road Administration Report, Borlänge, Sweden.
- Wimmer, M. 2007. An experimental investigation of blastability. Swebrec rpt. 2007:1. Lulea: Swedish Blasting Research Centre at Lulea University of Technology.
- Winzer, S. R. and Ritter, A. P. 1980. The Role of Stress Waves and Discontinuities in Rock Fragmentation: A Study of Fragmentation in Large Limestone Blocks. The 21st U.S. Symposium on Rock Mechanics (USRMS), American Rock Mechanics Association, Missouri: 362-367.
- Workman, L. 1991. Wall control, Technical Report, Calder and Workman Inc.

Worsey, P. N. and Chen, Q., 1986. The effect of rock strength on perimeter blasting and the “blastability” of massive rock. Proceedings of the 2nd symposium on explosives and blasting research, ISEE, Mini – Symp., Atlanta, Georgia: 118-131.

Worsey, P. 1996. Working group on rock assessment. Proc. Fragblast 5 workshop, Measurement of Blast Fragmentation, A. Franklin and T. Katsabanis (eds), Balkema.

Yang, Z.G. 1983. The influence from primary structure on fragmentation. Fragblast 1. Proc 1st Int. Symp. on Rock Fragmentation by Blasting, R. Holmberg and A. Rustan (eds.), Lulea University of Technology, Sweden, Vol.2: 581-604.

Zhu, G. 2015. Quantification of Cracks in Model Bench Blasting. The quantification of blast-induced cracks affected by hole position. Master thesis, Montanuniversitaet Leoben, Austria. Chair of Mining Engineering and Mineral Economics.

9. List of figures

Figure 1: Diagrammatic representation of collaring d_c , alignment d_a , deflection d_d and vertical depth d_z deviations (Sinkala, 1989).	4
Figure 2: Alignment deviation (horizontally projected) as a function of dip angle and azimuth error (Olsen, 2009).....	5
Figure 3: Deflection measures as a function of drillhole length (Olsen, 2009).....	6
Figure 4: Poor drilling result in the bottom of blast. Left/right: Top/bottom coordinates. Green line indicates bench face (Spilling, 2004)	8
Figure 5: Bull's-eye drilling error for Round 1481's face (Ouchterlony, Ivanova et al. 2013)	9
Figure 6: Effect of S/B ratio and layout on the maximum distance of any point and from any hole (Cunningham, 2005)	13
Figure 7: Square (left) and staggered layout (right) with influenced regions touching (Hustrulid, 1999).....	14
Figure 8: Dependence of n and x_c on drilling accuracy (Lownds, 1983).....	14
Figure 9: Comparison of RR and tRR fits to Split data from Sellers et al.(2013)	15
Figure 10: Backbreak due to excessive burden (Konya and Walter, 1991).....	18
Figure 11: Yokes at the Erzberg blasting site. They allow waves to escape from a test specimen. The inner yoke has room for the test block (Schimek, 2013)	20
Figure 12: Testing block with dimensions 660×280×210 mm.....	22
Figure 13: Cylinder sample geometry.....	24
Figure 14: Reference block pattern	26
Figure 15: Deviation pattern designing.....	27
Figure 16: Drillhole deviation blasthole pattern 13-7-3 (1st burden deviation) on the left, and blasthole pattern 2-3-7 (2nd burden deviation) on the right	28
Figure 17: Bull's eye diagrams: 250 Box-Muller pairs (Δx , Δy) (left) and the 21 values ultimately selected (right).....	29

Figure 18: Schematic description of staggered pattern	30
Figure 19: Drillhole deviation blasthole pattern 3-7-6 (S+B variations) on the left, and blasthole pattern S/4 shift on the right	31
Figure 20: Arrangement of blasting and delay between holes.....	32
Figure 21: Cylinder prepared for blasting	33
Figure 22: Contaminating material removed and weighed	36
Figure 23: Magnetic separation and brush cleaning of particles remaining on the mesh cloth.....	36
Figure 24: Surface cracks detection. Back side block CH01B04.....	39
Figure 25: Dye penetrant application, block CH01B04	40
Figure 26: Distance between slices to cut the testing block CH01B04.....	40
Figure 27: Clarification about the faces of the slices (e.g.3A-top, 3B-bottom) block CH01B04.....	41
Figure 28: Photo of the slice after using cleaner. Slice 2 block B04	41
Figure 29: Photo of the slice after using developer. Slice 2 block B04	41
Figure 30: Photos by zoom adjusting a) left; b) middle and c) right part. Slice 2 block B04.....	42
Figure 31: Drawing of crack traces horizontal slice. Slice 3 Block CH01B01	42
Figure 32: Digitized cracks on the horizontal sections. Slices 1-4 Block CH01B04...	43
Figure 33: Grid 2x2 cm	43
Figure 34: Grid 2x2 cm, representing the number of cracks (Navarro, 2015).....	44
Figure 35: Crack detection at the top of block after 1st row blast block B09	45
Figure 36: Detected cracks from blasting the 1st row of block B09	46
Figure 37: Graphical representation of the recognized crack families	47
Figure 38: Taking stereo photographic pictures	48
Figure 39: 2D Projection of 3D model of blasted surface CH01B04 R02	49
Figure 40: Capture of triangulation of the bench face imported into CAD.....	49

Figure 41: 2D Projection of contour	50
Figure 42: Projection of the contour and reference centre line of holes.....	50
Figure 43: Perpendicular distance of contour to the reference line	51
Figure 44: Distance of contour to the reference line histogram	51
Figure 45: Boxplots distance of contour line to the reference line	52
Figure 46: Percentile size x_{50} values plotted row wise, blast session 2013	68
Figure 47: Sieving curve block CH01B04 and Swebrec curve fit (1st burden deviation).....	69
Figure 48: Percentile size x_{30} values plotted row wise, blast session 2013	70
Figure 49: Percentile size x_{80} values plotted row wise blast session 2013	70
Figure 50: Coefficient of uniformity, blast session 2013	72
Figure 51: Percentile size x_{50} values plotted row wise for blast session 2014.....	75
Figure 52: Sieving curve 1st row block B07 and Swebrec curve fit (S/4 shift).....	76
Figure 53: Sieving curve 3rd row block B07 and Swebrec curve fit (S/4 shift).....	76
Figure 54: Percentile size x_{80} values plotted row wise for blast session 2014.....	77
Figure 55: Percentile size x_{30} values plotted row wise for blast session 2014.....	77
Figure 56: Coefficient of uniformity, blast session 2014	79
Figure 57: Equivalent n-values, blast session 2013 without invalid values.....	81
Figure 58: Equivalent n-values, blast session 2014 without invalid values.....	81
Figure 59: Front view after blasting of Reference block B06 row 1	87
Figure 60: Front view after blasting of 1st burden deviation pattern CH01B02, row 1	88
Figure 61: Front view after blasting of 2nd burden deviation pattern CH03B02, row 1	88
Figure 62: Front view after blasting of S+B variations pattern B04 row 1	89
Figure 63: Front view after blasting of S/4 shift pattern B07 row 1	89

Figure 64: D_{mean} for individual blocks, blast sessions 2013 and 2014	92
Figure 65: D_{mean} vs. P-wave velocity	93
Figure 66: D_{mean} data for individual blasthole pattern groups, blast sessions 2013 and 2014	94
Figure 67: D_{mean} values at 5, 10 and 15 cm height, session 2013	95
Figure 68: D_{mean} values at 5, 10 and 15 cm height, blast session 2014	96
Figure 69: MCD vs MCID, blocks session 2013 and 2014	100
Figure 70: Number of cracks in blocks for blast sessions 2013 and 2014	101
Figure 71: MCD values for blast sessions 2013 and 2014	101
Figure 72: Total number of cracks in different slices, blast session 2013	104
Figure 73: Total number of cracks in different slices and blocks, blast session 2014	107
Figure 74: Average number of cracks in different regions of blocks from reference drill pattern groups: reference (upper); S+B variations (middle), S/4 (lower).	110
Figure 75: Selected values and the variation from CDF	xv
Figure 76: Specimen CH01B03 (R01 upper, R02 mid, R03 down)	xviii
Figure 77: Specimen CH01B05 (R01 upper, R02 mid, R03 down)	xix
Figure 78: Specimen CH01B02 (R01 upper, R02 mid, R03 down)	xx
Figure 79: Specimen CH01B04 (R01 upper, R02 mid, R03 down)	xxi
Figure 80: Specimen CH03B01 (R01 upper, R02 mid, R03 down)	xxii
Figure 81: Specimen CH03B02 (R01 upper, R02 mid, R03 down)	xxiii
Figure 82: Specimen B01 (R01 upper, R02 mid, R03 down)	xxiv
Figure 83: Specimen B06 (R01 upper, R02 mid, R03 down)	xxv
Figure 84: Specimen B09 (R01 upper, R02 mid, R03 down)	xxvi
Figure 85: Specimen B03 (R01 upper, R02 mid, R03 down)	xxvii
Figure 86: Specimen B04 (R01 upper, R02 mid, R03 down)	xxviii
Figure 87: Specimen B10 (R01 upper, R02 mid, R03 down)	xxix

Figure 88: Specimen B02 (R01 upper, R02 mid, R03 down).....	xxx
Figure 89: Specimen B07 (R01 upper, R02 mid, R03 down).....	xxxI
Figure 90: Specimen B11 (R01 upper, R02 mid, R03 down).....	xxxII
Figure 91: Specimen CH01B03 (Reference).....	xxxIII
Figure 92: Specimen CH01B05 (Reference).....	xxxIV
Figure 93: Specimen CH01B02 (1 st burden deviation)	xxxV
Figure 94: Specimen CH01B04 (1st burden deviation)	xxxVI
Figure 95: Specimen CH03B01 (2nd burden deviation).....	xxxVII
Figure 96: Specimen CH03B02 (2nd burden deviation).....	xxxVIII
Figure 97: Specimen B01 (Reference).....	xxxIX
Figure 98: Specimen B06 (Reference).....	xI
Figure 99: Specimen B09 (Reference).....	xII
Figure 100: Specimen B03 (S+B variations).....	xIII
Figure 101: Specimen B04 (S+B variations).....	xIII
Figure 102: Specimen B10 (S+B variations).....	xIV
Figure 103: Specimen B02 (S/4 shift).....	xV
Figure 104: Specimen B07 (S/4 shift).....	xVI
Figure 105: Specimen B11 (S/4 shift).....	xVII
Figure 106: Cylinders, blast session 2013.....	xVIII
Figure 107: Cylinders, blast session 2014.....	xIX
Figure 108: Cracks from borehole in sectors between 90° - 80°.....	IV
Figure 109: Cracks from borehole in sectors between 80° - 30°.....	VI
Figure 110: Cracks from borehole in sectors between 30° - 0°.....	VI
Figure 111: Straight cracks from back side	IVII
Figure 112: Connections between boreholes	IVII
Figure 113: Parallel cracks to the surface	IVII

Figure 114: Cracks with direction to the boreholes in sectors between 90° - 80°	lviii
Figure 115: Cracks with direction to the boreholes in sectors between 80° - 30°	lviii
Figure 116: Cracks with direction to the boreholes in sectors between 30° - 0°	lviii
Figure 117: Short cracks from borehole	lix
Figure 118: Vertical cracks between two boreholes	lix
Figure 119: Block CH01B03 (Reference)	lx
Figure 120: Block CH01B05 (Reference)	lx
Figure 121: Block CH01B02 (1st burden variation).....	lxi
Figure 122: Block CH01B04 (1st burden variation)	lxi
Figure 123: Block CH03B01 (2nd burden variation).....	lxii
Figure 124: Block CH03B02 (2nd burden variation).....	lxii
Figure 125: Block B01 (Reference)	lxiii
Figure 126: Block B06 (Reference)	lxiii
Figure 127: Block B09 (Reference)	lxiv
Figure 128: Block B03 (S+B variations).....	lxiv
Figure 129: Block B04 (S+B variations).....	lxv
Figure 130: Block B10 (S+B variations).....	lxv
Figure 131: Block B02 (S/4 shift).....	lxvi
Figure 132: Block B07 (S/4 shift).....	lxvi
Figure 133: Block B11 (S/4 shift).....	lxvii
Figure 134: Crack detection on top Block B01 (Reference).....	lxxiii
Figure 135: Crack detection on top Block B06 (Reference).....	lxxiv
Figure 136: Crack detection on top Block B09 (Reference).....	lxxv
Figure 137: Crack detection on top Block B03 (S+B variations).....	lxxvi
Figure 138: Crack detection on top Block B04 (S+B variations).....	lxxvii
Figure 139: Crack detection on top Block B10 (S+B variations).....	lxxviii

Figure 140: Crack detection on top Block B02 (S/4 shift)	lxxix
Figure 141: Crack detection on top Block B07 (S/4 shift)	lxxx
Figure 142: Crack detection on top Block B11 (S/4 shift)	lxxxii
Figure 143: Total number of cracks in different regions of blocks from reference drill pattern groups: Reference B01, B06,B09 (upper); S+B variations B03, B04, B10 (middle), S/4 shift B02, B07, B11 (down).....	lxxxii
Figure 144: Roughness parameters specimen CH01B03 (Reference)	xcii
Figure 145: Roughness parameters specimen CH01B05 (Reference)	xciii
Figure 146: Roughness parameters specimen CH01B02 (1st burden deviation)....	xciv
Figure 147: Roughness parameters specimen CH01B04 (1st burden deviation)...	xcv
Figure 148: Roughness parameters specimen CH03B01 (2nd burden deviation)...	xcvi
Figure 149: Roughness parameters specimen CH03B02 (2nd burden deviation)...	xcvii
Figure 150: Roughness parameters specimen B01 (Reference).....	xcviii
Figure 151: Roughness parameters specimen B06 (Reference).....	xcix
Figure 152: Roughness parameters specimen B09 (Reference).....	c
Figure 153: Roughness parameters specimen B03 (S+B variations).....	ci
Figure 154: Roughness parameters specimen B04 (S+B variations).....	cii
Figure 155: Roughness parameters specimen B10 (S+B variations).....	ciii
Figure 156: Roughness parameters specimen B02 (S/4 shift)	civ
Figure 157: Roughness parameters specimen B07 (S/4 shift)	cv
Figure 158: Roughness parameters specimen B11 (S/4 shift)	cvii
Figure 159: D_{mean} values at 5, 10 and 15 cm height, drill patterns, session 2013....	cix
Figure 160: D_{mean} values at 5, 10 and 15 cm height, drill patterns, session 2014.....	

10. List of tables

Table 1: Literature findings summary of effects of drill hole deviations	16
Table 2: Ingredients of the magnetite concrete blocks	21
Table 3: List of the blocks produced and tested	23
Table 4: List of the blasthole patterns of blocks blasted	31
Table 5: Sieving procedure summary	37
Table 6: Crack families recognized.....	46
Table 7: Critical Chi-Square (χ^2) values.....	56
Table 8: Critical Chi-Square (χ^2) values for small samples (Conover, 1999):.....	56
Table 9: Average densities of core samples.....	59
Table 10: Density of blasted cylinders	60
Table 11: UCS and tensile strength of core samples.....	61
Table 12: P and S- wave velocities of sessions 2013 and 2014.....	61
Table 13: E-Modulus and Poisson's ratio values	62
Table 14: Sieving parameters of the cylinders [mm] and coefficient of uniformity [-]...	62
Table 15: Statistical evaluation of the material properties with MWU-Test ($\alpha = 0.05$)..	63
Table 16: Statistical evaluation of cylinders sieving parameters with MWU-Test ($\alpha = 0.05$).....	63
Table 17: Specific charge, density and cylinder's sieving parameters.....	65
Table 18: Sieving parameters blast session 2013.....	66
Table 19: Statistical evaluation of the sieving parameters with the KW-ANOVA ($\alpha=0.05$), 3x5 data,	71
Table 20: Coefficient of uniformity x_{80}/x_{30} evaluation with KW-ANOVA ($\alpha=0.05$), 3x5 data,	72
Table 21: Sieving parameters blast session 2014	73

Table 22: Statistical evaluation of the sieving parameters with the KW-ANOVA ($\alpha=0.05$), 3x3 data, blast session 2014.....	78
Table 23: Coefficient of uniformity x_{80}/x_{30} statistical evaluation with KW-ANOVA ($\alpha=0.05$), 3x3 data blast session 2014.....	79
Table 24: Statistical evaluation of n-values values with the KW-ANOVA ($\alpha=0.05$), 3x2 and 3x3 data, blast sessions 2013 and 2014	82
Table 25: Statistical evaluation of x_c -values values, with the KW-ANOVA ($\alpha=0.05$), 3x2 and 3x3 data, blast sessions 2013 and 2014	83
Table 26: Expected and obtained equivalent n-values, blast sessions 2013 and 2014	84
Table 27: Overview of the visual bench face control: blocks blast session 2013.....	90
Table 28: Overview of the visual bench face control: blocks blast session 2014.....	91
Table 29: Statistical evaluation of D_{mean} -values, with the two-sample t-test of variance ($\alpha=0.05$).....	93
Table 30: Statistical evaluation of D_{mean} of the individual line heights and patterns with the One-way ANOVA ($\alpha = 0.05$), per block, blast sessions 2013 and 2014	94
Table 31: Statistical evaluation of average D_{mean} of the average rows and line heights with One-way ANOVA ($\alpha = 0.05$), 6 blocks x 3 rows data (session 2013) and 8 blocks x 3 rows data (session 2014)	95
Table 32: Statistical evaluation of D_{mean} data of the individual rows and line heights with MWU-Test.....	96
Table 33: Statistical evaluation of D_{mean} of the individual rows and line heights with MWU-Test.....	97
Table 34: Correlation coefficient R matrix for total number of cracks created, MCD and MCID values, blast sessions 2013 and 2014.....	99
Table 35: Statistical analysis of damage session 2013 vs. session 2014 with the MWU-Test ($\alpha = 0.05$), 2 session groups x 6 blocks in 2013 and 9 blocks 2014	102
Table 36: Average number of cracks and average MCD values per slice, blast sessions 2013 and 2014	102

Table 37: Statistical analysis of average number of cracks in slices and average MCD values with the KW-ANOVA ($\alpha = 0.05$), 6 pattern groups x 4 slices data blast sessions 2013 and 2014	103
Table 38: Statistical evaluation of individual crack families with the KW-ANOVA ($\alpha = 0.05$),	104
Table 39: Total number of cracks in slices and MCD values, blast session 2013	105
Table 40: Statistical analysis of cracks in slices and MCD values with the KW-ANOVA ($\alpha = 0.05$), 6 blocks groups x 4 slices data, blast session 2013.....	105
Table 41: Statistical analysis of damage on the different slices with the KW-ANOVA ($\alpha = 0.05$)	106
Table 42: Statistical evaluation of crack families with the KW-ANOVA ($\alpha = 0.05$), 9 blocks groups x 4 slices data, blast session 2014	107
Table 43: Total number of cracks in slices and MCD values, blast session 2014	108
Table 44: Statistical analysis of cracks in slices and MCD values with the KW-ANOVA ($\alpha = 0.05$), 9 blocks groups x 4 slices data, blast session 2014.....	108
Table 45: Statistical analysis reference samples vs. samples with stochastic collaring errors, of number of cracks in slices and MCD values with the KW-ANOVA ($\alpha = 0.05$), 6 blocks groups x 4 slices data, blast session 2014	109
Table 46: Statistical analysis of damage on the n different slices with the KW-ANOVA ($\alpha = 0.05$), 4 slices groups x 9 blocks data, blast session 2014.....	109
Table 47: Correlation table for damage, blast sessions 2013 and 2014.....	113
Table 48: Correlation matrix, constructed to find relation between data.....	114
Table 49: Correlation matrix for D_{mean} values, n_{equiv} , x_{30} , x_{50} and x_{80} percentiles, blast sessions 2013	115
Table 50: Correlation matrix for D_{mean} values, n_{equiv} , number of cracks N , x_{30} , x_{50} and x_{80} percentiles, blast session 2014	115
Table 51: Summary of the literature review about influence of rock and rock mass parameters on blastability and fragmentation (Reichholf, 2013).....	123
Table 52: Drill patterns set up: random collaring positions in burden direction.....	x

Table 53: Drill patterns set up, blast session 2013	xii
Table 54: Drill patterns set up: Box-Muller method (part1)	xiii
Table 55: Drill patterns set up: Box-Muller method (part 2)	xiv
Table 56: Drill pattern 3-7-6 set up, session 2014	xvi
Table 57: Drill patterns S/4 set up, session 2014	xvii
Table 58: Equivalent n-values values, blast sessions 2013 and 2014.....	lii
Table 59: Equivalent x_c -values values, blast sessions 2013 and 2014.....	liii
Table 60: Equivalent x_c -values values, blast sessions 2013 and 2014.....	liv
Table 61: Color coded families of crack traces in horizontal slices.....	lv
Table 62: Total cracks at horizontal slices, MCD, MCID values and top cracks, sessions 2013 and 2014.....	lxviii
Table 63: Set of data used for the correlation analysis, session 2013.....	lxix
Table 64: Set of data used for the correlation analysis, session 2014.....	lxix
Table 65: Crack families at horizontal slices and drill patterns summary, blast sessions 2013 and 2014	lxx
Table 66: MCD and MCID for individual blocks with reference pattern, session 2013	lxxi
Table 67: MCD and MCID for individual blocks with 1st burden deviation pattern, session 2013	lxxi
Table 68: MCD and MCID for individual blocks with 2nd burden deviation pattern, session 2013	lxxi
Table 69: MCD and MCID for individual blocks with reference pattern, session 2014	lxxii
Table 70: MCD and MCID for individual blocks with S+B variations pattern, session 2014	lxxii
Table 71: MCD and MCID for individual blocks with S/4 shift pattern, session 2014.	lxxii
Table 72: Crack families on top Block B01 (Reference).....	lxxiii
Table 73: Crack families on top Block B06 (Reference).....	lxxiv
Table 74: Crack families on top Block B09 (Reference).....	lxxv

Table 75: Crack families on top B03 (S+B variations)	lxxvi
Table 76: Crack families on top B04 (S+B variations)	lxxvii
Table 77: Crack families on top B10 (S+B variations)	lxxviii
Table 78: Crack families on top B02 (S/4 shift)	lxxix
Table 79: Crack families on top B07 (S/4 shift)	lxxx
Table 80: Crack families on top B11 (S/4 shift)	lxxxi
Table 81: Summary of exterior and interior cracks, blast session 2014.....	lxxxiii
Table 82: D_{mean} values over height, blast session 2013.....	cvi
Table 83: D_{mean} values at 5, 10 and 15 cm height, blast session 2014.....	cviii

Appendix 1 Magnetite concrete ingredients: data sheets



Quarzwerte
CE

Datenblatt

Quarzsand ME 31 MESK31

Quarzsand ME31 ist ein aufbereiteter natürlicher Rohstoff. Der Quarzsand wird attritiert, gewaschen, hydroklassiert, gesiebt und ist von Kalk und organischen Verunreinigungen befreit. Durch sein gerundetes Korn und den chem. Inhaltsstoffen, ist diese Sorte speziell als Formgrundstoff für die Gießereindustrie geeignet. Durch laufende Kontrollen garantieren wir Ihnen eine hohe und gleichmäßige Qualität.

Lieferform : feucht oder trocken (feuergetrocknet)
lose, abgepackt in PE Säcken, foliert auf Palette

Korngrößenverteilung

Körnung in mm	Siebrückstand in %		Siebdurchgang in %
	Richtwert	Toleranz	Richtwert
0,71		max 0,5	100
0,5	1,5	max 3	98,5
0,355	26	20-35	72,5
0,25	49	40-60	23,5
0,125	23	18-28	0,5
0,063	0,5	max 2	
<		max 0,5	

Chemische Analyse (Gew.-%)

Element	Richtwert	Toleranz
SiO ₂	97	96-98
Al ₂ O ₃	1,7	max.2,2
Fe ₂ O ₃	0,17	max.0,25

Physikalische Eigenschaften

Schüttgewicht	1,5t/m ³	mittlere Korngröße	0,30 mm
Dichte	2,65t/m ³	AFS-Nummer	51
Härte	7Mohs	Glühverlust	<0,3%
Schlammstoffgehalt	<0,2%	Sinterbeginn*	~1420° C

*H.ÖGI

Quarzsand ist ein aufbereiteter natürlicher Rohstoff. Alle Daten sind Richtwerte mit vorkommens- und produktionsbedingter Toleranz. Sie dienen nur zur Beschreibung und stellen keine zugesicherten Eigenschaften dar. Größere und feinere Anteile sind in Spuren möglich. Dem Benutzer obliegt es, die Tauglichkeit für seinen Verwendungszweck zu prüfen. Wir geben auf Wunsch gerne Auskunft über Toleranzbreiten und anwendungstechnische Erfahrungen. Verkäufe erfolgen gemäß unseren Verkaufs- und Lieferbedingungen.

QUARZWERKE Österreich GmbH
Wachbergstr. 1
A-3390 Melk
www.quarzwerte.at

Telefon (02752) 50040-0
Telefax (02752) 50040-30

O541

04/07



Datenblatt

Quarzsand ME 0,1 - 0,4 mm

Quarzsand ME 0,1-0,4 ist ein aufbereiteter natürlicher Rohstoff. Der Quarzsand wird attritiert, gewaschen, hydroklassiert, gesiebt und ist von Kalk und organischen Verunreinigungen befreit. Durch laufende Kontrollen garantieren wir Ihnen eine hohe und gleichmäßige Qualität.

Lieferform : feucht oder trocken (feuergetrocknet)
lose, abgesackt in PE Säcken, foliert auf Palette

Korngrößenverteilung

Körnung in mm	Siebrückstand in %		Siebdurchgang in %
	Richtwert	Toleranz	Richtwert
0,71	0	0	100
0,5	1	max.2	99
0,355	10	5-15	89
0,25	36	30-55	53
0,125	50	40-60	3
0,063	3	1-6	
<		max.1	

Chemische Analyse (Gew.-%)

Element	Richtwert	Toleranz
SiO ₂	93	91-95
Al ₂ O ₃	4	3-5
Fe ₂ O ₃	0,2	0,1-0,4

Physikalische Eigenschaften

Schüttgewicht	1,5 t/m ³	
Dichte	2,65 t/m ³	
Härte	7 Mohs	

Quarzsand ist ein aufbereiteter natürlicher Rohstoff. Alle Daten sind Richtwerte mit vorkommens- und produktionsbedingter Toleranz. Sie dienen nur zur Beschreibung und stellen keine zugesicherten Eigenschaften dar. Größere und feinere Anteile sind in Spuren möglich. Dem Benutzer obliegt es, die Tauglichkeit für seinen Verwendungszweck zu prüfen. Wir geben auf Wunsch gerne Auskunft über Toleranzbreiten und anwendungstechnische Erfahrungen. Verkäufe erfolgen gemäß unseren Verkaufs- und Lieferbedingungen.

QUARZWERKE Österreich GmbH
Wachbergstr. 1
A-3390 Melk
www.quarzwerte.at

Telefon (02752) 50040-0
Telefax (02752) 50040-30

O535

04/07

Ferroxon® 618

Type:	Black iron oxide pigment
Form of delivery:	Powder, packed in PE-bags 25 kg or Big Bags

<u>Characteristics</u>		<u>Test methode</u>
Fe₃O₄-content:	90 - 95 M.-%	DIN ISO 1248
Matter volatile at 105 °C:	≤ 0,5 M.-%	DIN ISO 787-2
Water soluble content:	≤ 0,5 M.-%	DIN ISO 787-3
Loss on ignition:	≤ 1,0 M.-%	DIN ISO 4621
Oil absorption:	35 g/100 g	DIN ISO 787-5
pH-value:	5 – 8	DIN ISO 787-9
Sieving residue 46 µm-sieve:	≤ 0,1 M.-%	DIN ISO 787-7

Our technical advice – whether verbal, in writing or by way of trials – is given in good faith but without warranty. It does not release the customer from the obligation to test the products as to their suitability for the intended processes and uses. Our products are sold in accordance with the current version of our general conditions of sale and delivery.

Schlieper & Heyng GmbH + Co. KG, Postfach 27, 57647 Nistertal
Fon: 02661/940040, Fax: 02661/9400480

Appendix 2 Mechanical properties of mortar

Mechanical properties of mortar, blast session 2013:

Density

CH03	Sample	Diameter [mm]	Length [mm]	Weight [g]	Density [kg/m ³]
	BBK-241-5/1	51.25	102.85	486.33	2292.18
	BBK-241-6/1	51.29	103.59	495.11	2313.28
	BBK-241-7/1	51.35	24.85	116.10	2255.98
	BBK-241-10/1	51.02	24.94	117.71	2308.59
	BBK-241-12/1	51.02	25.96	118.45	2231.82
	Average				2280.37
	Stdev				35.25

CH01	Sample	Diameter [mm]	Length [mm]	Weight [g]	Density [kg/m ³]
	BBK-262-1/1	44.89	88.78	278.55	1982.43
	BBK-262-2/1	44.97	90.54	288.68	2007.43
	BBK-262-3/1	45.01	90.11	285.36	1990.27
	BBK-262-4/1	45.07	90.53	287.39	1989.82
	Average				1992.49
	Stdev				10.59

Young's Modulus, Uniaxial Compressive Strength

CH01	Sample	UCS [MPa]	Destruction work [kJ/m ³]	V-Modul [MPa]	E-Modul [MPa]	Poisson's ratio [1]
	BBK-241-1/1	63.67	188.81	23193	24853	0.12
	BBK-241-2/1	60.29	181.3	22267	23680	0.13
	Average	61.98	185.06	22730	24266	0.13
	Stdev	2.39	5.31	655	829	0.01

CH03	Sample	UCS [MPa]	Destruction work [kJ/m ³]	V-Modul [MPa]	E-Modul [MPa]	Poisson's ratio [1]
	BBK-241-5/1	49.53	153.81	20782	22514	0.1
	BBK-241-6/1	58.96	174.83	22511	24605	0.14
	Average	54.25	164.32	21646	23560	0.12
	Stdev	6.67	14.86	1223	1479	0.03

Brazilian Tensile Strength

CH01	Sample	STS [MPa]
	BBK-241-9/1	6.28
	BBK-241-13/1	4.62
	Average	5.45
	Stdev	1.17

CH03	Sample	STS [MPa]
	BBK-241-7/1	5.13
	BBK-241-10/1	5.62
	BBK-241-12/1	5.99
	Average	5.58
	Stdev	0.43

P Wave Velocity*

Block	P wave velocity [m/s]
CH01B03	Not measured
CH01B02	Not measured
CH01B04	3784
CH01B05	3835
Average	3809
Stdev	36.06
CH03B01	3647
CH03B02	3761
Average	3704
Stdev	80.61

* S-Wave not measured due to lack of instrument in Session 2013

Mechanical properties of mortar, blast session 2014:

Density

CH01	Sample	Diameter [mm]	Length [mm]	Weight [g]	Density [kg/m ³]
	BBK-262-1/1	44.89	88.78	278.55	1982.43
	BBK-262-2/1	44.97	90.54	288.68	2007.43
	BBK-262-3/1	45.01	90.11	285.36	1990.27
	BBK-262-4/1	45.07	90.53	287.39	1989.82
	Average				1992.49
	Stdev				10.59

CH02	Sample	Diameter [mm]	Length [mm]	Weight [g]	Density [kg/m ³]
	BBK-263-1/1	45.03	90.45	288.11	2000.12
	BBK-263-2/1	44.92	90.11	287.66	2014.36
	BBK-263-3/1	44.87	89.60	285.66	2016.23
	Average				2010.24
	Stdev				8.81

B14 x-dir	Sample	Diameter [mm]	Length [mm]	Weight [g]	Density [kg/m ³]
	BBK-264-1/1	50.35	99.85	401.96	2021.84
	BBK-264-2/1	50.70	100.16	406.44	2010.00
	BBK-264-3/1	50.87	100.15	405.43	1991.83
	BBK-264-4/1	50.56	100.24	404.46	2009.70
	BBK-264-5/1	50.79	26.76	103.34	1906.06
	BBK-264-6/1	50.77	26.76	104.06	1920.85
	BBK-264-7/1	50.71	25.73	101.50	1953.21
	BBK-264-8/1	50.26	26.50	103.04	1959.86
	Average				1971.67
	Stdev				43.43

B14 z-dir	Sample	Diameter [mm]	Length [mm]	Weight [g]	Density [kg/m ³]
	BBK-264-9/1	51.16	100.60	409.12	1978.34
	BBK-264-10/1	50.39	100.39	407.70	2036.44
	BBK-264-11/1	50.37	100.80	408.21	2032.31
	BBK-264-12/1	50.39	25.81	100.45	1951.57
	BBK-264-13/1	50.46	25.46	98.98	1944.04
	BBK-264-14/1	50.31	26.51	104.49	1982.74
	BBK-264-15/1	50.47	26.17	104.62	1998.27
	Average				1.989.10
	Stdev				36.03

Young's Modulus, Uniaxial Compressive Strength

CH01	Sample	UCS [MPa]	Destruction work [kJ/m ³]	V-Modul [MPa]	E-Modul [MPa]	Poisson's ratio [1]
	BBK-262-1/1	30.01	84.03	11541	12581	0.16
	BBK-262-2/1	40.77	161.37	12814	14263	0.15
	BBK-262-3/1	40.49	122.71	12533	14084	0.16
	BBK-262-4/1	33.99	99.69	12229	13894	0.18
	Average	36.32	116.95	12279	13706	0.16
	Stdev	5.24	33.61	547	765	0.01

CH02	Sample	UCS [MPa]	Destruction work [kJ/m ³]	V-Modul [MPa]	E-Modul [MPa]	Poisson's ratio [1]
	BBK-263-1/1	31.43	113.78	11463	13097	0.17
	BBK-263-2/1	29.27	83.42	11658	13800	0.15
	BBK-263-3/1	27.62	71.85	13299	16152	0.26
	Average	29.44	89.68	12140	14350	0.19
	Stdev	1.91	21.66	1009	1600	0.06

B14 x-dir	Sample	UCS [MPa]	Destruction work [kJ/m ³]	V-Modul [MPa]	E-Modul [MPa]	Poisson's ratio [1]
	BBK-264-1/1	35.27	150.84	12738	14108	0.17
	BBK-264-2/1	36.54	100.12	12493	13910	0.13
	BBK-264-3/1	38.49	199.20	12477	13974	0.17
	BBK-264-4/1	36.14	177.77	10893	12662	0.17
	Average	36.61	156.98	12150	13664	0.16
	Stdev	1.36	42.76	846	673	0.02

B14 z-dir	Sample	UCS [MPa]	Destruction work [kJ/m ³]	V-Modul [MPa]	E-Modul [MPa]	Poisson's ratio [1]
	BBK-264-9/1	40.89	163.63	12973	14550	0.18
	BBK-264-10/1	39.85	170.69	12518	14318	0.17
	BBK-264-11/1	39.88	145.36	13590	14386	0.17
	Average	40.21	159.89	13027	14418	0.17
	Stdev	0.59	13.07	538	119	0.01

Brazilian Tensile Strength

B14 x-direction	Sample	STS [MPa]
	BBK-264-5/1	2.78
	BBK-264-6/1	3.26
	BBK-264-7/1	3.34
	BBK-264-8/1	3.76
	Average	3.29
	Stdev	0.40

B14 z-direction	Sample	STS [MPa]
	BBK-264-12/1	3.25
	BBK-264-13/1	3.73
	BBK-264-14/1	3.71
	BBK-264-15/1	4.67
	Average	3.84
	Stdev	0.60

P-Wave and S-Wave Velocity,

Block	P wave velocity [m/s]	S-wave velocity[m/s]
B01	3064	
B02	3088	2002
B03	3101	1965
B04	3011	1982
B06	3038	2038
B07	3068	1962
B09	3098	2041
B10	3010	1938
B11	3031	1988
Average	3057	1990
Stdev	36	3

Possible changes in x_{50} by different material properties:

With regards to the Kuz-Ram formula for the median fragment size (see equation 5) the x_{50} is a function of A (rock mass factor) and explosive charge and strength. The rock factor A is a function of JF, RMD, HF and RDI. In sessions 2013 and 2014 the explosive charge and properties are constant, while the RDI value ((0.025.p) -50) would change because of the different density values. In addition changes in HF (E/3)

will appear. For our calculations we accept that JF=0, as by the formula development, Cunningham (2005) removed the JF parameter.

With regards to the equation 6, the following calculations were done to see what the possible changes in material properties are:

As the RDI: rock density influence is $(0.025 \cdot \rho) - 50$ [kg/m³]:

The 2013 value would be: $(0.025 \cdot \rho) - 50 = (0.025 \cdot 2362) - 50 = 9.05$ [kg/m³], thus $A_{2013} = 0.06 \cdot (50 + 0 + 9.05 + 4.08) = 3.78$

The 2014 value would be: 2014: $(0.025 \cdot \rho) - 50 = (0.025 \cdot 2024) - 50 = 0.6$ [kg/m³], thus

$$A_{2014} = 0.06 \cdot (50 + 0 + 0.6 + 4.66) = 3.31$$

The calculations of the changes in A, with regards to material properties changes, showed that the $\Delta A/A$ was estimated to be roughly 13 %.

If we look to the possible effect of the c_p changes (Kou and Rustan, 1993), who gives the following x_{50} formula:

$$x_{50} = 0.01 \cdot (\rho \cdot c) \cdot B^{0.2} (S/B)^{0.5} \cdot (H/L_{tot})^{0.7} / (D^{0.4} q) \quad \text{Equation 37}$$

where the symbols are given in abbreviation table.

Refereing to the ρ and c_p values for the blasted block samples in sessions 2013 and 2014, assuming that the conditions with regards to the rest of the parameters are roughly the same, the following differences on average will be observed:

In session p=2013 kg/m³ and c= 2274 m/s (see pages iv - v)

In session 2014: p=1986 and c=3056 m/s (see pages vi - vii)

Thus the average difference with regards to the ρ and c values may become roughly 30 %. The results from possible changes are summarized below:

Session	RMD if massive	JF	RDI	HF(E/3)	A (Kuz-Ram)	(p.c)
2013	50	1	9.05	7.96	3.84	8.54
2014	50	1	0.6	4.66	3.37	6.06

Drill patterns set-up, blast session 2013:

Table 53: Drill patterns set up, blast session 2013

Reference							
	45	row 1	25	row 2	25	row 3	25
	95	col 7	70	col 3	140	col 2	210
Hole	x		y		y		y
1	45	-0.84	48.9	0.75	158.8	-0.07	208.3
2	140	0.84	90.9	-0.02	139.6	-0.99	185.3
3	235	-0.43	59.3	-0.36	131.1	-0.98	185.6
4	330	-0.25	63.7	-0.63	124.3	0.72	228.0
5	425	0.30	77.5	0.88	162.0	0.37	219.2
6	520	0.99	94.9	-0.26	133.6	0.28	217.1
7	615	-0.60	55.1	-0.29	132.6	0.60	225.0
	Average:	0.002		0.012		-0.009	0.002
	Stdev	0.718		0.580		0.710	0.638
2-3-7 (1st burden deviation)							
	45	row 1	25	row 2	25	row 3	25
	95	col 2	70	col 3	140	col 7	210
Hole	x		y		y		y
1	45	-0.07	68.3	0.75	158.8	-0.84	188.9
2	140	-0.99	45.3	-0.02	139.6	0.84	230.9
3	235	-0.98	45.6	-0.36	131.1	-0.43	199.3
4	330	0.72	88.0	-0.63	124.3	-0.25	203.7
5	425	0.37	79.2	0.88	162.0	0.30	217.5
6	520	0.28	77.1	-0.26	133.6	0.99	234.9
7	615	0.60	85.0	-0.29	132.6	-0.60	195.1
	Average:	-0.009		0.012		0.002	0.002
	Stdev	0.710		0.580		0.718	0.638
13-7-3 (2nd burden deviation)							
	45	row 1	25	row 2	25	row 3	25
	95	col 13	70	col 7	140	col 3	210
Hole	x		y		y		y
1.0	45.0	0.57	84.2	-0.84	118.9	0.75	228.8
2.0	140.0	-0.94	46.6	0.84	160.9	-0.02	209.6
3.0	235.0	0.54	83.5	-0.43	129.3	-0.36	201.1
4.0	330.0	-0.73	51.8	-0.25	133.7	-0.63	194.3
5.0	425.0	0.27	76.7	0.30	147.5	0.88	232.0
6.0	520.0	0.76	89.0	0.99	164.9	-0.26	203.6
7.0	615.0	-0.58	55.5	-0.60	125.1	-0.29	202.6
	Average:	-0.015		0.002		0.012	0.000
	Stdev	0.708		0.718		0.580	0.637

The values are based on the same principle with random uncorrelated numbers, x gives the spacing, y gives the positions in the burden directions.

Table 55: Drill patterns set up: Box-Muller method (part 2)

TC2D constant	0,772			1,132277			0,657	1,175			1,175		
	sorted		0,866				sorted	rescaled			sorted	rescaled	
R	R	P		G(r)		R	R	R	P		R	R	P
0,6618	1,9685	100,0	2,273	99,4	N1	0,7117	1,5212	1,7875	100,0				
0,3937	1,9240	99,0	2,222	99,3		1,3241	1,5199	1,7859	96,4				
1,3700	1,8316	98,0	2,115	98,9		0,5034	1,4432	1,6958	92,9				
0,3013	1,7649	97,0	2,038	98,4		0,5893	1,3571	1,5947	89,3				
0,4288	1,6892	96,0	1,951	97,8		1,1167	1,3241	1,5559	85,7				
1,2620	1,6241	95,0	1,875	97,0		0,5807	1,1235	1,3201	82,1				
1,3905	1,5877	94,0	1,833	96,5		1,0929	1,1167	1,3121	78,6				
1,0226	1,5535	93,0	1,794	96,0	N2	0,6323	1,1154	1,3106	75,0	N2-N4	1,5212	1,7875	100,0
0,7370	1,5377	92,0	1,776	95,7		0,6098	1,0929	1,2842	71,4		1,5199	1,7859	95,2
0,1357	1,5212	91,0	1,757	95,4		1,5199	1,0189	1,1972	67,9		1,4432	1,6958	90,5
0,7048	1,5199	90,0	1,755	95,4		0,5249	1,0176	1,1958	64,3		1,3571	1,5947	85,7
0,4360	1,4785	89,0	1,707	94,6		0,2567	0,9655	1,1345	60,7		1,1235	1,3201	81,0
1,1339	1,4432	88,0	1,667	93,8		1,4432	0,8456	0,9936	57,1		1,1154	1,3106	76,2
1,3184	1,4399	87,0	1,663	93,7		0,6069	0,7936	0,9325	53,6		1,0189	1,1972	71,4
0,5504	1,4366	86,0	1,659	93,6	N3	0,8456	0,7117	0,8362	50,0		1,0176	1,1958	66,7
1,4785	1,4129	85,0	1,632	93,0		1,0189	0,6323	0,7429	46,4		0,9655	1,1345	61,9
1,5877	1,4122	84,0	1,631	93,0		0,5161	0,6098	0,7165	42,9		0,8456	0,9936	57,1
1,2616	1,3905	83,0	1,606	92,4		0,9655	0,6069	0,7131	39,3		0,7936	0,9325	52,4
1,3668	1,3700	82,0	1,582	91,8		1,3571	0,5893	0,6925	35,7		0,6323	0,7429	47,6
0,5028	1,3668	81,0	1,578	91,7		1,1235	0,5807	0,6823	32,1		0,6098	0,7165	42,9
1,4399	1,3571	80,0	1,567	91,4		1,5212	0,5581	0,6558	28,6		0,6069	0,7131	38,1
0,7117	1,3263	79,0	1,532	90,4	N4	0,4205	0,5249	0,6167	25,0		0,5581	0,6558	33,3
1,3241	1,3241	78,0	1,529	90,3		0,5581	0,5161	0,6064	21,4		0,5249	0,6167	28,6
0,5034	1,3184	77,0	1,522	90,1		0,4397	0,5034	0,5915	17,9		0,5161	0,6064	23,8
0,5893	1,3176	76,0	1,522	90,1		0,4170	0,4397	0,5167	14,3		0,4397	0,5167	19,0
1,1167	1,3025	75,0	1,504	89,6		1,0176	0,4205	0,4941	10,7		0,4205	0,4941	14,3
0,5807	1,2698	74,0	1,466	88,4		1,1154	0,4170	0,4899	7,1		0,4170	0,4899	9,5
1,0929	1,2620	73,0	1,457	88,0		0,7936	0,2567	0,3016	3,6		0,2567	0,3016	4,8
1,2698	1,2616	72,0	1,457	88,0									
0,7618	1,2553	71,0	1,450	87,8		28					21		
1,1545	1,2055	70,0	1,392	85,6									
1,6241	1,1783	69,0	1,361	84,3									
1,3025	1,1564	68,0	1,335	83,2									
1,4366	1,1545	67,0	1,333	83,1									
0,9793	1,1531	66,0	1,332	83,0									
1,9240	1,1519	65,0	1,330	83,0									
0,8739	1,1396	64,0	1,316	82,3									
0,8107	1,1339	63,0	1,309	82,0									
0,9070	1,1235	62,0	1,297	81,4									
0,7834	1,1167	61,0	1,289	81,0									
0,9652	1,1154	60,0	1,288	81,0									
0,3963	1,0929	59,0	1,262	79,7									
1,5377	1,0676	58,0	1,233	78,1									
0,2030	1,0226	57,0	1,181	75,2									
0,7304	1,0189	56,0	1,177	74,9									
0,3608	1,0176	55,0	1,175	74,9									
0,6323	0,9793	54,0	1,131	72,2									
0,6098	0,9655	53,0	1,115	71,1									

*The number of points used for the Box-Muller method is 250

a) Consequences:

1. Blasting pattern with almost uncorrelated collaring errors ΔS and ΔB in S and directions respectively
2. Blasting pattern with almost uncorrelated collaring errors between rows
3. Blasting pattern with almost same average burden volume for each row and as consequence almost same nominal specific charge

4. Blasting patterns where collaring errors in burden and spacing directions can be tested separately or together
5. Chosen $3 \times 7 = 21$ numbers Δx and Δy when ordered deviate somewhat from bivariate normal distribution CDF

The bivariate normal distribution for two orthogonal components with $R = \sqrt{(x^2 + y^2)}$ and σ stdev is:

$$CDF \cdot G(r) = 1 - e^{-(R/\sigma)^2} \text{Equation 38}$$

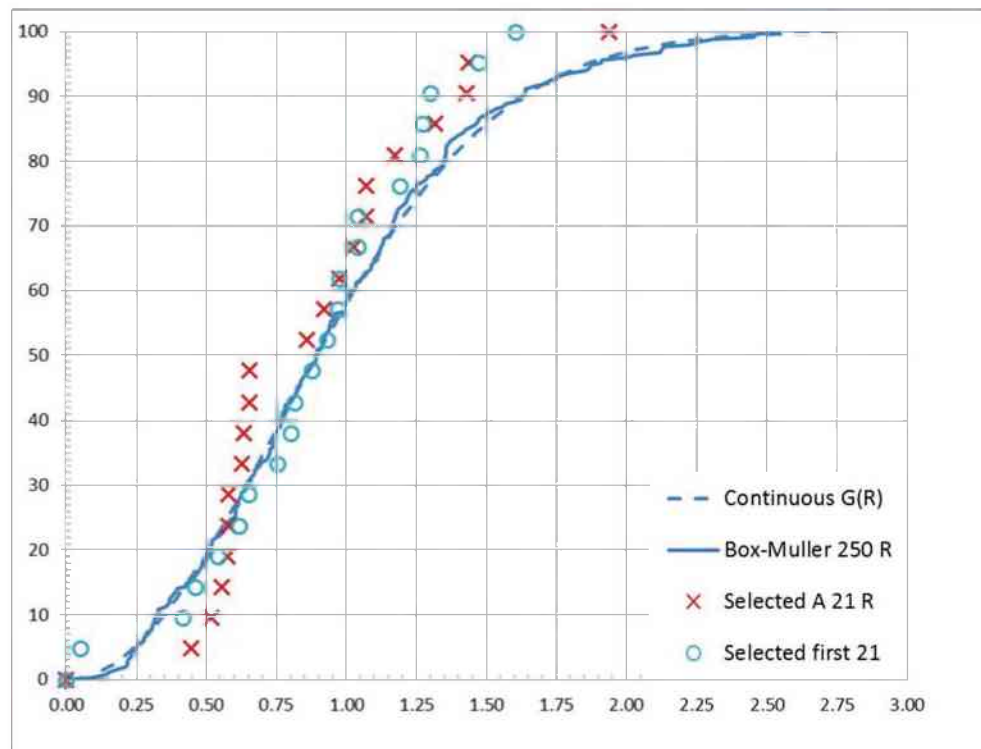


Figure 75: Selected values and the variation from CDF

S+B variations (3-7-6) pattern:

Table 56: Drill pattern 3-7-6 set up, session 2014

					0	95	190	285	380	475	570	
	S	B		R1	47.5	142.5	237.5	332.5	427.5	522.5	617.5	S0
N3	0.22	0.53	0.57	R1	70	70	70	70	70	70	70	B0
0.07	0.45	0.97	1.07	0.04	0.2	0.5	-1.1	-0.1	-0.1	0.8	0.3	S1
0.59	-	-	-	-	0.5	1	0.2	-1.3	-0.5	-0.5	0.3	B1
	0.10	1.31	1.32		51.9	151.5	216.6	330.6	424.9	538.4	623.9	x1
	0.13	0.54	0.56		89.6	89.5	74.6	43.7	59.2	60.6	76.2	y1
	0.79	0.47	0.92									
	0.32	0.31	0.44									
N7	0.46	0.46	0.66	R2	47.5	142.5	237.5	332.5	427.5	522.5	617.5	S0
0.01	0.35	0.46	0.58	0.02	140	140	140	140	140	140	140	B0
0.69	0.20	-0.6	0.63	0.68	0.5	0.4	-0.2	0.1	0.2	0.6	-1.4	S1
	0.13	0.97	0.98		-0.5	0.5	-0.6	1	0.6	-0.8	0	B1
	0.16	0.62	0.64		56.8	149.5	233.6	335.1	430.6	534.9	588.8	x2
	0.62	0.82	1.03		130.7	149.2	128.1	159.4	152.3	123.6	139.2	y2
	1.44	0.04	1.44									
N6	1.14	1.57	1.94	R3								
0.03	0.19	0.84	0.86	0.05	47.5	142.5	237.5	332.5	427.5	522.5	617.5	S0
0.83	0.92	1.09	1.43	0.89	210	210	210	210	210	210	210	B0
	0.50	0.11	0.52		-1.1	-0.2	-0.9	0.5	1.2	0.5	0.4	S1
	1.17	0.10	1.17		-1.6	0.8	1.1	0.1	-0.1	-0.5	0.5	B1
	0.46	0.46	0.66		39.7	138.8	219.2	342.6	450.9	531.8	624.5	x3
	0.35	0.46	0.58		178.7	226.8	231.9	212.2	207.9	200.7	219.2	y3
	0.67	0.75										

The values are based on the random uncorrelated numbers, x gives the spacing, y gives the positions in the burden directions. N3 (row 1), N7 (row2) and N6 (row 3) are the three combination sequences with a very low correlation selected.

Systematic collaring errors in spacing direction (S/4 shift):

S/4 shift pattern:

Table 57: Drill patterns S/4 set up, session 2014

	45	row 1	25	row 2	25	row 3	25
	95	col 2	70	col 3	140	col 7	210
Hole	x		x1		x2		x3
1	45	-0.07	68.8	0.75	36.3	-0.84	68.8
2	140	-0.99	163.8	-0.02	116.3	0.84	163.8
3	235	-0.98	258.8	-0.36	211.3	-0.43	258.8
4	330	0.72	353.8	-0.63	306.3	-0.25	353.8
5	425	0.37	448.8	0.88	401.3	0.30	448.8
6	520	0.28	543.8	-0.26	496.3	0.99	543.8
7	615	0.60	623.8	-0.29	591.3	-0.60	623.8
	Average:	-0.009		0.012		0.002	0.002
	Stdev	0.710		0.580		0.718	0.638

Appendix 4 Documentation of the blasting tests

CH01B03 (Reference)

Block	Row	X ₃₀ [mm]	X ₅₀ [mm]	X ₈₀ [mm]	Planned delay [μs]	Delay per m burden [ms/m]	Delay measured [μs]							Mean	Stdev [μs]	Range
							Hole 2	Hole 3	Hole 4	Hole 5	Hole 6	Hole 7				
CH01B03 (Reference)	1	26.08	57.61	91.35	73	1	Not measured, oscilloscope failure							71.50	1.21	3.0
	2	9.94	21.36	73.09	73	1	70.0	72.0	73.0	70.0	72.0	71.0				
	3	8.50	17.51	43.12	73	1	71.0	72.0	73.0	71.0	73.0	72.0				



Figure 76: Specimen CH01B03 (R01 upper, R02 mid, R03 down)

CH01B05 (Reference)

Block	Row	X_{50} [mm]	X_{50} [mm]	X_{80} [mm]	Planned delay [μ s]	Delay per m burden [ms/m]	Delay measured [μ s]							Mean	Stdev [μ s]	Range
							Hole 2	Hole 3	Hole 4	Hole 5	Hole 6	Hole 7				
CH01B05 (Reference)	1	15.64	32.43	64.29	73	1	71.5	71.5	73.5	72.0	77.5	69.0	71.75	2.85	8.5	
	2	10.41	22.42	54.45	73	1	74.0	71.5	73.0	73.5	74.0	72.5	73.25	0.97	2.5	
	3	7.71	14.54	37.00	73	1	72.5	72.0	75.0	71.5	74.5	74.5	73.50	1.51	3.5	



Figure 77: Specimen CH01B05 (R01 upper, R02 mid, R03 down)

CH01B02 (1st burden deviation)

Block	Row	X_{30} [mm]	X_{50} [mm]	X_{90} [mm]	Planned delay [μ s]	Delay per m burden [ms/m]	Delay measured [μ s]							Mean	Stdev [μ s]	Range
							Hole 2	Hole 3	Hole 4	Hole 5	Hole 6	Hole 7				
CH01B02 (1st burden deviation)	1	13.74	30.14	110.05	73	1	67.5	67.5	68.0	66.0	67.5	66.5	67.50	0.75	2.0	
	2	11.63	23.61	61.67	73	1	71.0	72.0	72.0	71.5	72.5	no data	72.00	0.57	1.5	
	3	10.12	19.95	52.05	73	1	73.5	71.5	71.5	71.5	71.5	71.5	71.50	0.82	2.0	



Figure 78: Specimen CH01B02 (R01 upper, R02 mid, R03 down)

CH01B04 (1st burden deviation)

Block	Row	X_{30} [mm]	X_{50} [mm]	X_{90} [mm]	Planned delay [μ s]	Delay per m burden [ms/m]	Delay measured [μ s]							Mean	Stdev [μ s]	Range
							Hole 2	Hole 3	Hole 4	Hole 5	Hole 6	Hole 7				
CH01B04 (1st burden deviation)	1	13.56	25.87	84.61	73	1	72.0	72.0	75.5	74.0	71.5	72.5	72.25	1.53	4.0	
	2	9.77	18.96	47.81	73	1	73.0	72.0	73.0	73.5	73.0	73.0	73.00	0.49	1.5	
	3	7.53	13.86	33.84	73	1	72.0	73.5	72.0	73.0	73.5	72.5	72.75	0.69	1.5	



Figure 79: Specimen CH01B04 (R01 upper, R02 mid, R03 down)

CH03B01 (2nd burden deviation)

Block	Row	X ₃₀ [mm]	X ₅₀ [mm]	X ₉₀ [mm]	Planned delay [μs]	Delay per m burden [ms/m]	Delay measured [μs]							Mean	Stdev [μs]	Range
							Hole 2	Hole 3	Hole 4	Hole 5	Hole 6	Hole 7				
CH03B01 (2nd burden deviation)	1	16.55	54.42	117.74	73	1	70.0	71.5	72.5	74.5	72.5	73.0	72.50	1.51	4.5	
	2	10.87	25.61	79.76	73	1	73.0	71.5	72.5	73.0	70.0	73.0	72.75	1.21	3.0	
	3	8.96	18.09	46.15	73	1	73.5	69.0	74.5	74.5	73.0	74.0	73.75	2.08	5.5	



Figure 80: Specimen CH03B01 (R01 upper, R02 mid, R03 down)

CH03B02 (2nd burden deviation)

Block	Row	X ₃₀ [mm]	X ₅₀ [mm]	X ₉₀ [mm]	Planned delay [μs]	Delay per m burden [ms/m]	Delay measured [μs]							Mean	Stdev [μs]	Range
							Hole 2	Hole 3	Hole 4	Hole 5	Hole 6	Hole 7				
CH03B02 (2nd burden deviation)	1	20.28	44.74	88.13	73	1	72.5	72.5	74.5	66.5	75.5	74.5	73.50	3.25	9.0	
	2	9.53	24.53	79.05	73	1	73.5	71.5	72.0	74.0	73.5	72.0	72.75	1.04	2.5	
	3	9.78	19.38	55.32	73	1	72.5	71.5	73.0	72.5	72.5	74.0	72.50	0.82	2.5	



Figure 81: Specimen CH03B02 (R01 upper, R02 mid, R03 down)

B01 (Reference)

Block	Row	x30 [mm]	x50 [mm]	x80 [mm]	Planned delay [μ s]	Delay per m burden [ms/m]	Delay measured [μ s]							Mean	Stdev [μ s]	Range
							Hole 2	Hole 3	Hole 4	Hole 5	Hole 6	Hole 7				
B01 (Reference)	1	56.96	90.63	>125	73	1	72.0	71.5	74.5	72.0	73.0	73.0	72.67	1.08	3.0	
	2	12.28	29.07	67.07	73	1	71.0	74.0	74.0	71.5	73.0	73.5	72.83	1.29	3.0	
	3	9.06	19.63	50.85	73	1	71.0	73.0	74.0	74.5	73.5	72.5	73.08	1.24	3.5	



Figure 82: Specimen B01 (R01 upper, R02 mid, R03 down)

B06 (Reference)

Block	Row	x30 [mm]	x50 [mm]	x80 [mm]	Planned delay [μ s]	Delay per m burden [ms/m]	Delay measured [μ s]							Mean	Stdev [μ s]	Range
							Hole 2	Hole 3	Hole 4	Hole 5	Hole 6	Hole 7				
B06 (Reference)	1	11.34	22.03	48.47	73	1	74.0	72.5	73.0	72.5	73.5	72.5	73.00	0.63	1.5	
	2	8.65	18.60	44.07	73	1	72.5	74.0	73.0	72.0	73.0	73.0	72.92	0.66	2.0	
	3	5.83	12.61	33.94	73	1	74.0	73.0	73.5	70.5	73.5	73.0	72.92	1.24	3.5	



Figure 83: Specimen B06 (R01 upper, R02 mid, R03 down)

B09 (Reference)

Block	Row	x30 [mm]	x50 [mm]	x80 [mm]	Planned delay [μ s]	Delay per m burden [ms/m]	Delay measured [μ s]							Mean	Stdev [μ s]	Range
							Hole 2	Hole 3	Hole 4	Hole 5	Hole 6	Hole 7				
B09 (Reference)	1	16.95	38.05	83.93	73	1	73.5	73.0	74.5	73.5	74.0	72.0	73.42	0.86	2.5	
	2	8.07	16.37	39.24	73	1	72.5	72.5	74.5	73.5	74.0	75.0	73.67	1.03	2.5	
	3	5.86	12.76	36.44	73	1	73.5	73.0	74.0	73.5	73.5	73.5	73.50	0.32	1.0	



Figure 84: Specimen B09 (R01 upper, R02 mid, R03 down)

B03 (S+B variations)

Block	Row	x30 [mm]	x50 [mm]	x80 [mm]	Planned delay [μ s]	Delay per m burden [ms/m]	Delay measured [μ s]							Mean	Stdev [μ s]	Range
							Hole 2	Hole 3	Hole 4	Hole 5	Hole 6	Hole 7				
B03 (S+B variations)	1	9.41	23.69	71.03	73	1	72.0	73.0	72.5	73.5	74.0	71.5	72.75	0.94	2.5	
	2	7.23	16.58	45.86	73	1	73.0	73.5	73.0	71.5	72.5	70.0	72.25	1.29	3.5	
	3	9.17	19.25	49.62	73	1	72.0	73.5	72.5	66.0	73.0	72.5	71.58	2.78	7.5	



Figure 85: Specimen B03 (R01 upper, R02 mid, R03 down)

B04 (S+B variations)

Block	Row	x30 [mm]	x50 [mm]	x80 [mm]	Planned delay [μ s]	Delay per m burden [ms/m]	Delay measured [μ s]							Mean	Stdev [μ s]	Range
							Hole 2	Hole 3	Hole 4	Hole 5	Hole 6	Hole 7				
B04 (S+B variations)	1	9.02	20.58	61.30	73	1	72.7	72.7	74.0	73.0	73.3	73.0	73.12	0.49	1.3	
	2	6.30	15.67	53.50	73	1	74.0	74.0	72.0	74.5	72.5	73.5	73.42	0.97	2.5	
	3	6.52	13.97	37.48	73	1	73.5	74.5	74.5	73.0	73.5	76.5	74.25	1.25	3.5	



Figure 86: Specimen B04 (R01 upper, R02 mid, R03 down)

B10 (S+B variations)

Block	Row	x30 [mm]	x50 [mm]	x80 [mm]	Planned delay [μ s]	Delay per m burden [ms/m]	Delay measured [μ s]							Mean	Stdev [μ s]	Range
							Hole 2	Hole 3	Hole 4	Hole 5	Hole 6	Hole 7				
B10 (S+B variations)	1	19.07	43.76	103.83	73	1	74.0	73.0	73.5	73.5	75.5	75.0	74.08	0.97	2.5	
	2	11.70	25.58	101.59	73	1	74.0	73.5	76.5	72.5	74.0	75.0	74.25	1.37	4.0	
	3	9.44	18.62	42.23	73	1	74.5	73.5	66.5	71.0	74.5	74.5	72.42	3.20	8.0	



Figure 87: Specimen B10 (R01 upper, R02 mid, R03 down)

B02 (S/4 shift)

Block	Row	x30 [mm]	x50 [mm]	x80 [mm]	Planned delay [μ s]	Delay per m burden [ms/m]	Delay measured [μ s]							Mean	Stdev [μ s]	Range
							Hole 2	Hole 3	Hole 4	Hole 5	Hole 6	Hole 7				
B02 (S/4 shift)	1	19.67	46.92	90.01	73	1	73.0	73.0	72.5	73.5	74.0	71.5	72.92	0.86	2.5	
	2	21.64	49.19	89.24	73	1	72.5	73.5	74.5	72.0	72.5	71.5	72.75	1.08	3.0	
	3	11.42	22.02	48.24	73	1	73.0	80.0	83.0	80.0	79.0	78.5	78.92	3.29	10.0	



Figure 88: Specimen B02 (R01 upper, R02 mid, R03 down)

B07 (S/4 shift)

Block	Row	x30 [mm]	x50 [mm]	x80 [mm]	Planned delay [μ s]	Delay per m burden [ms/m]	Delay measured [μ s]						Mean	Stdev [μ s]	Range
							Hole 2	Hole 3	Hole 4	Hole 5	Hole 6	Hole 7			
B07 (S/4 shift)	1	30.14	79.13	102.74	73	1	73.0	73.5	74.0	73.5	73.0	73.0	73.33	0.41	1.0
	2	15.43	39.55	81.46	73	1	72.5	75.0	72.5	72.5	73.0	73.5	73.17	0.98	2.5
	3	8.80	17.80	42.68	73	1	73.0	73.0	73.0	72.0	75.5	75.0	73.58	1.36	3.5



Figure 89: Specimen B07 (R01 upper, R02 mid, R03 down)

B11 (S/4 shift)

Block	Row	x30 [mm]	x50 [mm]	x80 [mm]	Planned delay [μs]	Delay per m burden [ms/m]	Delay measured [μs]							Mean	Stdev[μs]	Range
							Hole 2	Hole 3	Hole 4	Hole 5	Hole 6	Hole 7				
B11 (S/4 shift)	1	17.83	39.12	90.75	73	1	Oscilloscope failure									
	2	11.73	28.27	71.78	73	1	Oscilloscope failure									
	3	10.89	21.49	48.83	73	1	Oscilloscope failure									



Figure 90: Specimen B11 (R01 upper, R02 mid, R03 down)

Appendix 5 Sieving data and Swebrec fit summary

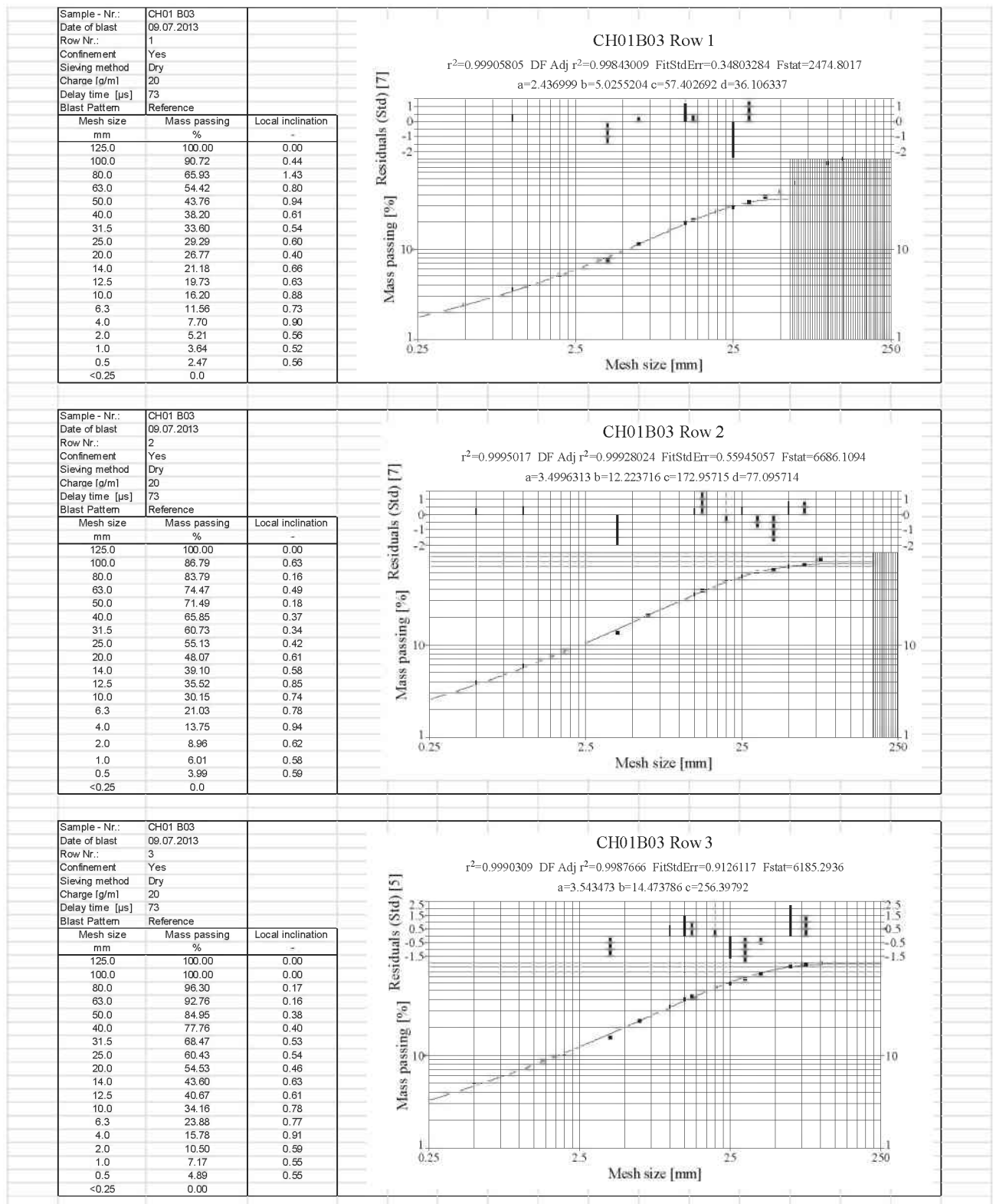
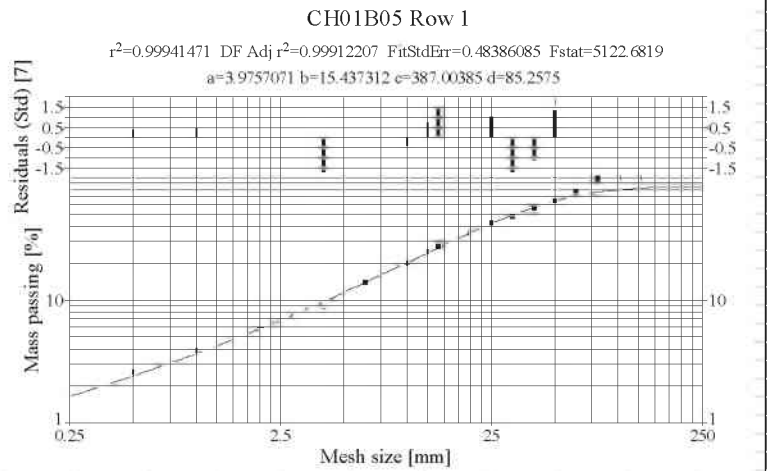
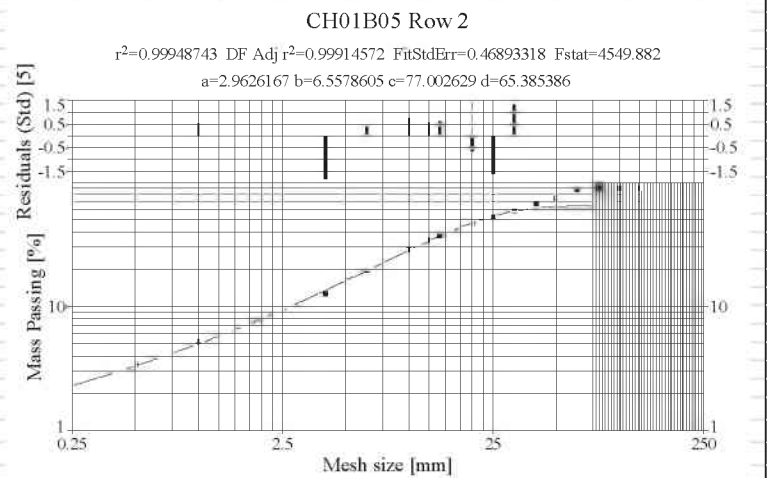


Figure 91: Specimen CH01B03 (Reference)

Sample - Nr.:	CH01 B05	
Date of blast	10.09.2013	
Row Nr.:	1	
Confinement	Yes	
Sieving method	Dry	
Charge [g/m]	20	
Delay time [μs]	73	
Blast Pattern	Reference	
Mesh size mm	Mass passing %	Local inclination -
125.0	100.00	0.00
100.0	100.00	0.00
80.0	100.00	0.00
63.0	78.36	1.02
50.0	65.49	0.78
40.0	57.25	0.60
31.5	49.10	0.64
25.0	43.04	0.57
20.0	35.82	0.82
14.0	27.80	0.71
12.5	24.99	0.94
10.0	20.28	0.93
6.3	13.97	0.81
4.0	8.98	0.97
2.0	5.83	0.62
1.0	3.92	0.57
0.5	2.61	0.59
<0.25	0.0	



Sample - Nr.:	CH01 B05	
Date of blast	10.09.2013	
Row Nr.:	2	
Confinement	Yes	
Sieving method	Dry	
Charge [g/m]	20	
Delay time [μs]	73	
Blast Pattern	Reference	
Mesh size mm	Mass passing %	Local inclination -
125.0	90.74	0.00
100.0	90.74	0.00
80.0	90.74	0.00
63.0	89.26	0.07
50.0	75.17	0.74
40.0	68.41	0.42
31.5	59.50	0.58
25.0	52.91	0.51
20.0	47.27	0.50
14.0	37.70	0.63
12.5	34.60	0.76
10.0	29.09	0.78
6.3	19.79	0.83
4.0	12.68	0.98
2.0	7.98	0.67
1.0	5.30	0.59
0.5	3.45	0.62
<0.25	0.0	



Sample - Nr.:	CH01 B05	
Date of blast	10.09.2013	
Row Nr.:	3	
Confinement	Yes	
Sieving method	Dry	
Charge [g/m]	20	
Delay time [μs]	73	
Blast Pattern	Reference	
Mesh size mm	Mass passing %	Local inclination -
125.0	100.00	0.00
100.0	100.00	0.00
80.0	95.37	0.21
63.0	95.37	0.00
50.0	90.02	0.25
40.0	82.54	0.39
31.5	75.34	0.38
25.0	71.05	0.25
20.0	62.48	0.58
14.0	48.76	0.69
12.5	45.58	0.60
10.0	37.93	0.82
6.3	25.13	0.89
4.0	16.28	0.96
2.0	10.50	0.63
1.0	6.92	0.60
0.5	4.37	0.66
<0.25	0.00	

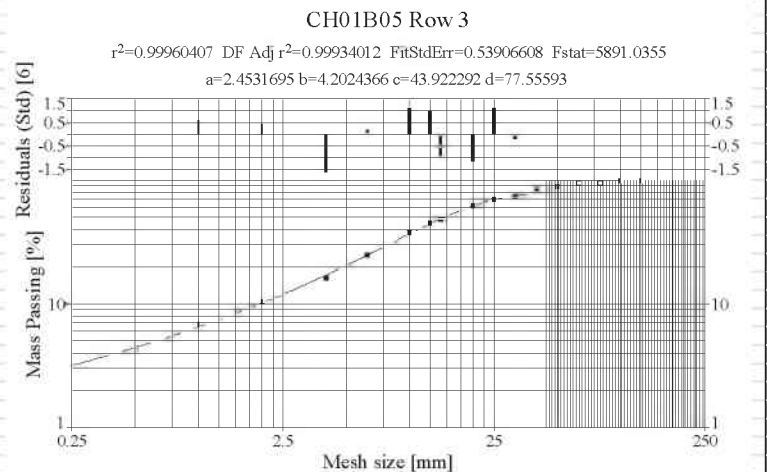
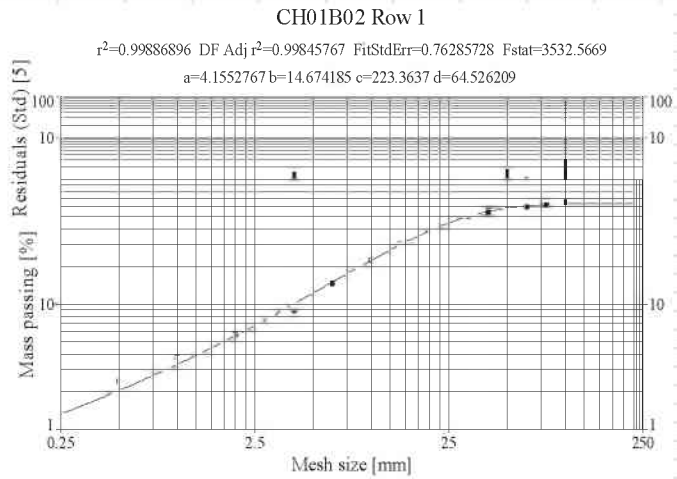
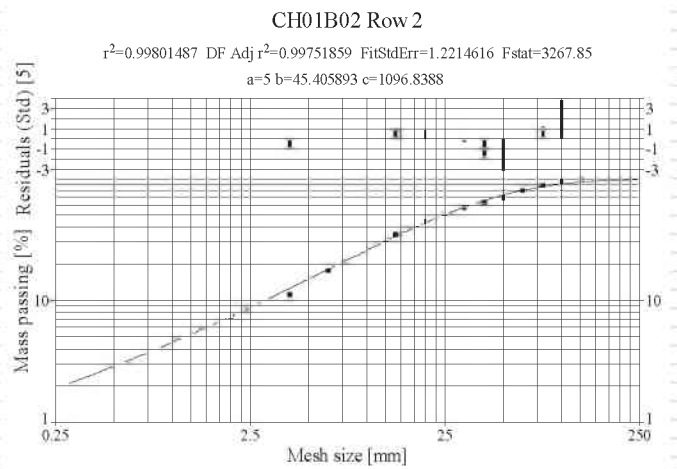


Figure 92: Specimen CH01B05 (Reference)

Sample - Nr.:	CH01 B02	
Date of blast	22.08.2013	
Row Nr.:	1	
Confinement	Yes	
Sieving method	Dry	
Charge [g/m]	20	
Delay time [µs]	73	
Blast Pattern	1st burden deviation	
Mesh size mm	Mass passing %	Local inclination -
125.0	100.00	0.00
100.0	66.56	1.82
80.0	63.09	0.24
63.0	60.95	0.14
50.0	57.63	0.24
40.0	55.22	0.19
31.5	50.98	0.33
25.0	46.28	0.42
20.0	39.78	0.68
14.0	30.55	0.74
12.5	27.39	0.97
10.0	22.76	0.83
6.3	14.87	0.92
4.0	8.97	1.11
2.0	5.81	0.63
1.0	3.84	0.60
0.5	2.43	0.66
<0.25	0.0	



Sample - Nr.:	CH01 B02	
Date of blast	22.08.2013	
Row Nr.:	2	
Confinement	Yes	
Sieving method	Dry	
Charge [g/m]	20	
Delay time [µs]	73	
Blast Pattern	1st burden deviation	
Mesh size mm	Mass passing %	Local inclination -
125.0	100.00	0.00
100.0	95.78	0.19
80.0	88.27	0.37
63.0	81.11	0.35
50.0	70.29	0.62
40.0	64.80	0.36
31.5	58.39	0.44
25.0	51.92	0.51
20.0	45.02	0.64
14.0	35.03	0.70
12.5	31.80	0.85
10.0	26.64	0.79
6.3	17.87	0.86
4.0	11.25	1.02
2.0	7.46	0.59
1.0	4.70	0.67
0.5	2.84	0.73
<0.25	0.0	



Sample - Nr.:	CH01 B02	
Date of blast	22.08.2013	
Row Nr.:	3	
Confinement	Yes	
Sieving method	Dry	
Charge [g/m]	20	
Delay time [µs]	73	
Blast Pattern	1st burden deviation	
Mesh size mm	Mass passing %	Local inclination -
125.0	100.00	0.00
100.0	100.00	0.00
80.0	100.00	0.00
63.0	85.26	0.67
50.0	80.89	0.23
40.0	75.25	0.32
31.5	65.35	0.59
25.0	58.62	0.47
20.0	50.10	0.70
14.0	38.74	0.72
12.5	35.48	0.78
10.0	29.73	0.79
6.3	20.24	0.83
4.0	12.22	1.11
2.0	8.11	0.59
1.0	5.26	0.62
0.5	3.34	0.65
<0.25	0.00	

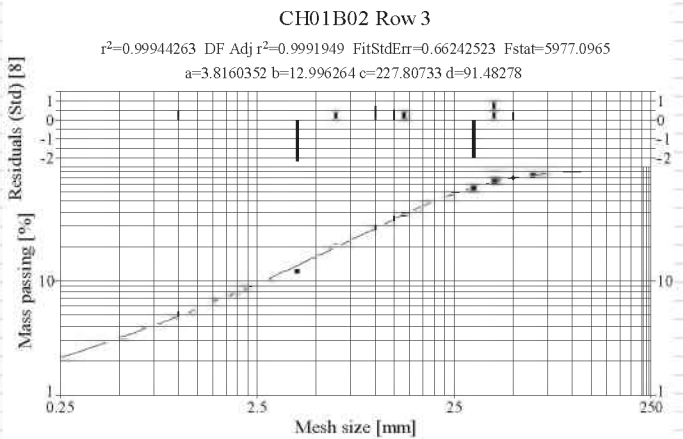
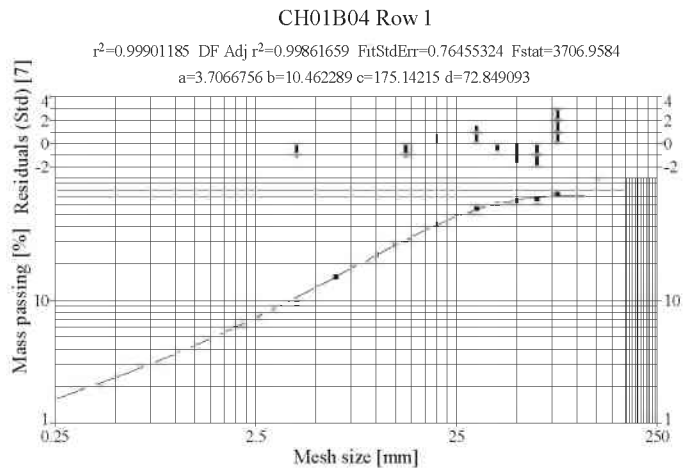
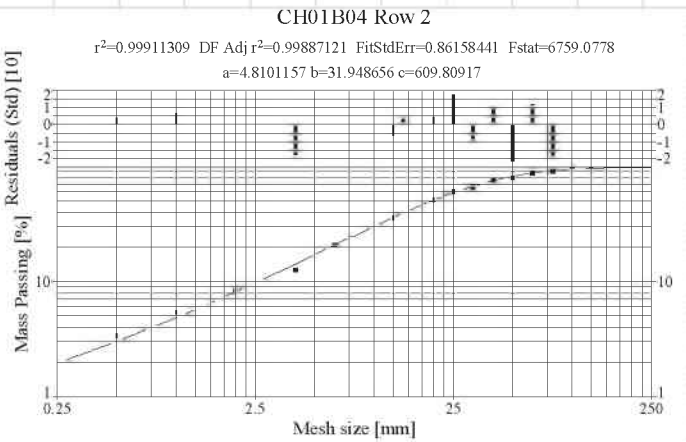


Figure 93: Specimen CH01B02 (1st burden deviation)

Sample - Nr.:	CH01 B04	
Date of blast	04.09.2013	
Row Nr.:	1	
Confinement	Yes	
Sieving method	Dry	
Charge [g/m]	20	
Delay time [µs]	73	
Blast Pattern	1st burden deviation	
Mesh size mm	Mass passing %	Local inclination -
125.0	100.00	0.00
100.0	100.00	0.00
80.0	74.00	1.35
63.0	67.91	0.36
50.0	65.04	0.19
40.0	61.23	0.27
31.5	56.64	0.33
25.0	48.97	0.63
20.0	42.27	0.66
14.0	30.53	0.91
12.5	28.73	0.54
10.0	23.84	0.84
6.3	15.74	0.90
4.0	9.71	1.06
2.0	6.45	0.59
1.0	4.11	0.65
0.5	2.42	0.76
<0.25	0.0	



Sample - Nr.:	CH01 B04	
Date of blast	04.09.2013	
Row Nr.:	2	
Confinement	Yes	
Sieving method	Dry	
Charge [g/m]	20	
Delay time [µs]	73	
Blast Pattern	1st burden deviation	
Mesh size mm	Mass passing %	Local inclination -
125.0	100.00	0.00
100.0	100.00	0.00
80.0	91.25	0.41
63.0	89.45	0.08
50.0	80.84	0.44
40.0	76.98	0.22
31.5	67.19	0.57
25.0	61.19	0.40
20.0	52.06	0.72
14.0	40.15	0.73
12.5	35.91	0.99
10.0	30.59	0.72
6.3	20.92	0.82
4.0	12.73	1.09
2.0	8.35	0.61
1.0	5.49	0.60
0.5	3.43	0.68
<0.25	0.0	



Sample - Nr.:	CH01 B04	
Date of blast	04.09.2013	
Row Nr.:	3	
Confinement	Yes	
Sieving method	Dry	
Charge [g/m]	20	
Delay time [µs]	73	
Blast Pattern	1st burden deviation	
Mesh size mm	Mass passing %	Local inclination -
125.0	100.00	0.00
100.0	100.00	0.00
80.0	97.08	0.13
63.0	97.08	0.00
50.0	94.24	0.13
40.0	86.11	0.40
31.5	77.68	0.43
25.0	69.82	0.46
20.0	62.42	0.50
14.0	50.40	0.60
12.5	45.93	0.82
10.0	39.17	0.71
6.3	25.42	0.94
4.0	16.49	0.95
2.0	10.31	0.68
1.0	6.43	0.68
0.5	3.98	0.69
<0.25	0.00	

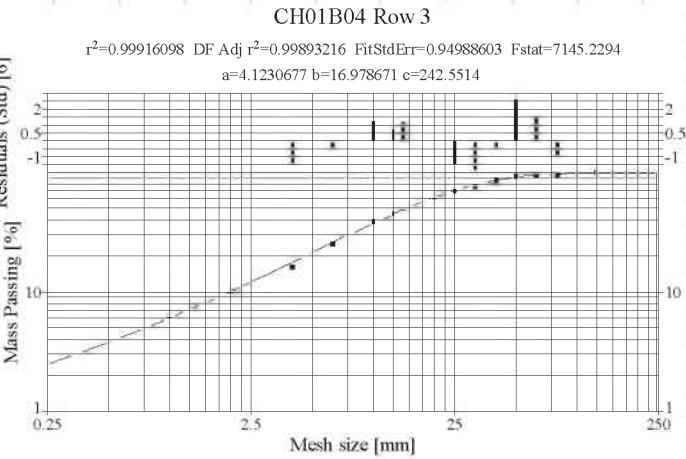
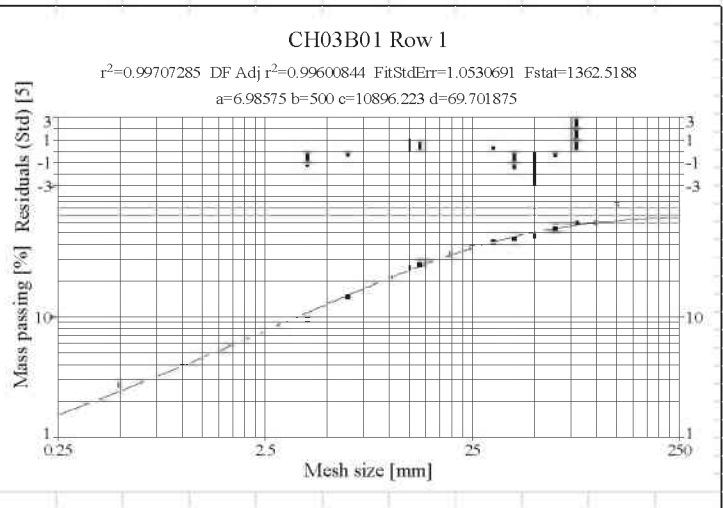
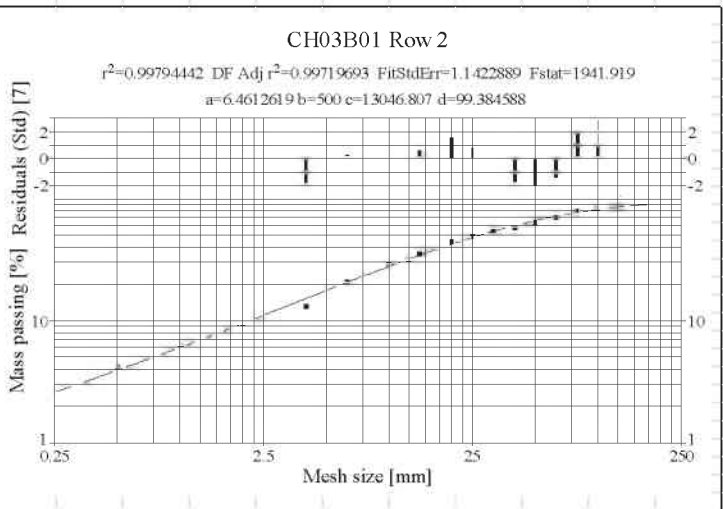


Figure 94: Specimen CH01B04 (1st burden deviation)

Sample - Nr.:	CH03 B01	
Date of blast	02.10.2013	
Row Nr.:	1	
Confinement	Yes	
Sieving method	Dry	
Charge [g/m]	20	
Delay time [μs]	73	
Blast Pattern	2nd burden deviation	
Mesh size mm	Mass passing %	Local inclination -
125.0	87.60	0.00
100.0	61.45	1.59
80.0	61.45	0.00
63.0	54.32	0.52
50.0	47.77	0.56
40.0	45.13	0.26
31.5	42.62	0.24
25.0	38.29	0.46
20.0	33.49	0.60
14.0	27.42	0.56
12.5	25.92	0.50
10.0	21.55	0.83
6.3	14.79	0.81
4.0	9.50	0.97
2.0	6.30	0.59
1.0	4.19	0.59
0.5	2.75	0.61
<0.25	0.0	



Sample - Nr.:	CH03 B01	
Date of blast	02.10.2013	
Row Nr.:	2	
Confinement	Yes	
Sieving method	Dry	
Charge [g/m]	20	
Delay time [μs]	73	
Blast Pattern	2nd burden deviation	
Mesh size mm	Mass passing %	Local inclination -
125.0	100.00	0.00
100.0	83.52	0.81
80.0	80.13	0.19
63.0	70.75	0.52
50.0	64.42	0.41
40.0	58.92	0.40
31.5	54.69	0.31
25.0	49.51	0.43
20.0	44.76	0.45
14.0	35.52	0.65
12.5	32.37	0.82
10.0	28.74	0.53
6.3	21.14	0.66
4.0	13.23	1.03
2.0	9.41	0.49
1.0	6.40	0.56
0.5	4.26	0.59
<0.25	0.0	



Sample - Nr.:	CH03 B01	
Date of blast	02.10.2013	
Row Nr.:	3	
Confinement	Yes	
Sieving method	Dry	
Charge [g/m]	20	
Delay time [μs]	73	
Blast Pattern	2nd burden deviation	
Mesh size mm	Mass passing %	Local inclination -
125.0	100.00	0.00
100.0	100.00	0.00
80.0	94.58	0.25
63.0	87.32	0.33
50.0	82.54	0.24
40.0	75.94	0.37
31.5	67.87	0.47
25.0	60.71	0.48
20.0	53.95	0.53
14.0	41.54	0.73
12.5	38.58	0.65
10.0	32.56	0.76
6.3	23.49	0.71
4.0	15.20	0.96
2.0	10.40	0.55
1.0	7.17	0.54
0.5	4.79	0.58
<0.25	0.00	

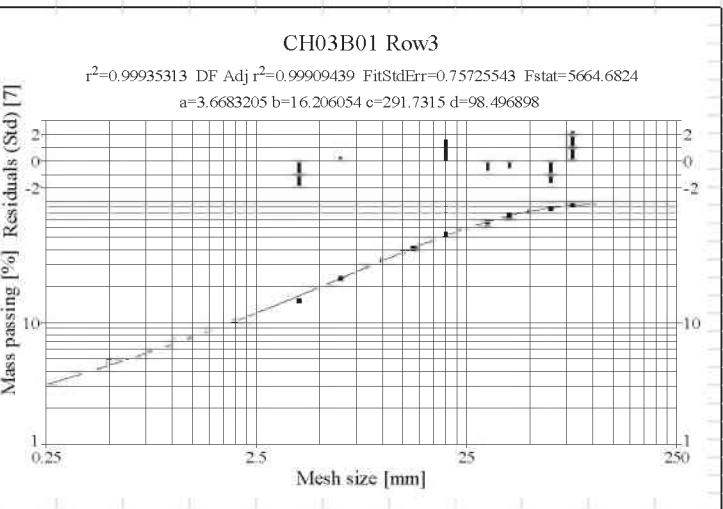


Figure 95: Specimen CH03B01 (2nd burden deviation)

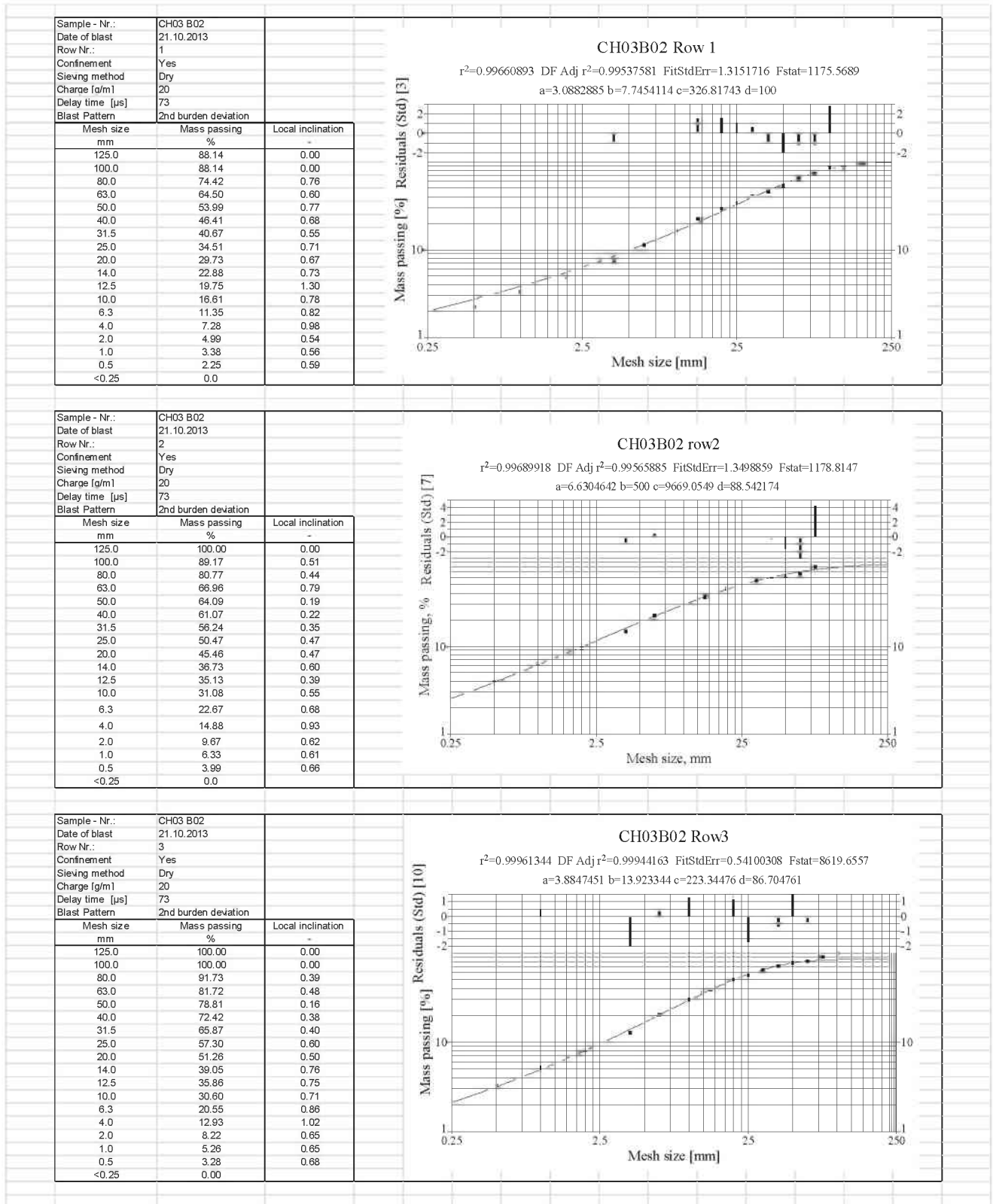
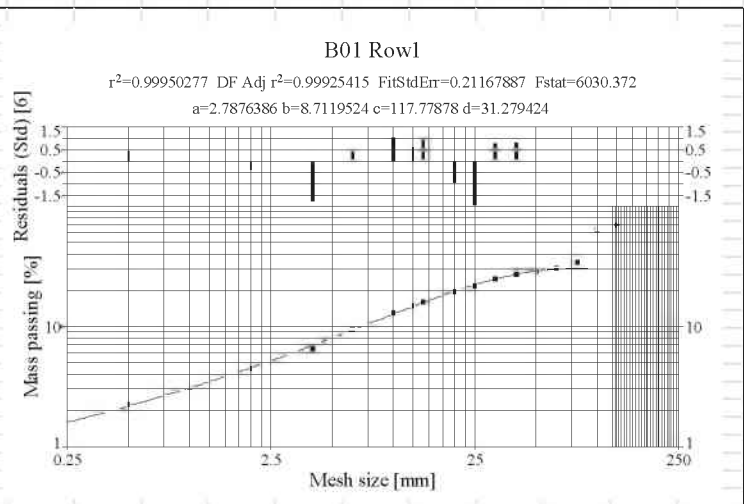
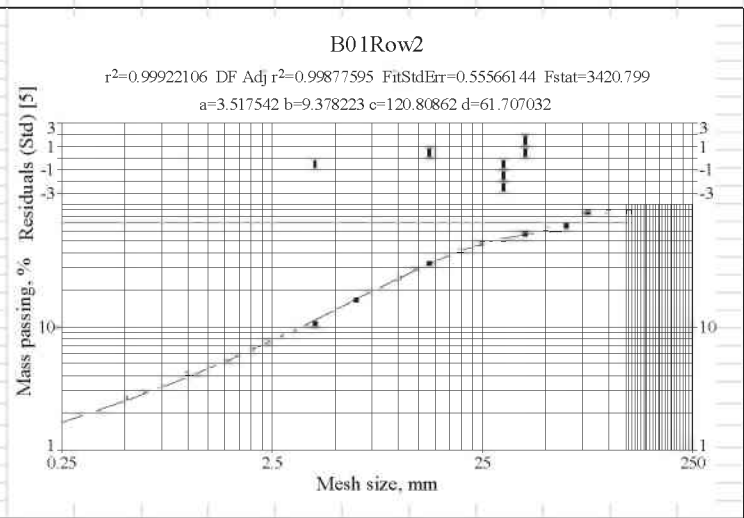


Figure 96: Specimen CH03B02 (2nd burden deviation)

Sample - Nr.:	B01	
Date of blast	03.06.2014	
Row Nr.:	1	
Confinement	Yes	
Sieving method	Dry	
Charge [g/m]	20	
Delay time [µs]	73	
Blast Pattern	Reference	
Mesh size mm	Mass passing %	Local inclination -
125.0	69.98	0.00
100.0	63.36	0.45
80.0	34.83	2.68
63.0	30.84	0.51
50.0	29.03	0.26
40.0	27.52	0.24
31.5	25.16	0.37
25.0	22.02	0.58
20.0	19.67	0.51
14.0	16.19	0.55
12.5	15.00	0.67
10.0	13.05	0.62
6.3	9.54	0.68
4.0	6.62	0.81
2.0	4.49	0.56
1.0	3.15	0.51
0.5	2.29	0.46
<0.25		



Sample - Nr.:	B01	
Date of blast	03.06.2014	
Row Nr.:	2	
Confinement	Yes	
Sieving method	Dry	
Charge [g/m]	20	
Delay time [µs]	73	
Blast Pattern	Reference	
Mesh size mm	Mass passing %	Local inclination -
125.0	88.10	0.00
100.0	88.10	0.00
80.0	88.10	0.00
63.0	67.52	1.11
50.0	63.61	0.26
40.0	58.10	0.41
31.5	51.19	0.53
25.0	48.01	0.28
20.0	42.19	0.58
14.0	33.37	0.66
12.5	30.49	0.80
10.0	25.02	0.89
6.3	16.89	0.85
4.0	10.76	0.99
2.0	6.53	0.72
1.0	4.20	0.64
0.5	2.66	0.66
<0.25		



Sample - Nr.:	B01	
Date of blast	03.06.2014	
Row Nr.:	3	
Confinement	Yes	
Sieving method	Dry	
Charge [g/m]	20	
Delay time [µs]	73	
Blast Pattern	Reference	
Mesh size mm	Mass passing %	Local inclination -
125.0	100.00	0.00
100.0	100.00	0.00
80.0	91.83	0.38
63.0	86.08	0.27
50.0	79.57	0.34
40.0	69.93	0.58
31.5	62.43	0.47
25.0	57.20	0.38
20.0	50.50	0.56
14.0	42.26	0.50
12.5	38.34	0.86
10.0	32.49	0.74
6.3	22.71	0.78
4.0	16.30	0.73
2.0	10.98	0.57
1.0	7.63	0.52
0.5	5.20	0.55
<0.25	0.00	

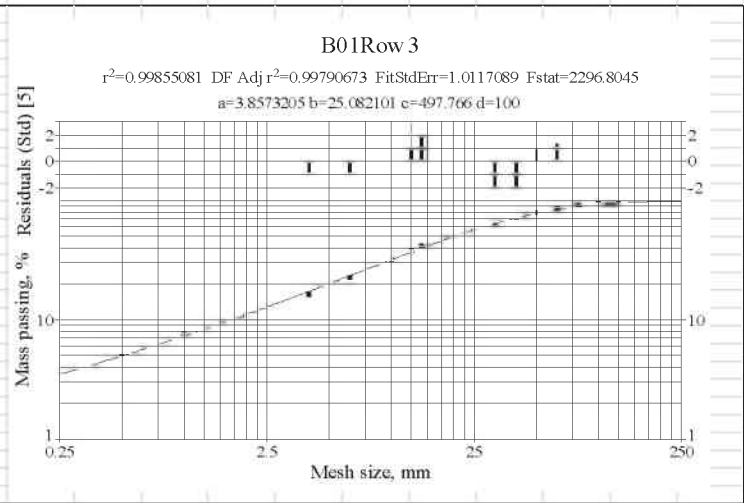


Figure 97: Specimen B01 (Reference)

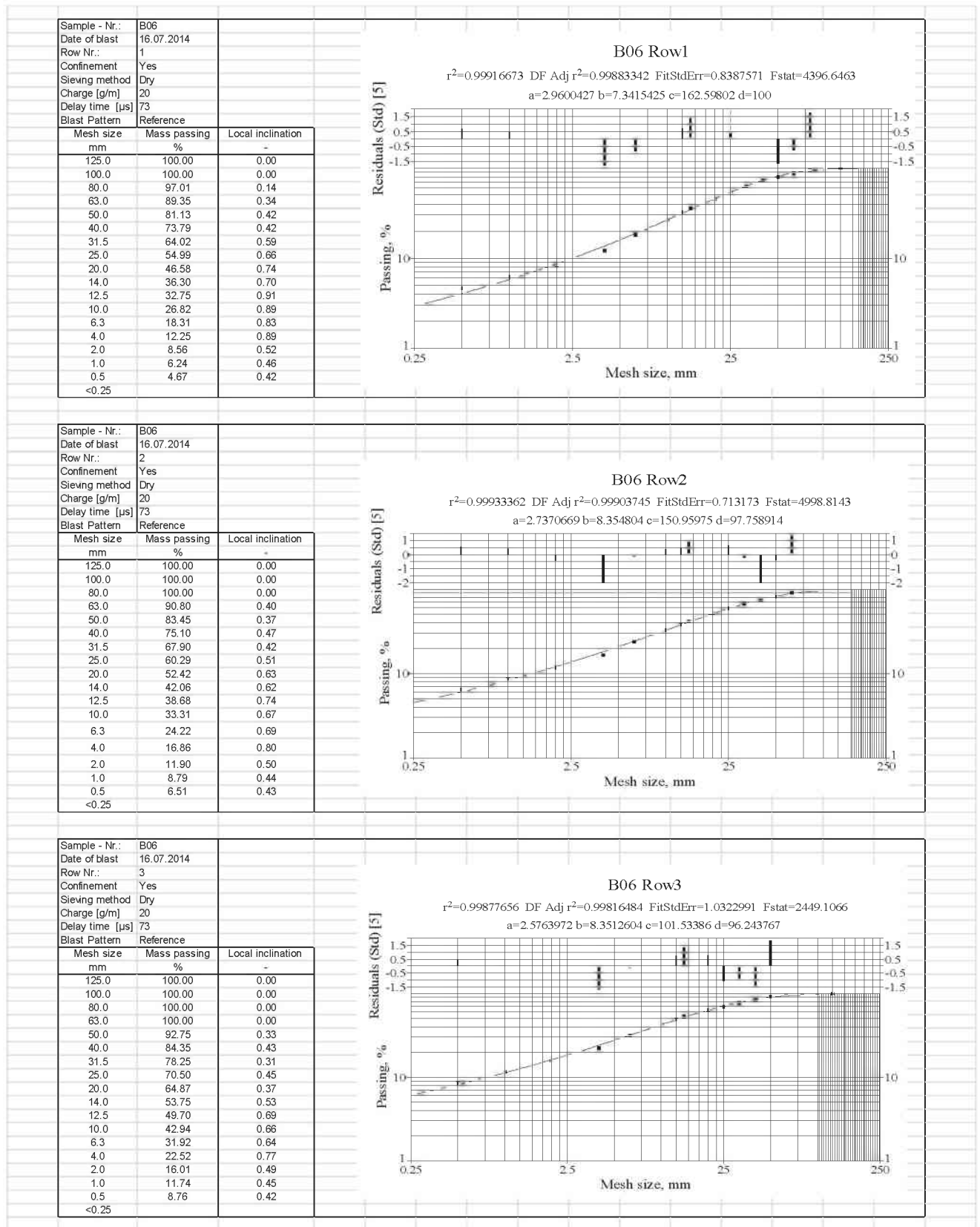


Figure 98: Specimen B06 (Reference)

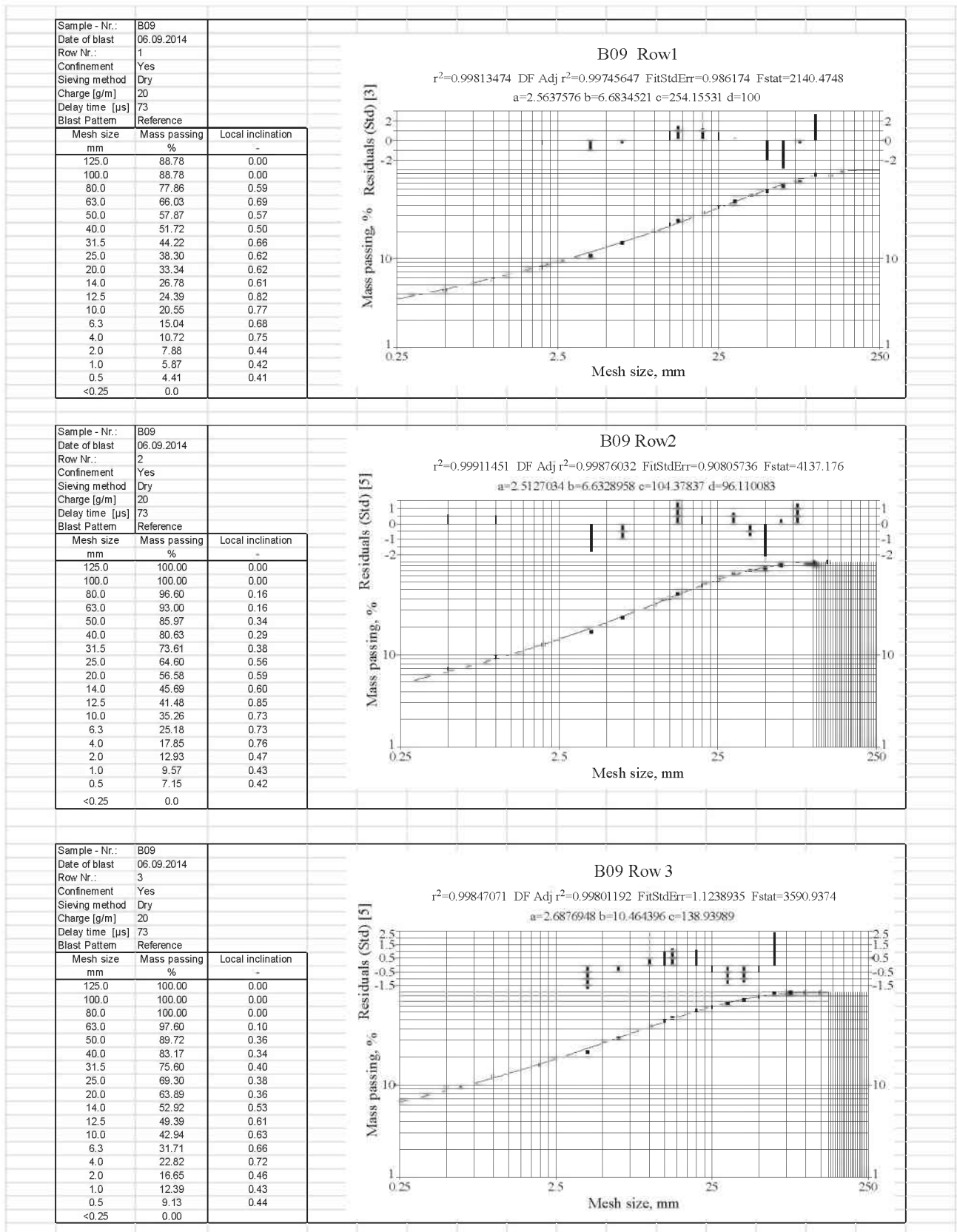
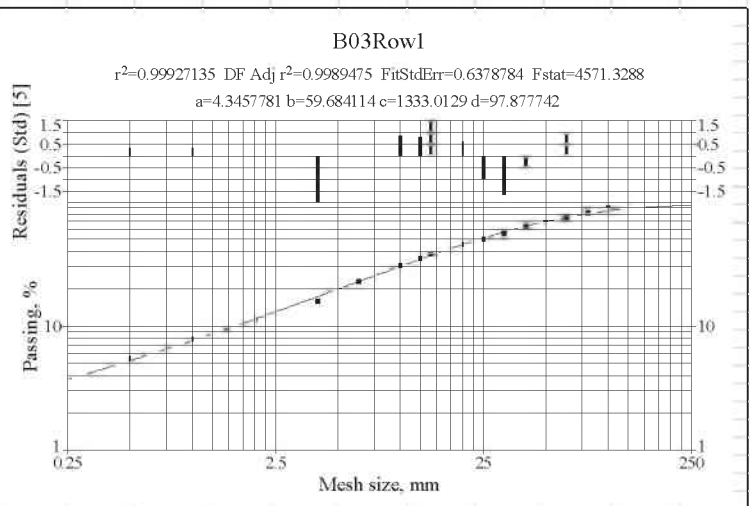
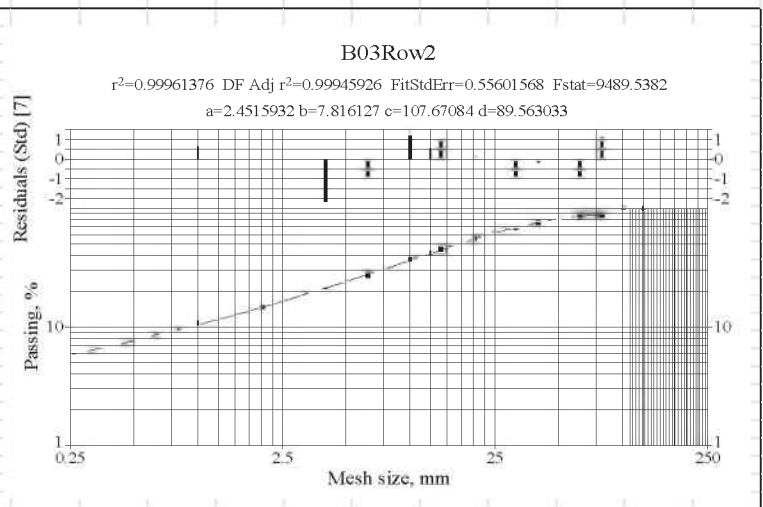


Figure 99: Specimen B09 (Reference)

Sample - Nr.:	B03	
Date of blast	23.06.2014	
Row Nr.:	1	
Confinement	Yes	
Sieving method	Dry	
Charge [g/ml]	20	
Delay time [µs]	73	
Blast Pattern	S+B variations	
Mesh size mm	Mass passing %	Local inclination -
125.0	100.00	0.00
100.0	92.33	0.36
80.0	83.26	0.46
63.0	77.08	0.32
50.0	70.69	0.37
40.0	64.42	0.42
31.5	57.10	0.51
25.0	51.25	0.47
20.0	46.51	0.43
14.0	38.57	0.52
12.5	35.73	0.67
10.0	31.32	0.59
6.3	23.07	0.66
4.0	16.22	0.78
2.0	11.35	0.52
1.0	7.95	0.51
0.5	5.53	0.52
<0.25		



Sample - Nr.:	B03	
Date of blast	23.06.2014	
Row Nr.:	2	
Confinement	Yes	
Sieving method	Dry	
Charge [g/ml]	20	
Delay time [µs]	73	
Blast Pattern	S+B variations	
Mesh size mm	Mass passing %	Local inclination -
125.0	100.00	0.00
100.0	100.00	0.00
80.0	89.42	0.50
63.0	85.78	0.17
50.0	82.37	0.18
40.0	76.65	0.32
31.5	69.21	0.43
25.0	62.60	0.43
20.0	55.66	0.53
14.0	45.74	0.55
12.5	42.57	0.64
10.0	37.58	0.56
6.3	27.47	0.68
4.0	20.27	0.67
2.0	14.75	0.46
1.0	10.90	0.44
0.5	7.91	0.46
<0.25		



Sample - Nr.:	B03	
Date of blast	23.06.2014	
Row Nr.:	3	
Confinement	Yes	
Sieving method	Dry	
Charge [g/ml]	20	
Delay time [µs]	73	
Blast Pattern	S+B variations	
Mesh size mm	Mass passing %	Local inclination -
125.0	100.00	0.00
100.0	100.00	0.00
80.0	93.09	0.32
63.0	87.61	0.25
50.0	80.30	0.38
40.0	72.50	0.46
31.5	65.80	0.41
25.0	58.37	0.52
20.0	51.31	0.58
14.0	40.89	0.64
12.5	37.26	0.82
10.0	32.00	0.68
6.3	23.07	0.71
4.0	16.48	0.74
2.0	11.66	0.50
1.0	8.59	0.44
0.5	6.29	0.45
<0.25		

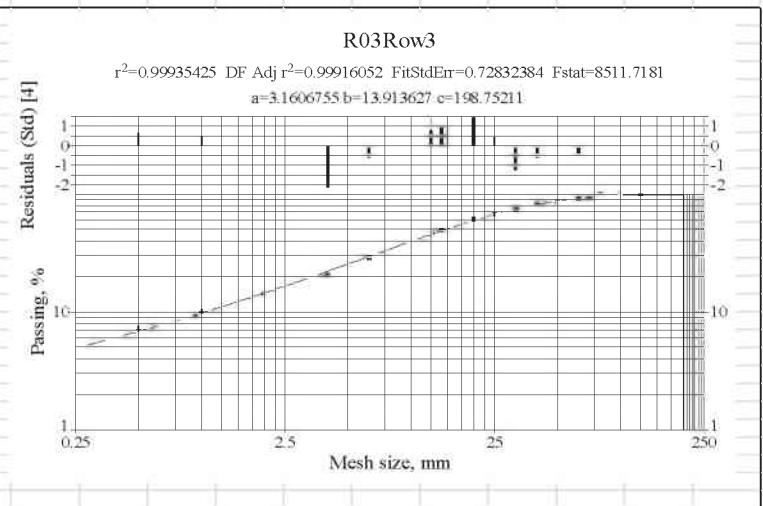
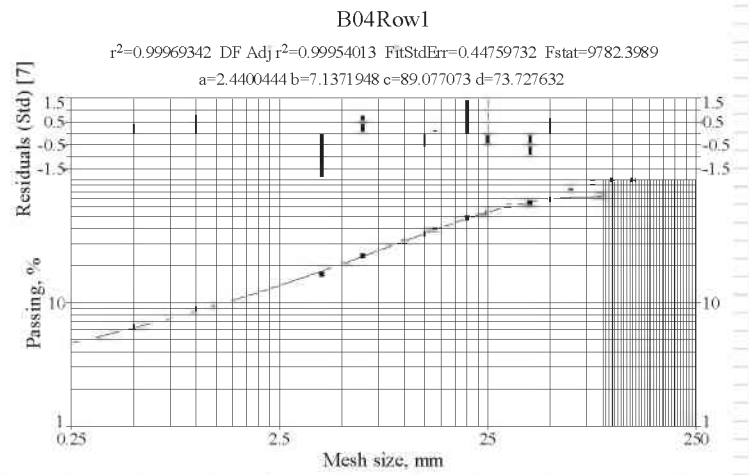
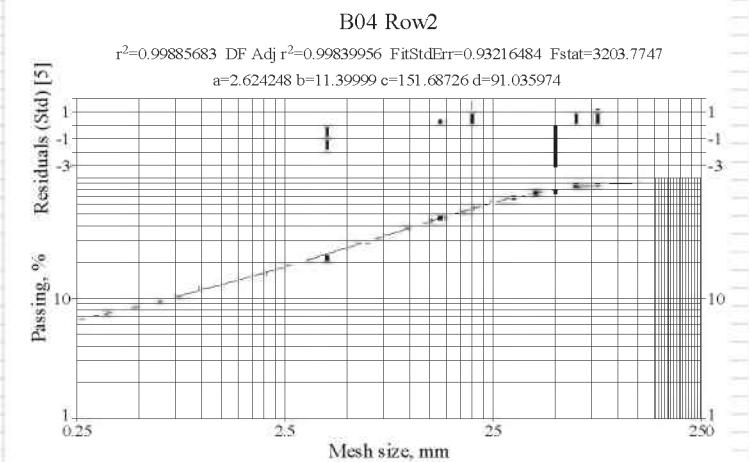


Figure 100: Specimen B03 (S+B variations)

Sample - Nr.:	B04	
Date of blast	04.07.2014	
Row Nr.:	1	
Confinement	Yes	
Sieving method	Dry	
Charge [a/m]	20	
Delay time [μs]	73	
Blast Pattern	S+B variations	
Mesh size mm	Mass passing %	Local inclination -
125.0	100.00	0.00
100.0	100.00	0.00
80.0	95.69	0.20
63.0	81.43	0.68
50.0	70.49	0.62
40.0	65.85	0.31
31.5	60.86	0.33
25.0	54.63	0.47
20.0	49.39	0.45
14.0	39.62	0.62
12.5	36.64	0.69
10.0	32.05	0.60
6.3	24.33	0.60
4.0	17.37	0.74
2.0	12.42	0.48
1.0	9.02	0.46
0.5	6.50	0.47
<0.25		



Sample - Nr.:	B04	
Date of blast	04.07.2014	
Row Nr.:	2	
Confinement	Yes	
Sieving method	Dry	
Charge [a/m]	20	
Delay time [μs]	73	
Blast Pattern	S+B variations	
Mesh size mm	Mass passing %	Local inclination -
125.0	100.00	0.00
100.0	100.00	0.00
80.0	89.56	0.49
63.0	86.09	0.17
50.0	77.75	0.44
40.0	75.26	0.15
31.5	69.00	0.36
25.0	62.96	0.40
20.0	57.23	0.43
14.0	47.20	0.54
12.5	44.35	0.55
10.0	39.38	0.53
6.3	30.00	0.59
4.0	21.80	0.70
2.0	16.22	0.43
1.0	12.24	0.41
0.5	9.11	0.43
<0.25		



Sample - Nr.:	B04	
Date of blast	04.07.2014	
Row Nr.:	3	
Confinement	Yes	
Sieving method	Dry	
Charge [g/ml]	20	
Delay time [μs]	73	
Blast Pattern	S+B variations	
Mesh size mm	Mass passing %	Local inclination -
125.0	100.00	0.00
100.0	100.00	0.00
80.0	100.00	0.00
63.0	92.86	0.31
50.0	88.23	0.22
40.0	82.25	0.31
31.5	74.64	0.41
25.0	68.34	0.38
20.0	61.68	0.46
14.0	50.08	0.58
12.5	46.67	0.62
10.0	40.19	0.67
6.3	29.35	0.68
4.0	20.77	0.76
2.0	14.50	0.52
1.0	10.26	0.50
0.5	7.42	0.47
<0.25		

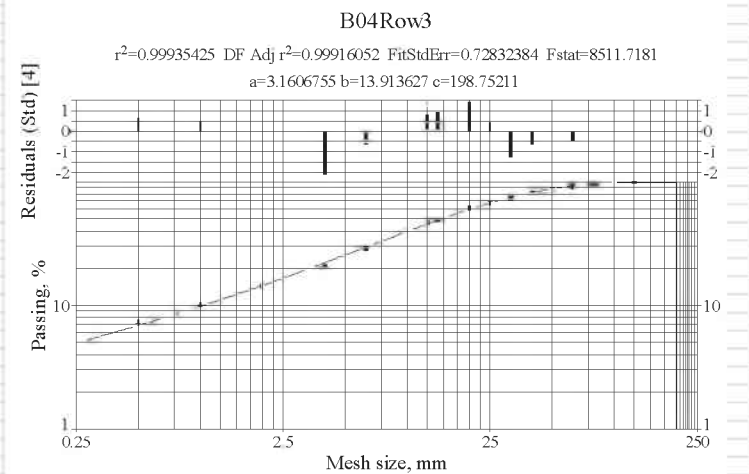
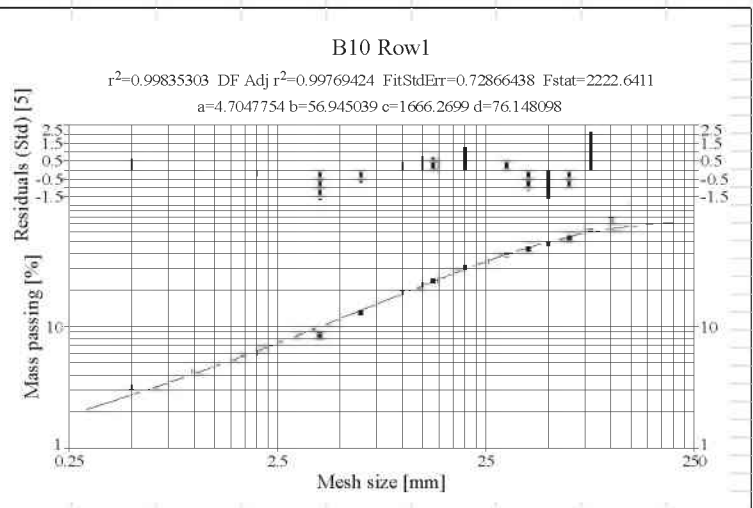
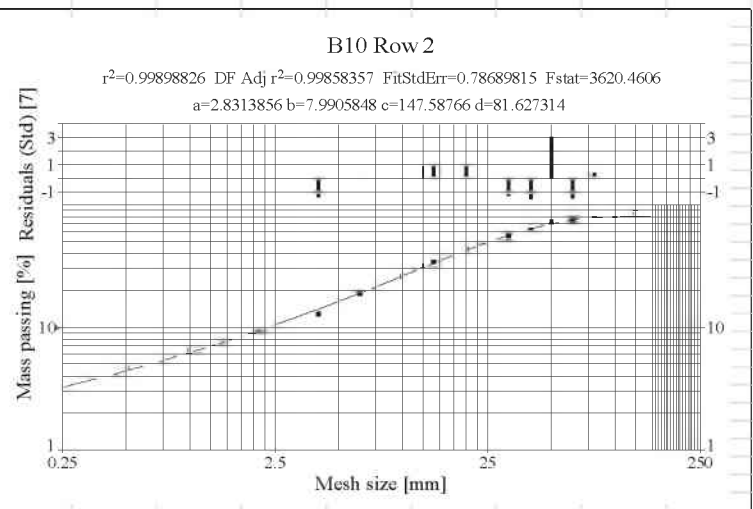


Figure 101: Specimen B04 (S+B variations)

Sample - Nr.:	B10	
Date of blast	07.10.2014	
Row Nr.:	1	
Confinement	Yes	
Sieving method	Dry	
Charge [g/m]	20	
Delay time [µs]	73	
Blast Pattern	S+B variations	
Mesh size mm	Mass passing %	Local inclination -
125.0	100.00	0.00
100.0	76.38	1.21
80.0	61.95	0.94
63.0	54.77	0.52
50.0	49.14	0.47
40.0	44.36	0.46
31.5	40.03	0.43
25.0	34.74	0.61
20.0	31.05	0.50
14.0	24.28	0.69
12.5	22.58	0.64
10.0	19.22	0.72
6.3	13.17	0.82
4.0	8.81	0.89
2.0	6.08	0.53
1.0	4.36	0.48
0.5	3.24	0.43
<0.25	0.0	



Sample - Nr.:	B10	
Date of blast	07.10.2014	
Row Nr.:	2	
Confinement	Yes	
Sieving method	Dry	
Charge [g/m]	20	
Delay time [µs]	73	
Blast Pattern	S+B variations	
Mesh size mm	Mass passing %	Local inclination -
125.0	87.96	0.00
100.0	79.46	0.46
80.0	79.46	0.00
63.0	74.39	0.28
50.0	72.92	0.09
40.0	63.13	0.65
31.5	55.95	0.51
25.0	49.41	0.54
20.0	43.80	0.54
14.0	34.43	0.68
12.5	31.73	0.72
10.0	26.32	0.84
6.3	19.01	0.70
4.0	13.01	0.84
2.0	9.15	0.51
1.0	6.49	0.50
0.5	4.75	0.45
<0.25	0.0	



Sample - Nr.:	B10	
Date of blast	07.10.2014	
Row Nr.:	3	
Confinement	Yes	
Sieving method	Dry	
Charge [g/m]	20	
Delay time [µs]	73	
Blast Pattern	S+B variations	
Mesh size mm	Mass passing %	Local inclination -
125.0	100.00	0.00
100.0	100.00	0.00
80.0	100.00	0.00
63.0	94.60	0.23
50.0	87.31	0.35
40.0	77.90	0.51
31.5	69.90	0.45
25.0	61.55	0.55
20.0	52.77	0.69
14.0	40.73	0.73
12.5	37.08	0.83
10.0	31.42	0.74
6.3	21.98	0.77
4.0	14.97	0.85
2.0	10.17	0.56
1.0	7.13	0.51
0.5	5.27	0.44
<0.25	0.00	

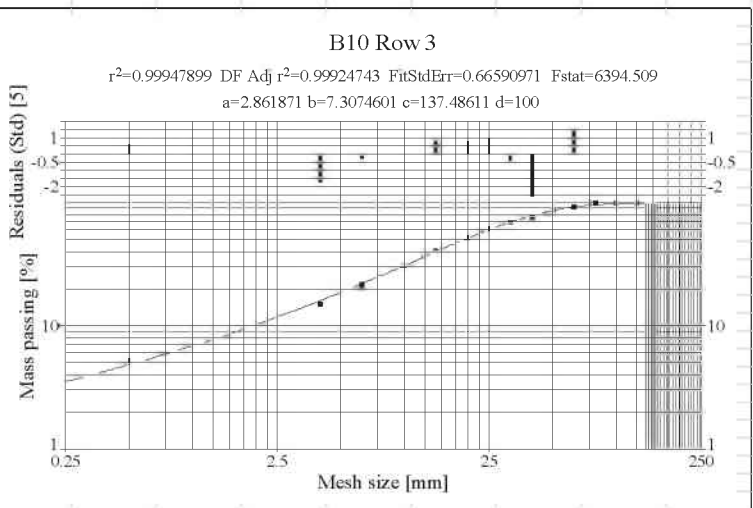
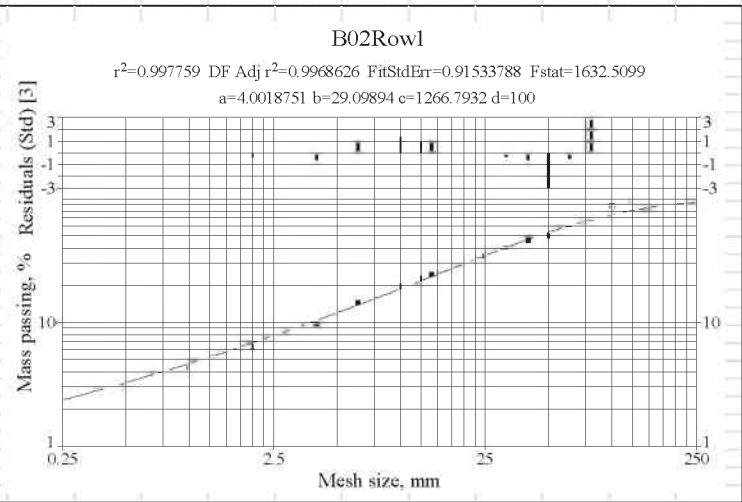
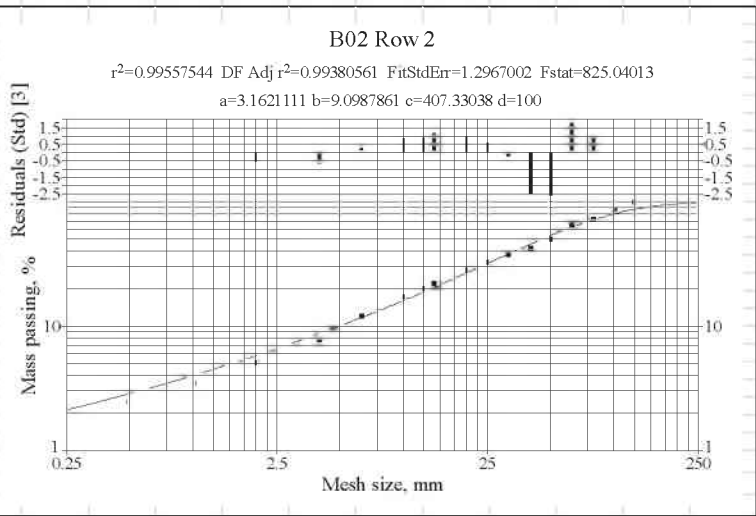


Figure 102: Specimen B10 (S+B variations)

Sample - Nr.:	B02	
Date of blast	11.06.2014	
Row Nr.:	1	
Confinement	Yes	
Sieving method	Dry	
Charge [g/ml]	20	
Delay time [μs]	73	
Blast Pattern	S/4 shift	
Mesh size mm	Mass passing %	Local inclination -
125.0	100.00	0.00
100.0	88.51	0.55
80.0	71.48	0.96
63.0	60.89	0.67
50.0	51.37	0.74
40.0	46.93	0.40
31.5	40.58	0.61
25.0	35.16	0.62
20.0	30.31	0.67
14.0	24.69	0.57
12.5	23.01	0.62
10.0	20.28	0.57
6.3	14.68	0.70
4.0	9.90	0.87
2.0	6.48	0.61
1.0	4.32	0.58
0.5	2.98	0.54
<0.25		



Sample - Nr.:	B02	
Date of blast	11.06.2014	
Row Nr.:	2	
Confinement	Yes	
Sieving method	Dry	
Charge [g/ml]	20	
Delay time [μs]	73	
Blast Pattern	S/4 shift	
Mesh size mm	Mass passing %	Local inclination -
125.0	100.00	0.00
100.0	87.50	0.60
80.0	73.56	0.78
63.0	65.34	0.50
50.0	50.63	1.10
40.0	42.85	0.75
31.5	38.17	0.48
25.0	33.05	0.62
20.0	28.52	0.66
14.0	22.30	0.69
12.5	20.30	0.83
10.0	17.39	0.69
6.3	12.20	0.77
4.0	7.88	0.96
2.0	5.14	0.62
1.0	3.53	0.54
0.5	2.48	0.51
<0.25		



Sample - Nr.:	B02	
Date of blast	11.06.2014	
Row Nr.:	3	
Confinement	Yes	
Sieving method	Dry	
Charge [g/ml]	20	
Delay time [μs]	73	
Blast Pattern	S/4 shift	
Mesh size mm	Mass passing %	Local inclination -
125.0	100.00	0.00
100.0	100.00	0.00
80.0	96.43	0.16
63.0	88.59	0.35
50.0	81.79	0.35
40.0	71.60	0.60
31.5	63.90	0.48
25.0	54.16	0.72
20.0	47.17	0.62
14.0	36.18	0.74
12.5	32.56	0.93
10.0	26.93	0.85
6.3	18.91	0.76
4.0	12.80	0.86
2.0	8.62	0.57
1.0	6.09	0.50
0.5	4.30	0.50
<0.25		

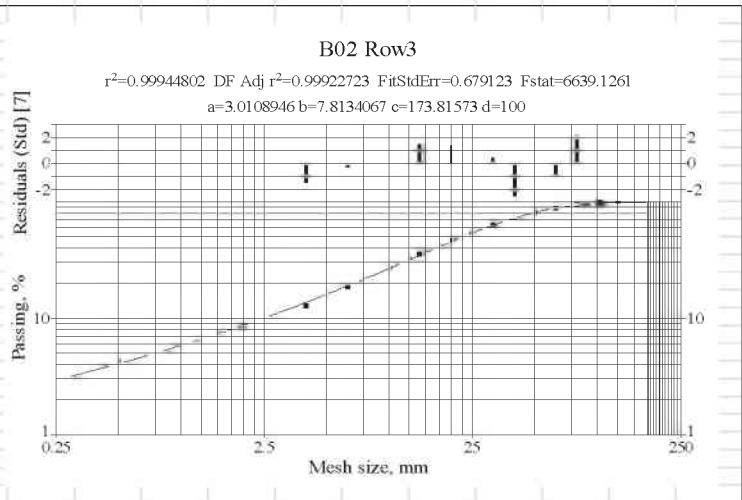
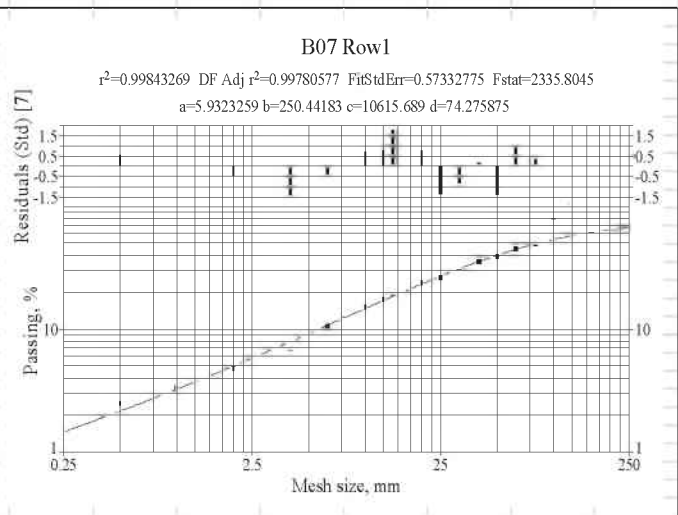
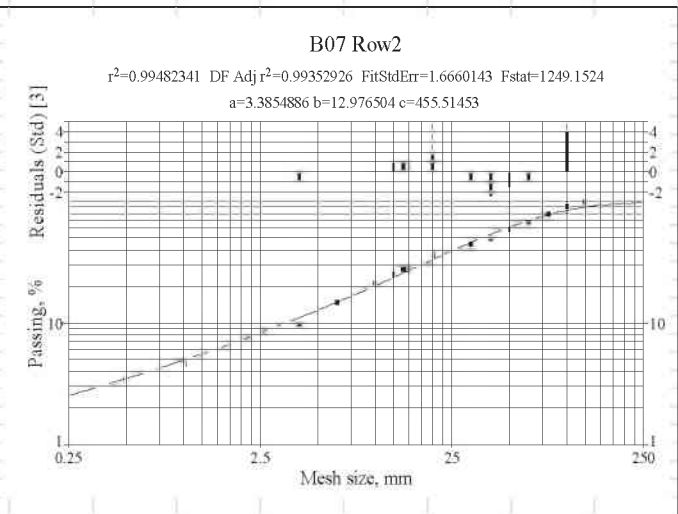


Figure 103: Specimen B02 (S/4 shift)

Sample - Nr.:	B07	
Date of blast	18.07.2014	
Row Nr.:	1	
Confinement	Yes	
Sieving method	Dry	
Charge [g/m]	20	
Delay time [µs]	73	
Blast pattern	S/4 shift	
Mesh size mm	Mass passing %	Local inclination °
125.0	100.00	0.00
100.0	77.54	1.14
80.0	50.23	1.95
63.0	45.79	0.39
50.0	39.65	0.62
40.0	36.10	0.42
31.5	30.92	0.65
25.0	26.52	0.66
20.0	24.17	0.42
14.0	19.80	0.56
12.5	17.85	0.91
10.0	15.35	0.68
6.3	10.62	0.80
4.0	7.08	0.89
2.0	4.81	0.56
1.0	3.39	0.51
0.5	2.51	0.43
<0.25		



Sample - Nr.:	B07	
Date of blast	18.07.2014	
Row Nr.:	2	
Confinement	Yes	
Sieving method	Dry	
Charge [g/m]	20	
Delay time [µs]	73	
Blast pattern	S/4 shift	
Mesh size mm	Mass passing %	Local inclination °
125.0	100.00	0.00
100.0	92.26	0.36
80.0	79.04	0.69
63.0	68.95	0.57
50.0	59.74	0.62
40.0	50.28	0.77
31.5	45.01	0.46
25.0	40.73	0.43
20.0	36.47	0.50
14.0	27.97	0.74
12.5	25.58	0.79
10.0	21.45	0.79
6.3	14.78	0.81
4.0	9.84	0.90
2.0	6.57	0.58
1.0	4.62	0.51
0.5	3.45	0.42
<0.25		



Sample - Nr.:	B07	
Date of blast	18.07.2014	
Row Nr.:	3	
Confinement	Yes	
Sieving method	Dry	
Charge [g/m]	20	
Delay time [µs]	73	
Blast pattern	S/4 shift	
Mesh size mm	Mass passing %	Local inclination °
125.0	100.00	0.00
100.0	100.00	0.00
80.0	100.00	0.00
63.0	93.12	0.30
50.0	86.23	0.33
40.0	77.72	0.47
31.5	69.45	0.47
25.0	61.68	0.51
20.0	54.55	0.55
14.0	42.17	0.72
12.5	38.23	0.86
10.0	32.61	0.71
6.3	24.56	0.61
4.0	16.76	0.84
2.0	11.48	0.55
1.0	8.08	0.51
0.5	6.01	0.43
<0.25		

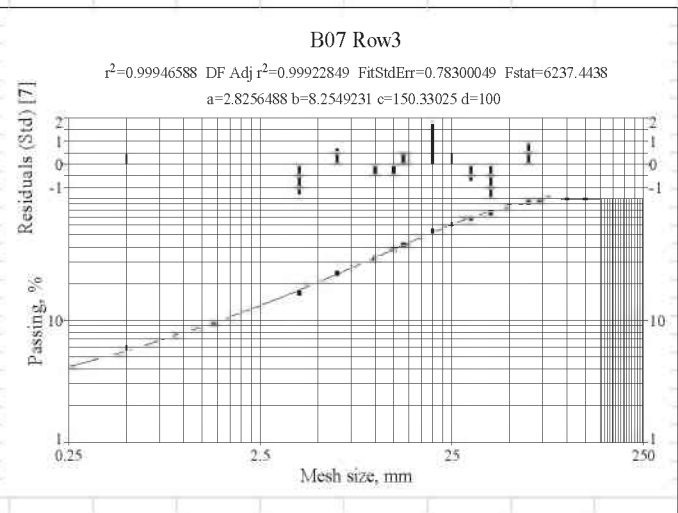
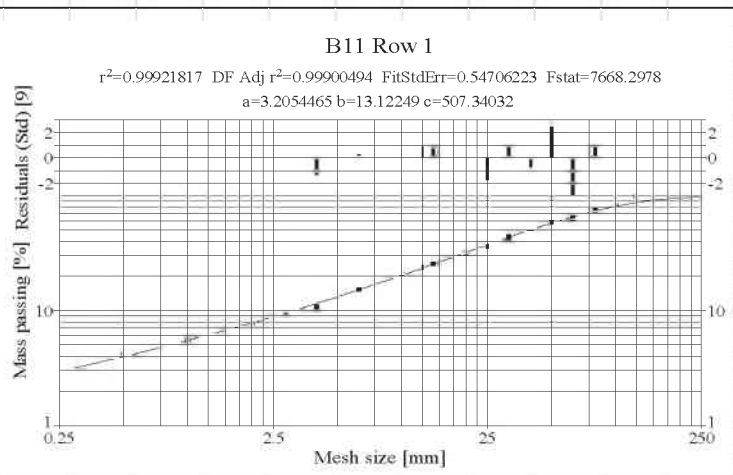
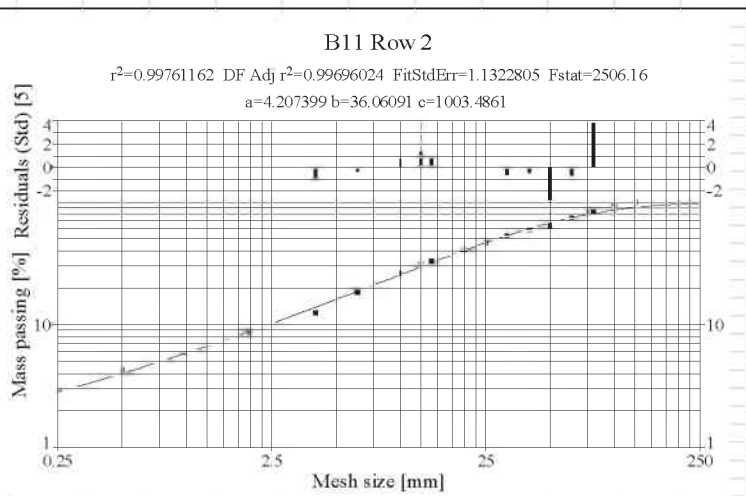


Figure 104: Specimen B07 (S/4 shift)

Sample - Nr.:	B11	
Date of blast	13.10.2014	
Row Nr.:	1	
Confinement	Yes	
Sieving method	Dry	
Charge [g/m]	20	
Delay time [µs]	73	
Blast pattern	S/4 shift	
Mesh size mm	Mass passing %	Local inclination -
125.0	100.00	0.00
100.0	84.31	0.76
80.0	74.99	0.52
63.0	64.65	0.62
50.0	59.72	0.34
40.0	50.64	0.74
31.5	44.44	0.55
25.0	36.74	0.82
20.0	32.26	0.58
14.0	26.01	0.60
12.5	24.26	0.62
10.0	20.86	0.68
6.3	15.48	0.65
4.0	10.88	0.78
2.0	7.74	0.49
1.0	5.61	0.46
0.5	4.22	0.41
<0.25	0.0	



Sample - Nr.:	B11	
Date of blast	13.10.2014	
Row Nr.:	2	
Confinement	Yes	
Sieving method	Dry	
Charge [g/m]	20	
Delay time [µs]	73	
Blast pattern	S/4 shift	
Mesh size mm	Mass passing %	Local inclination -
125.0	100.00	0.00
100.0	93.32	0.31
80.0	85.65	0.38
63.0	73.96	0.61
50.0	64.72	0.58
40.0	60.40	0.31
31.5	52.96	0.55
25.0	47.01	0.52
20.0	41.13	0.60
14.0	33.21	0.60
12.5	31.50	0.47
10.0	26.64	0.75
6.3	18.42	0.80
4.0	12.58	0.84
2.0	8.59	0.55
1.0	6.06	0.50
0.5	4.33	0.48
<0.25	0.0	



Sample - Nr.:	B11	
Date of blast	13.10.2014	
Row Nr.:	3	
Confinement	Yes	
Sieving method	Dry	
Charge [g/m]	20	
Delay time [µs]	73	
Blast pattern	S/4 shift	
Mesh size mm	Mass passing %	Local inclination -
125.0	100.00	0.00
100.0	100.00	0.00
80.0	95.47	0.21
63.0	91.47	0.18
50.0	80.98	0.53
40.0	72.63	0.49
31.5	62.60	0.62
25.0	55.91	0.49
20.0	47.50	0.73
14.0	36.59	0.73
12.5	32.60	1.02
10.0	28.06	0.67
6.3	19.95	0.74
4.0	13.47	0.86
2.0	9.12	0.56
1.0	6.33	0.53
0.5	4.46	0.51
<0.25	0.00	

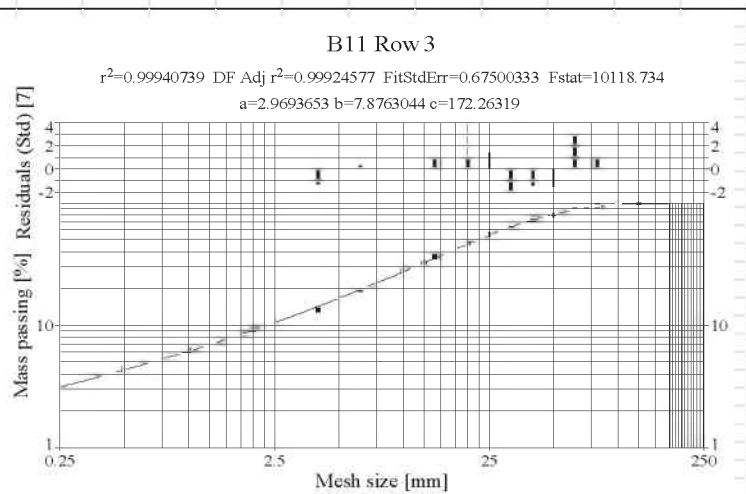
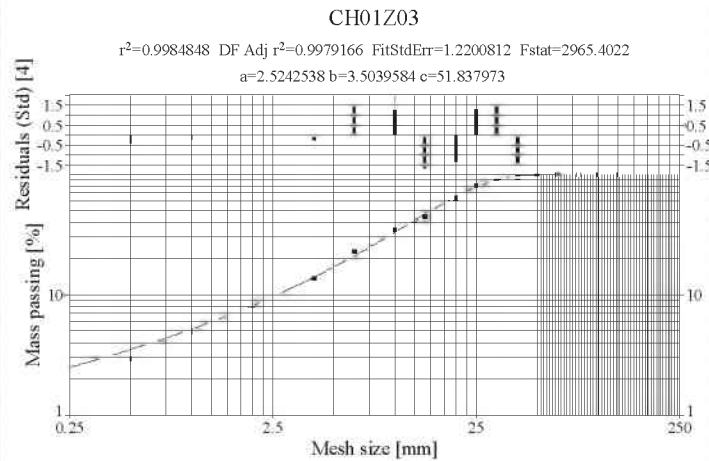
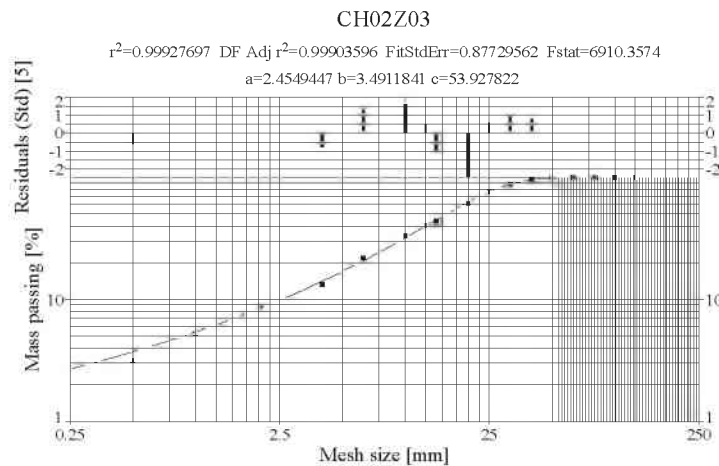


Figure 105: Specimen B11 (S/4 shift)

Sample - Nr.:	CH01Z03	
Date of blast	27.06.2013	
Confinement	No	
Sieving method	Dry	
Charge [g/m]	20	
Mesh size	Mass passing	Local inclination
mm	%	-
125.0		
100.0		
80.0		
63.0		
50.0		
40.0	96.29	0.17
31.5	92.93	0.15
25.0	81.29	0.58
20.0	65.02	1.00
14.0	45.20	1.02
12.5	41.76	0.70
10.0	35.02	0.79
6.3	23.20	0.89
4.0	13.91	1.14
2.0	9.21	0.75
1.0	4.97	0.72
0.5	2.98	0.74
<0.25		



Sample - Nr.:	CH02Z03	
Date of blast	27.06.2013	
Confinement	No	
Sieving method	Dry	
Charge [g/m]	20	
Mesh size	Mass passing	Local inclination
mm	%	-
125.0		
100.0		
80.0		
63.0		
50.0		
40.0	97.82	0.10
31.5	89.71	0.36
25.0	77.25	0.65
20.0	61.70	1.01
14.0	44.49	0.92
12.5	40.92	0.74
10.0	33.99	0.84
6.3	22.07	0.93
4.0	13.50	1.08
2.0	9.66	0.64
1.0	5.34	0.70
0.5	3.20	0.74
<0.25		



Sample - Nr.:	CH03Z03	
Date of blast	27.06.2013	
Confinement	No	
Sieving method	Dry	
Charge [g/m]	20	
Mesh size	Mass passing	Local inclination
mm	%	-
125.0		
100.0		
80.0		
63.0		
50.0		
40.0	99.11	0.04
31.5	96.35	0.12
25.0	89.01	0.39
20.0	69.95	1.03
14.0	49.10	0.99
12.5	45.24	0.72
10.0	37.26	0.87
6.3	24.05	0.95
4.0	14.57	1.10
2.0	9.71	0.74
1.0	5.34	0.70
0.5	3.13	0.77
<0.25		

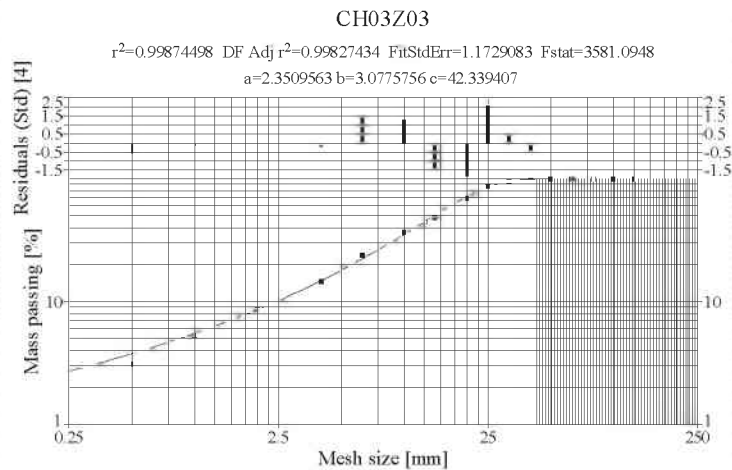


Figure 106: Cylinders, blast session 2013

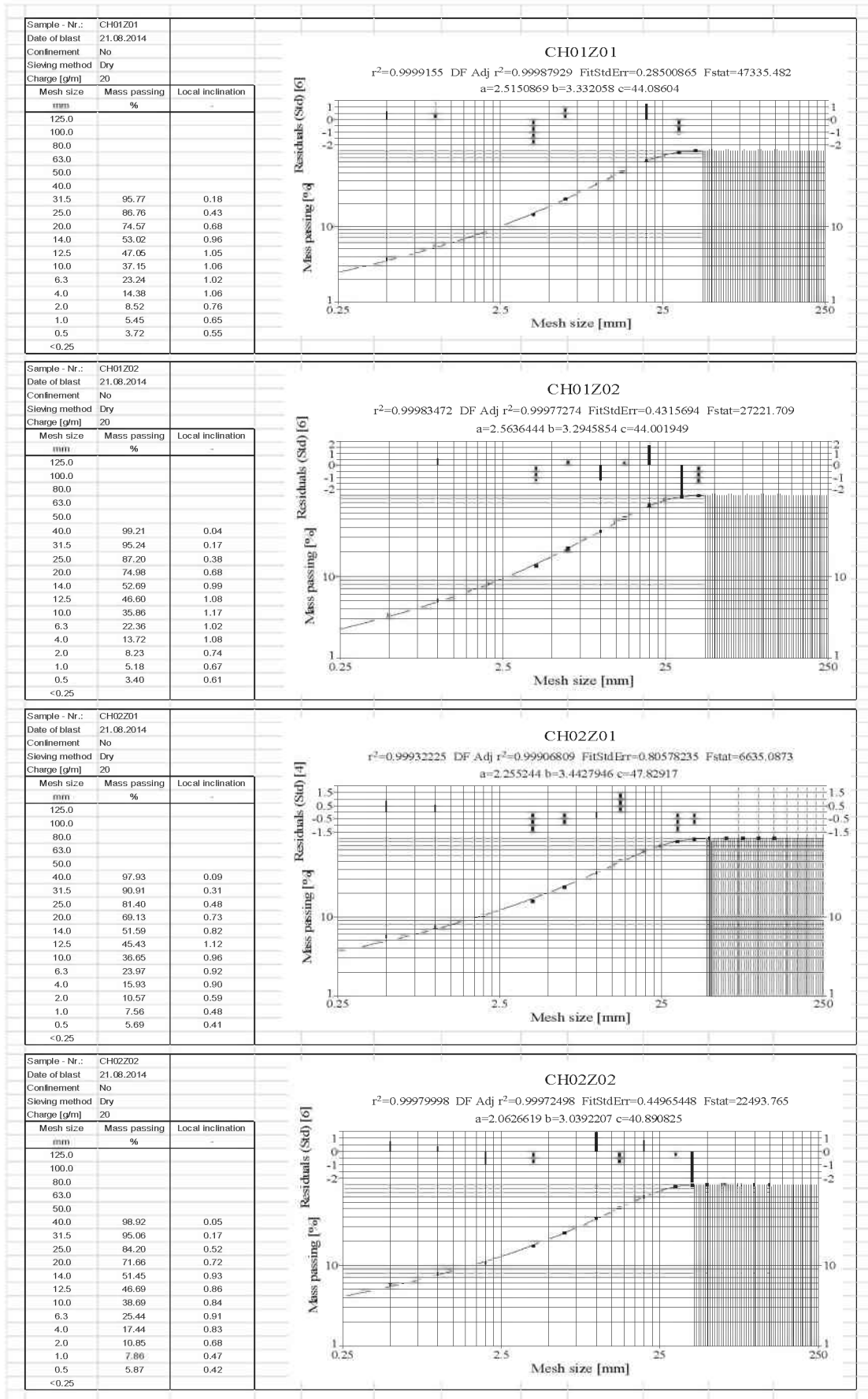


Figure 107: Cylinders, blast session 2014

Swebrec fits summary:

Swebrec fits summary							
Cylinders							
Sample	Curve fit Equation	a b	b x_{max}/x_{50}	c x_{max}	d A	r^2	Obs.
CH01 Z03		2.52	3.50	51.84	100.00	0.9985	*50
CH02 Z03		2.45	3.49	53.93	100.00	0.9993	*63
CH03 Z03		2.35	3.08	42.34	100.00	0.9987	*50
CH01 Z01		2.51	3.33	44.08	100.00	0.9999	*50
CH01 Z02		2.56	3.29	44.00	100.00	0.9998	**50
CH02 Z01		2.25	3.44	47.82	100.00	0.9993	*50
CH02 Z02		2.06	3.03	40.89	100.00	0.9997	*50
Blocks							
Sample	Curve fit Equation	a b	b x_{max}/x_{50}	c x_{max}	d A	r^2	Obs.
CH01 B02	1	4.16	14.67	223.36	64.53	0.9989	*125
	2	5.00	45.40	1096.83	100.00	0.9980	*125
	3	3.81	13.00	227.81	91.48	0.9994	*80
CH01 B03	1	2.43	5.02	57.40	36.10	0.9990	*40
	2	3.50	12.22	172.96	77.10	0.9995	*80
	3	3.54	14.47	256.40	100.00	0.9990	*100
CH01 B04	1	3.71	10.46	175.14	72.85	0.9990	*100
	2	4.81	31.95	609.81	100.00	0.9991	*100
	3	4.12	16.98	242.55	100.00	0.9992	*100
CH01 B05	1	3.98	15.44	387.00	85.25	0.9994	*63
	2	2.96	6.56	77.00	65.39	0.9995	*40
	3	2.46	4.20	43.92	77.75	0.9996	*40
CH03 B01	1	6.98	500.00	10896.22	69.70	0.9970	*125
	2	6.46	500.00	13046.81	99.38	0.9979	*100
	3	3.67	16.20	291.73	98.50	0.9994	*100
CH03 B02	1	3.08	7.74	326.81	100.00	0.9966	*125
	2	6.63	500.00	9669.05	88.54	0.9968	*80
	3	3.88	13.92	223.34	86.70	0.9996	*80
B01	1	2.79	8.71	117.78	31.28	0.9995	*63
	2	3.52	9.38	120.81	61.71	0.9992	*50
	3	3.86	25.08	497.77	100.00	0.9986	*63
B02	1	4.00	29.10	1266.79	100.00	0.9978	*100
	2	3.16	9.10	407.33	100.00	0.9956	*125
	3	3.01	7.81	173.82	100.00	0.9994	*100
B03	1	4.35	59.68	1333.01	97.88	0.9993	*80
	2	2.45	7.82	107.67	89.56	0.9996	*100
	3	3.16	13.91	198.75	100.00	0.9994	*80

B04	1	2.44	7.14	89.08	73.73	0.9997	*63
	2	2.62	11.40	151.69	91.04	0.9989	*100
	3	3.16	13.91	198.75	100.00	0.9993	*80
B06	1	2.96	7.34	162.60	100.00	0.9992	*100
	2	2.73	8.35	150.96	97.76	0.9993	*80
	3	2.58	8.35	101.53	96.24	0.9988	*63
B07	1	5.93	250.44	10615.69	74.28	0.9984	*100
	2	3.39	12.98	455.51	100.00	0.9948	*125
	3	2.83	8.25	150.33	100.00	0.9995	*80
B09	1	2.57	6.68	254.16	100.00	0.9981	*125
	2	2.51	6.63	104.38	96.11	0.9991	*100
	3	2.69	10.46	138.94	100.00	0.9985	*80
B10	1	4.70	56.95	1666.27	76.15	0.9984	*100
	2	2.83	7.99	147.59	81.63	0.9990	*100
	3	2.86	7.31	137.49	100.00	0.9995	*80
B11	1	3.21	13.12	507.34	100.00	0.9992	*100
	2	4.23	36.95	1.026.82	100.00	0.9976	*100
	3	2.97	7.88	172.26	100.00	0.9994	*100

Where:

d (A) represents the fitting parameter which enables scaling. In this case it is given as 1 when there is 100 % scaling parameter or not given in the figures of Appendix 5, otherwise the scaling factor is less than 1 or 100 %.

r^2 is the coefficient of determination, which indicates how well data fits a specified line/curve.

The column Obs.(observations) contains information about how the data set, which may include data up to 125 mm mesh size, fitted into the Swebrec function (the size of the largest sieve value used in the fit curve, e.g. *63 means all mesh sizes up to and including 63 mm

Equivalent calculated n-values in sessions 2013 and 2014:

Table 58: Equivalent n-values values, blast sessions 2013 and 2014

Blocks session 2013	Equivalent n value ($1.506/\ln(x_{80}/x_{30})$)			Average n 2+3 row
	1 row	2 row	3 row	
CH01B03 (Reference)	1.20*	0.76	0.91	0.83
CH01B05 (Reference)	1.07*	0.82	1.03	0.92
Average row	0.72*	0.79	0.97	0.88
Stdev row	0.91*	0.05	0.08	0.12
CH01B02 (1st burden deviation)	0.72*	0.90	0.95	0.93
CH01B04 (1st burden deviation)	0.91*	0.95	0.71	0.83
Average row		0.93	0.83	0.88
Stdev row		0.03	0.17	0.11
CH03B01 (2nd burden deviation)	0.77*	0.76	0.71	0.73
CH03B02 (2nd burden deviation)	0.96	1.00	0.87	0.94
Average row		0.88	0.79	0.84
Stdev row		0.17	0.11	0.13

Blocks 2014	Equivalent n value ($1.506/\ln(x_{80}/x_{30})$)			Average n 2+3 row
	1 row	2 row	3 row	
B01 (Reference)		0.89*	0.87*	
B06 (Reference)	1.04	0.93	0.86	0.89
B09 (Reference)	0.94	0.95	0.82	0.89
Average row	0.99	0.94	0.84	0.89
Stdev row	0.07	0.02	0.02	0.06
B03 (S+B variations)	0.75	0.82	0.89	0.85
B04 (S+B variations)	0.79*	0.70	0.86	0.78
B10 (S+B variations)	0.89*	0.70	1.01	0.85
Average row	0.75	0.74	0.92	0.83
Stdev row		0.07	0.08	0.12
B02 (S/4 shift)	0.99*	1.06	1.05	1.05
B07 (S/4 shift)	1.23*	0.91	0.95	0.93
B11 (S/4 shift)	0.93	0.83	1.00	0.92
Average row	0.93	0.93	1.00	0.97
Stdev row		0.11	0.06	0.09

* These values are judged as invalid and excluded in the further analysis.

Equivalent calculated x_c -values in sessions 2013 and 2014:

Table 59: Equivalent x_c -values values, blast sessions 2013 and 2014

Blocks 2013	Equivalent x_c values			Average x_c 2+3 row
Row	1 row	2 row	3 row	
CH01B03 (Reference)	75.97*	35.59	27.24	31.42
CH01B05 (Reference)	47.23*	35.03	20.42	27.72
Average row	61.60*	35.31	23.83	29.57
Stdev row	20.32*	0.40	4.82	7.19
CH01B02 (1st burden deviation)	80.61*	37.88	29.42	33.65
CH01B04 (1st burden deviation)	45.17*	27.18	20.53	23.85
Average row	62.89*	32.53	24.97	28.75
Stdev row	25.06*	7.57	6.29	7.16
CH03B01 (2nd burden deviation)	101.67*	47.78	27.26	37.52
CH03B02 (2nd burden deviation)	61.39*	47.06	29.47	38.27
Average row	81.53*	47.42	28.37	37.89
Stdev row	28.48*	0.51	1.57	11.04

Blocks 2014	Equivalent x_c values			Average x_c 2+3 row
Row	1 row	2 row	3 row	
B01 (Reference)	99.89*	49.26*	32.37*	40.82*
B06 (Reference)	30.91*	27.49	19.10	23.29
B09 (Reference)	58.50*	24.13	19.62	21.88
Average row	63.10*	33.62	19.36	22.58
Stdev row	19.51*	2.38	0.37	3.97
B03 (S+B variations)	38.58*	25.59	29.22	27.41
B04 (S+B variations)	35.49*	25.25	21.14	23.20
B10 (S+B variations)	81.73*	40.08	26.29	33.18
Average row	51.93*	30.31	25.55	27.93
Stdev row	25.85*	8.46	4.09	6.49
B02 S/4 shift	66.71*	61.11	31.03	46.07
B07 S/4 shift	89.50*	54.89	26.27	40.58
B11 S/4 shift	59.17*	46.49	32.00	39.25
Average row	71.79*	54.16	29.77	41.96
Stdev row	15.79*	7.34	3.07	14.27

* These values are judged as invalid and excluded in the further analysis.

Calculated coefficient of uniformity x_{30}/x_{80} -values in sessions 2013 and 2014:

Table 60: Equivalent x_c -values values, blast sessions 2013 and 2014

Block	Coefficient of uniformity (x_{80}/x_{30})		
	1 row	2 row	3 row
Row			
CH01B03 (Reference)	3.50	7.35	5.23
CH01B05 (Reference)	4.11	6.24	4.35
Average row	3.81	6.80	4.79
Stdev row	0.43	0.79	0.63
CH01B02 (1st burden deviation)	8.01	5.30	4.89
CH01B04 (1st burden deviation)	5.23	4.89	8.29
Average row	6.62	5.10	6.59
Stdev row	1.96	0.29	2.41
CH03B01 (2nd burden deviation)	7.11	7.34	8.29
CH03B02(2nd burden deviation)	4.80	4.49	5.66
Average row	5.96	5.92	6.98
Stdev row	1.64	2.01	1.87

Block	Coefficient of uniformity (x_{80}/x_{30})		
	1 row	2 row	3 row
Row			
B01 (Reference)		5.46	5.61
B06 (Reference)	4.27	5.09	5.82
B09 (Reference)	4.95	4.86	6.22
Average row	4.61	5.14	5.88
Stdev row	0.48	0.30	0.31
B03 (S+B variations)	7.55	6.35	5.41
B04 (S+B variations)	6.80	8.49	5.75
B10 (S+B variations)	5.44	8.68	4.47
Average row	6.60	7.84	5.21
Stdev row	1.07	1.30	0.66
B02 S/4 shift	4.58	4.12	4.23
B07 S/4 shift	3.41	5.28	4.85
B11 S/4 shift	5.09	6.12	4.49
Average row	4.36	5.17	4.52
Stdev row	0.86	1.00	0.31

Appendix 6 Crack families detailed description

Table 61: Color coded families of crack traces in horizontal slices

Colour	Description	Abbreviation
1	Cracks connecting with the borehole with an angle between 90° - 80°	CB 90° - 80°
2	Cracks connecting with the borehole with an angle between 80° - 30°	CB 80° - 30°
3	Cracks connecting with the borehole with an angle between 30° - 0°	CB 30° - 0°
4	Straight cracks between holes coming from the back side	SCB
5	Connections cracks between neighbouring boreholes	Connect
6	Parallel cracks to the bench surface	Parallel
7	Cracks with direction to the boreholes with an angle between 90° - 80°	CD 90° - 80°
8	Cracks with direction to the boreholes with an angle between 80° - 30°	CD 80° - 30°
9	Cracks with direction to the boreholes with an angle between 30° - 0°	CD 30° - 0°
10	Short radial cracks around the borehole	SC
11	Vertical cracks between boreholes, starting at face	VCB

Below, a detailed description of each family is given:

- 1- *Cracks from boreholes* in sectors *between 90° - 80°* cracks that start from the borehole and develop a trajectory limited by sectors between 90° - 80° counted from both sides of the free face, i.e. sector 80° - 100° counted from one side. These cracks are divided according to their lengths from the center of the blast hole: long (> 3 cm) and short (between 1 cm and 3 cm). Cracks shorter than 1 cm belong to family no. 10, see below.

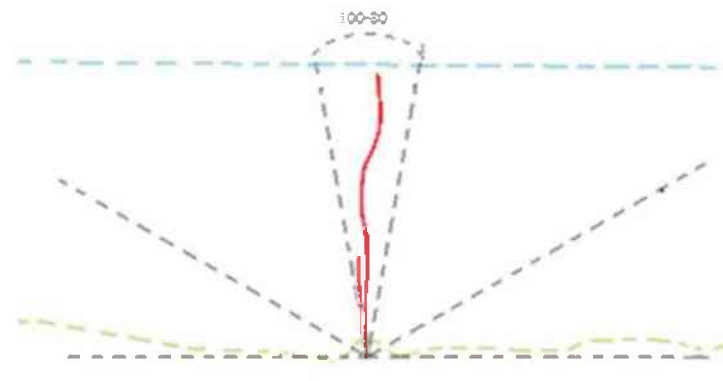


Figure 108: Cracks from borehole in sectors between 90° - 80°

- 2- *Cracks from borehole* in sectors *between 80° - 30°* : cracks that start from the borehole and develop a trajectory limited by sectors between 80° - 30° at both sides

of the borehole. These cracks are divided according to their lengths from the center of the blast hole: large (> 3 cm) and short (between 1 cm and 3 cm). Cracks shorter than 1 cm belong to family no. 10, see below.

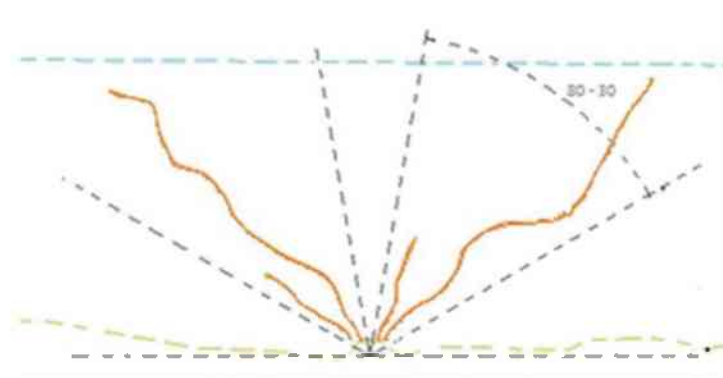


Figure 109: Cracks from borehole in sectors between $80^\circ - 30^\circ$

- 3- *Cracks from borehole in sectors between $30^\circ - 0^\circ$* : cracks that start from the borehole and develop a trajectory limited by sectors between $30^\circ - 0^\circ$ at both sides of the borehole. These cracks are divided according to their lengths from the center of the blast hole: large (> 3 cm) and short (between 1 cm and 3 cm). Cracks shorter than 1 cm belong to family no. 10, see below.

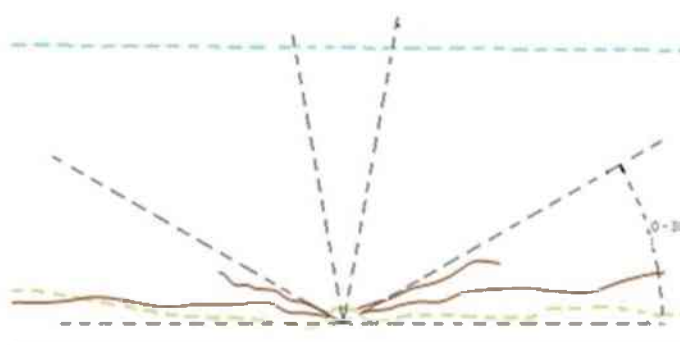


Figure 110: Cracks from borehole in sectors between $30^\circ - 0^\circ$

- 4- *Straight cracks from back side*: cracks which seem to start from the back side of the slice and that follow a trajectory in a different direction to the borehole. These cracks are also divided according to their lengths: large (>3 cm) and short (between 1 and 3 cm).

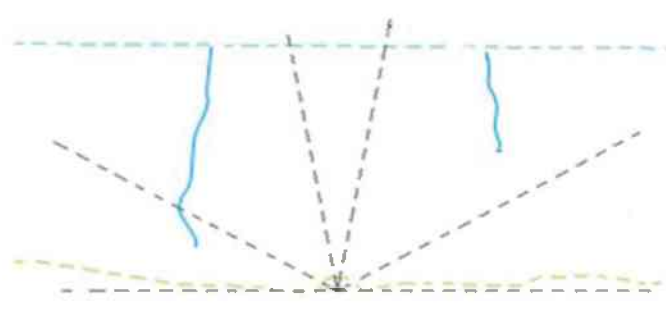


Figure 111: Straight cracks from back side

- 5- *Connections between boreholes*: sometimes cracks with an angle between 30° - 0° starting from two neighboring boreholes are connected, creating an arc shaped connection between boreholes, roughly with the shape of a banana.

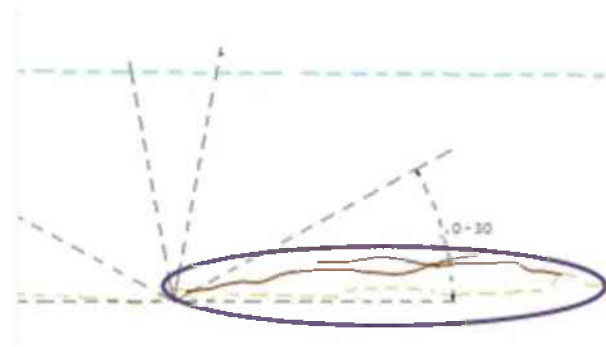


Figure 112: Connections between boreholes

- 6- *Parallel to the surface*: parallel cracks which are created along the slice. These cracks are also divided according to their lengths: large (>3 cm) and short (between 1 and 3 cm).

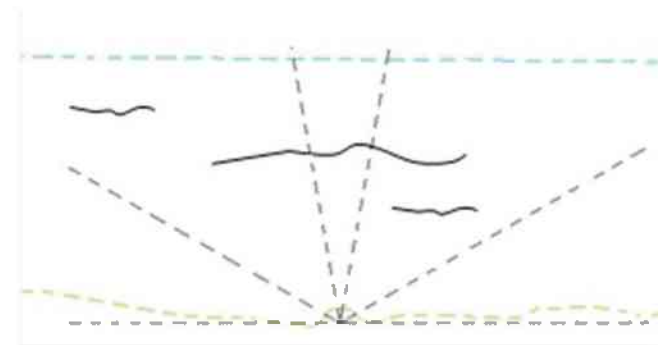


Figure 113: Parallel cracks to the surface

- 7- *Cracks with direction to the boreholes in sectors between 90° - 80°* : These cracks do not start from the borehole but develop a trajectory with a direction towards the hole and are limited by a sector between 90° - 80° from both sides of the borehole. These cracks are also divided according to their lengths: large (>3 cm) and short (between 1 and 3 cm).

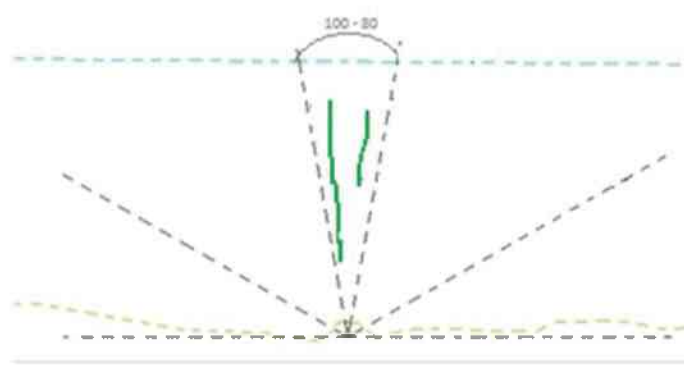


Figure 114: Cracks with direction to the boreholes in sectors between $90^\circ - 80^\circ$

- 8- *Cracks with direction to the boreholes in sectors between $80^\circ - 30^\circ$* : These cracks do not start from the borehole but develop a trajectory with a direction towards the hole and are limited by a sector between $90^\circ - 80^\circ$ from both sides of the borehole. These cracks are also divided according to their lengths: large (> 3cm) and short (between 1 and 3 cm).

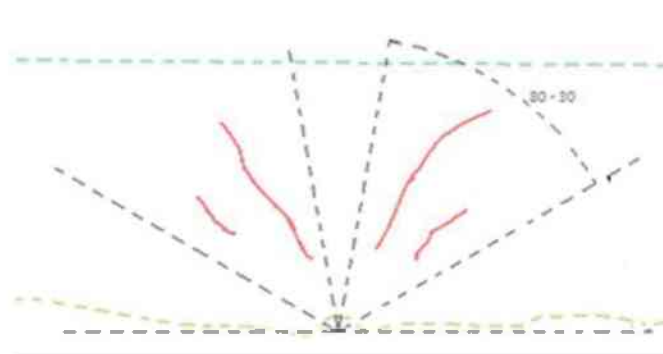


Figure 115: Cracks with direction to the boreholes in sectors between $80^\circ - 30^\circ$

- 9- *Cracks with direction to the boreholes in sectors between $30^\circ - 0^\circ$* : These cracks do not start from the borehole but develop a trajectory with a direction towards the hole and are limited by a sector between $90^\circ - 80^\circ$ from both sides of the borehole. These cracks are also divided according to their lengths: large (> 3 cm) and short (between 1 and 3 cm).

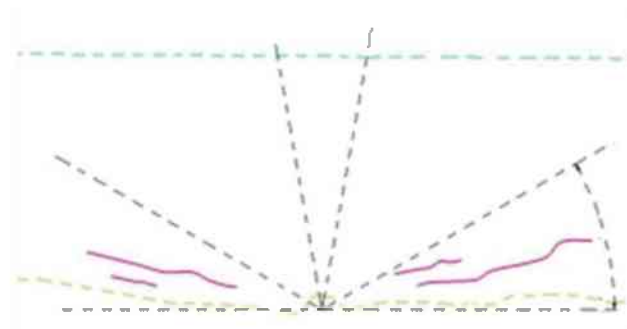


Figure 116: Cracks with direction to the boreholes in sectors between $30^\circ - 0^\circ$

10-*Short cracks from borehole*: short cracks which start from the borehole. The lengths of these cracks are smaller than 1 cm and can appear in all directions.

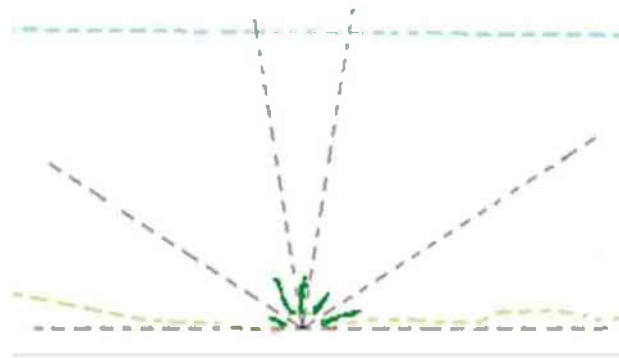


Figure 117: Short cracks from borehole

11-*Vertical cracks between two boreholes*: These are cracks between two boreholes, perpendicular to the bench face starting at face.

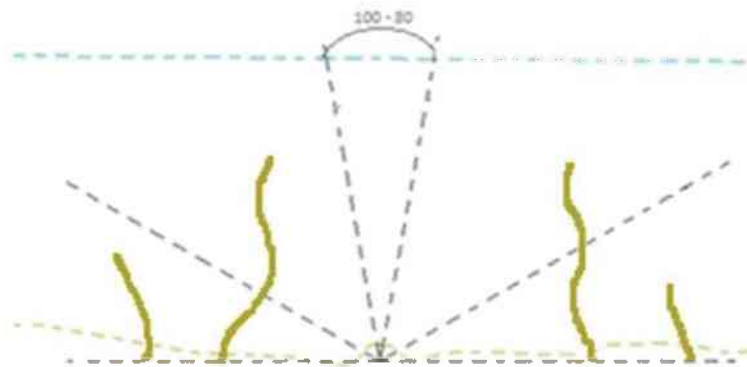


Figure 118: Vertical cracks between two boreholes

Appendix 7 Crack families in horizontal sections on slices

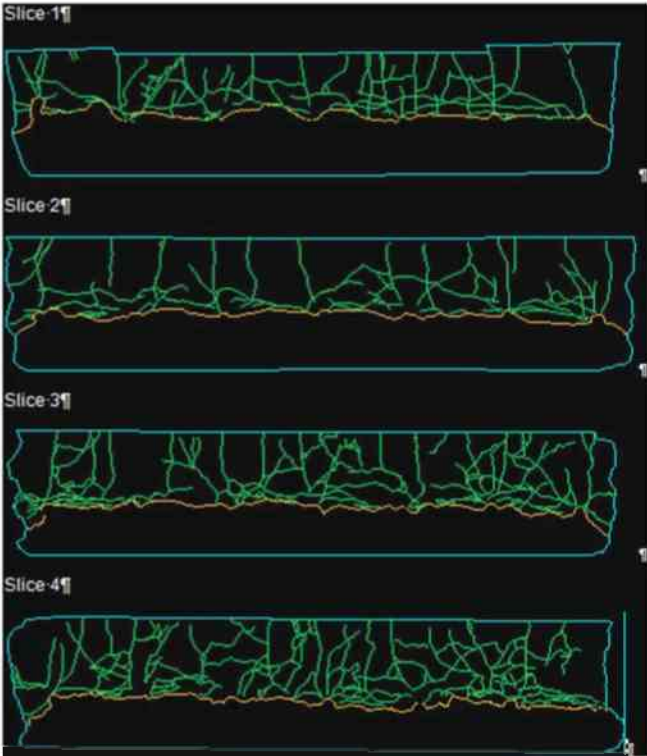


Figure 119: Block CH01B03 (Reference)

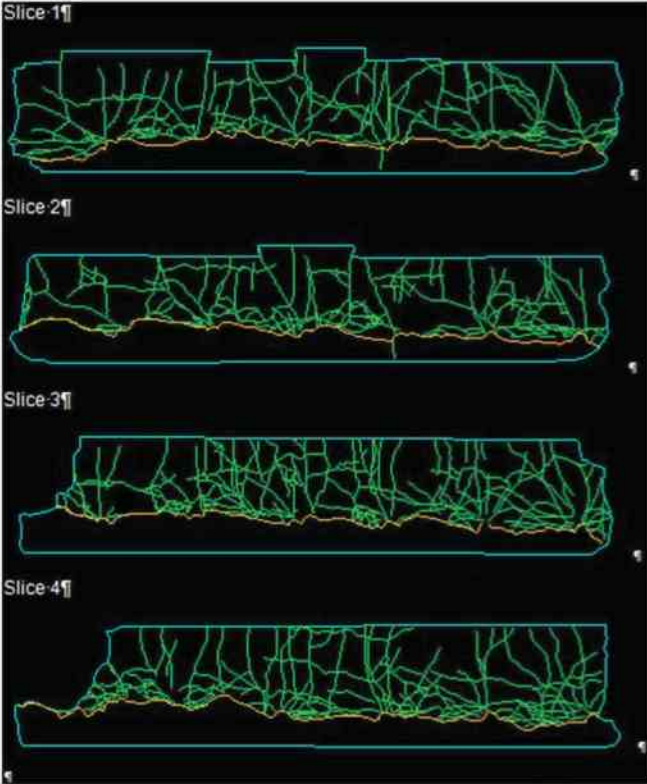


Figure 120: Block CH01B05 (Reference)

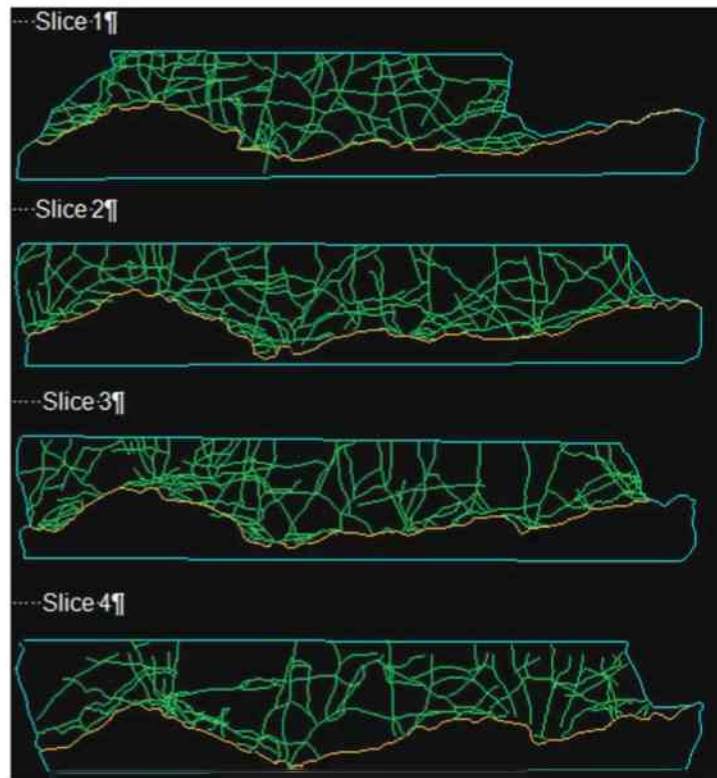


Figure 121: Block CH01B02 (1st burden variation)

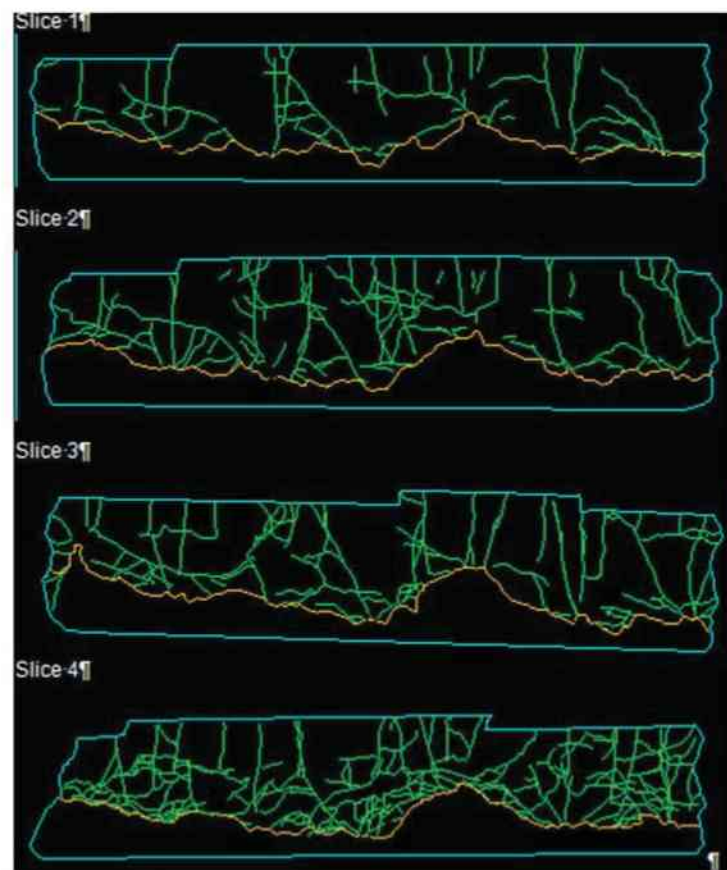


Figure 122: Block CH01B04 (1st burden variation)

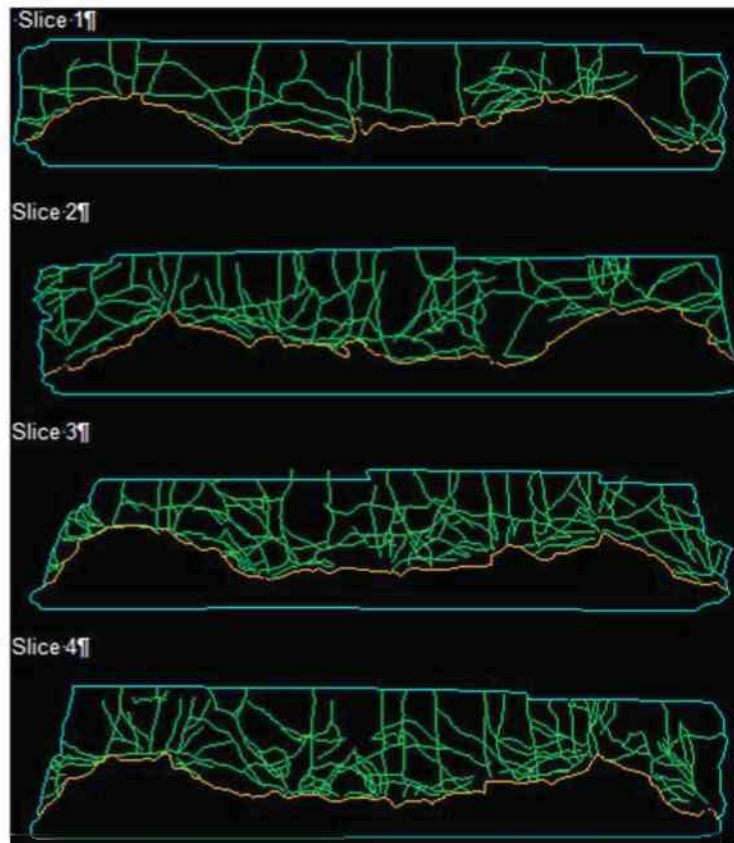


Figure 123: Block CH03B01 (2nd burden variation)

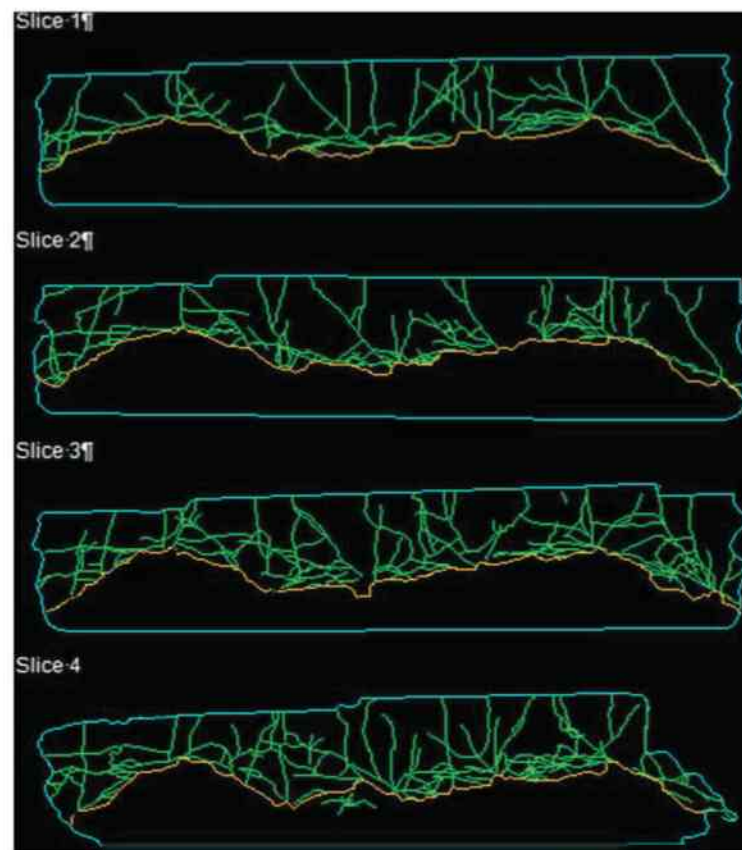


Figure 124: Block CH03B02 (2nd burden variation)

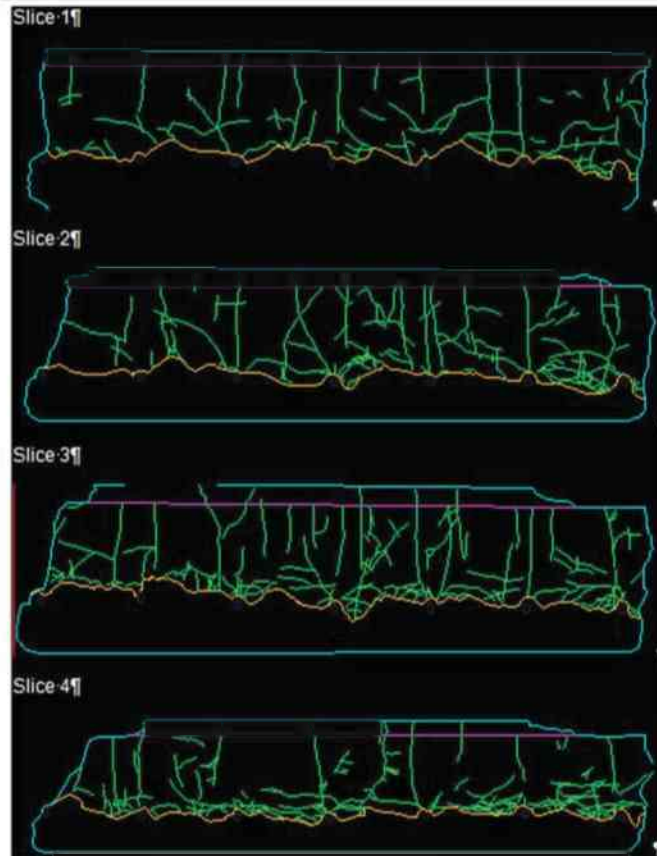


Figure 125: Block B01 (Reference)

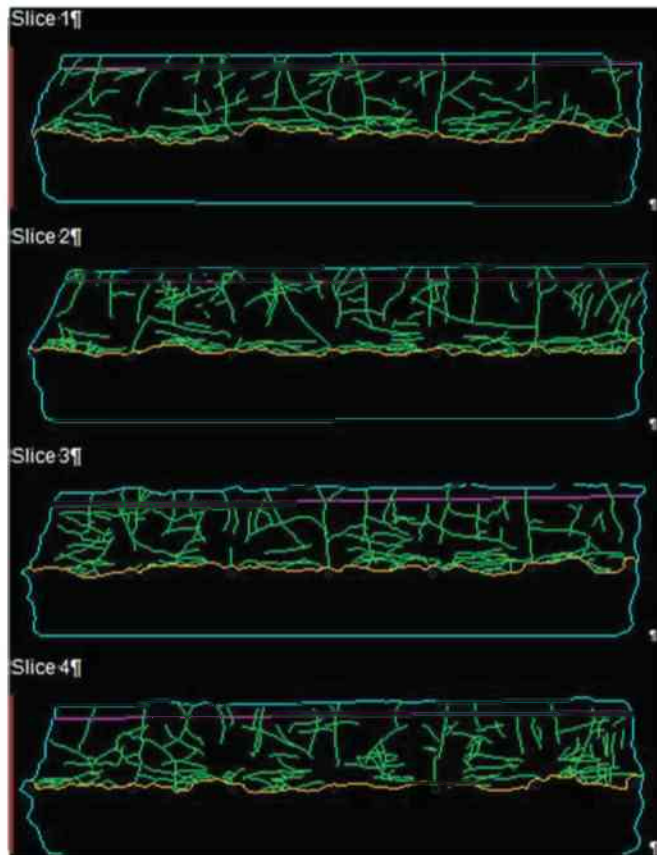


Figure 126: Block B06 (Reference)

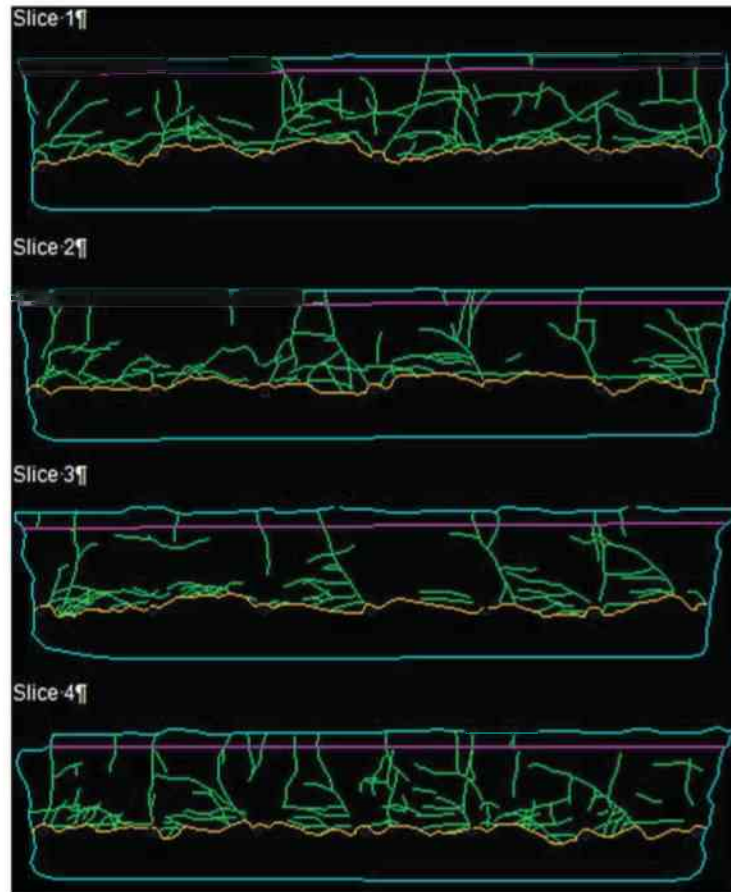


Figure 127: Block B09 (Reference)

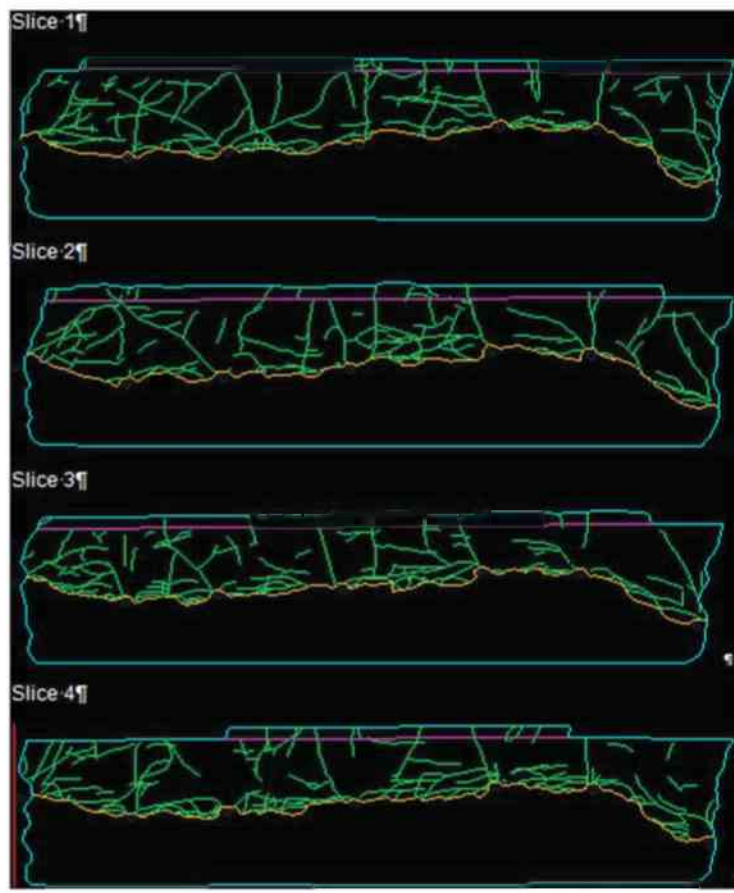


Figure 128: Block B03 (S+B variations)

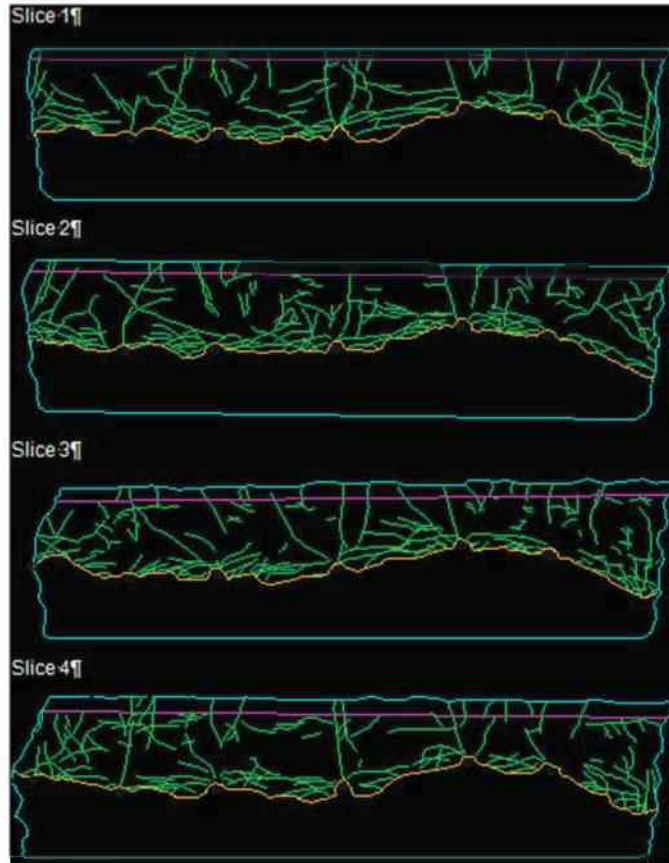


Figure 129: Block B04 (S+B variations)

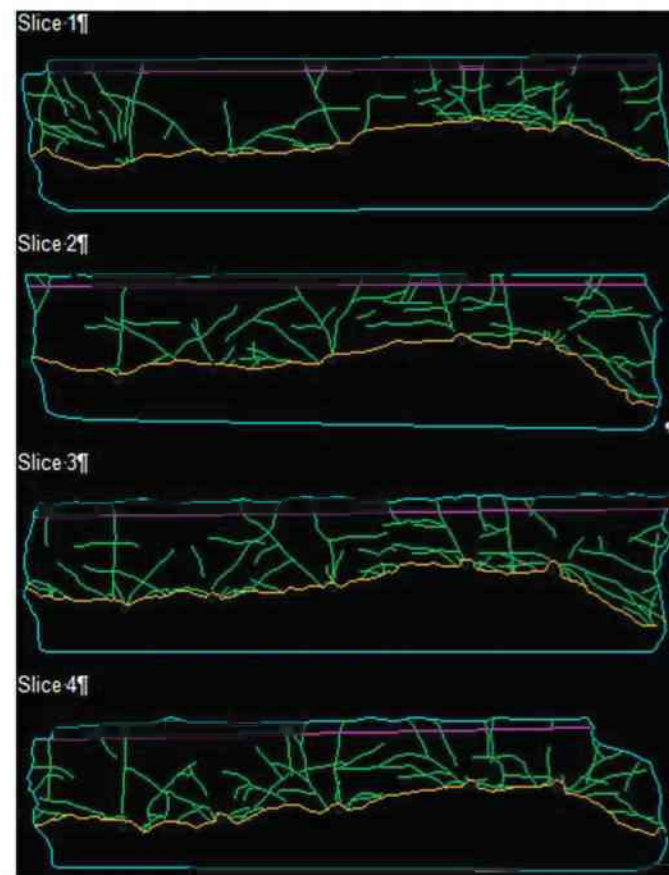


Figure 130: Block B10 (S+B variations)

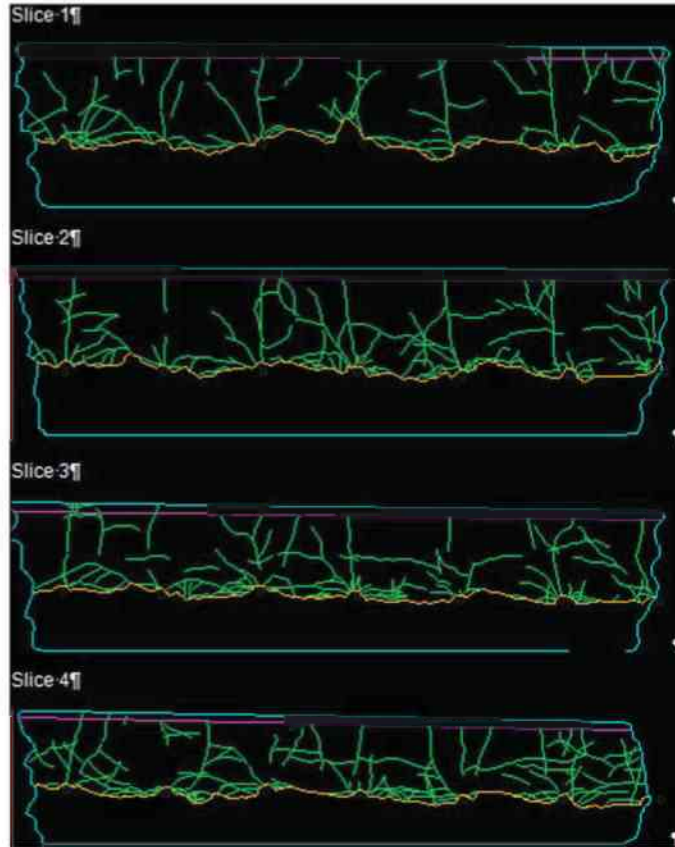


Figure 131: Block B02 (S/4 shift)

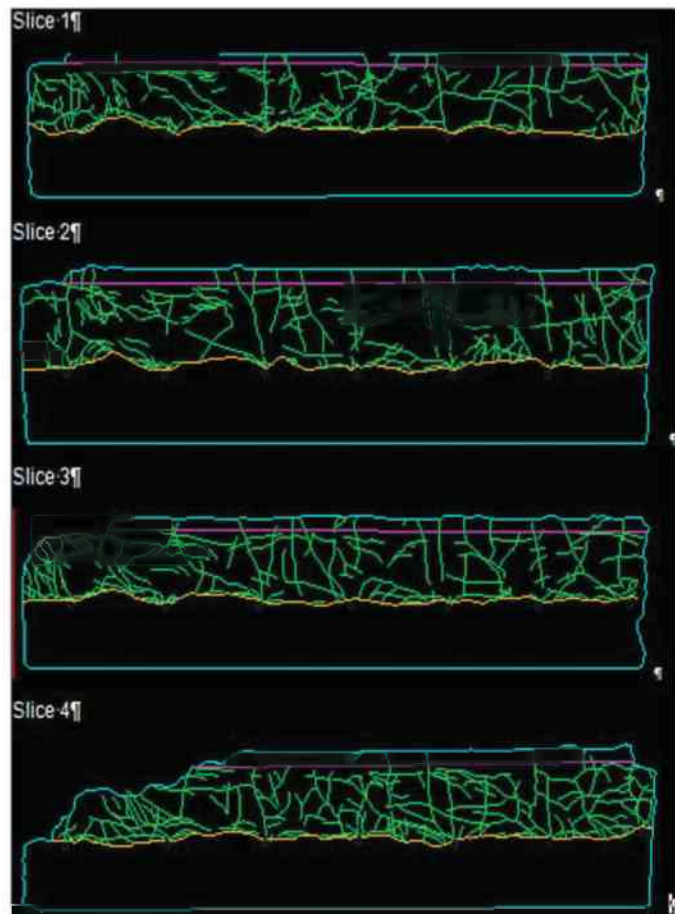


Figure 132: Block B07 (S/4 shift)

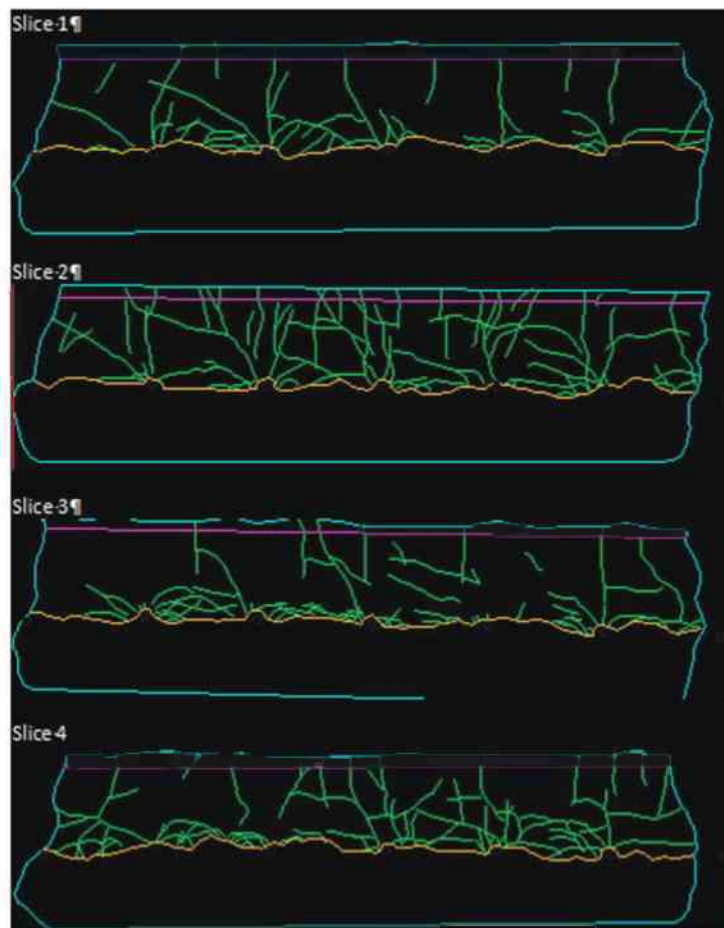


Figure 133: Block B11 (S/4 shift)

Table 62: Total cracks at horizontal slices, MCD, MCID values and top cracks, sessions 2013 and 2014

Block	Slice	Total cracks	MCD [-]	MCID [-]	Row	Top cracks
CH01B02	1	51			0	-
	2	79	2.34	1.68	1	-
	3	80	2.24	1.63	2	-
	4	70	1.94	1.25	3	-
CH01B03	1	79	1.06	0.55	0	-
	2	72	1.06	0.47	1	-
	3	93	1.47	0.77	2	-
	4	119	1.88	1.30	3	-
CH01B04	1	85	1.53	0.66	0	-
	2	110	2.04	1.19	1	-
	3	123	2.24	1.52	2	-
	4	117	2.02	1.37	3	-
CH01B05	1	104	2.03	1.28	0	-
	2	96	1.98	1.38	1	-
	3	102	2.42	1.58	2	-
	4	81	2.36	1.50	3	-
CH03B01	1	39	0.82	0.32	0	-
	2	91	1.59	0.87	1	-
	3	104	1.86	1.22	2	-
	4	91	1.66	0.97	3	-
CH03B02	1	77	1.01	0.54	0	-
	2	72	1.02	0.56	1	-
	3	77	1.25	0.65	2	-
	4	95	1.30	0.70	3	-
B01	1	50	0.83	0.25	0	6
	2	78	1.12	0.59	1	25
	3	80	1.34	0.64	2	82
	4	96	1.35	0.89	3	51
B02	1	80	0.92	0.31	0	24
	2	69	1.00	0.42	1	50
	3	69	1.12	0.46	2	50
	4	77	1.34	0.64	3	42
B03	1	83	1.07	0.50	0	30
	2	81	1.04	0.48	1	73
	3	84	1.00	0.38	2	73
	4	81	1.08	0.50	3	65
B04	1	97	1.19	0.46	0	22
	2	107	1.35	0.63	1	118
	3	98	1.24	0.46	2	95
	4	91	1.08	0.44	3	59
B06	1	99	1.36	0.62	0	21
	2	126	1.52	0.76	1	145
	3	109	1.34	0.63	2	94
	4	116	1.35	0.69	3	70
B07	1	106	1.47	0.81	0	35
	2	112	1.54	0.83	1	81
	3	98	1.36	0.60	2	90
	4	119	1.64	0.89	3	63
B09	1	75	1.16	0.56	0	8
	2	52	0.94	0.49	1	113
	3	64	0.92	0.44	2	97
	4	78	1.16	0.57	3	63
B10	1	62	0.74	0.27	0	0
	2	54	0.72	0.21	1	49
	3	60	0.82	0.24	2	86
	4	62	0.80	0.32	3	47
B11	1	48	0.59	0.16	0	0
	2	68	1.01	0.33	1	62
	3	64	0.70	0.26	2	71
	4	64	0.84	0.38	3	44

Table 63: Set of data used for the correlation analysis, session 2013

	1	2	3	4	5	6	7	8	9	10	11	12	13	14	15	16	17	18
D_0, D_1, D_2	0	5.14	8.56	0	4.59	8.20	0	2.37	7.71	0	3.20	7.47	0	2.74	4.32	0	7.72	5.48
x_{30}	26.08	9.94	8.50	15.64	10.41	7.71	13.74	11.63	10.12	13.56	9.77	7.53	16.55	10.87	8.96	20.28	9.53	9.78
X_{60}	57.61	21.36	17.51	32.43	22.42	14.54	30.14	23.61	19.95	25.87	18.96	13.86	54.42	25.61	18.09	44.74	24.53	19.38
X_{80}	91.35	73.09	43.12	64.29	54.45	37.00	110.05	61.67	52.05	84.61	47.81	33.84	117.74	79.76	46.15	88.13	79.05	55.32
n	0	0.76	0.91	0	0.82	1.03	0	0.9	0.95	0	0.95	0.71	0	0.76	0.71	0.96	1.00	0.87
D_1, D_2, D_3	5.14	8.56	2.67	4.59	8.20	6.41	2.37	7.71	5.46	3.20	7.47	4.11	2.74	4.32	6.00	7.72	5.48	4.67

Table 64: Set of data used for the correlation analysis, session 2014

	1	2	3	4	5	6	7	8	9	10	11	12	13	14	15	16	17	18	19	20	21	22	23	24	25	26	27
D_0, D_1, D_2	0	2.06	8.17	0	3.30	4.46	0	2.47	9.90	0	3.30	4.00	0	3.52	2.60	0	4.27	4.60	0	1.65	7.24	0	2.56	7.20	0	2.51	3.60
N_0, N_1, N_2	6.00	25.00	82.00	21.00	145.00	94.00	8.00	113.00	97.00	30.00	73.00	73.00	22.00	118.00	95.00	0.00	49.00	86.00	24.00	50.00	50.00	35.00	81.00	90.00	0.00	62.00	71.00
x_{30}	56.96	12.28	9.06	11.34	8.65	5.83	16.95	8.07	5.86	9.41	7.23	9.17	9.02	6.30	6.52	19.07	11.70	9.44	19.67	21.64	11.42	30.14	15.43	8.80	17.83	11.73	10.89
X_{60}	90.63	29.07	19.63	22.03	18.60	12.61	38.05	16.37	12.76	23.69	16.58	19.25	20.58	15.67	13.97	43.76	25.58	18.62	46.92	49.19	22.02	79.13	39.55	17.80	39.12	28.27	21.49
X_{80}	125.00	67.07	50.85	48.47	44.07	33.94	83.93	39.24	36.44	71.03	45.86	49.62	61.30	53.50	37.48	103.83	101.59	42.23	90.01	89.24	48.24	102.74	81.46	42.68	90.75	71.78	48.83
n	0	0.89	0.87	1.04	0.93	0.86	0.94	0.95	0.82	0.75	0.82	0.89	0	0.70	0.86	0	0.70	1.01	0	1.06	1.05	0	0.91	0.95	0.93	0.83	1.00
D_1, D_2, D_3	2.06	8.17	3.66	3.30	4.46	2.54	2.47	9.90	3.49	3.30	4.00	5.59	3.52	2.60	0.79	4.27	4.60	1.63	1.65	7.24	4.79	2.56	7.20	0.75	2.51	3.60	1.14
N_1, N_2, N_3	25	82	45	145	94	70	113	97	63	73	73	65	118	95	66	49	86	47	50	50	42	81	90	63	62	71	44

Table 65: Crack families at horizontal slices and drill patterns summary, blast sessions 2013 and 2014

Pattern/Block/Family		CB 90-80	CB 80-30	CB 30-0	SCB	Connect	Parallel	CD 90-80	CD 80-30	CD 30-0	SC	VCD	Total
2013													
Reference	CH01B03	10	49	19	49	47	39	5	44	45	24	32	363
	CH01B05	12	42	25	39	34	26	19	63	75	16	32	383
	Total	22	91	44	88	81	65	24	107	120	40	64	746
1Bdev.	CH01B02	9	42	17	21	34	23	10	40	48	7	29	280
	CH01B04	12	40	28	49	44	43	16	99	65	16	27	439
	Total	21	82	45	70	78	66	26	139	113	23	56	719
2Bdev.	CH03B01	13	22	21	30	43	30	17	85	43	6	15	325
	CH03B02	15	36	27	23	49	28	12	41	50	16	24	321
	Total	28	58	48	53	92	58	29	126	93	22	39	646
Total cracks		71	231	137	211	251	189	79	372	326	85	159	2111
2014													
Reference	B01	13	31	22	26	40	29	10	48	38	7	40	304
	B06	12	17	27	29	66	52	20	99	77	6	45	450
	B09	7	19	19	16	36	37	12	43	47	2	31	269
	Total	32	67	68	71	142	118	42	190	162	15	116	1023
S+B var.	B03	10	23	34	21	69	37	14	47	44	6	24	329
	B04	7	26	40	31	64	46	16	56	68	9	30	393
	B10	12	26	41	17	25	27	5	33	28	10	14	238
	Total	29	75	115	69	158	110	35	136	140	25	68	960
S/4 shift	B02	14	35	45	14	46	28	9	42	18	18	26	295
	B07	15	46	29	28	44	70	9	64	65	12	53	435
	B011	11	37	44	22	30	18	14	17	23	10	18	244
	Total	40	118	118	64	120	116	32	123	106	40	97	974
Total cracks		101	260	301	204	420	344	109	449	408	80	281	2957

Appendix 8 Damage in individual blocks and patterns

Table 66: MCD and MCID for individual blocks with reference pattern, session 2013

Block	MCD [-]		MCID [-]	
	CH01B03	CH01B05	CH01B03	CH01B05
Drill pattern	Reference		Reference	
Slice 1	1.06	2.03	0.55	1.28
Slice 2	1.06	1.98	0.47	1.38
Slice 3	1.47	2.42	0.77	1.58
Slice 4	1.88	2.36	1.30	1.50
Average	1.37	2.2	0.77	1.43
Stdev	0.39	0.23	0.38	0.13

Table 67: MCD and MCID for individual blocks with 1st burden deviation pattern, session 2013

Block	MCD [-]		MCID [-]	
	CH01B02	CH01B04	CH01B02	CH01B04
Drill pattern	1st burden deviation		1st burden deviation	
Slice 1	-	1.53	-	0.66
Slice 2	2.34	2.04	1.68	1.19
Slice 3	2.24	2.24	1.63	1.52
Slice 4	1.94	2.02	1.25	1.37
Average	2.2	2.0	1.5	1.2
Stdev	0.2	0.3	0.2	0.4

Table 68: MCD and MCID for individual blocks with 2nd burden deviation pattern, session 2013

Block	MCD [-]		MCID [-]	
	CH03B01	CH03B02	CH03B01	CH03B02
Drill pattern	2nd burden deviation		2nd burden deviation	
Slice 1	0.82	1.01	0.32	0.54
Slice 2	1.59	1.02	0.87	0.56
Slice 3	1.86	1.25	1.22	0.65
Slice 4	1.66	1.30	0.97	0.70
Average	1.5	1.1	0.8	0.6
Stdev	0.5	0.1	0.4	0.1

Table 69: MCD and MCID for individual blocks with reference pattern, session 2014

Block	MCD [-]			MCID [-]		
	B01	B06	B09	B01	B06	B09
Drill pattern						
Slice 1	0.83	1.36	1.16	0.25	0.62	0.56
Slice 2	1.12	1.52	0.94	0.59	0.76	0.49
Slice 3	1.34	1.34	0.92	0.64	0.63	0.44
Slice 4	1.35	1.35	1.16	0.89	0.69	0.57
Average	1.2	1.4	1.0	0.6	0.7	0.5
Stdev	0.2	0.1	0.1	0.3	0.1	0.1

Table 70: MCD and MCID for individual blocks with S+B variations pattern, session 2014

Block	MCD [-]			MCID [-]		
	B03	B04	B10	B03	B04	B10
Drill pattern						
Slice 1	1.07	1.19	0.74	0.50	0.46	0.27
Slice 2	1.04	1.35	0.72	0.48	0.63	0.21
Slice 3	1.00	1.24	0.82	0.38	0.46	0.24
Slice 4	1.08	1.08	0.80	0.50	0.44	0.32
Average	1.0	1.2	0.8	0.5	0.5	0.3
Stdev	0.0	0.1	0.0	0.1	0.1	0.0

Table 71: MCD and MCID for individual blocks with S/4 shift pattern, session 2014

Block	MCD [-]			MCID [-]		
	B02	B07	B11	B02	B07	B11
Drill pattern	S/4 shift			S/4 shift		
Slice 1	0.92	1.47	0.59	0.31	0.81	0.16
Slice 2	1.00	1.54	1.01	0.42	0.83	0.33
Slice 3	1.12	1.36	0.70	0.46	0.60	0.26
Slice 4	1.34	1.64	0.84	0.64	0.89	0.38
Average	1.1	1.5	0.8	0.5	0.8	0.3
Stdev	0.2	0.1	0.2	0.1	0.1	0.1

Appendix 9 Crack families on top of test blocks

B01 (Reference)



Figure 134: Crack detection on top Block B01 (Reference)

Table 72: Crack families on top Block B01 (Reference)

Block reference	Crack family	BEFORE BLASTING					1 ROW BLASTED					2 ROW BLASTED					3 ROW BLASTED				
		0row	1 row	2 row	3 row	Total	0row	1 row	2 row	3 row	Total	0row	1 row	2 row	3 row	Total	0row	1 row	2 row	3 row	Total
CB1	long	0	0	0	0	0	0	0	1	1	2	0	0	2	4	6	0	0	0	2	2
	short	1	0	0	0	1	0	2	0	0	2	0	0	4	4	4	0	0	0	0	0
CB 80-30	long	0	0	0	0	0	0	1	1	2	4	0	0	0	2	2	0	0	0	1	3
	short	0	0	0	0	0	0	0	0	0	0	0	0	1	1	1	0	0	0	8	8
CB 30-0	long	0	0	0	0	0	0	3	0	3	0	0	1	0	1	0	0	0	0	1	
	short	0	0	0	0	0	0	0	0	0	0	0	2	0	2	0	0	0	1	1	
SCB	long	1	0	0	0	1	0	1	0	1	0	0	3	2	5	0	0	0	2	2	
	short	0	0	0	0	0	0	1	0	1	0	0	6	2	8	0	0	0	4	4	
Connect	long	0	0	0	0	0	0	0	0	0	0	0	0	0	0	0	0	0	0	0	
	short	0	0	0	0	0	0	0	0	0	0	0	0	0	0	0	0	0	0	0	
Parallel	long	0	0	0	0	0	0	1	0	1	0	0	2	1	3	0	0	0	0	1	
	short	1	0	0	0	1	0	0	1	1	0	0	4	4	8	0	0	0	7	7	
CB 90-0	long	0	0	0	0	0	0	0	0	0	0	0	3	0	3	0	0	0	1	3	
	short	1	0	0	0	1	0	0	0	0	0	0	1	0	1	0	0	0	3	3	
CB 80-30	long	0	0	0	1	1	0	2	0	1	3	0	0	5	0	5	0	0	0	4	6
	short	0	0	0	0	0	0	3	0	3	0	0	12	6	18	0	0	0	7	6	
CB 30-0	long	0	0	0	0	0	0	0	0	0	0	0	1	0	1	0	0	0	0	0	
	short	0	0	0	1	1	0	0	0	0	0	0	4	0	4	0	0	0	1	1	
SC	long	0	0	0	0	0	0	2	0	2	0	0	5	0	5	0	0	0	0	0	
	short	0	0	0	0	0	0	0	0	0	0	0	0	0	0	0	0	0	0	0	
VCB	long	0	0	0	0	0	0	1	1	2	0	0	0	1	1	0	0	0	2	2	
	short	0	0	0	0	0	0	0	0	0	0	0	2	2	4	0	0	0	1	1	
Totals		4	0	0	2	6	0	17	4	4	25	0	0	58	24	82	0	0	0	45	51

Block B06 (Reference)



Figure 135: Crack detection on top Block B06 (Reference)

Table 73: Crack families on top Block B06 (Reference)

B06 (reference)		BEFORE BLASTING						1 ROW BLASTED						2 ROW BLASTED						3 ROW BLASTED					
		0 row	1 row	2 row	3 row	Total	0 row	1 row	2 row	3 row	Total	0 row	1 row	2 row	3 row	Total	0 row	1 row	2 row	3 row	Total				
CBS	long	0	0	0	1	1	0	1	7	2	10	0	0	6	6	12	0	0	0	0	6	6			
	short	0	0	0	0	0	0	1	0	1	2	0	0	0	0	0	0	0	0	0	1	1			
CB 80-30	long	0	1	0	0	1	0	3	5	2	10	0	0	4	3	7	0	0	0	0	5	5			
	short	0	0	0	0	0	0	4	1	1	6	0	0	3	0	3	0	0	0	0	1	1			
CB 30-0	long	0	0	0	0	0	0	1	0	0	1	0	0	2	0	2	0	0	0	0	1	1			
	short	0	0	0	0	0	0	3	1	0	4	0	0	2	0	2	0	0	0	0	1	1			
SCB	long	2	0	0	0	2	0	1	3	0	4	0	0	5	3	8	0	0	0	0	3	3			
	short	2	1	1	0	4	0	11	2	4	17	0	0	3	7	10	0	0	0	0	11	11			
Connect	long	0	0	0	0	0	0	0	0	0	0	0	0	0	0	0	0	0	0	0	0	0			
	short	0	0	0	0	0	0	0	0	0	0	0	0	0	0	0	0	0	0	0	0	0			
Parallel	long	2	0	0	0	2	0	7	1	1	9	0	0	4	1	5	0	0	0	0	8	8			
	short	3	0	1	3	7	0	14	0	4	18	0	0	3	5	8	0	0	0	0	10	10			
CD 90-0	long	0	0	0	0	0	0	1	0	1	2	0	0	1	0	1	0	0	0	0	0	0			
	short	0	0	0	0	0	0	7	0	0	7	0	0	1	0	1	0	0	0	0	1	1			
CD 80-30	long	0	1	1	0	2	0	7	4	1	12	0	0	4	1	5	0	0	0	0	3	3			
	short	0	0	0	0	0	0	22	0	2	24	0	0	9	1	10	0	0	0	0	5	5			
CD 30-0	long	0	0	0	0	0	0	1	0	0	1	0	0	0	0	0	0	0	0	0	0	0			
	short	0	0	0	0	0	0	0	1	0	1	0	0	0	0	0	0	0	0	0	0	0			
SC	long	0	0	0	0	0	0	4	1	0	5	0	0	6	0	6	0	0	0	0	5	5			
	short	0	0	0	0	0	0	4	2	1	7	0	0	4	3	7	0	0	0	0	4	4			
VCB	long	0	1	1	0	2	0	1	1	3	5	0	0	4	3	7	0	0	0	0	4	4			
	short	0	0	0	0	0	0	4	2	1	7	0	0	4	3	7	0	0	0	0	4	4			
Totals		9	4	4	4	21	0	93	29	23	145	0	0	61	33	94	0	0	0	0	70	70			

B09 (Reference)

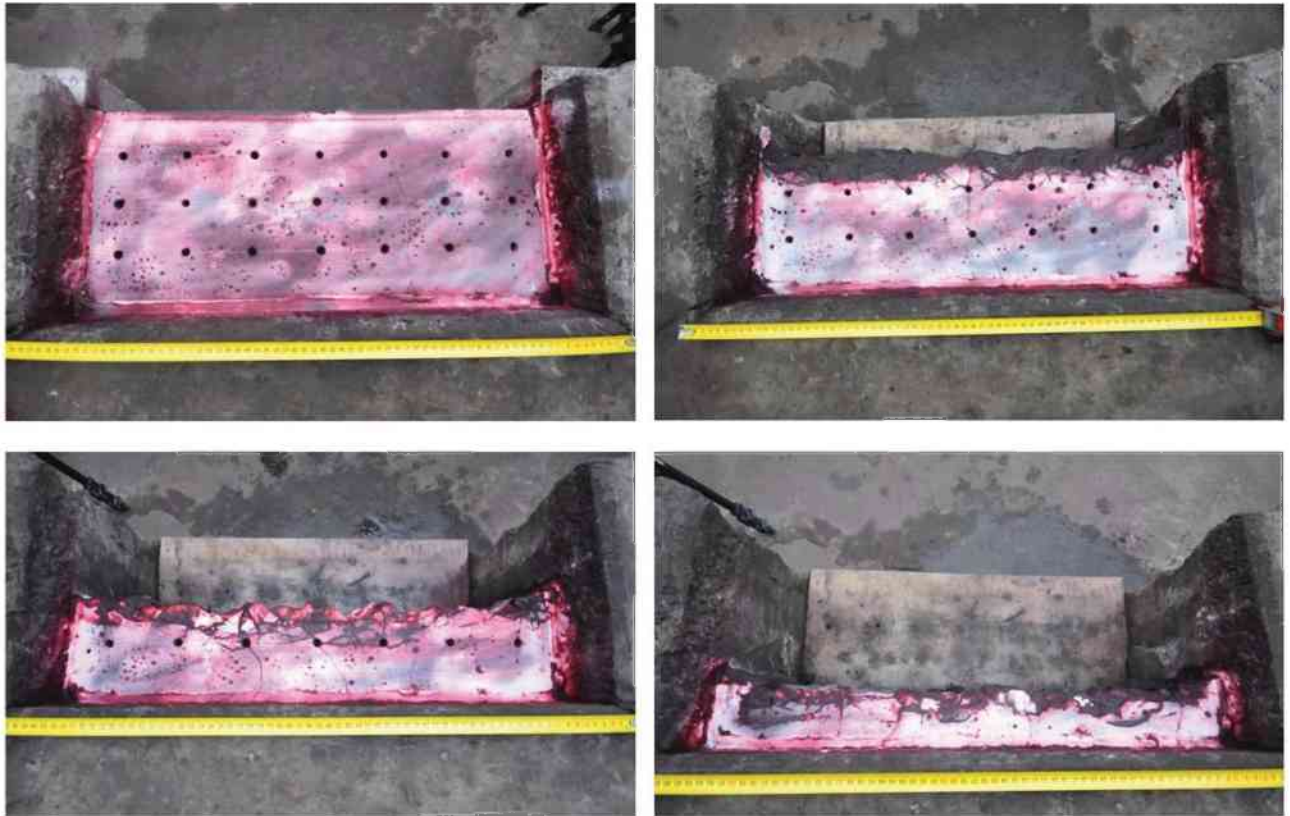


Figure 136: Crack detection on top Block B09 (Reference)

Table 74: Crack families on top Block B09 (Reference)

B09 (reference)		BEFORE BLASTING					1 ROW BLASTED					2 ROW BLASTED					3 ROW BLASTED				
		0 row	1 row	2 row	3 row	Total	0 row	1 row	2 row	3 row	Total	0 row	1 row	2 row	3 row	Total	0 row	1 row	2 row	3 row	Total
CB5	long	0	0	0	0	0	0	4	6	0	10	0	0	5	2	7	0	0	0	3	3
	short	0	0	0	0	0	0	0	0	0	0	0	0	0	4	4	0	0	0	3	3
CB 80-30	long	0	1	1	0	2	0	1	4	2	7	0	0	3	1	4	0	0	0	3	3
	short	0	0	0	0	0	0	4	1	1	6	0	0	4	3	7	0	0	0	4	4
CB 30-0	long	0	0	0	0	0	0	0	0	0	0	0	0	1	2	3	0	0	0	0	0
	short	0	0	0	0	0	0	1	1	1	3	0	0	0	1	1	0	0	0	4	4
SCB	long	0	0	0	0	0	0	0	6	0	6	0	0	0	0	0	0	0	0	0	0
	short	1	0	1	0	2	0	19	1	1	21	0	0	9	1	10	0	0	0	11	11
Connect	long	0	0	0	0	0	0	0	0	0	0	0	0	0	1	1	0	0	0	0	0
	short	0	0	0	0	0	0	0	0	0	0	0	0	0	0	0	0	0	0	0	0
Parallel	long	0	0	0	0	0	0	0	1	0	1	0	0	0	0	0	0	0	0	3	3
	short	0	0	0	0	0	0	12	1	0	13	0	0	18	1	19	0	0	0	5	5
CD 90-80	long	0	0	0	0	0	0	3	0	0	3	0	0	3	1	4	0	0	0	3	3
	short	0	0	0	0	0	0	4	0	0	4	0	0	2	0	2	0	0	0	1	1
CD 80-30	long	0	0	0	0	0	0	3	0	0	3	0	0	4	0	4	0	0	0	2	2
	short	0	0	0	0	0	0	14	0	1	15	0	0	5	2	7	0	0	0	7	7
CD 30-0	long	0	0	0	0	0	0	0	0	0	0	0	0	1	0	1	0	0	0	0	0
	short	0	0	0	0	0	0	3	0	0	3	0	0	0	0	0	0	0	0	3	3
SC	short	0	0	0	0	0	0	5	0	0	5	0	0	3	0	3	0	0	0	5	5
	long	0	1	0	1	2	0	0	2	1	3	0	0	7	1	8	0	0	0	1	1
VCB	long	0	0	0	0	0	0	7	1	2	10	0	0	10	2	12	0	0	0	5	5
	short	0	0	1	1	2	0	7	1	2	10	0	0	10	2	12	0	0	0	5	5
Totals:		1	2	3	2	8	0	80	24	9	113	0	0	75	22	97	0	0	0	63	63

B03 (S+B variations)

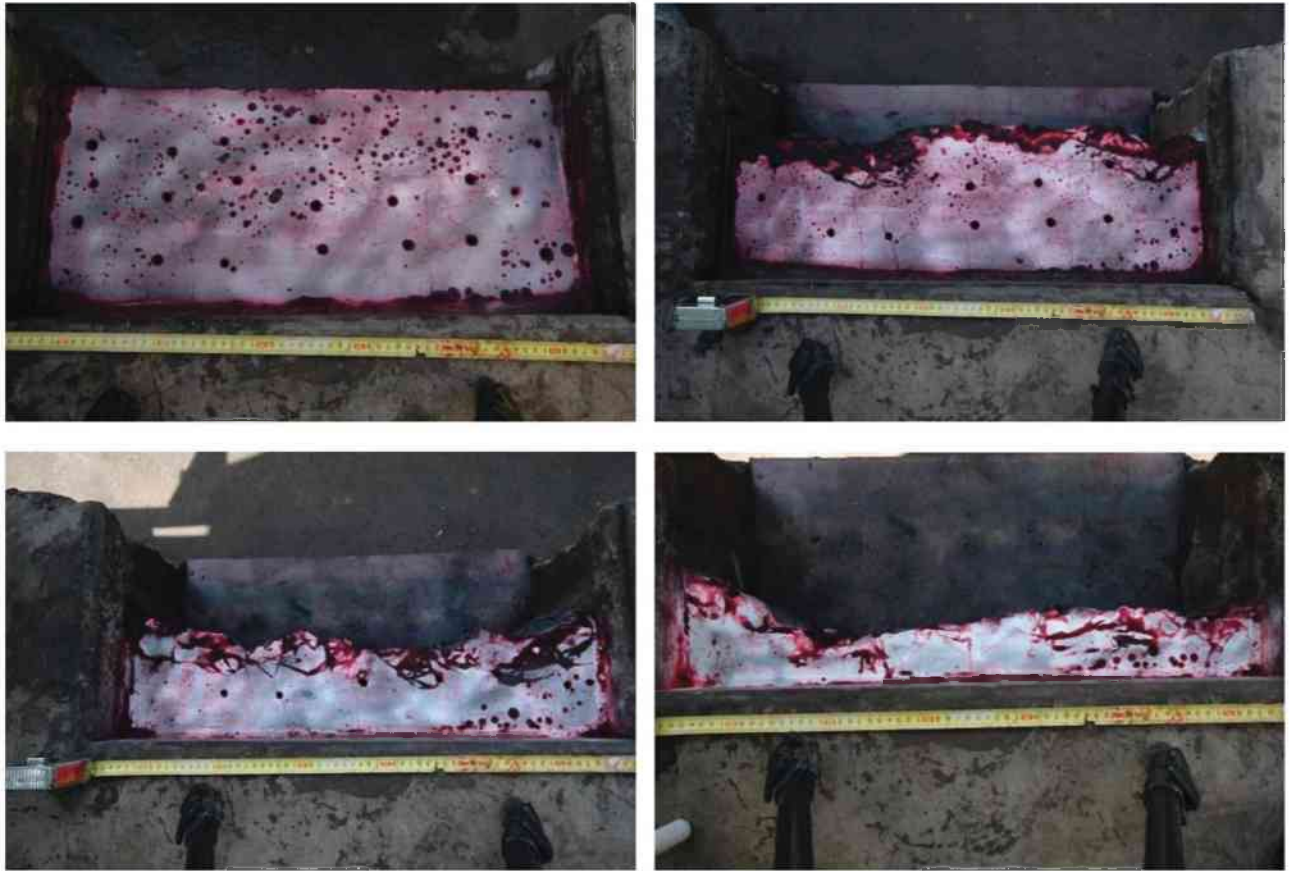


Figure 137: Crack detection on top Block B03 (S+B variations)

Table 75: Crack families on top B03 (S+B variations)

B03 (3-7-6)		BEFORE BLASTING					1 ROW BLASTED					2 ROW BLASTED					3 ROW BLASTED				
		0 row	1 row	2 row	3 row	Total	0 row	1 row	2 row	3 row	Total	0 row	1 row	2 row	3 row	Total	0 row	1 row	2 row	3 row	Total
CBS	long	0	0	1	1	2	0	1	4	3	8	0	0	4	5	9	0	0	0	3	3
	short	0	0	0	0	0	0	0	0	1	1	0	0	0	0	0	0	0	0	4	4
CB 80-30	long	0	1	2	0	3	0	1	3	1	5	0	0	4	1	5	0	0	0	4	4
	short	0	0	0	0	0	0	0	4	0	4	0	0	1	0	1	0	0	0	1	1
CB 30-0	long	0	0	0	0	0	0	0	1	0	1	0	0	2	0	2	0	0	0	2	2
	short	0	0	0	0	0	0	1	2	0	3	0	0	3	0	3	0	0	0	2	2
SCB	long	0	0	0	1	1	0	2	1	1	4	0	0	2	2	4	0	0	0	6	6
	short	1	1	3	0	5	0	4	2	3	9	0	0	7	2	9	0	0	0	3	3
Connect	long	0	0	0	0	0	0	0	1	0	1	0	0	0	0	0	0	0	0	0	0
	short	0	0	0	0	0	0	0	0	0	0	0	0	0	0	0	0	0	0	0	0
Parallel	long	1	1	1	1	4	0	1	1	0	2	0	0	9	0	9	0	0	0	4	4
	short	1	2	1	0	4	0	0	2	0	2	0	0	10	1	11	0	0	0	7	7
CD 90-80	long	0	0	0	0	0	0	2	0	2	0	0	0	0	0	0	0	0	0	0	0
	short	0	0	0	0	0	0	4	0	4	0	0	2	0	2	0	0	0	0	1	1
CD 80-30	long	0	0	1	0	1	0	0	2	0	2	0	0	4	0	4	0	0	0	0	0
	short	0	0	1	1	2	0	8	2	0	10	0	0	1	1	2	0	0	0	8	8
CD 30-0	long	0	0	0	0	0	0	1	0	0	1	0	0	0	0	0	0	0	0	0	0
	short	0	0	0	0	0	0	0	0	0	0	0	0	0	0	0	0	0	0	0	0
SC	long	0	0	0	0	0	0	0	0	0	0	0	0	2	0	2	0	0	0	6	6
	short	3	1	0	1	5	0	0	6	4	10	0	0	7	4	6	0	0	0	3	3
VCB	long	1	0	0	2	3	0	0	4	0	4	0	0	4	0	4	0	0	0	11	11
	short	1	0	0	2	3	0	0	4	0	4	0	0	4	0	4	0	0	0	11	11
Totals		7	6	10	7	30	0	25	35	13	73	0	0	57	16	73	0	0	0	65	65

B04 (S+B variations)



Figure 138: Crack detection on top Block B04 (S+B variations)

Table 76: Crack families on top B04 (S+B variations)

B04 (3-7-6)		BEFORE BLASTING					1 ROW BLASTED					2 ROW BLASTED					3 ROW BLASTED				
Crack family		0 row	1 row	2 row	3 row	Total	0 row	1 row	2 row	3 row	Total	0 row	1 row	2 row	3 row	Total	0 row	1 row	2 row	3 row	Total
CBS	long	0	0	0	1	1	0	4	4	3	11	0	0	3	5	8	0	0	0	5	5
	short	0	0	0	0	0	0	1	1	0	2	0	0	2	0	2	0	0	0	0	0
CB 80-30	long	0	0	0	0	0	0	1	4	2	7	0	0	4	1	5	0	0	0	3	3
	short	0	0	0	0	0	0	3	0	0	3	0	0	1	1	2	0	0	0	2	2
CB 30-B	long	0	0	0	0	0	0	1	1	0	2	0	0	3	0	3	0	0	0	4	4
	short	0	0	0	0	0	0	4	0	0	4	0	0	4	1	5	0	0	0	2	2
SCB	long	0	0	0	0	0	0	5	3	0	8	0	0	3	0	3	0	0	0	2	2
	short	2	0	1	0	3	0	5	3	1	9	0	0	11	3	14	0	0	0	11	11
Connect	long	0	0	0	0	0	0	0	1	0	1	0	0	0	0	0	0	0	0	0	0
	short	0	0	0	0	0	0	0	0	0	0	0	0	0	0	0	0	0	0	0	0
Parallel	long	0	3	0	2	5	0	5	3	2	10	0	0	5	1	6	0	0	0	8	4
	short	0	0	1	0	1	0	5	4	1	10	0	0	10	3	13	0	0	0	8	7
CD 50-80	long	0	0	1	0	1	0	0	0	0	0	0	0	1	0	1	0	0	0	0	0
	short	0	0	0	0	0	0	4	0	2	6	0	0	2	0	2	0	0	0	3	1
CD 80-30	long	0	0	0	0	0	0	4	0	0	4	0	0	2	0	2	0	0	0	1	1
	short	0	1	0	0	1	0	8	1	0	9	0	0	11	0	11	0	0	0	4	4
CD 80-B	long	0	0	1	0	1	0	2	1	0	3	0	0	2	0	2	0	0	0	0	0
	short	0	0	0	0	0	0	5	0	0	5	0	0	2	0	2	0	0	0	2	2
SC	long	0	0	0	0	0	0	1	3	0	4	0	0	3	2	5	0	0	0	6	6
	short	5	1	0	1	7	0	3	3	4	10	0	0	3	4	7	0	0	0	2	2
VCB	long	2	0	0	0	2	0	4	6	0	10	0	0	2	0	2	0	0	0	3	3
	short	2	0	0	0	2	0	4	6	0	10	0	0	2	0	2	0	0	0	3	3
Totals		9	5	4	4	22	0	65	38	15	118	0	0	74	21	95	0	0	0	66	59

B10 (S+B variations)

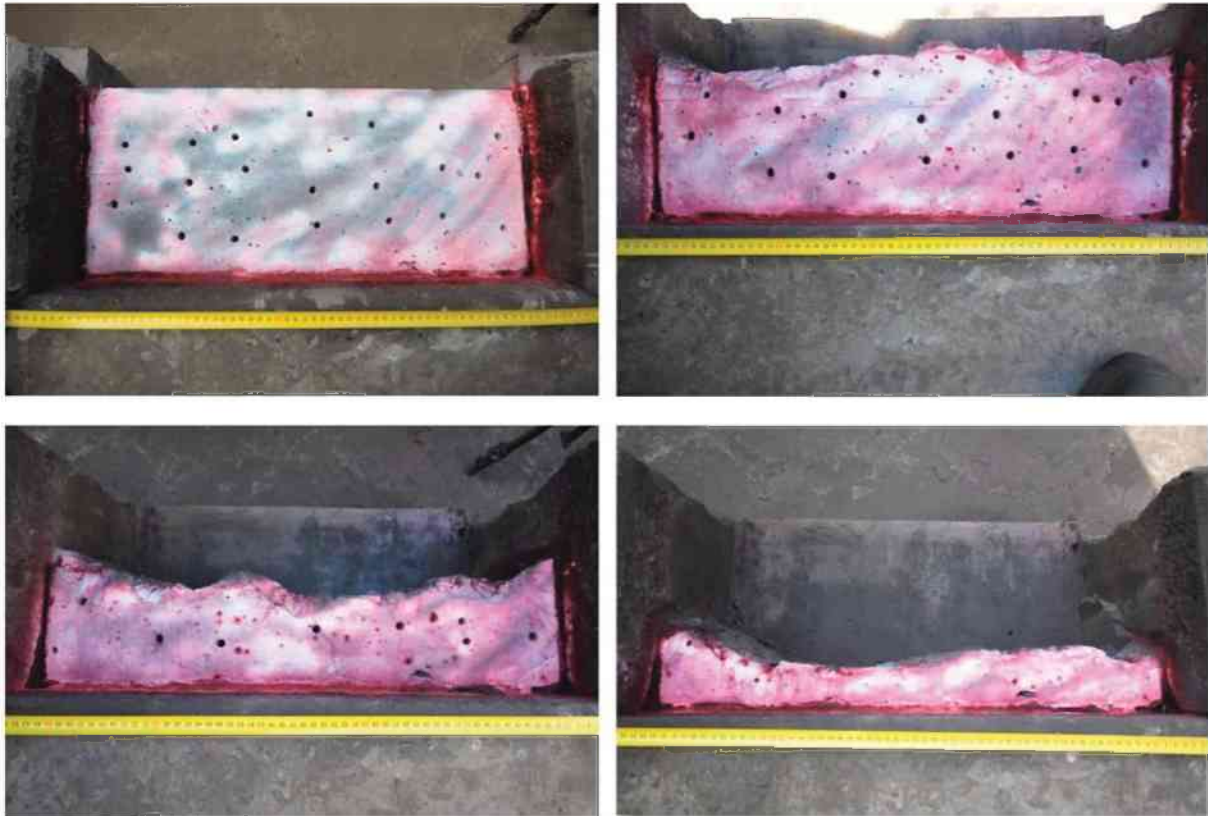


Figure 139: Crack detection on top Block B10 (S+B variations)

Table 77: Crack families on top B10 (S+B variations)

B10 (3-7-6)		BEFORE BLASTING					1 ROW BLASTED					2 ROW BLASTED					3 ROW BLASTED				
Crack family		0 row	1 row	2 row	3 row	Total	0 row	1 row	2 row	3 row	Total	0 row	1 row	2 row	3 row	Total	0 row	1 row	2 row	3 row	Total
CB	long	0	0	0	0	0	0	1	1	0	2	0	0	3	2	5	0	0	0	3	3
	short	0	0	0	0	0	0	1	1	0	2	0	0	3	1	4	0	0	0	2	2
CB 80-30	long	0	0	0	0	0	0	1	0	1	2	0	0	1	1	2	0	0	0	0	1
	short	0	0	0	0	0	0	3	1	0	4	0	0	11	0	11	0	0	0	3	3
CB 30-0	long	0	0	0	0	0	0	1	1	0	2	0	0	5	0	5	0	0	0	0	0
	short	0	0	0	0	0	0	2	0	0	2	0	0	5	0	5	0	0	0	1	1
SCB	long	0	0	0	0	0	0	0	1	1	2	0	0	2	1	3	0	0	0	1	1
	short	0	0	0	0	0	0	1	0	0	1	0	0	5	0	5	0	0	0	2	2
Connect	long	0	0	0	0	0	0	0	0	0	0	0	0	0	0	0	0	0	0	0	0
	short	0	0	0	0	0	0	0	0	0	0	0	0	0	0	0	0	0	0	0	0
Parallel	long	0	0	0	0	0	0	0	0	0	0	0	0	0	0	0	0	0	0	0	0
	short	0	0	0	0	0	0	5	0	0	5	0	0	3	0	3	0	0	0	4	4
CD 90-80	long	0	0	0	0	0	0	1	0	0	1	0	0	0	0	0	0	0	0	1	1
	short	0	0	0	0	0	0	2	0	0	2	0	0	3	0	3	0	0	0	2	2
CD 80-30	long	0	0	0	0	0	0	0	0	1	1	0	0	2	0	2	0	0	0	1	1
	short	0	0	0	0	0	0	2	1	0	3	0	0	8	1	9	0	0	0	6	6
CD 20-0	long	0	0	0	0	0	0	0	0	0	0	0	0	0	0	0	0	0	0	0	0
	short	0	0	0	0	0	0	3	0	0	3	0	0	4	0	4	0	0	0	0	0
SC	long	0	0	0	0	0	0	11	0	1	12	0	0	10	0	10	0	0	0	13	13
	short	0	0	0	0	0	0	0	0	1	1	0	0	1	0	1	0	0	0	1	1
VCB	long	0	0	0	0	0	0	4	0	0	4	0	0	13	1	14	0	0	0	6	6
	short	0	0	0	0	0	0	0	0	0	0	0	0	0	0	0	0	0	0	0	0
Totals		0	0	0	0	0	0	38	6	5	49	0	0	79	7	86	0	0	0	47	47

B02 (S/4 shift)

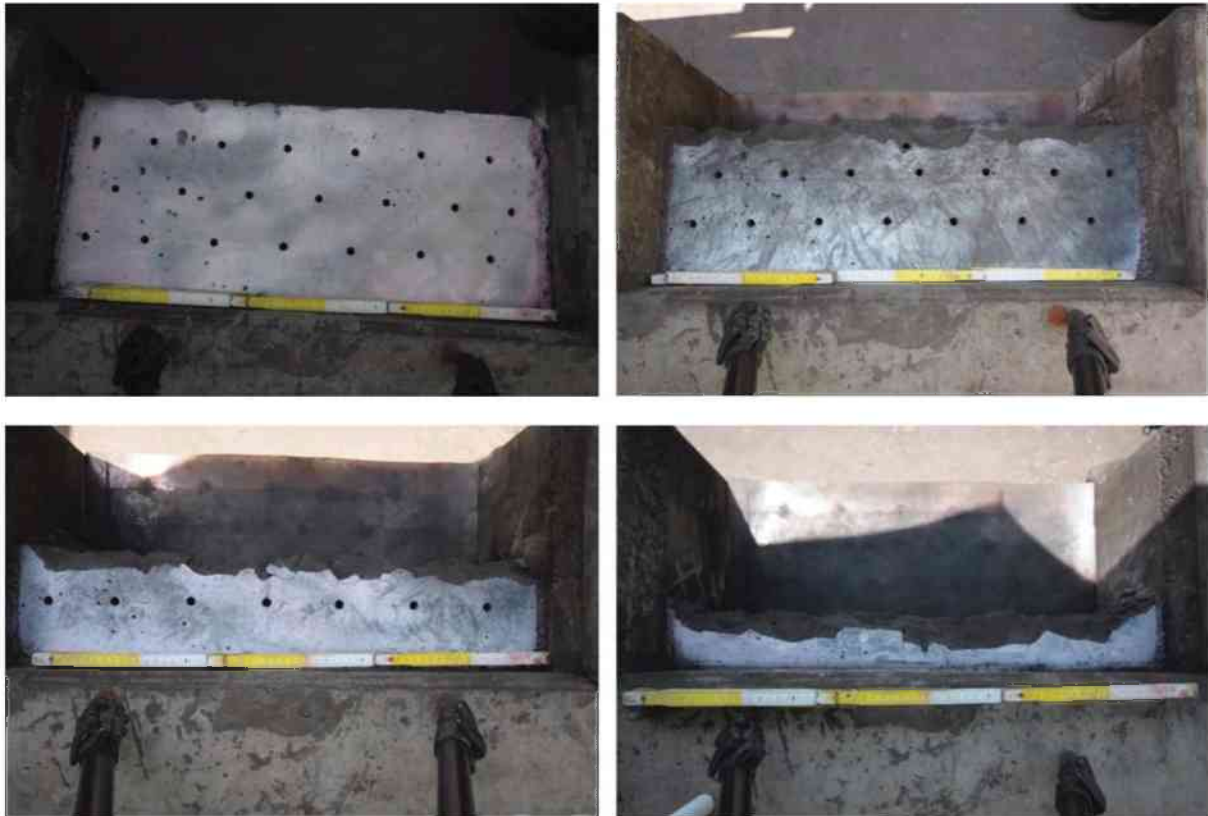


Figure 140: Crack detection on top Block B02 (S/4 shift)

Table 78: Crack families on top B02 (S/4 shift)

B02 (S/4 shift)		BEFORE BLASTING					1 ROW BLASTED					2 ROW BLASTED					3 ROW BLASTED				
Crack family		0 row	1 row	2 row	3 row	Total	0 row	1 row	2 row	3 row	Total	0 row	1 row	2 row	3 row	Total	0 row	1 row	2 row	3 row	Total
CBS	long	0	1	0	1	2	0	1	0	2	3	0	0	2	4	6	0	0	0	7	7
	short	0	0	0	0	0	0	5	1	0	6	0	0	2	0	2	0	0	0	0	0
CB 80-30	long	0	1	0	0	1	0	5	1	0	6	0	0	5	0	5	0	0	0	5	5
	short	3	0	0	0	3	0	9	0	0	9	0	0	2	0	2	0	0	0	2	2
CB 30-0	long	1	0	0	0	1	0	2	0	2	0	0	4	0	4	0	0	0	0	2	2
	short	0	0	0	0	0	0	3	0	3	0	0	2	0	2	0	0	0	0	4	4
SCB	long	1	0	0	0	1	0	0	0	0	0	0	0	1	1	2	0	0	0	0	0
	short	1	0	0	0	1	0	1	0	1	0	0	0	0	0	0	0	0	0	0	0
Connect	long	0	0	0	0	0	0	0	0	0	0	0	0	0	0	0	0	0	0	0	0
	short	0	0	0	0	0	0	0	0	0	0	0	0	0	0	0	0	0	0	0	0
Parallel	long	0	3	2	0	5	0	0	3	0	3	0	0	1	0	1	0	0	0	0	0
	short	0	0	0	0	0	0	0	0	0	0	0	0	6	0	6	0	0	0	2	2
CD 90-80	long	0	0	0	0	0	0	0	0	0	0	0	0	0	0	0	0	0	0	0	0
	short	0	0	0	0	0	0	1	0	1	0	0	0	0	0	0	0	0	0	0	0
CD 80-30	long	0	0	0	0	0	0	1	0	1	2	0	0	1	0	1	0	0	0	2	2
	short	0	0	0	0	0	0	0	0	0	0	0	0	4	0	4	0	0	0	0	0
CD 30-0	long	0	0	0	0	0	0	0	0	0	0	0	0	1	0	1	0	0	0	0	0
	short	0	0	0	0	0	0	0	0	0	0	0	0	1	0	1	0	0	0	0	0
SC	long	0	0	0	0	0	0	10	0	10	0	0	7	0	7	0	0	0	0	12	12
	short	0	0	0	0	0	0	0	0	0	0	0	1	0	1	0	0	0	0	0	0
VCB	long	3	2	2	0	7	0	0	1	0	1	0	0	2	1	3	0	0	0	1	1
	short	3	0	0	0	3	0	3	0	3	0	0	3	0	3	0	3	0	0	5	5
Totals		12	7	4	1	24	0	41	6	3	50	0	0	44	6	50	0	0	0	42	42

B07 (S/4 shift)

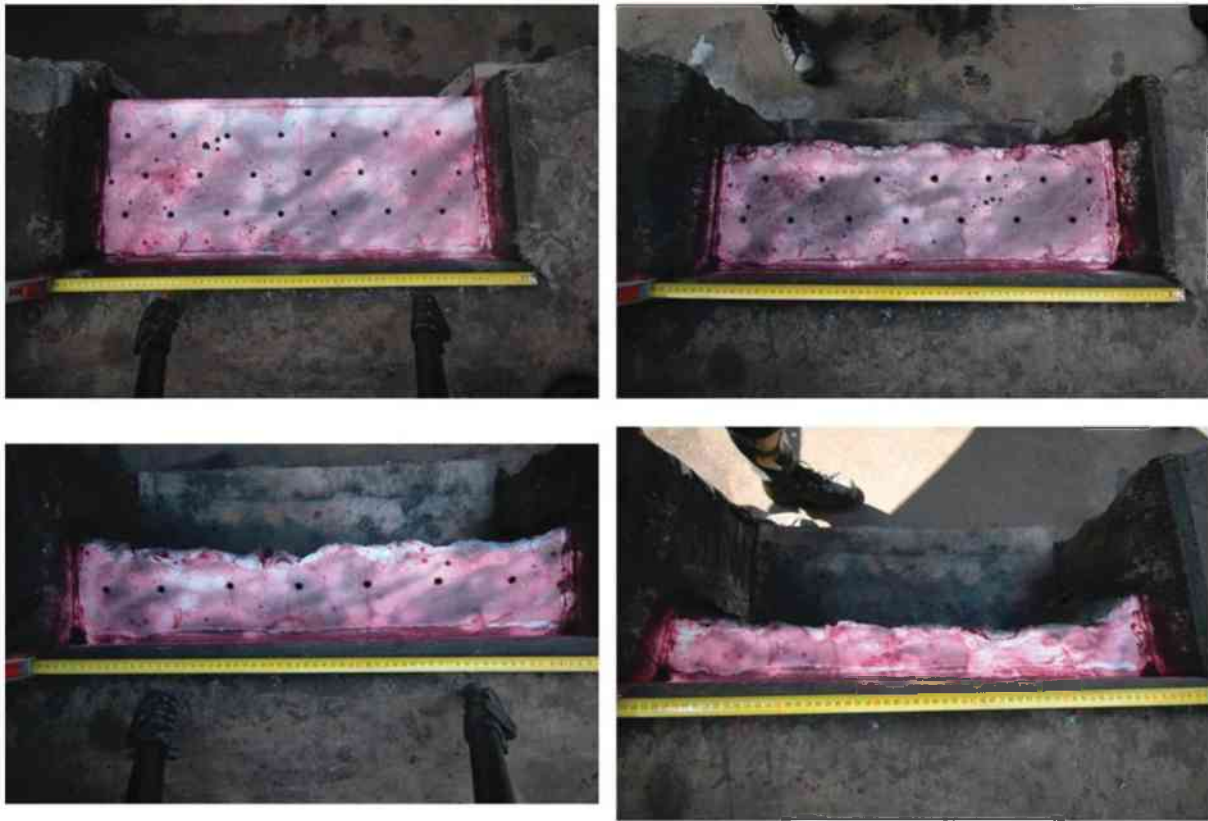


Figure 141: Crack detection on top Block B07 (S/4 shift)

Table 79: Crack families on top B07 (S/4 shift)

B07 (S/4 shift)	BEFORE BLASTING					1 ROW BLASTED					2 ROW BLASTED					3 ROW BLASTED					
	0 row	1 row	2 row	3 row	Total	0 row	1 row	2 row	3 row	Total	0 row	1 row	2 row	3 row	Total	0 row	1 row	2 row	3 row	Total	
CRS	long	0	0	0	0	0	3	0	2	5	0	0	2	4	6	0	0	0	4	4	
	short	0	0	0	0	0	3	1	0	4	0	0	3	0	3	0	0	0	1	1	
CR 80-30	long	0	0	1	0	1	1	2	0	3	0	0	4	0	4	0	0	0	3	3	
	short	0	0	1	0	1	0	3	0	3	0	0	5	0	5	0	0	0	4	4	
CR 30-0	long	0	0	1	0	1	0	3	1	4	0	0	2	0	2	0	0	0	1	1	
	short	0	0	0	0	0	6	0	0	6	0	0	7	0	7	0	0	0	11	11	
SQB	long	0	0	0	2	2	0	0	2	2	0	0	2	4	6	0	0	0	0	0	
	short	0	0	1	5	6	0	1	1	2	4	0	0	4	4	8	0	0	0	5	5
Conspic	long	0	0	0	0	0	0	0	0	0	0	0	0	0	0	0	0	0	0	0	
	short	0	0	0	0	0	0	0	0	0	0	0	0	0	0	0	0	0	0	0	
Parallel	long	0	1	0	3	4	0	2	0	3	5	0	0	2	3	5	0	0	0	6	6
	short	0	1	0	3	4	0	1	0	3	4	0	0	1	3	4	0	0	0	7	7
CD 90-90	long	0	0	0	0	0	0	0	0	0	0	0	1	0	1	0	0	0	1	1	
	short	0	0	1	0	1	0	1	1	3	0	0	0	0	0	0	0	0	0	0	
CD 80-30	long	0	1	1	2	4	0	2	1	4	0	0	0	0	0	0	0	0	0	0	
	short	0	1	1	0	2	0	3	0	2	5	0	0	7	2	9	0	0	0	3	3
CD 40-0	long	0	0	2	0	2	0	0	2	2	0	0	0	0	0	0	0	0	0	0	
	short	0	0	0	0	0	0	0	0	0	0	0	2	0	2	0	0	0	3	3	
SC	long	0	0	0	0	0	0	7	0	7	0	0	10	0	10	0	0	0	5	5	
	short	1	1	1	2	5	0	3	1	2	6	0	0	1	2	3	0	0	0	2	2
VCB	long	1	1	1	2	5	0	3	1	2	6	0	0	1	2	3	0	0	0	2	2
	short	1	1	0	0	2	0	10	3	1	14	0	0	15	0	15	0	0	0	7	7
Totals	2	6	10	17	35	0	49	13	19	81	0	0	68	22	90	0	0	0	63	63	

B11 (S/4 shift)

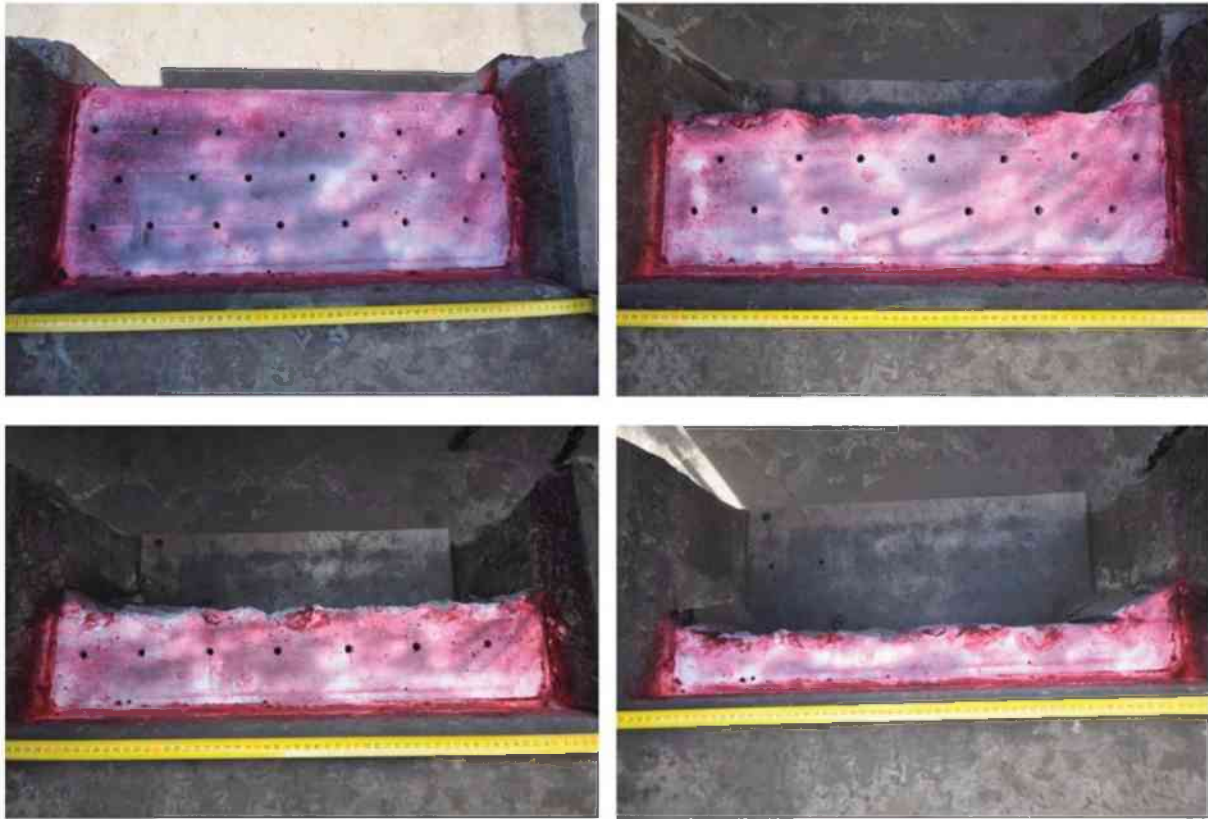


Figure 142: Crack detection on top Block B11 (S/4 shift)

Table 80: Crack families on top B11 (S/4 shift)

B11 (S/4 shift)	BEFORE BLASTING					1 ROW BLASTED					2 ROW BLASTED					3 ROW BLASTED					
	0 row	1 row	2 row	3 row	Total	0 row	1 row	2 row	3 row	Total	0 row	1 row	2 row	3 row	Total	0 row	1 row	2 row	3 row	Total	
CBS	long	0	0	0	0	0	2	0	1	3	0	0	0	2	2	0	0	0	0	4	4
	short	0	0	0	0	0	0	0	0	0	0	0	2	0	2	0	0	0	0	1	1
CB 80-30	long	0	0	0	0	0	0	2	1	3	0	0	3	1	4	0	0	0	0	2	2
	short	0	0	0	0	0	5	0	0	5	0	0	6	0	6	0	0	0	0	3	3
CB 30-0	long	0	0	0	0	0	0	0	0	0	0	0	0	0	0	0	0	0	0	1	1
	short	0	0	0	0	0	8	0	0	8	0	0	5	0	6	0	0	0	0	3	3
SCB	long	0	0	0	0	0	1	0	0	1	0	0	1	0	1	0	0	0	0	0	0
	short	0	0	0	0	0	1	0	3	4	0	0	5	3	8	0	0	0	0	3	3
Connect	long	0	0	0	0	0	0	0	0	0	0	0	0	0	0	0	0	0	0	0	0
	short	0	0	0	0	0	0	0	0	0	0	0	0	0	0	0	0	0	0	0	0
Parallel	long	0	0	0	0	0	0	0	0	0	0	0	1	0	1	0	0	0	0	0	0
	short	0	0	0	0	0	4	0	0	4	0	0	7	0	7	0	0	0	0	5	5
CD 90-80	long	0	0	0	0	0	0	0	0	0	0	0	0	0	0	0	0	0	0	0	0
	short	0	0	0	0	0	1	0	0	1	0	0	2	0	2	0	0	0	0	1	1
CB 80-30	long	0	0	0	0	0	1	0	0	1	0	0	0	0	0	0	0	0	0	1	1
	short	0	0	0	0	0	7	0	0	7	0	0	11	0	11	0	0	0	0	2	2
CD 30-0	long	0	0	0	0	0	1	0	0	1	0	0	0	0	0	0	0	0	0	0	0
	short	0	0	0	0	0	4	0	0	4	0	0	5	0	5	0	0	0	0	1	1
SC	long	0	0	0	0	0	15	0	0	15	0	0	14	0	14	0	0	0	0	10	10
	short	0	0	0	0	0	0	0	0	0	0	0	1	0	1	0	0	0	0	0	0
VCB	long	0	0	0	0	0	4	1	0	5	0	0	1	0	1	0	0	0	0	0	0
	short	0	0	0	0	0	4	1	0	5	0	0	1	0	1	0	0	0	0	7	7
Totals	0	0	0	0	0	0	54	3	5	62	0	0	65	6	71	0	0	0	44	44	

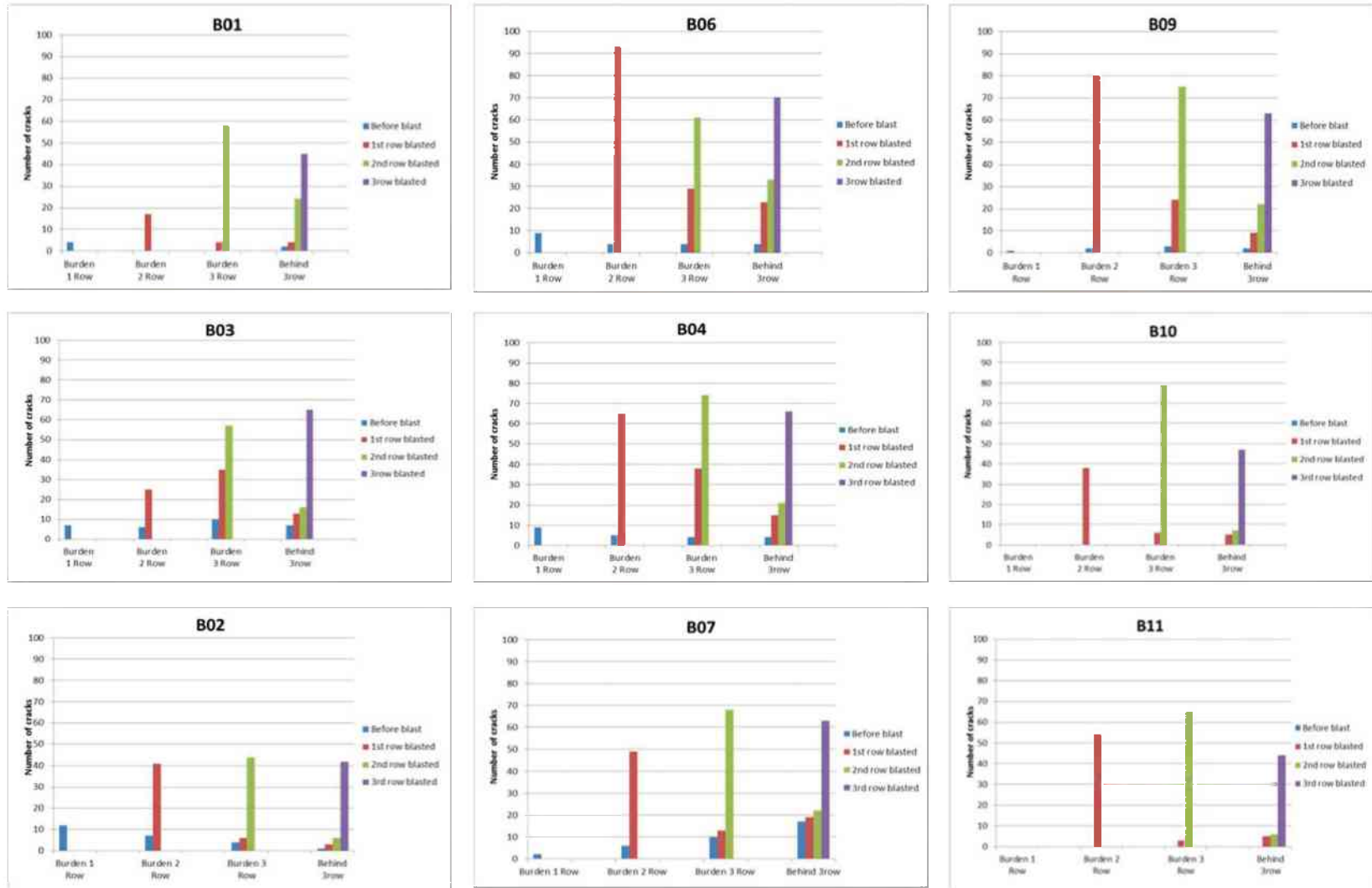


Figure 143: Total number of cracks in different regions of blocks from reference drill pattern groups: Reference B01, B06, B09 (upper); S+B variations B03, B04, B10 (middle), S/4 shift B02, B07, B11 (down).

Table 81: Summary of exterior and interior cracks, blast session 2014

Reference pattern					
Block	Top cracks behind 3 row	Slice 1	Slice 2	Slice 3	Slice 4
B01	45	50	78	80	96
B06	70	99	126	109	116
B09	63	75	52	64	78
Min	45	50	52	64	78
Max	70	99	126	109	116
Range	25	49	74	45	38
S+B variations pattern					
Block	Top cracks behind 3 row	Slice 1	Slice 2	Slice 3	Slice 4
B03	65	83	81	84	81
B04	66	97	107	98	91
B10	47	62	54	60	62
Min	47	62	54	60	62
Max	66	97	107	98	91
Range	19	35	53	38	29
S/4 shift pattern					
Block	Top cracks behind 3 row	Slice 1	Slice 2	Slice 3	Slice 4
B02	42	80	69	69	77
B07	63	106	112	98	119
B10	44	48	68	64	64
Min	42	48	68	64	64
Max	63	106	112	98	119
Range	21	58	44	34	55

Appendix 10 Surface damage analysis methodology

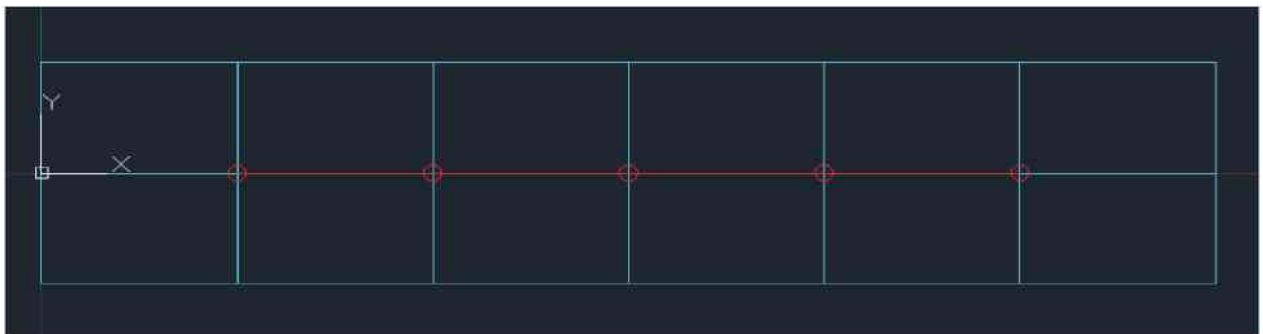
Source: Thomas SEIDL

1) *Blast Metrix*

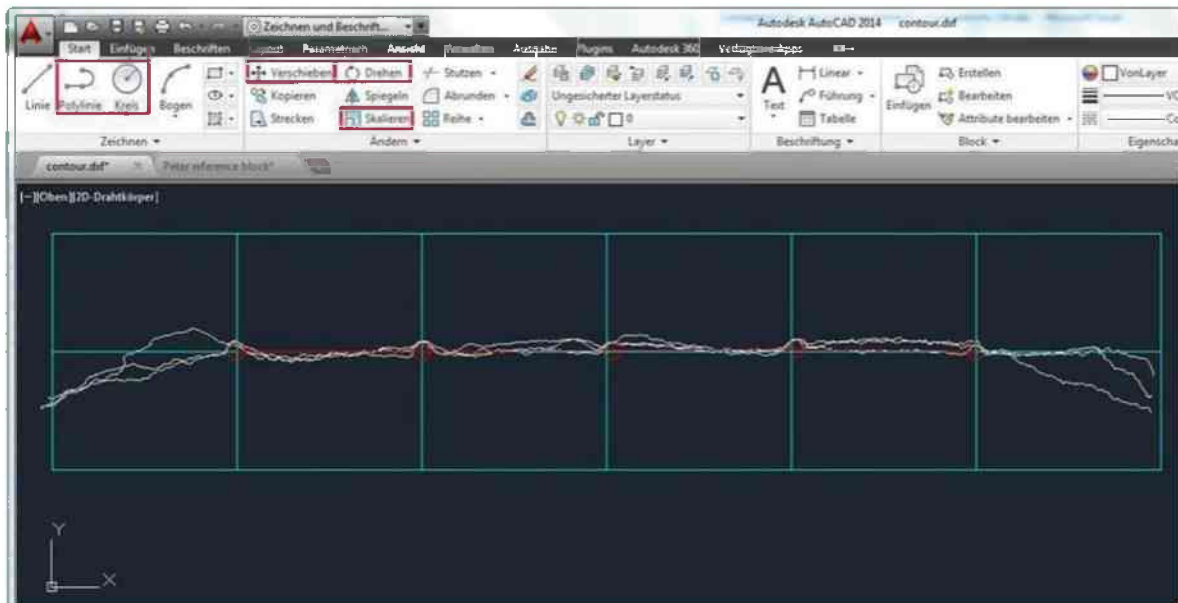
- Generate 3D-model from images using Blast Metrix.
- Export surface model as .dxf for 3D analysis (used later)
- Create three sections (at 5cm, 10cm, 15cm) and export contour as .dxf file for 2D-analysis.
- See Blast Metrix Manual for detailed information

2) *Place drillhole reference in AutoCAD®*

- Open contour.dxf
- If available for current drill pattern, copy & paste block template into contour file. Place template in x-y-plane using the left bottom front corner as centre of coordinate system. ($x=0$, $y=0$, $z=0$)
- A block template should consist of:
 - Planned drill grid
 - Circles (10mm diameter) representing the holes
 - Polyline connecting the centres of the circles (at $z=0$)



- Place drill holes on actual position, with regard to the half cast pattern in the contour line.
- Suggested workflow using a template (relevant tools marked):
 - Paste block template matching the block-coordinate system
 - Move contours, fitting at least one hole to its half cast
 - If required, rotate contours around matched hole (make sure to be in top-view)
 - If required, scale contours (NOTE: z-coordinates are affected as well)
 - If required, move single holes from the defined pattern to the actual position. Check image of block taken before blasting to identify inaccurate drill holes.
Also move corresponding point of Polyline to new centre of drillhole.



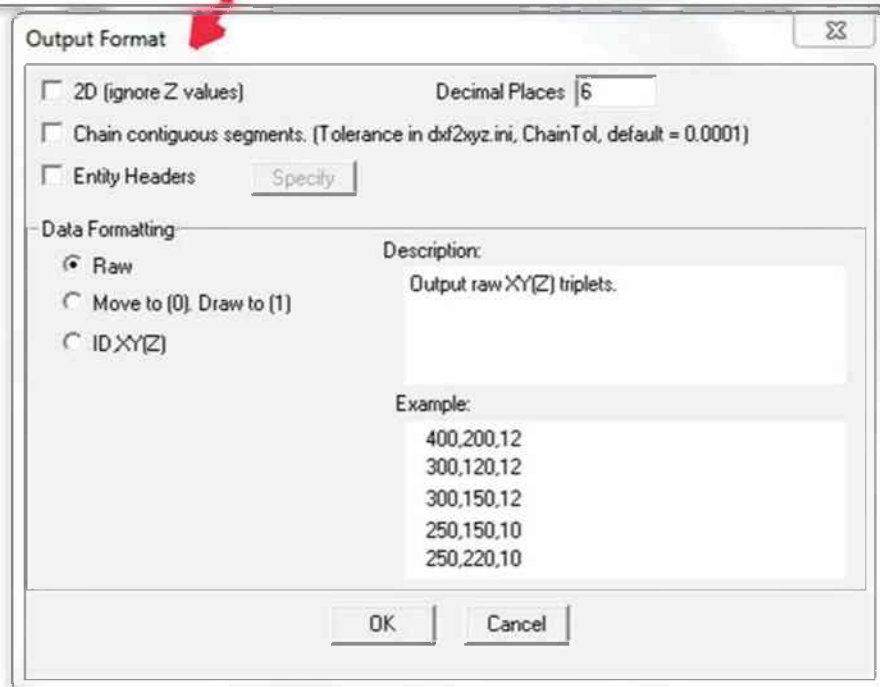
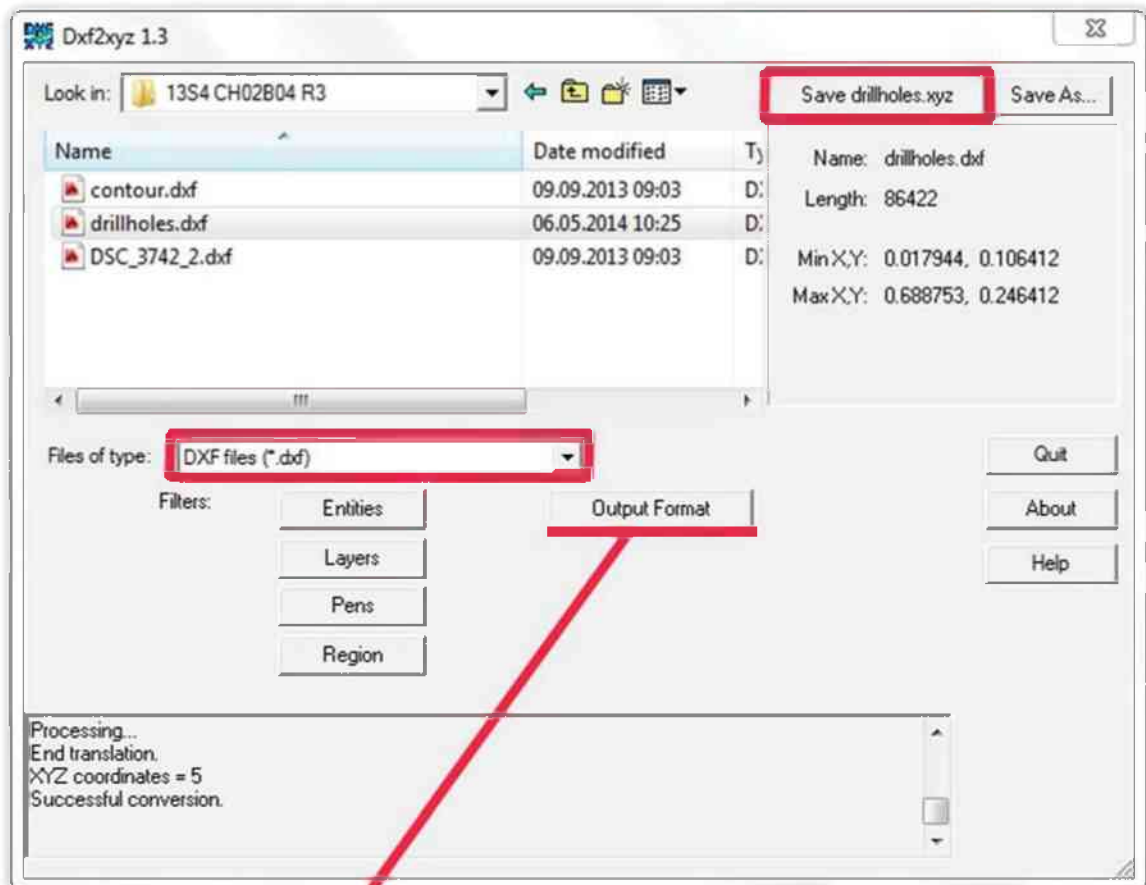
- Save as DWG-file
- Delete everything except drillhole-polyline and profiled and save as DXF-file
- Optional all rows of one block can be place in one DWG-file (recommended for blocks with irregular pattern). Create an individual DXF-file for each row. Use “delete” and “UnDo” to create the DXF files containing only profiles and drillhole-polyline.

3) Preparation of Data

Conversion of DXF-files to XYZ-files is done using the freeware tool “dxf2xyz” by “Guthrie CAD/GIS Software”



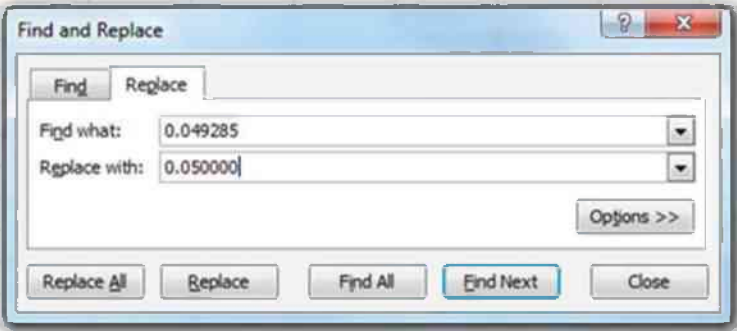
- Open dxf2xyz.exe
- Select files to be converted
- Save XYZ-file. Name is taken from original file, or can be specified using “Save As...”



- Open new Excel file
- Open XYZ-file with "Editor", "Notepad" or similar
- Copy all (Shortcuts: "Ctrl+A" + "Ctrl+C")
- Paste data to Excel ("Ctrl+V")

- Use function “Data” - “Text to Columns” with comma as delimiter when pasting (Sometimes the conversion to columns works directly when pasting the data, sometimes it has to be initiated manually)
- Split drill holes ($z=0$, mostly at top or bottom) from contour data ($z \neq 0$)
- Save Excel file
- NOTE: Points with z-coordinate other than 0.05, 0.10 or 0.15 can be deleted, but they can also remain as they are ignored by the processing algorithms anyway.
- NOTE: In case the contour data was scaled in AutoCAD®, the z-values are not exactly at 5cm intervals and would be ignored by the processing algorithms. Therefore the profiles need to be shifted using the “Find and Replace” function in Excel.

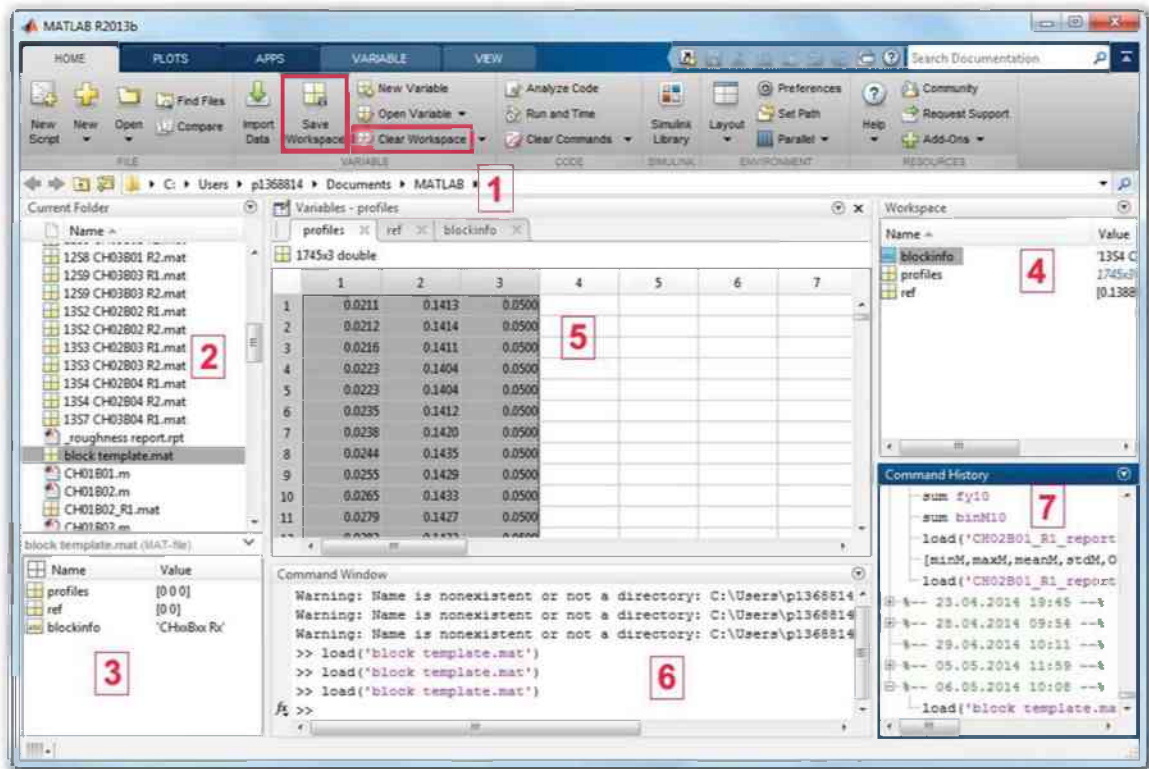
	A	B	C	D	E	F	G	H	I	J	K
722	0.046019	0.029976	0.049285								
723	0.045821	0.030047	0.049285								
724	0.044578	0.030221	0.049285								
725	0.043742	0.030449	0.049285								
726	0.043480	0.030535	0.049285								
727	0.701482	0.100387	0.098569								
728	0.701578	0.100612	0.098569								
729	0.701192	0.100496	0.098569								
730	0.699716	0.100249	0.098569								
731	0.699158	0.100093	0.098569								
732	0.698074	0.099946	0.098569								
733	0.697081	0.099678	0.098569								



4) Short general introduction to MATLAB® GUI

- [1] Path of current folder
- [2] Content of current folder
- [3] Preview of file or description of function
- [4] Workspace (list of active variables)
- [5] Variables editor (activated by double clicking of variable in workspace)
- [6] Command window
- [7] Command history
- [red] Command buttons for workspace handling

- All MATLAB® files have to be in the Current folder. Its path is indicated (and can be changed) at [1], and its contents are listed in [2].
- This Manual is based on MATLAB® Version “R2013b”

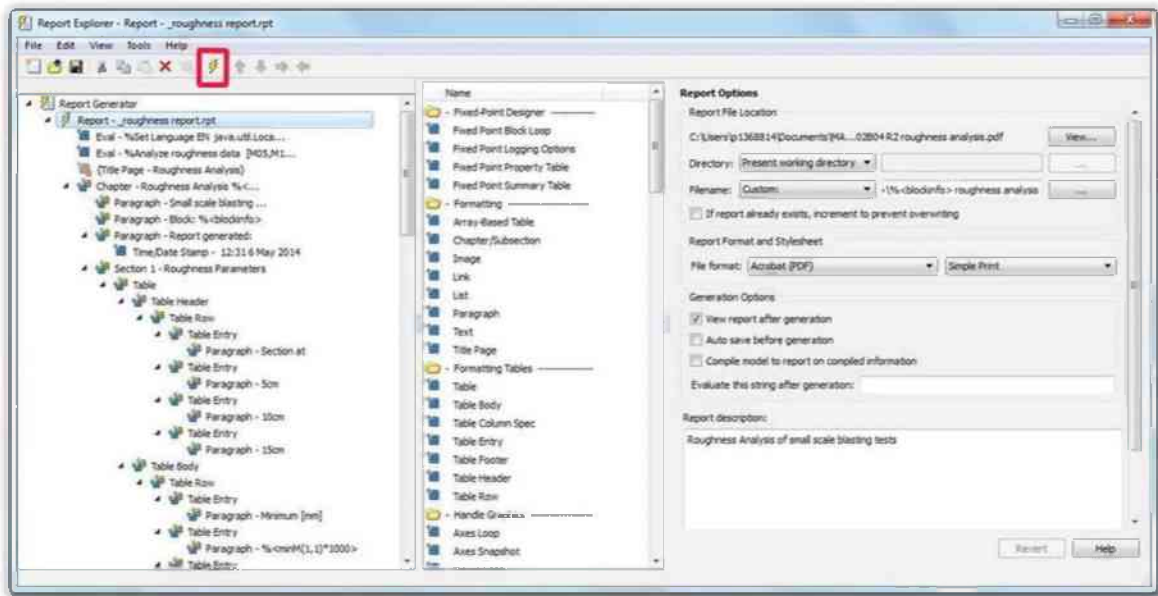


5) Report generation in MATLAB® (automated)

- Clear workspace first in case of existing variables
- Create variables “blockinfo”, “profiles” and “ref” for basic information in workspace. This task is performed when opening “block template.mat”
NOTE: Names of variables have to be **exactly** like mentioned above
- Enter name of block and blasted row in “blockinfo”. This name will be displayed on the report and the graphs. Filename and saving location of the result files also use this name.
- Enter x, y, z coordinates into “profiles” (copy & paste from Excel file)
- Enter x, y coordinates of drill holes in “ref” (copy & paste from Excel file). Drill holes must be sorted ascending in x-direction
- Save workspace (recommendation: use same name as stored in “blockinfo”)

Name	Value	Min	Max
blockinfo	'1354 CH02B04 R3'		
profiles	1745x3 double	0.0179	0.6876
ref	[0.1388 0.1764; 0.2488 ...	0.1388	0.5788

- Open “_roughness report.rpt” -> Report Explorer launches
- Run report generation by clicking the “flash”-symbol
- NOTE: all MATLAB® files have to be in current MATLAB® working directory (path [1])



- The following tasks are performed by the report generator:
 - Analysis of the data and generation of graphs
 - Creation of folder named according to “block info” for result files as a subdirectory of the current working directory
 - Saving of PDF report
 - Saving of graphs in PNG format
 - Creation of export-variable for further use of data in Excel
 - Saving of analysed workspace
- The data in the export-variable can now be copied into an Excel-file
NOTE: “Use Text import wizard” in Excel and choose “Tab” as delimiter when pasting into Excel-sheet.
- The export variable contains 15x4 values (5, 10, 15 cm & combined), sorted as follows:
 - Number of Points [-]
 - Length of section [-]
 - Distance Minimum [mm]
 - Distance Maximum [mm]
 - Distance Mean [mm]
 - Distance Standard Deviation [mm]
 - Overbreak [mm²/mm]
 - Underbreak [mm²/mm]
 - Total Area [mm²/mm]
 - Area Replacement [mm²/mm]
 - Inclination Normalized [-]
 - Inclination Minimum [-]

- Inclination Maximum [-]
- Inclination Mean [-]
- Inclination Standard Deviation [-]

6) **Histogram comparison from multiple rows**

- Open saved analysed workspace of first row to compare (“*block name analyzed.mat*” in folder containing the pdf-report and saved histograms)
- Run “`plothisto comparisonStart.m`” to initiate plot and add first curve. Therefore type as follows in Command Window [6]:

```
plothistocomparisonStart(ME05,ME10,ME15,blockinfo);
```

- Load next analysed workspace and run “`plothistocomparisonAdd.m`”:

```
plothistocomparisonAdd(ME05,ME10,ME15,blockinfo);
```

- Repeat previous step until second to last data set.
- Load last analysed workspace
- Run “`plothistocomparisonFinish.m`” to add last data set and save plot:

```
plothistocomparisonFinish(ME05,ME10,ME15,blockinfo);
```

- Desired formatting of plot (e.g. fixed range of axis) can be applied by adopting the code-section “complete plot” of “`plothistocomparisonFinish.m`”. All available parameters are listed in the MATLAB[®] documentation of “plot” (2-D line plot).
- For comparison of 2 rows, only “Start” and “Finish” are required.
- NOTE: The created histograms are saved to the folder “Histogram Comparison” in the MATLAB[®] working directory. If this folder doesn’t exist and problems occur while saving the histogram: create the folder manually.
- NOTE: The comparison code is programmed for 7 curves with individual colour for each (caused by 7 available colours in MATLAB[®]). The 8th curve will be black again, more than 8 curves are not possible and will cause an error.

Appendix 11 Surface damage characteristics diagrams

CH01B03 (Reference)

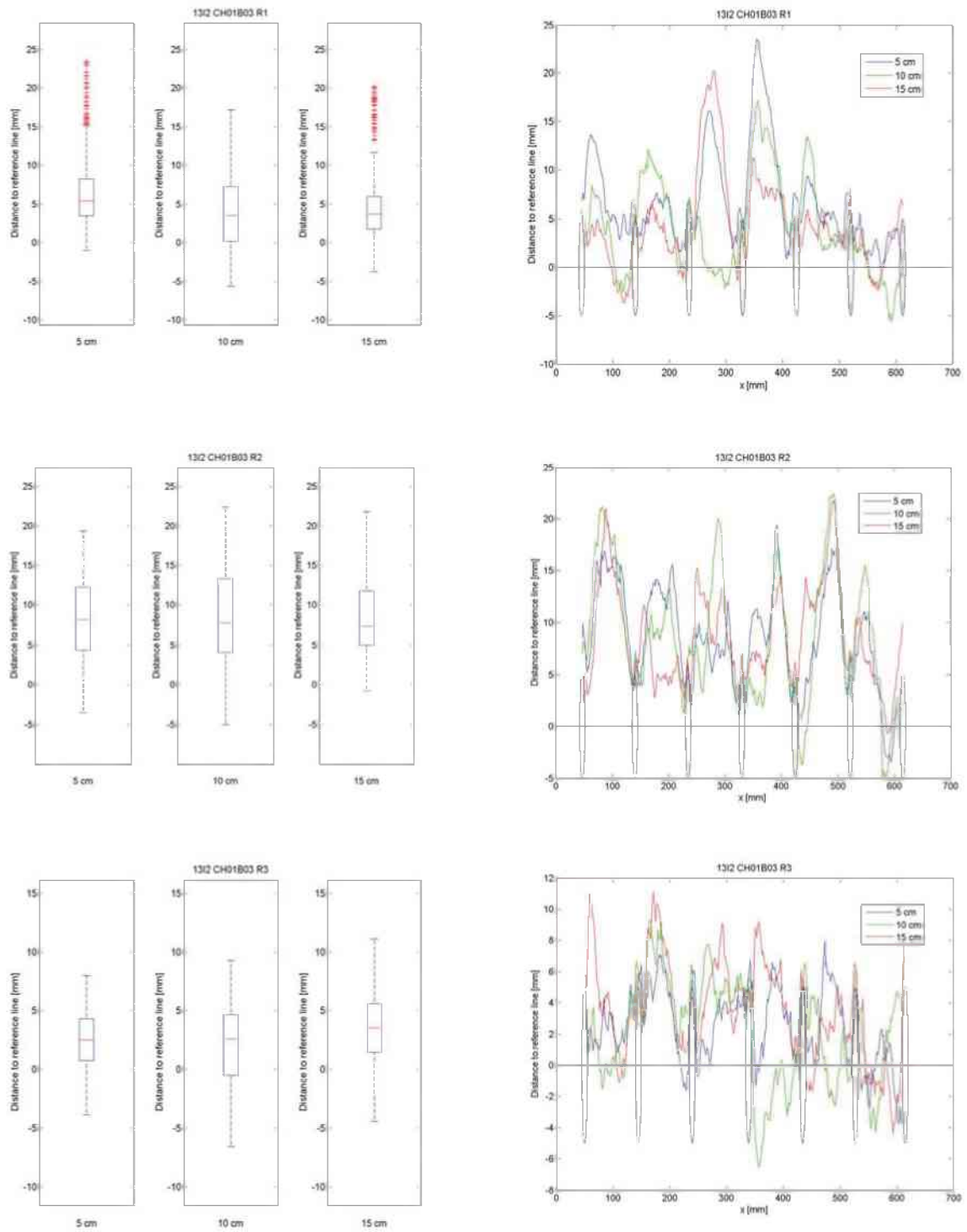


Figure 144: Roughness parameters specimen CH01B03 (Reference)

CH01B05 (Reference)

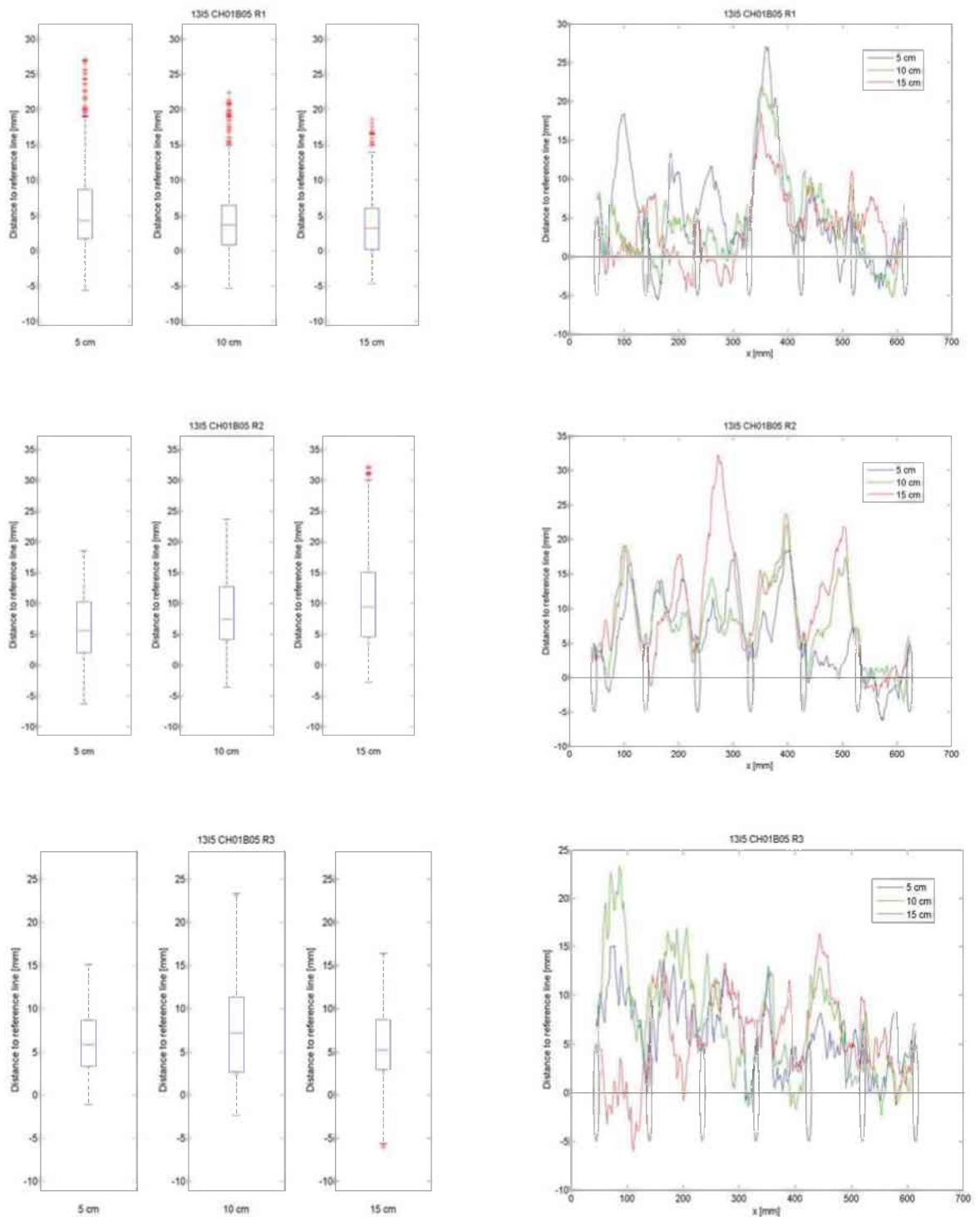


Figure 145: Roughness parameters specimen CH01B05 (Reference)

CH01B02 (1st burden deviation)

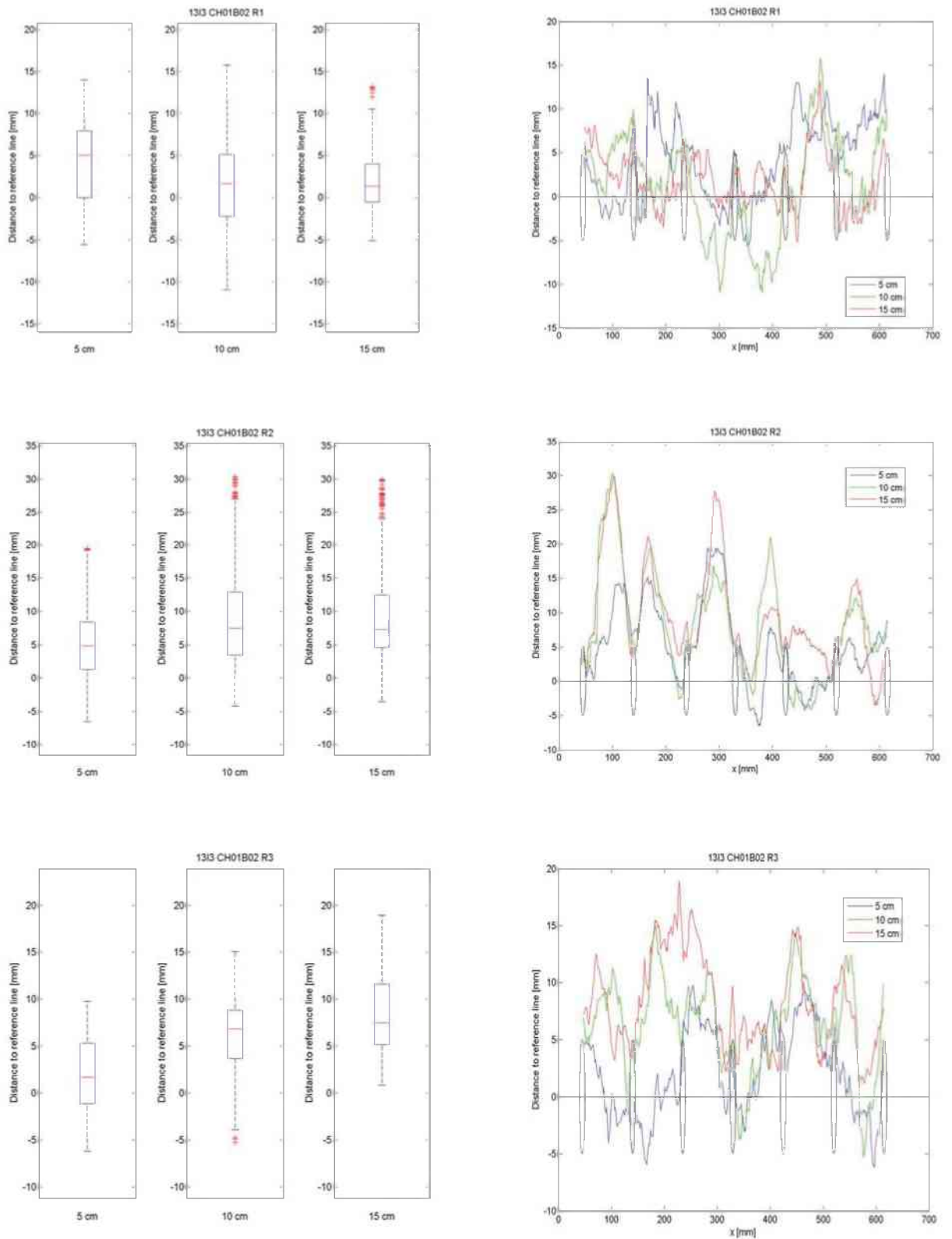


Figure 146: Roughness parameters specimen CH01B02 (1st burden deviation)

CH01B04 (1st burden deviation)

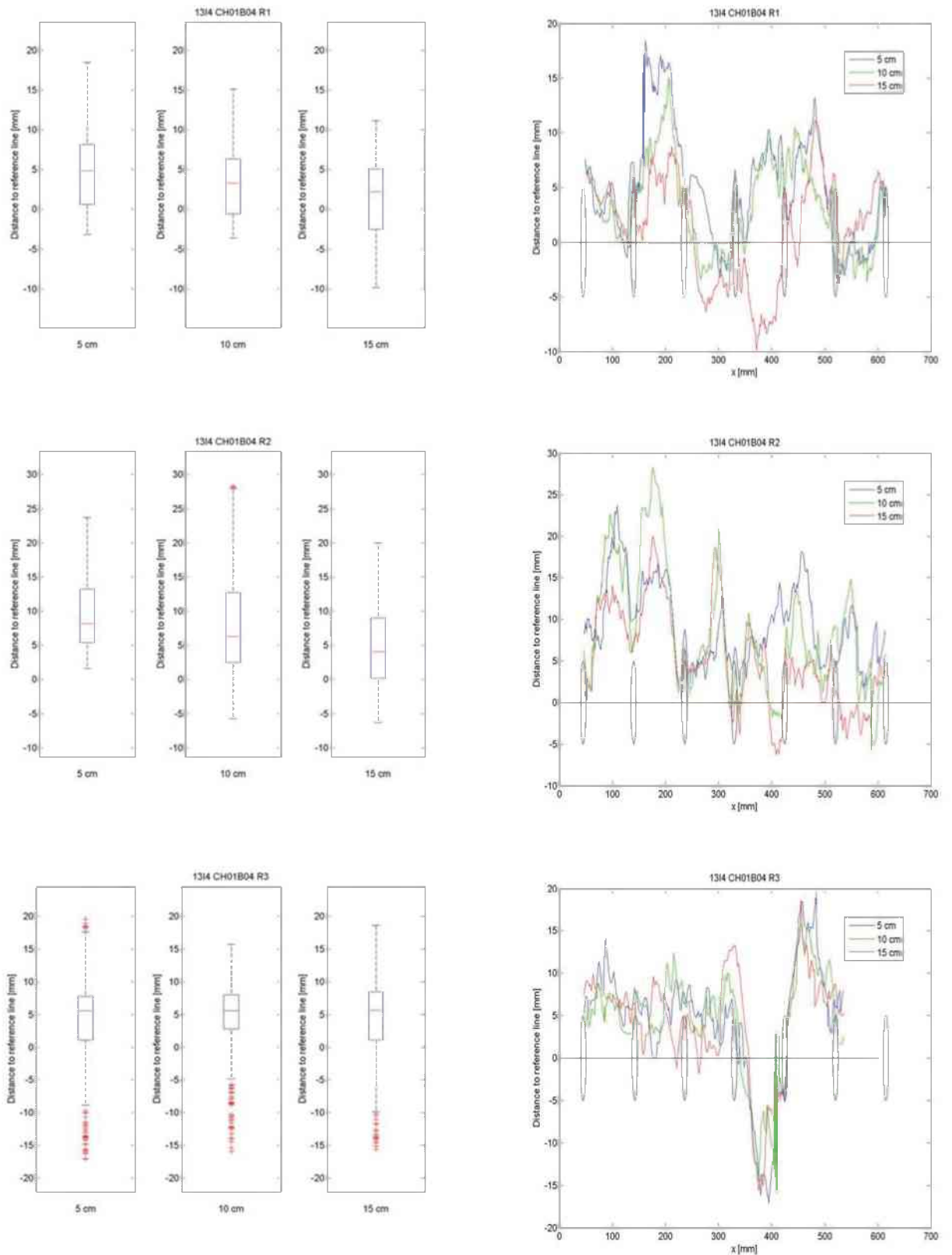


Figure 147: Roughness parameters specimen CH01B04 (1st burden deviation)

CH03B01 (2nd burden deviation)

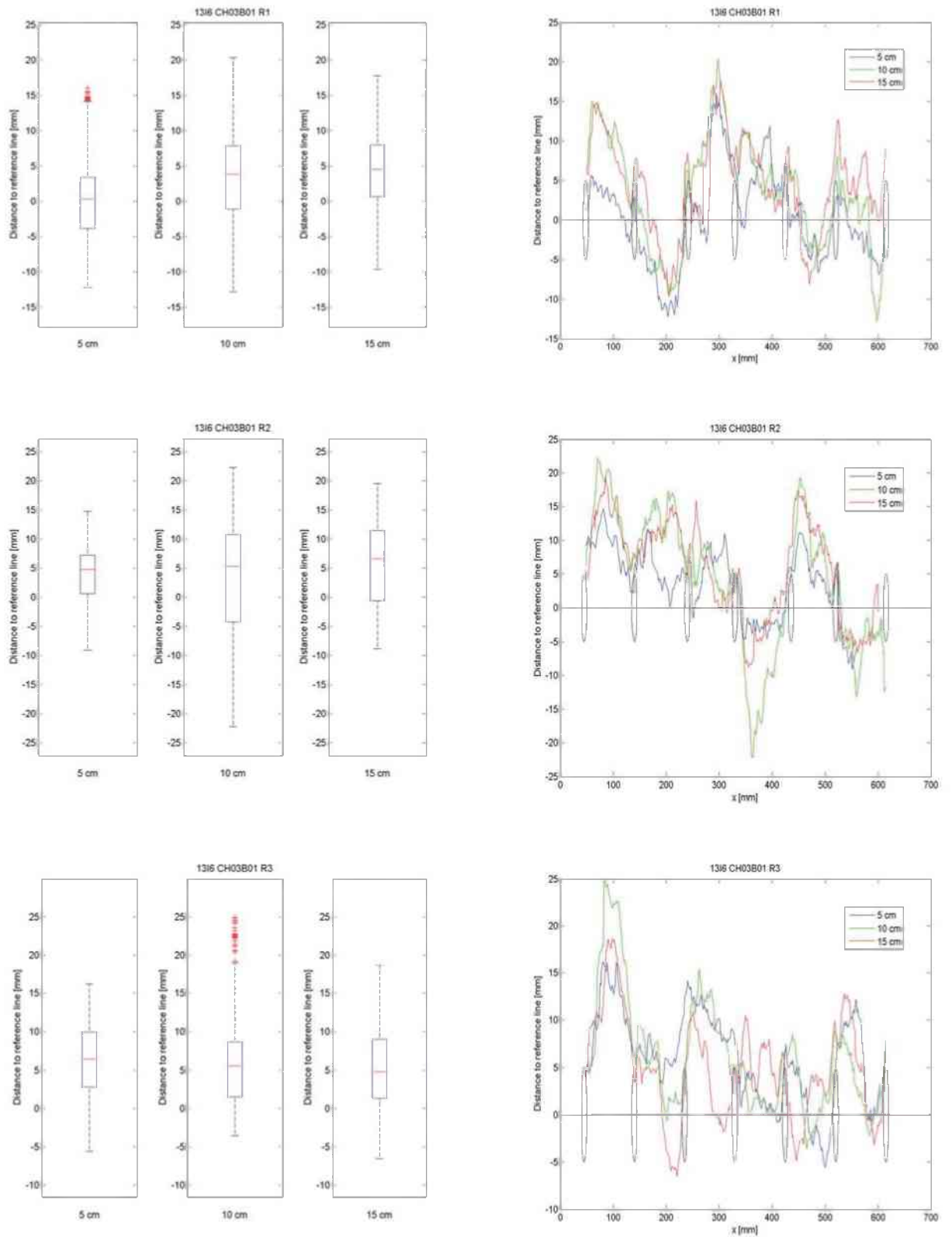


Figure 148: Roughness parameters specimen CH03B01 (2nd burden deviation)

CH03B02 (2nd burden deviation)

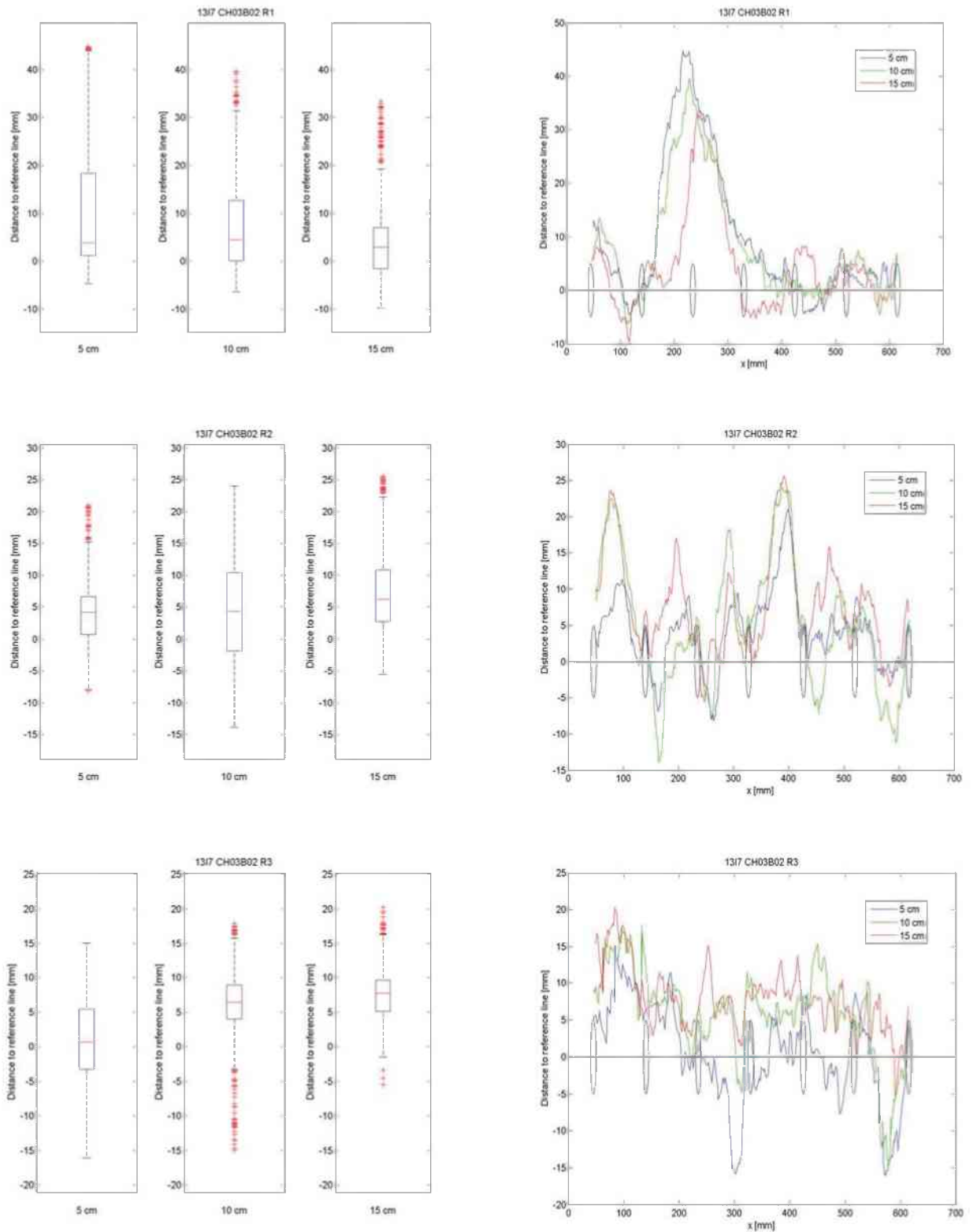


Figure 149: Roughness parameters specimen CH03B02 (2nd burden deviation)

B01 (Reference)

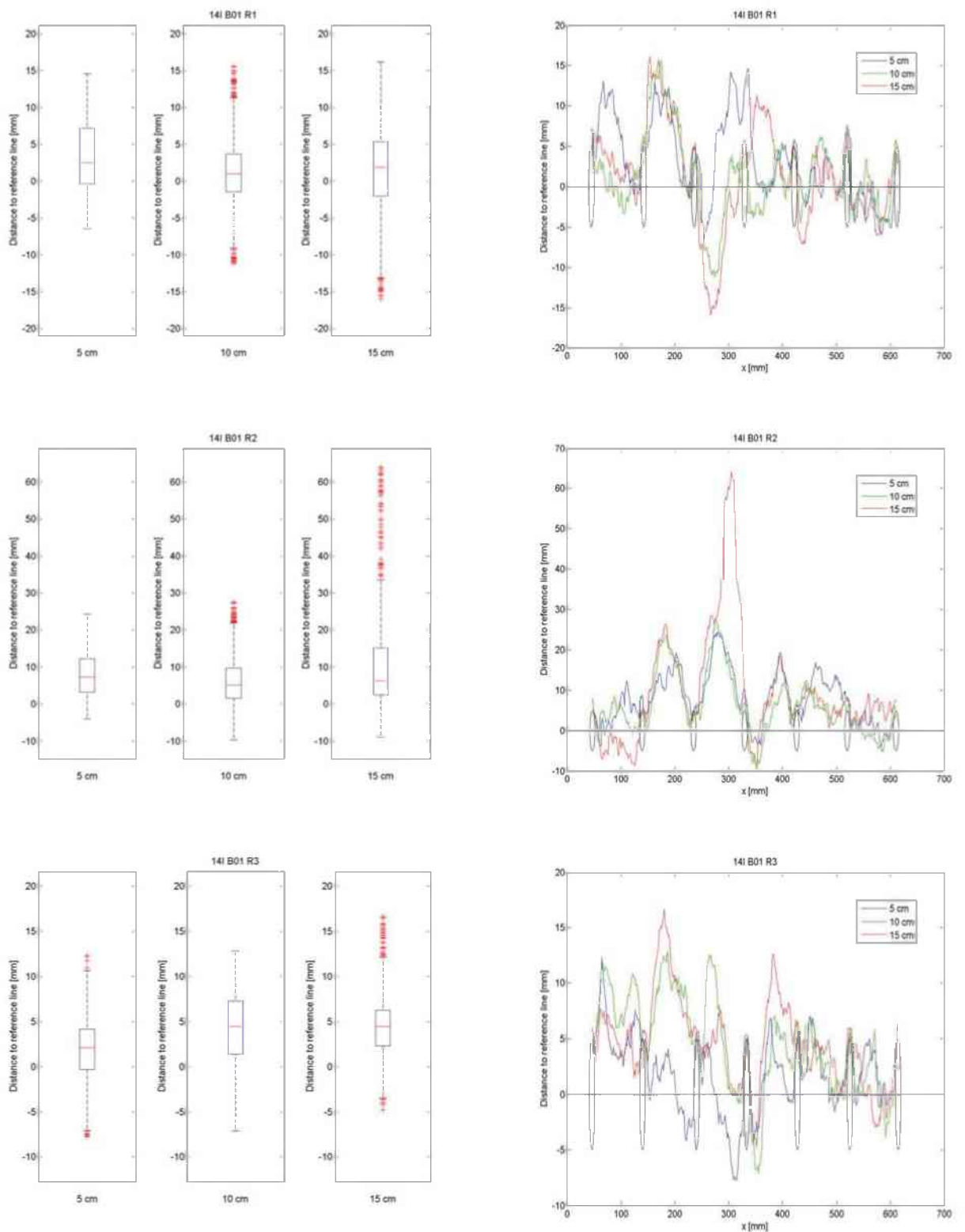


Figure 150: Roughness parameters specimen B01 (Reference)

B06 (Reference)

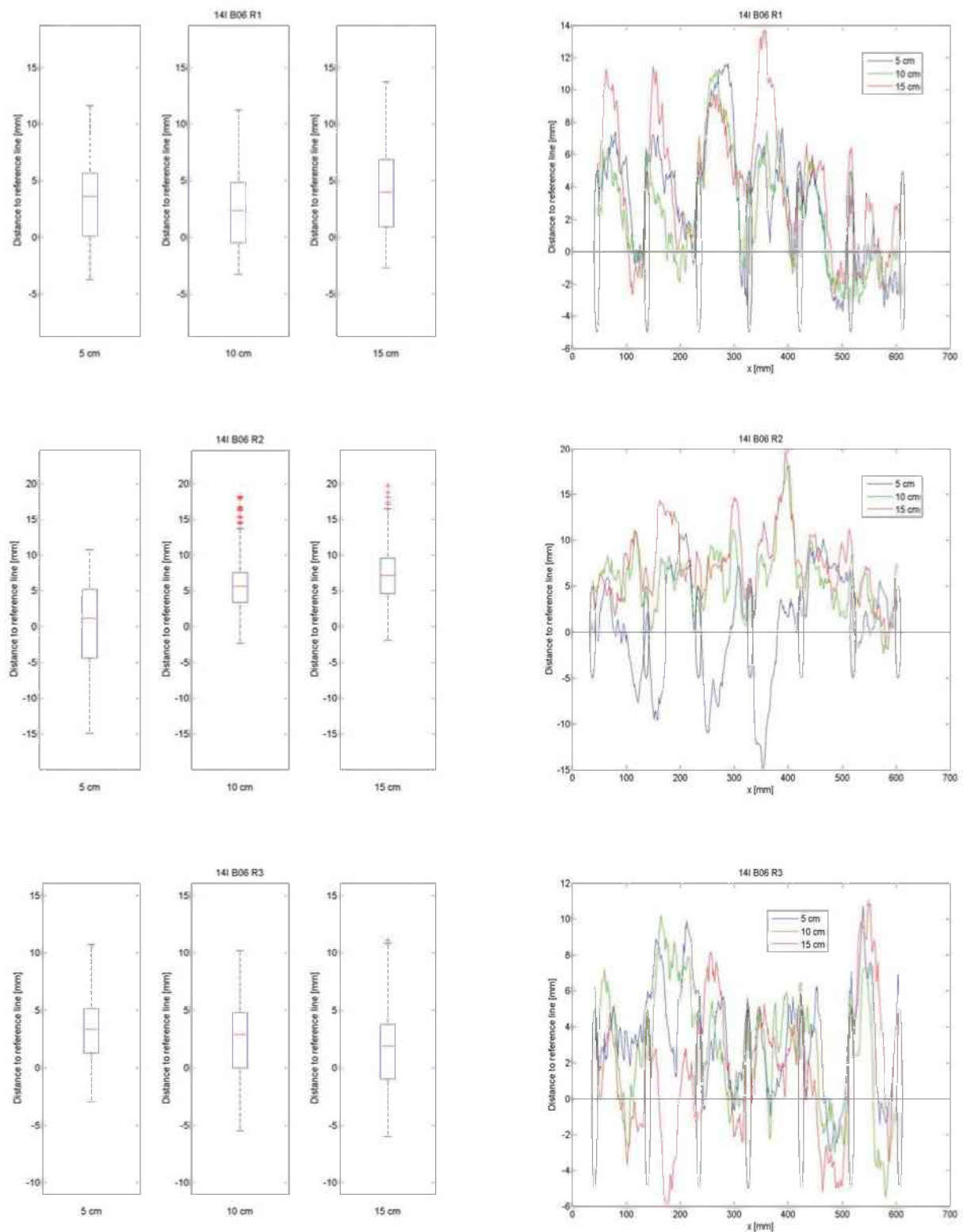


Figure 151: Roughness parameters specimen B06 (Reference)

B09 (Reference)

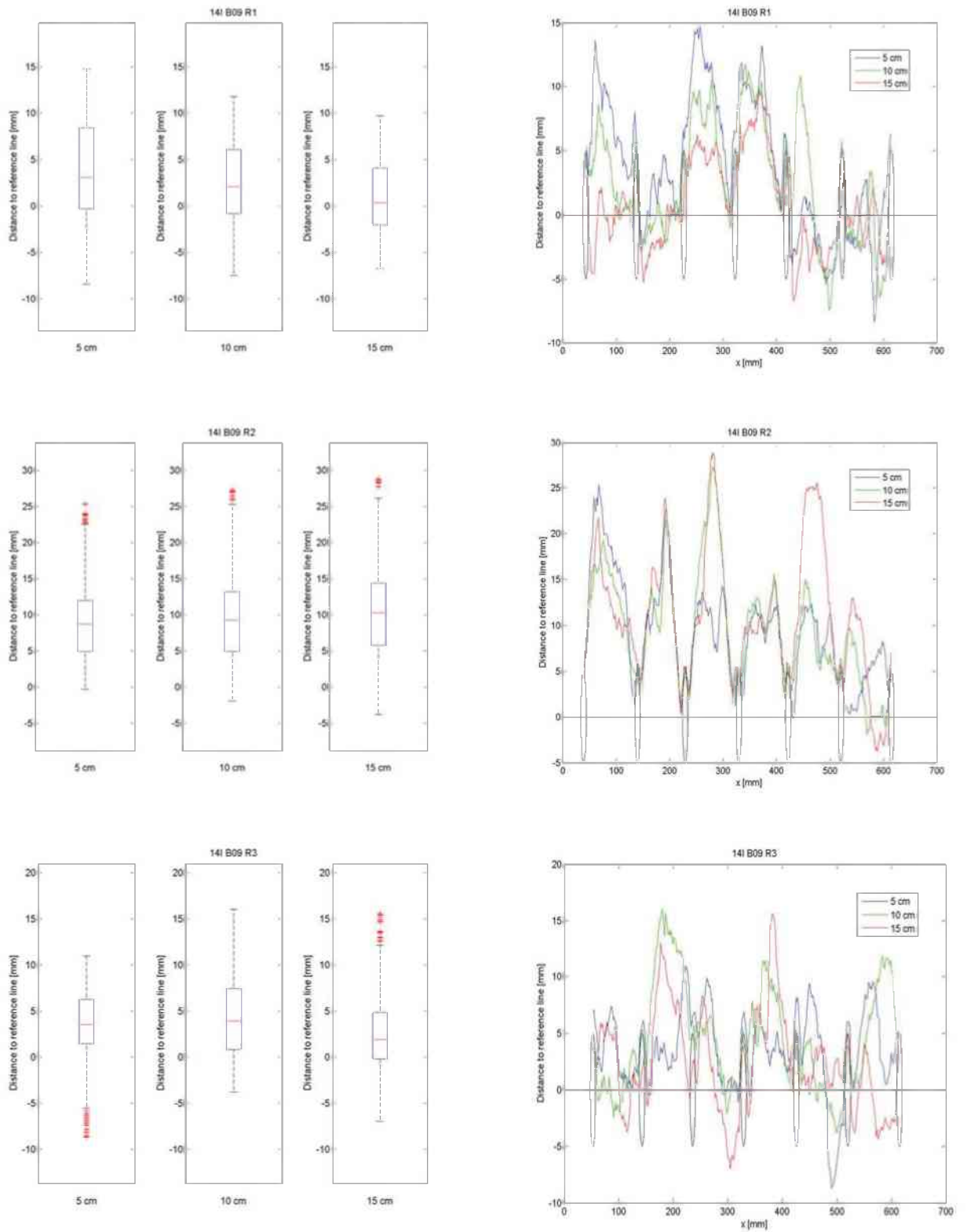


Figure 152: Roughness parameters specimen B09 (Reference)

B03 (S+B variations)

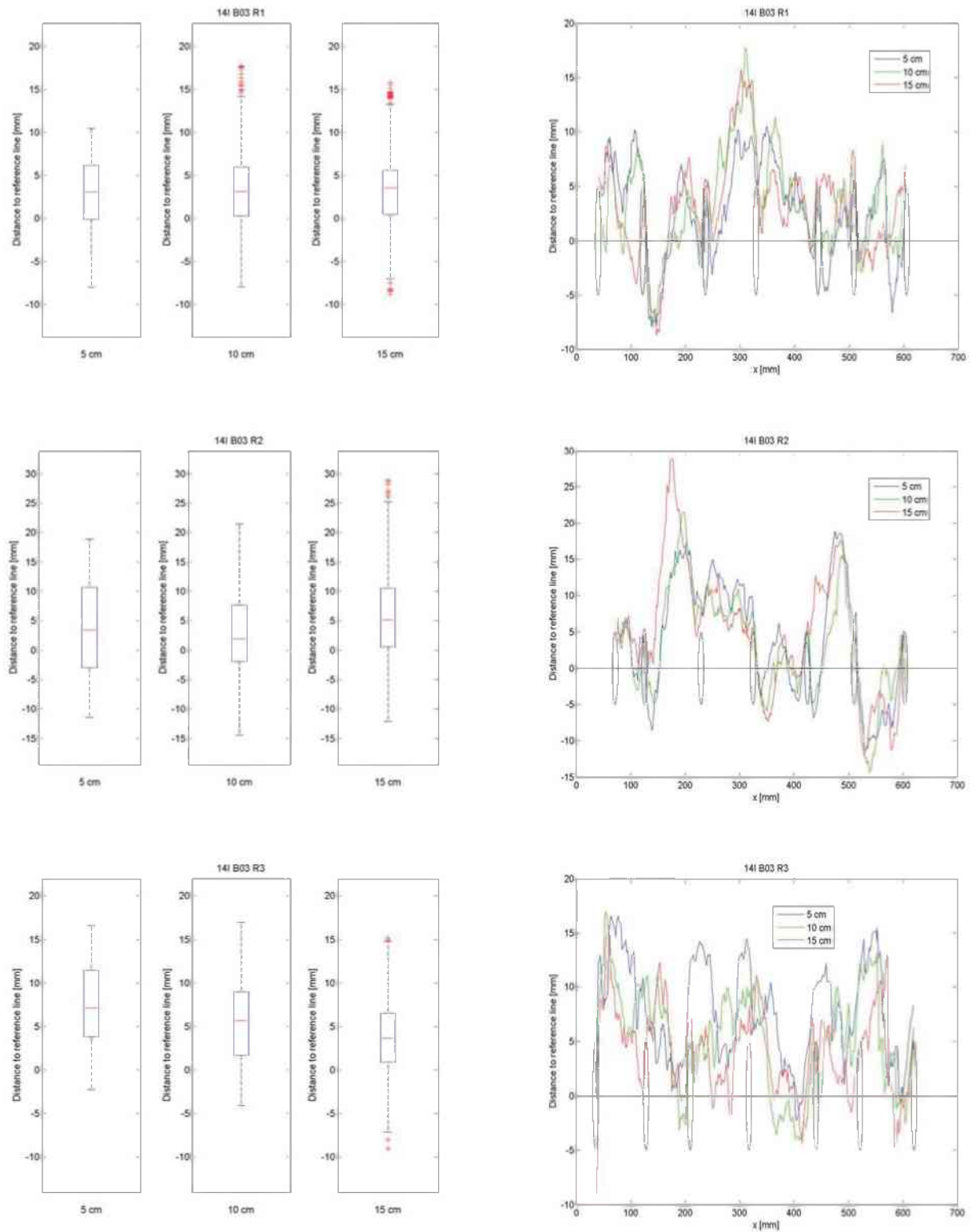


Figure 153: Roughness parameters specimen B03 (S+B variations)

B04 (S+B variations)

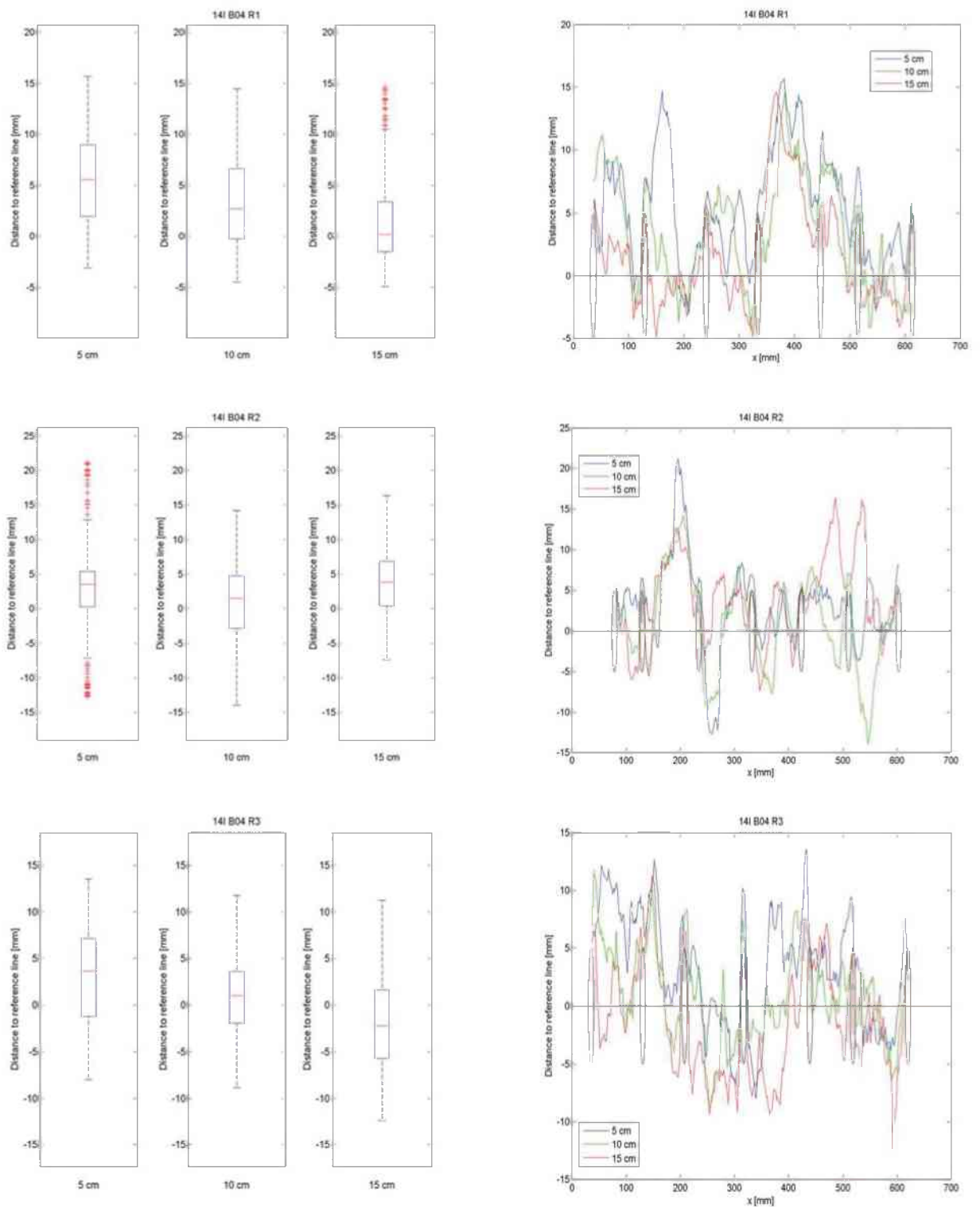


Figure 154: Roughness parameters specimen B04 (S+B variations)

B10 (B+B variations)

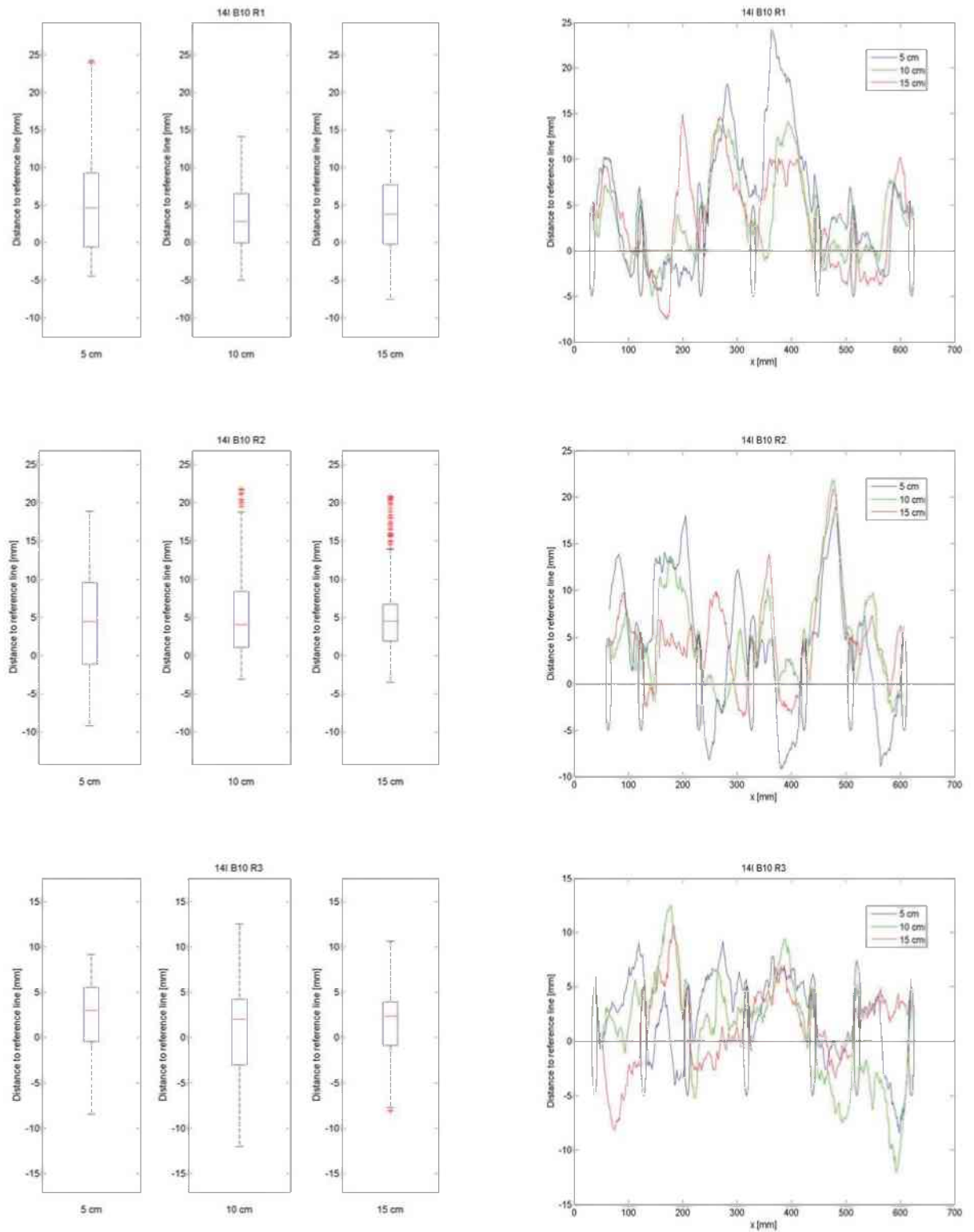


Figure 155: Roughness parameters specimen B10 (S+B variations)

B02 (S/4 shift)

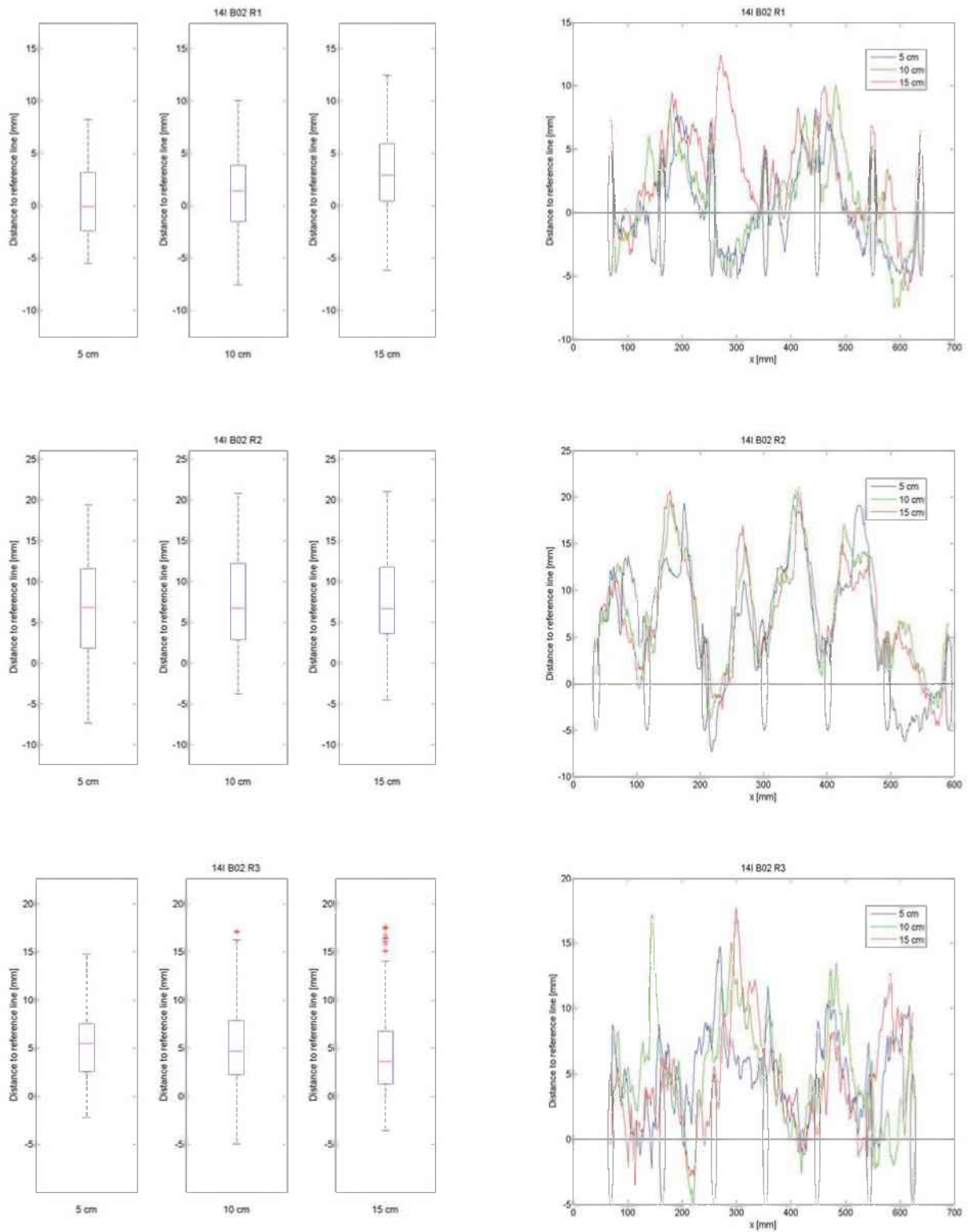


Figure 156: Roughness parameters specimen B02 (S/4 shift)

B07 (S/4 shift)

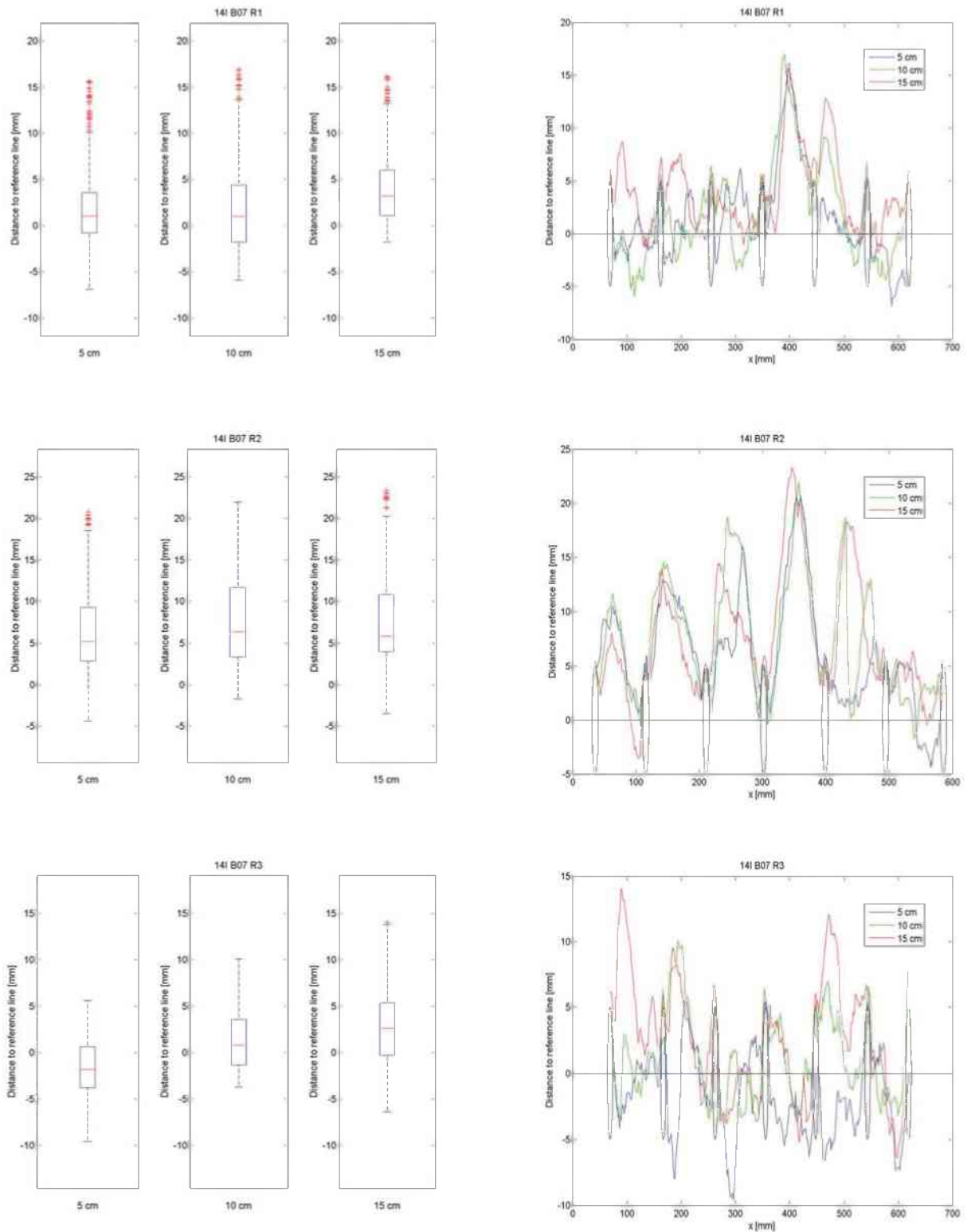


Figure 157: Roughness parameters specimen B07 (S/4 shift)

B11 (S/4 shift)

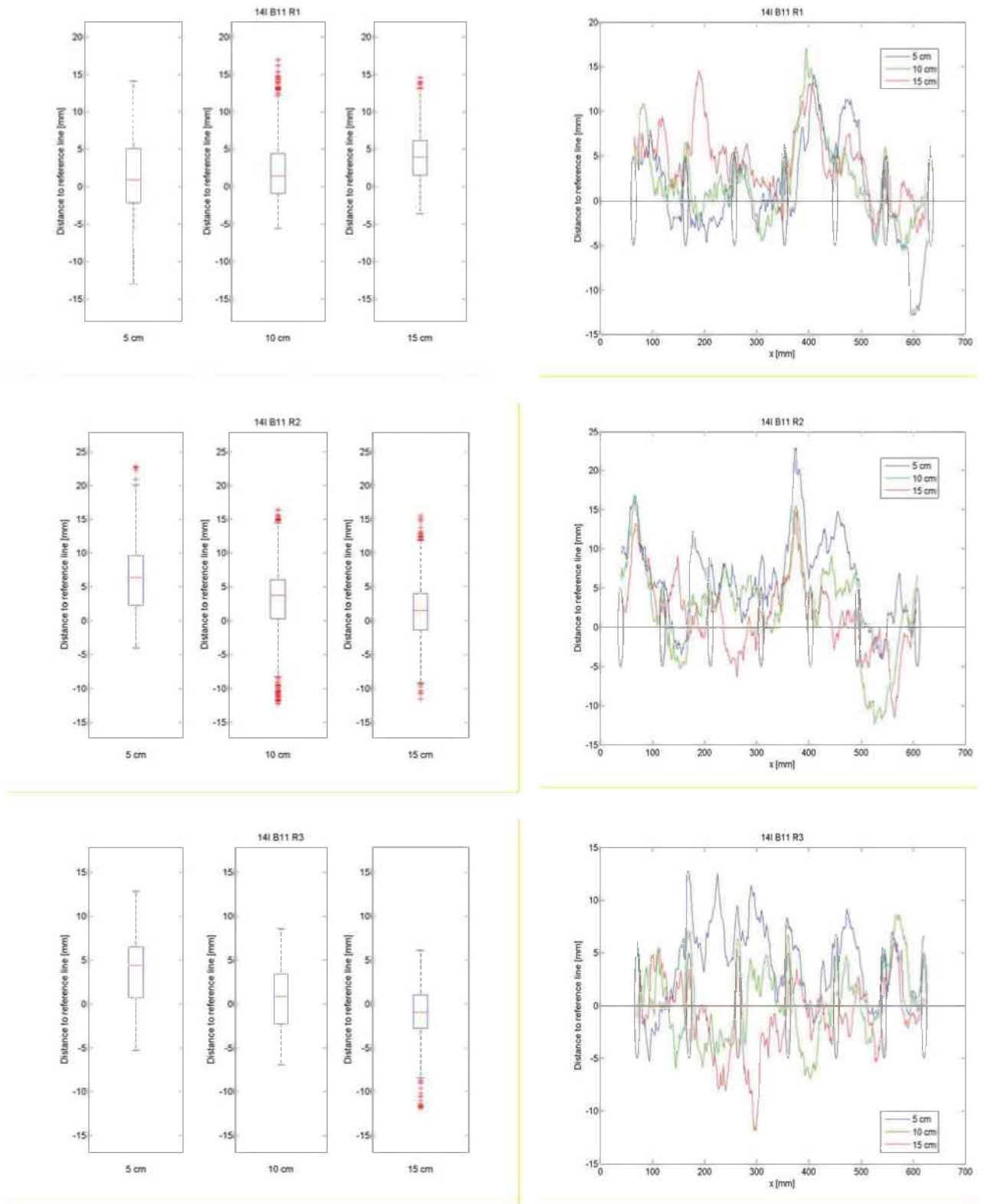


Figure 158: Roughness parameters specimen B11 (S/4 shift)

Appendix 12 Surface damage characteristics data

Blast session 2013:

Table 82: D_{mean} values over height, blast session 2013

Block	Row	D_{mean} value [mm] at			Average row	Stdev row	Average D_{mean} in pattern [mm]
		5	10	15			
CH01B03 (Reference)	1	6.75	4.16	4.52	5.14	1.40	5.93
	2	8.33	8.73	8.61	8.56	0.21	
	3	2.44	2.07	3.50	2.67	0.74	
CH01B05 (Reference)	1	5.71	4.48	3.59	4.59	1.07	
	2	6.10	8.12	10.39	8.20	2.14	
	3	6.06	7.55	5.63	6.41	1.01	
CH01B02 (1st burden deviation)	1	4.25	1.02	1.83	2.37	1.68	5.05
	2	5.34	8.50	9.29	7.71	2.09	
	3	2.01	6.13	8.23	5.46	3.16	
CH01B04 (1st burden deviation)	1	5.10	3.16	1.34	3.20	1.88	
	2	9.31	8.17	4.94	7.47	2.26	
	3	3.98	4.15	4.19	4.11	0.12	
CH03B01 (2nd burden deviation)	1	0.30	3.61	4.32	2.74	2.15	5.16
	2	3.89	3.61	5.44	4.32	0.98	
	3	6.30	6.53	5.17	6.00	0.73	
CH03B02 (2nd burden deviation)	1	10.59	7.87	4.68	7.72	2.96	
	2	4.14	4.74	7.56	5.48	1.83	
	3	0.37	5.79	7.87	4.67	3.87	

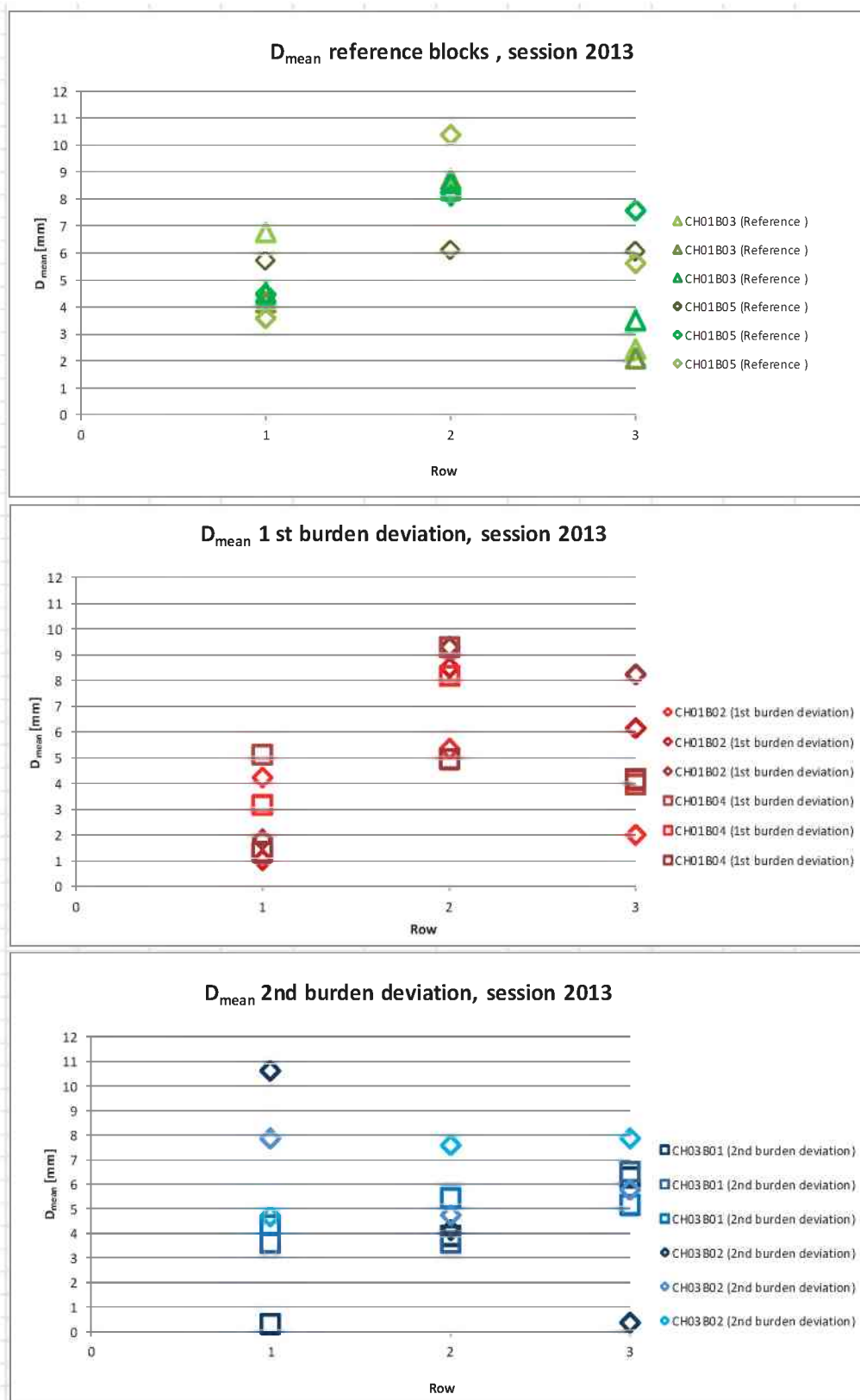


Figure 159: D_{mean} values at 5, 10 and 15 cm height, drill patterns, session 2013

Blast session 2014:

Table 83: D_{mean} values at 5, 10 and 15 cm height, blast session 2014

Block	Row	D_{mean} value[mm] at			Average row	Stdev row	Average D_{mean} in pattern [mm]
		5	10	15			
B01* (Reference)	1	3.30	1.31	1.57	2.06	1.08	4.36
	2	7.85	6.11	10.54	8.17	2.23	
	3	1.87	4.54	4.55	3.66	1.55	
B06 (Reference)	1	3.31	2.41	4.18	3.30	0.88	
	2	0.31	5.76	7.31	4.46	3.68	
	3	3.28	2.62	1.71	2.54	0.79	
B09 (Reference)	1	3.80	2.64	0.97	2.47	1.42	
	2	9.16	9.55	11.00	9.90	0.97	
	3	3.60	4.51	2.35	3.49	1.09	
B03 (S+B variations)	1	2.92	3.54	3.42	3.30	0.33	3.37
	2	3.72	2.91	5.38	4.00	1.26	
	3	7.56	5.31	3.89	5.59	1.85	
B04 (S+B variations)	1	5.67	3.36	1.52	3.52	2.08	
	2	3.05	0.85	3.89	2.60	1.57	
	3	3.21	0.89	-1.73	0.79	2.47	
B10 (S+B variations)	1	5.37	3.75	3.69	4.27	0.96	
	2	4.04	4.96	4.81	4.60	0.49	
	3	2.32	0.93	1.65	1.63	0.69	
B02 (S/4 shift)	1	0.51	1.22	3.21	1.65	1.40	3.49
	2	6.55	7.57	7.60	7.24	0.60	
	3	5.13	5.01	4.24	4.79	0.48	
B07 (S/4 shift)	1	1.81	1.89	3.97	2.56	1.22	
	2	6.26	7.79	7.57	7.20	0.83	
	3	-1.67	1.26	2.66	0.75	2.21	
B11 (S/4 shift)	1	1.20	2.26	4.09	2.51	1.46	
	2	6.40	2.65	1.74	3.60	2.47	
	3	3.98	0.64	-1.19	1.14	2.62	

Block B01 is a fragmentation outlier, but the D_{mean} data is presented

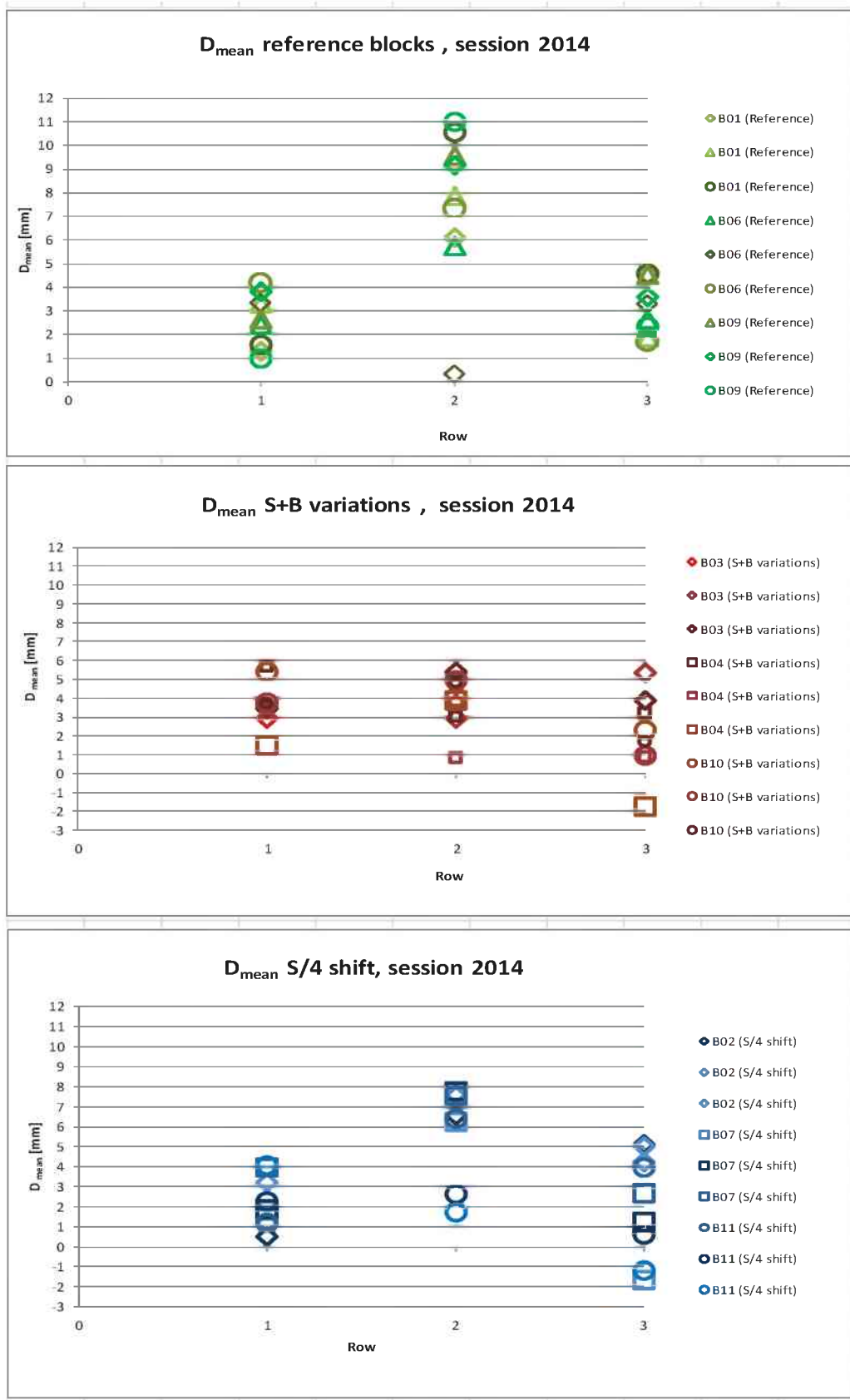


Figure 160: D_{mean} values at 5, 10 and 15 cm height, drill patterns, session 2014

Snorm evaluation:

The normalized slope inclination of the individual sections of the contour lines (S_{norm}) was used as a comparative figure for the roughness of the fresh blasted surface. The development of S_{norm} by the statistical evaluation of the data showed that except some samples in the 1st burden deviation pattern in session 2013, all the data in both 2013 and 2014 sessions are not samples which are drawn from the same underlying population. Schimek (2015) also has found similar results, by evaluating the S_{norm} data from 8 blocks in his Stage 2. All the blocks were blasted with the same pre-conditioning (140 μ s) in the first row. The statistical evaluation of the means of the individual rows showed that there was significant difference between the values for the individual blocks. No other simple model to apply for evaluation of the data was found either. The S_{norm} was judged as parameter with no physical meaning of describing the surface properties and was removed from the further analysis.